

MEETING THE CHALLENGES: CARBON-HYDROGEN BOND ACTIVATION AND
CANCER TREATMENT

by

HONGWANG WANG

B.A., Inner Mongolia University, China, 2000
M.S., Lanzhou Institute of Chemical Physics, Chinese Academy of Sciences, China, 2003

AN ABSTRACT OF A DISSERTATION

submitted in partial fulfillment of the requirements for the degree

DOCTOR OF PHILOSOPHY

Department of Chemistry
College of Arts and Sciences

KANSAS STATE UNIVERSITY
Manhattan, Kansas

2009

Abstract

My thesis is divided into two parts. The first part is focused on studies of N-heterocyclic carbene (NHC) palladium(IV) intermediates, which are involved in oxidative addition mediated C-C, and C-O bond formation processes as well as in C-Cl bond forming reactions via a reductive elimination process. Bis-NHC-Pd(II) complexes have been reported as effective catalysts to mediate direct conversion of methane into methanol. However, a H-D exchange study revealed that the bis-NHC-Pd(II) complexes are not the active species responsible for the C-H bond activation reaction. This unexpected result implies that the high oxidation state bis-NHC-Pd(IV) species may be the real catalyst! The oxidative addition of methyl iodide to the bis-NHC-Pd(II)-Me₂ complex led to the successful observation of the formation of a transient trimethyl bis-NHC-Pd(IV) intermediate by both ¹H-NMR and ¹³C-NMR spectroscopy. Different oxidants such as O₂, PhI(OAc)₂, PhI(OTFA)₂ and Cl₂ reacted with the bis-NHC-Pd(II)-Me₂ complex, and competitive C-C and C-O bond formations, as well as C-C and C-Cl bond formations were observed. Dioxygen triggered C-C bond formation under dry condition and both C-C and C-O bond formation in the presence of H₂O gave strong indications that the bis-NHC-Pd(II)-Me₂ complex can be oxidized to a bis-NHC-Pd(IV) intermediate by dioxygen. The reaction between the hypervalent iodine reagents PhI(OAc)₂ and PhI(OTFA)₂ and the bis-NHC-Pd(II)-Me₂ complex gave only reductive elimination products. Therefore, this system can act as a model system, which is able to providing valuable information of the product forming (functionalization) step of the C-H bond activation system. The reaction between chlorine and the bis-NHC-Pd(II)-Me₂ complex resulted in a relatively stable bis-NHC-Pd(IV)-Cl₄ complex, which was characterized by ¹H-NMR spectroscopy and mass spectroscopy. The structure of bis-NHC-Pd(IV)-Cl₄ was unambiguously established by X-ray crystallography.

The second part of this thesis describes the synthesis of functionalized bimagnetic core/shell iron/iron oxide nanoparticles for the treatment of cancer. Biocompatible dopamine-oligoethylene glycol functionalized bimagnetic core/shell Fe/Fe₃O₄ nanoparticles were prepared via ligand exchange, and purified by repeated dispersion/magneto-precipitation cycles. A porphyrin (TCPP) has been tethered to the stealth nanoparticles to enhance their uptake by tumor cells and (neural) stem cells. The stealth nanoparticles have been delivered in a mouse model to tumor sites intravenously by using the EPR (enhanced permeation and retention) effect.

Magnetic hyperthermia proved to be very effective against B16-F10 mouse melanomas in Charles River black mice. After hyperthermia, the nanoparticles have shown a significant effect on the growth of tumor (up to 78% growth inhibition).

MEETING THE CHALLENGES: CARBON-HYDROGEN BOND ACTIVATION AND
CANCER TREATMENT

by

HONGWANG WANG

B.A., Inner Mongolia University, China, 2000
M.S., Lanzhou Institute of Chemical Physics, Chinese Academy of Sciences, China, 2003

A DISSERTATION

submitted in partial fulfillment of the requirements for the degree

DOCTOR OF PHILOSOPHY

Department of Chemistry
College of Arts and Sciences

KANSAS STATE UNIVERSITY
Manhattan, Kansas

2009

Approved by:

Major Professor
Dr. Stefan H. Bossmann

Copyright

Hongwang Wang

2009

Abstract

My thesis is divided into two parts. The first part is focused on studies of N-heterocyclic carbene (NHC) palladium(IV) intermediates, which are involved in oxidative addition mediated C-C, and C-O bond formation processes as well as in C-Cl bond forming reactions via a reductive elimination process. Bis-NHC-Pd(II) complexes have been reported as effective catalysts to mediate direct conversion of methane into methanol. However, a H-D exchange study revealed that the bis-NHC-Pd(II) complexes are not the active species responsible for the C-H bond activation reaction. This unexpected result implies that the high oxidation state bis-NHC-Pd(IV) species may be the real catalyst! The oxidative addition of methyl iodide to the bis-NHC-Pd(II)-Me₂ complex led to the successful observation of the formation of a transient trimethyl bis-NHC-Pd(IV) intermediate by both ¹H-NMR and ¹³C-NMR spectroscopy. Different oxidants such as O₂, PhI(OAc)₂, PhI(OTFA)₂ and Cl₂ reacted with the bis-NHC-Pd(II)-Me₂ complex, and competitive C-C and C-O bond formations, as well as C-C and C-Cl bond formations were observed. Dioxygen triggered C-C bond formation under dry condition and both C-C and C-O bond formation in the presence of H₂O gave strong indications that the bis-NHC-Pd(II)-Me₂ complex can be oxidized to a bis-NHC-Pd(IV) intermediate by dioxygen. The reaction between the hypervalent iodine reagents PhI(OAc)₂ and PhI(OTFA)₂ and the bis-NHC-Pd(II)-Me₂ complex gave only reductive elimination products. Therefore, this system can act as a model system, which is able to providing valuable information of the product forming (functionalization) step of the C-H bond activation system. The reaction between chlorine and the bis-NHC-Pd(II)-Me₂ complex resulted in a relatively stable bis-NHC-Pd(IV)-Cl₄ complex, which was characterized by ¹H-NMR spectroscopy and mass spectroscopy. The structure of bis-NHC-Pd(IV)-Cl₄ was unambiguously established by X-ray crystallography.

The second part of this thesis describes the synthesis of functionalized bimagnetic core/shell iron/iron oxide nanoparticles for the treatment of cancer. Biocompatible dopamine-oligoethylene glycol functionalized bimagnetic core/shell Fe/Fe₃O₄ nanoparticles were prepared via ligand exchange, and purified by repeated dispersion/magneto-precipitation cycles. A porphyrin (TCPP) has been tethered to the stealth nanoparticles to enhance their uptake by tumor cells and (neural) stem cells. The stealth nanoparticles have been delivered in a mouse model to tumor sites intravenously by using the EPR (enhanced permeation and retention) effect.

Magnetic hyperthermia proved to be very effective against B16-F10 mouse melanomas in Charles River black mice. After hyperthermia, the nanoparticles have shown a significant effect on the growth of tumor (up to 78% growth inhibition).

Table of Contents

List of Figures	xiii
List of Tables	xxii
Acknowledgements	xxiii
CHAPTER 1 - Introduction	1
1.1 What is C-H bond activation?.....	1
1.2 Transition metal mediated aromatic C-H bond activation.....	2
1.3 Transition metal mediated alkane C-H bond activation	4
1.4 Transition metal catalyzed methane oxidation	6
1.4.1 The Shilov System	7
1.4.2 The Catalytica System	13
1.4.3 The NHC-Pd system by Strassner.....	16
1.5 Research Goals	19
CHAPTER 2 - NHC-Pd Complexes-mediated Aryl C-H bond activation study	23
2.1 Possible reaction pathways of the NHC-Pd catalyzed methane oxidation reaction.	23
2.2 NHC-Pd Complex Mediated Aryl H-D Exchange.....	25
2.2.1 Synthesis of NHC-Pd(II) Complexes.....	25
2.2.2 H-D Exchange Study	26
2.3 Study of Bis-NHC-Pd(II) Mediated C-H Bond Activation in the Presence of Potassium Peroxodisulfate	30
2.4 Discussion of the Experimental Findings	31
2.5 Experimental.....	32
2.5.1 Synthesis of 1, 1'-Dimethyl-3,3'-methylene-diimidazolium dibromide (2.1)	32
2.5.2 Synthesis of (1, 1'-Dimethyl-3,3'-methylene-diimidazoline-2,2'-diylidene) palladium(II) dibromide (2.2).	33
2.5.3 Synthesis of (1, 1'-Dimethyl-3,3'-methylene-diimidazoline-2,2'-diylidene) palladium(II) bis(trifluoroacetate) (2.3a).	33
2.5.4 Synthesis of (1, 1'-Dimethyl-3,3'-methylene-diimidazoline-2,2'-diylidene) palladium(II) diacetate (2.3b).	33

2.5.5 Bis-NHC-Pd-Br ₂ complex 2.2 mediated H-D toluene exchange.....	34
2.5.6 Control experiment of toluene H-D exchange	34
2.5.7 Bis-NHC-Pd-(OOCF ₃) ₂ complex 2.3a mediated toluene H-D exchange.....	35
2.5.8 Bis-NHC-Pd-(OOCF ₃) ₂ complex 2.3a mediated p-xylene H-D exchange	35
2.5.9 Control experiment of p-xylene H-D exchange study	35
2.5.10 Bis-NHC-Pd(II)-Br ₂ complex 2.2 mediated C-H bond activation of toluene in the presence of potassium peroxodisulfate.	35
CHAPTER 3 - Study of NHC-Pd(IV) Species	38
3.1 Introduction.....	38
3.2 Oxidation of NHC-Pd(II)-(OOCCH ₃) ₂ and NHC-Pd(II)-(OOCF ₃) ₂	40
3.3 Oxidation of NHC-Pd(II)-Br ₂ with Br ₂	41
3.4 Synthesis of Tripodal NHC-Pd Complexes	42
3.4.1 Examples of Pd(IV) Complexes that are Stabilized with Tripod ligands	42
3.4.2 Tripod ligand design and synthesis.....	42
3.4.3 Synthesis of tripod bis-NHC-Pd(II) complexes.....	44
3.5 Discussion of the experimental findings.....	48
3.6 Experimental.....	48
3.6.1 Synthesis of the α -chloro-epoxide 3.17	48
3.6.2 Synthesis of the bis-imidazole alcohol 3.18	49
3.6.3 Tips-protection of hydroxyl group to form 3.19	49
3.6.4 Tips-protected bis-imidazolium diiodide 3.20.....	50
3.6.5 Synthesis of tripod-bis-imidazolium diiodide 3.24.....	50
3.6.6 Synthesis of tripod-bis-NHC-Pd(II)-I ₂ complex 3.25	50
CHAPTER 4 - Direct Observation of Trimethyl Bis-NHC-Pd(IV) Species	53
4.1 The Principle of Microscopic Reversibility.....	53
4.2 Synthesis of a Bis-NHC-Pd-Me ₂ Complex.....	54
4.3 Oxidative Addition of MeI to Bis-NHC-Pd-Me ₂ Complex	55
4.4 Oxidative Addition of ¹³ CH ₃ I to Bis-NHC-Pd-Me ₂ Complex.....	57
4.5 Mechanistic Discussion of the Oxidative Addition of MeI to the Bis-NHC-Pd(II)-Me ₂ Complex and the Reductive Elimination from the Trimethyl Bis-NHC-Pd(IV) Species.....	60
4.5.1 Pathway for the Oxidative Addition.....	60

4.5.2 Pathway for the Reductive Elimination.....	62
4.6 Experimental.....	65
4.6.1 Synthesis of bis-NHC-Pd(II)-(CH ₃) ₂ complex.....	65
4.6.2 VT-NMR study of the reaction between bis-NHC-Pd(II)-(CH ₃) ₂ and CH ₃ I.....	65
4.6.3 VT-NMR study of the reaction between bis-NHC-Pd(II)-(CH ₃) ₂ and ¹³ CH ₃ I.....	65
4.6.4 VT-NMR study of the reaction between bis-NHC-Pd(II)-(CH ₃) ₂ and ¹³ CH ₃ I in the presence of DMAP.....	66
CHAPTER 5 - Dioxygen Triggered C-C Bond Formation vs. C-O Bond Formation from the Bis- NHC-Pd(II)-Me ₂ Complex	69
5.1 Introduction.....	69
5.1.1 Examples of Reaction between Dioxygen and Pt(II) Complexes.....	69
5.1.2 Examples of Reaction between Dioxygen and Pd(0), Pd(II) complexes.....	71
5.2 Synthesis of 1,1'-Di(n-butyl)-3,3'-Methylene-4-Diimidazolin-2,2'-Diyliidene Palladium(II) Dimethyl Complex.....	72
5.3 Oxygen Triggered C-C Bond Formation.....	73
5.4 Oxygen Triggered C-C Bond Formation and C-O Bond Formation in the Presence of Water.....	75
5.5 Experimental.....	79
5.5.1 Synthesis of n-butyl-imidazole 5.11.....	79
5.5.2 Synthesis of 1,1'-di-n-butyl-3,3'-methylenediimidazolium dibromide 5.12.....	79
5.5.3 Synthesis of (1,1'-di-n-butyl-3,3'-methylenediimidazoline-2,2'-diylidene)palladium(II) dibromide 5.13.....	79
5.5.4 Synthesis of (1,1'-di-n-butyl-3,3'-methylenediimidazoline-2,2'-diylidene)palladium(II) dimethyl 5.14.....	80
5.5.5 Synthesis of (1,1'-di-n-butyl-3,3'-methylenediimidazoline-2,2'-diylidene)palladium(II) di(¹³ C-methyl) 5.14'.....	80
5.5.6 Reaction between bis-NHC-Pd(II)-Me ₂ complex 5.14 and O ₂	80
5.5.7 Reaction between bis-NHC-Pd(II)-Me ₂ complex 5.14 and O ₂ in the presence of H ₂ O.....	80
CHAPTER 6 - PhI(OAc) ₂ and PhI(OTFA) ₂ Triggered C-C Bond and C-O Bond Formation from Bis-NHC-Pd(II)-(CH ₃) ₂ Complex	83

6.1 Introduction.....	83
6.2 PhI(OAc) ₂ Triggered C-C Bond Formation from Bis-NHC-Pd(II)-(CH ₃) ₂ Complex.....	84
6.3 PhI(OTFA) ₂ Triggered C-C Bond and C-O Bond Formation from Bis-NHC-Pd(II)-(CH ₃) ₂ Complex.....	86
6.4 Mechanistic Discussion of the PhI(OAc) ₂ Triggered C-C Bond Formation vs PhI(OTFA) ₂ Triggered C-C and C-O Bond Formation.	89
6.5 Experimental.....	95
6.5.1 The reaction between PhI(OAc) ₂ and bis-NHC-Pd(II)-(CH ₃) ₂ complex 5.14.....	95
6.5.2 The reaction between PhI(OTFA) ₂ and bis-NHC-Pd(II)-(CH ₃) ₂ complex 5.14.....	95
6.5.3 Mono-protonation of bis-NHC-Pd(II)-(CH ₃) ₂ complex with diisopropylethylammonium trifluoroacetate salt and further reaction with PhI(OTFA) ₂	95
6.5.4 Mono-protonation of bis-NHC-Pd(II)-(CH ₃) ₂ complex to form bis-NHC-Pd(II)-(CH ₃)-(4-Cl-C ₆ H ₄ O) complex.....	96
6.5.5 The reaction between PhI(OTFA) ₂ and bis-NHC-Pd(II)-(CH ₃)-(4-Cl-C ₆ H ₄ O) complex.....	96
CHAPTER 7 - Chlorine Triggered C-C Bond Formation Vs C-Cl Bond Formation from Bis-NHC-Pd(II)-Me ₂ Complex	99
7.1 Introduction.....	99
7.2 Chlorine Triggered C-C Bond and C-Cl Bond Formation at Lower Temperature.....	100
7.3 Chlorine Triggered C-C Bond and C-Cl Bond Formation at Room Temperature.	101
7.4 Mass Spectroscopy Characterization of the Final Product.....	102
7.5 Discussion of The Mechanism of the Reaction between the Bis-NHC-Pd(II)-(CH ₃) ₂ Complex and Chlorine.....	103
7.6 The Stability of the Bis-NHC-Pd(IV)-Cl ₄ in Solution.....	104
7.7 Crystal Structure of a Isolated Bis-NHC-Pd(IV)-Cl ₄ Complex.....	107
7.8 Experimental.....	109
CHAPTER 8 - Conclusion and Future Work on the Bis-NHC-Pd(IV) Studies	
CHAPTER 9 - Synthesis of Functionalized Bimagnetic Core/Shell Fe/Fe ₃ O ₄ Nanoparticles for the Treatment of Cancer.....	113
9.1 Introduction.....	113
9.2 Research Goal.....	115

9.3 Surface Modification of the Fe/Fe ₃ O ₄ Core/Shell Nanoparticles.....	116
9.3.1 Synthesis of the Organic Ligands.....	116
9.3.2 Tethering the Ligands on the Nanoparticles and Introduction of a TCPP Porphyrin as Targeting Tag.....	118
9.4 Magnetic Heating of Nanoparticles.....	120
9.5 Light-Absorption and Emission Properties of Fe/Fe ₃ O ₄ Core/Shell Nanoparticles Featuring Chemically Attached Porphyrin Units (TCPP).....	121
9.6 NMR-Measurement of T ¹ and T ² -Relaxation Times.....	122
9.7 Hyperthermia Experiments of Charles River Mice Featuring Impregnated B16-F10-Melanomas.....	125
9.7.1 Cytotoxicity of Magnetic Nanoparticles on B16-F10 cells.....	125
9.7.2 Temperature Measurement on Mice.....	126
9.7.3 Intratumoral Administration of MNPs with AMF Exposure.....	127
9.7.4 Intravenous Administration of MNPs with AMF Exposure.....	128
9.8 Conclusion.....	131
9.9 Experimental.....	131
9.9.1. Synthesis of porphyrin (TCPP).....	131
9.9.2. Boc-protection of Dopamine.....	132
9.9.3 Benzyl-protection of Boc-dopamine.....	132
9.9.4 Deprotect of Boc-group.....	133
9.9.5 Amide Formation.....	134
9.9.6 Synthesis of ligand I.....	134
9.9.7 Synthesis of glycine-tipped ligand (ligand II).....	136
9.9.8 Modification of Fe/Fe ₃ O ₄ nanoparticles with dopamine-based ligands I and II and introducing of porphyrin (TCPP).....	137

List of Figures

Figure 1.1 Ru(0)(dmpe) ₂ complex mediated C-H bond activation of naphthalene.....	3
Figure 1.2 Proposed mechanisms for the platinum(II) mediated aromatic H-D exchange	4
Figure 1.3 Iridium complex 1.4 mediated C-H bond activation of alkanes.....	5
Figure 1.4 Iridium complex 1.8 mediated C-H bond activation of alkanes.....	5
Figure 1.5 Rhodium complex 1.9 mediated C-H bond activation of propane.....	6
Figure 1.6 Syn-gas method to convert methane to methanol.....	6
Figure 1.7 Pt(II) mediated methane oxidation.....	7
Figure 1.8 Proposed mechanism for the methane oxidation in Shilov System	8
Figure 1.9 Proposed S _N 2 pathway (a) and concerted pathway (b) in the product forming step.....	8
Figure 1.10 Evidence for the S _N 2 pathway in the product forming step for the Shilov System.....	9
Figure 1.11 Two possible pathways for oxidation of the alkylpalladium(II) intermediate by [PtCl ₆] ²⁻	10
Figure 1.12 Oxidation of Zeise's salt by [PtCl ₆] ²⁻	10
Figure 1.13 Two possible pathways for alkane C-H bond activation by Pt(II)	11
Figure 1.14 Oxidative addition of HCl to (tmeda)Pt(II)(CH ₃)Cl complex.....	12
Figure 1.15 Possible pathway for multiple deuterium incorporation into methane.....	12
Figure 1.16 Four individual steps of the platinum catalyzed C-H bond activation	13
Figure 1.17 (bpym)PtCl ₂ catalyzed methane oxidation in concentrated sulfuric acid.....	13
Figure 1.18 Process scheme for the net oxidation of methane to methanol	14
Figure 1.19 Proposed mechanism for the methane oxidation for the Catalytica System	15
Figure 1.20 NHC-Pd(II) complexes catalyzed methane oxidation.....	16
Figure 1.21 Stepwise replacement of halogen with trifluoroacetate.....	18
Figure 2.1 Possible methane oxidation pathway I for the Strassner System	23
Figure 2.2 Possible methane oxidation pathway II for the Strassner System.....	24
Figure 2.3 Possible methane oxidation pathway III for the Strassner System.....	25
Figure 2.4 Synthesis of bis-NHC-Pd(II) complexes.....	26
Figure 2.5 Stacked ¹ H-NMR of the bis-NHC-Pd(II)-Br ₂ mediated toluene H-D exchange reaction in CF ₃ COOD (expanded aromatic area, the spectrum was recorded every 5 hours).....	27

Figure 2.6 Possible pathways for the bis-NHC-Pd(II)-Br ₂ complex mediated aromatic H-D exchange reaction.....	28
Figure 2.7 Test of cationic NHC-Pd(II) species for aromatic H-D exchange reaction.....	30
Figure 2.8 The hypothetical sequence for the formation of p-toluenesulfonic acid	31
Figure 2.9 Demonstration of the π -backdonating effect.....	32
Figure 3.1 Oxidation of Pd(II) complexes to Pd(IV) complexes by chlorine.....	38
Figure 3.2 Reductive elimination of ethane from a Pd(IV) intermediate	39
Figure 3.3 Bis-pyridine ligand stabilized Pd(IV) complexes formation.....	39
Figure 3.4 Tris(pyrazol-1-yl)borate ligand supported palladium(IV)cyclopentane complexes formation.....	39
Figure 3.5 Phenylpyridine ligand supported Pd(IV) complexes formation.....	40
Figure 3.6 Proposed reversible reaction between NHC-ligated Pd(II) and Pd(IV)	41
Figure 3.7 Stronger donor ligand stabilize Pd(IV) species better	42
Figure 3.8 Tripod ligand design.....	43
Figure 3.9 Synthesis of the tripodal ligand	44
Figure 3.10 Proposed approach to tripodal ligand stabilized Pd(IV) species.....	45
Figure 3.11 Synthesis of tripodal bis-NHC-Pd(II)-I ₂ complex 25.....	45
Figure 3.12 X-ray structure of complex 25 (a: Thermal ellipsoid plot drawn at the 50% probability level; b: The hydrogen atoms are omitted for clarity reasons).....	46
Figure 4.1 Energy diagram of a reversible reaction (a: reductive elimination; b: oxidative addition)	53
Figure 4.2 Synthesis of bis-NHC-Pd(II)-Me ₂ complex using MeLi.....	54
Figure 4.3 Synthesis of bis-NHC-Pd(II)-Me ₂ complex using MeMgBr.....	55
Figure 4.4 Stacked ¹ H-NMR spectra recorded during the reaction process at -50 °C in 10 min intervals.....	56
Figure 4.5 Proposed reaction pathway between bis-NHC-Pd(II)-(CH ₃) ₂ complex 4.1 and MeI...57	
Figure 4.6 Stacked ¹³ C-NMR of the reaction between bis-NHC-Pd(II)-Me ₂ and ¹³ CH ₃ I (blue: After 20 minutes reaction at -50 °C, ¹³ C-NMR recorded at -70 °C; green: After 20 minutes reaction at -50 °C, ¹³ C-NMR recorded at -70 °C with carbon-hydrogen coupling; black: After 60 minutes reaction at -50 °C, ¹³ C-NMR recorded at -50 °C)	58
Figure 4.7 ¹ H-NMR for the products after reductive elimination form the Pd(IV) species	59

Figure 4.8 Oxidation of bpy-Pt(II)-Me ₂ complex with methyl iodide.....	60
Figure 4.9 Oxidation of bpy-Pd(II)-Me ₂ complex with methyl iodide.....	61
Figure 4.10 Hammett plot for electronic effects on reductive elimination.....	62
Figure 4.11 Proposed reaction mechanism for the reductive elimination reaction.....	63
Figure 4.12 Stacked ¹³ C-NMR of the reaction between bis-NHC-Pd(II)-Me ₂ and ¹³ CH ₃ I in the presence of DMAP (blue: reaction at -50 °C for 20 min; green: reaction at -30 °C for 20 minutes; gray: reaction at -30 °C for 40 minutes; black: reaction at -30 °C for 60 minutes)	64
Figure 5.1 Wacker process.....	69
Figure 5.2 Oxidation of Pt(II) complexes to Pt(IV) complexes by dioxygen.....	69
Figure 5.3 A two-step mechanism for the oxidation (tmeda)Pd(II)Me ₂ to (tmeda)Pd(IV)Me ₂ (OH)(OCH ₃) by dioxygen.....	70
Figure 5.4 Proposed two pathways for the interaction of dioxygen with Pt(II) complexes	71
Figure 5.5 The oxidation of (IMes) ₂ Pd(0) with dioxygen to form η ² -peroxo (IMes) ₂ Pd(O ₂) complex, and protonation of this complex to form the hydroperoxopalladium(II) complex	71
Figure 5.6 Dioxygen insertion into a Pd-H bond.....	72
Figure 5.7 One of the proposed pathways for the dioxygen insertion into Pd-H bond	72
Figure 5.8 Synthesis of the bis-NHC-Pd(II)-Me ₂ complex 5.14	73
Figure 5.9 Proposed pathway for the reaction between the Pd(II) dimethyl complex 5.14 and dioxygen.....	74
Figure 5.10 Stacked ¹ H-NMR spectrum for the reaction between the palladium(II) dimethyl complex 5.14 with dioxygen in the presence of H ₂ O.	76
Figure 5.11 Expanded methanol region for the reaction between the bis-NHC-Pd(II)-(¹³ CH ₃) ₂ complex and dioxygen in the presence of H ₂ O.....	77
Figure 5.12 Expanded ethane region for the reaction between the bis-NHC-Pd(II)-(¹³ CH ₃) ₂ complex and dioxygen in the presence of H ₂ O.....	77
Figure 5.13 Two proposed pathways for the reaction between the palladium(II) dimethyl complex 5.14 with dioxygen in the presence of H ₂ O.	78
Figure 6.1 O insertion into a Pd ^{II} -C bond with (C ₆ F ₅ I=O) _n	83
Figure 6.2 Double amination of palladacycle 6.4	83
Figure 6.3 Oxidation of Pd ^{II} to Pd ^{IV} with PhICl ₂	84
Figure 6.4 Oxidation of Pd ^{II} to Pd ^{IV} with PhI(O ₂ CPh) ₂	84

Figure 6.5 Stacked ¹ H-NMR spectrum for the reaction between bis-NHC-Pd(II)-Me ₂ complex 5.14 and PhI(OAc) ₂	85
Figure 6.6 Proposed reaction pathway between bis-NHC-Pd(II)-Me ₂ and PhI(OAc) ₂	86
Figure 6.7 Stacked ¹ H-NMR spectrum for the reaction between bis-NHC-Pd(II)-(CH ₃) ₂ and PhI(OTFA) ₂ . (blue: bis-NHC-Pd(II)-(CH ₃) ₂ at -40 °C; green: adding 1 equivalent of PhI(OTFA) ₂ at -40 oC for 5 minutes; black: after adding 0.50 equivalent of PhI(OTFA) ₂ at room temperature).....	87
Figure 6.8 Stacked ¹ H-NMR spectrum for the reaction between bis-NHC-Pd(II)-(¹³ CH ₃) ₂ complex and PhI(OTFA) ₂ . (blue: bis-NHC-Pd(II)-(¹³ CH ₃) ₂ at -40 °C; green: adding 1 equivalent of PhI(OTFA) ₂ at -40 °C for 5 minutes; black: after adding 0.20 equivalent of PhI(OTFA) ₂ at room temperature).....	88
Figure 6.9 Stacked ¹³ C-NMR spectrum for the reaction between bis-NHC-Pd(II)-(¹³ CH ₃) ₂ complex and PhI(OTFA) ₂ . (blue: bis-NHC-Pd(II)-(¹³ CH ₃) ₂ at -40 °C; black: adding 1 equivalent of PhI(OTFA) ₂ at -40 °C for 5 minutes).....	89
Figure 6.10 Proposed pathway for the C-C bond formation process.....	90
Figure 6.11 Proposed C-O bond formation pathway via external attack.....	90
Figure 6.12 Proposed C-O bond formation pathway via reductive elimination from Pd(IV) species	91
Figure 6.13 Stacked ¹ H-NMR spectrum for the reaction between bis-NHC-Pd(II)-(¹³ CH ₃) ₂ complex and diisopropylethylammonium trifluoroacetate salt, and the further reaction with PhI(OTFA) ₂ . (blue: bis-NHC-Pd(II)-(¹³ CH ₃) ₂ at -40 °C; green: adding 1 equivalent of diisopropylethylammonium trifluoroacetate salt at -40 °C for 5 minutes; black: after adding 1.0 equivalent of PhI(OTFA) ₂ at room temperature).....	92
Figure 6.14 Protonation of bis-NHC-Pd(II)-(CH ₃) ₂ and further oxidative addition triggered C-O reductive elimination.	92
Figure 6.15 Protonation of the bis-NHC-Pd(II)-(CH ₃) ₂ complex with p-chlorophenol and the further oxidation of the bis-NHC-Pd(II)-(CH ₃)-(p-Cl-C ₆ H ₄) with PhI(OTFA) ₂	94
Figure 6.16 Stacked ¹ H-NMR spectrum of the protonation of the bis-NHC-Pd(II)-(CH ₃) ₂ complex with p-chlorophenol and the further oxidation with PhI(OTFA) ₂ . (blue: bis-NHC-Pd(II)-(CH ₃) ₂ at -20 oC; green: After adding one equivalent of p-chlorophenol for 2 minutes at -20 oC; gray: After adding one equivalent of PhI(OTFA) ₂ for 1 minute at room	

temperature; black: After adding one equivalent of $\text{PhI}(\text{OTFA})_2$ for 5 minutes at room temperature).	94
Figure 7.1 Chlorine oxidation of bidentate ligands supported Pd(II) to Pd(IV)	99
Figure 7.2 Chlorine oxidation of terdentate ligand supported Pd(II) to Pd(IV)	99
Figure 7.3 Stacked $^1\text{H-NMR}$ spectrum (expended area to show the methyl chloride and ethane of the reaction between the bis-NHC-Pd(II)- $(\text{CH}_3)_2$ complex 5.14 and chlorine gas at $-40\text{ }^\circ\text{C}$. (blue: bis-NHC-Pd(II)- $(\text{CH}_3)_2$ at $-40\text{ }^\circ\text{C}$; the green and black spectrum were recorded after adding chlorine gas with 10 minutes intervals; the pink spectrum was recorded after adding chlorine gas for 50 minutes)	101
Figure 7.4 Stacked $^1\text{H-NMR}$ spectrum of the reaction between the bis-NHC-Pd(II)- $(\text{CH}_3)_2$ complex and chlorine gas at $25\text{ }^\circ\text{C}$. (blue: bis-NHC-Pd(II)- $(\text{CH}_3)_2$ at $25\text{ }^\circ\text{C}$; green: right after the addition of chlorine; the other two spectrum were recorded after adding chlorine gas with 5 minutes intervals)	102
Figure 7.5 ESI $^+$ Mass spectroscopy of the bis-NHC-Pd(IV)- Cl_4	103
Figure 7.6 Proposed pathway for the reaction between the bis-NHC-Pd(II)- $(\text{CH}_3)_2$ complex and chlorine gas.	104
Figure 7.7 The bis-NHC-Pd(IV)- Cl_4 complex was reduced back to the bis-NHC-Pd(II)- Cl_2 complex in the absence of chlorine	105
Figure 7.8 The bis-NHC-Pd(II)- Cl_2 complex was oxidized back to the bis-NHC-Pd(IV)- Cl_4 complex in the presence of chlorine.	106
Figure 7.9 Reversible reaction between bis-NHC-ligand supported Pd(II) complex and Pd(IV) complex	106
Figure 7.10 Formation of single crystals of a bis-NHC-Pd(IV)- Cl_4 complex	107
Figure 7.11 X-ray structure of the bis-NHC-Pd(IV)- Cl_4 complex (a: Thermal ellipsoid plot drawn at 50% probability level; b: the boat conformation of the six-membered ring)	107
Figure 9.1 Synthesis of dopamine-anchored tetraethylene glycole ligand for the stabilization of Fe/ Fe_3O_4 -nanoparticles (t-Bu: tertiary butylate, Bn: benzyl, EDC: 1-Ethyl-3-[3-dimethylaminopropyl]carbodiimide, DMAP: 4-Dimethyl-aminopyridine, DMF: Dimethylformamide). ^{41,42}	117
Figure 9.2 Synthesis of “glycine-tipped” dopamine-anchored tetraethylene glycol ligands for the stabilization of Fe/ Fe_3O_4 -nanoparticles (Bn: benzyl, EDC: 1-Ethyl-3-[3-	

dimethylaminopropyl]carbodiimide, DMAP: 4-Dimethyl-aminopyridine, Fmoc: Fluorenylmethyloxycarbonyl-). ^{43,44}	118
Figure 9.3 Synthesis of dopamine-anchored stealth nanoparticles using two ligands: dopamine-anchored tetraethylene glycol (I) and “glycine-tipped” dopamine-anchored tetraethylene glycol (II). A molar ratio of 95 mol percent (I) and 5 mol percent (II) was used for the organic stealth layers of all Fe/Fe ₃ O ₄ core/shell nanoparticles synthesized here. Mesotetrakis-4-(carboxylphenyl)porphyrin was attached by using an EDC/NHS standard protocol in THF (EDC: 1-Ethyl-3-[3-dimethylaminopropyl]carbodiimide, NHS: N-Hydroxysuccinimide). ^{45,46}	119
Figure 9.4 UV/Vis-spectra of Fe/Fe ₃ O ₄ core/shell nanoparticles (#4, see Table 1) containing 0, 1.2 and 5 TCPP units per nanoparticle (statistical average) in 0.05M aqueous phosphate buffer (pH=7.2).....	121
Figure 9.5 Fluorescence emission of Fe/Fe ₃ O ₄ core/shell nanoparticles (#4, see Table 1) 1.2 and 5 TCPP units per nanoparticle (statistical average) in 0.05M aqueous phosphate buffer (pH=7.2); excitation wavelength: 400 nm.....	122
Figure 9.6 T ¹ -relaxation times of H ₂ O/D ₂ O (9/1) at 9.4T in dependence on the concentration of Fe/Fe ₃ O ₄ -NPs (#4, see Table 1).....	124
Figure 9.7 T ² -relaxation times of H ₂ O/D ₂ O (9/1) at 9.4T in dependence on the concentration of NPs (Fe/Fe ₃ O ₄ : #4, Fe _x O _y : #5, see Table 1).....	124
Figure 9.8 <i>In vitro</i> cell viability of B16-F10’s cultured in medium containing increasing concentration of MNPs, as measured by iron concentration. *Statistically significant (p-value less than 0.05).....	126
Figure 9.9 Temperature change at MNP injection site and in body core during AMF exposure, measure with a fiber optic temperature probe.....	127
Figure 9.10 Effect on tumor burden of intratumoral injection of MNPs followed by alternating magnetic field (AFM) treatments. Graph depicting average tumor volumes over time of B16-F10 tumor bearing mice which were later injected with either saline or MNP intratumorally and with or without AMF treatments. *Statistically significant (p-value less than 0.1).....	128
Figure 9.11 Effect of intravenous injection of MNPs and AMF on tumor weight. *Statistically significant (p-value less than 0.1) between control and IV MNPs+AMF groups.....	129
Figure 9.12 Tumor volume comparison of IV MNP+AMF experiment on day 14 and 18.....	130

Figure 9.13 Prussian blue staining of tumor section (picture A), lung section (picture B) and liver section (picture C) after in vivo experiment.....	130
Figure A.1 $^1\text{H-NMR}$ of 2.1(in $\text{DMSO-}d_6$).....	145
Figure A.2 $^1\text{H-NMR}$ of 2.2 (in $\text{DMSO-}d_6$).....	146
Figure A.3 $^1\text{H-NMR}$ of 2.3a (in $\text{DMSO-}d_6$).....	147
Figure A.4 $^1\text{H-NMR}$ of 2.3b (in $\text{DMSO-}d_6$).....	148
Figure A.5 (a) Stacked $^1\text{H-NMR}$ of 2.2 mediated toluene H-D exchange in CF_3COOD ; (b) Expanded aromatic area.....	149
Figure A.6 (a) Stacked $^1\text{H-NMR}$ of control toluene H-D exchange in CF_3COOD ; (b) Expanded aromatic area.....	150
Figure A.7 Stacked $^1\text{H-NMR}$ of 2.3a mediated <i>para</i> -xylene H-D exchange in CF_3COOD	151
Figure A.8 Stacked $^1\text{H-NMR}$ of control <i>para</i> -xylene H-D exchange in CF_3COOD	152
Figure A.9 Stacked $^1\text{H-NMR}$ of 2.2 mediated toluene C-H activation in CF_3COOD in the presence of oxane. (a) 2.2 and oxane in a mixture of CF_3COOD and trifluoroacetic anhydride; (b) Toluene was converted to p-toluenesulfonic acid.....	153
Figure A.10 (a) $^1\text{H-NMR}$ and (b) $^{13}\text{C-NMR}$ of 3.17 (in CDCl_3).....	154
Figure A.11 (a) $^1\text{H-NMR}$ and (b) $^{13}\text{C-NMR}$ of 3.18 (in CDCl_3).....	155
Figure A.12 $^1\text{H-NMR}$ 3.19 (in CDCl_3).....	156
Figure A.13 $^1\text{H-NMR}$ 3.20 (in $\text{DMSO-}d_6$).....	157
Figure A.14 $^1\text{H-NMR}$ 3.24 (in $\text{DMSO-}d_6$).....	158
Figure A.15 $^1\text{H-NMR}$ 3.25 (in $\text{DMSO-}d_6$).....	159
Figure A.16 $^1\text{H-NMR}$ 4.1 (in $\text{THF-}d_8$).....	160
Figure A.17a Stacked $^1\text{H-NMR}$ spectrum of the reaction between palladium complex 4.1 and MeI at $-50\text{ }^\circ\text{C}$. (NMR spectrum was recorded every 10 minutes in $\text{THF-}d_8$).....	161
Figure A.17b Stacked $^1\text{H-NMR}$ spectrum of the reaction between palladium complex 4.1 and MeI at $-50\text{ }^\circ\text{C}$; (NMR spectrum was recorded every 10 minutes in $\text{THF-}d_8$, expended imidazole and methylene bridge area).....	162
Figure A.17c Stacked $^1\text{H-NMR}$ spectrum of the reaction between palladium complex 4.1 and MeI at $-50\text{ }^\circ\text{C}$; (NMR spectrum was recorded every 10 minutes in $\text{THF-}d_8$, expended N-methyl area).....	163

Figure A.17d Stacked $^1\text{H-NMR}$ spectrum of the reaction between palladium complex 4.1 and MeI at $-50\text{ }^\circ\text{C}$; (NMR spectrum was recorded every 10 minutes in THF- d_8 , expended palladium coordinated methyl groups area).....	164
Figure A.18 $^1\text{H-NMR}$ of 4.4 (Spectrum recorded after the completion of the reaction between palladium complex 4.1 and MeI).....	165
Figure A.19 Stacked $^{13}\text{C-NMR}$ spectrum of the reaction between palladium complex 4.1 and $^{13}\text{CH}_3\text{I}$ (blue: After 20 minutes reaction at $-50\text{ }^\circ\text{C}$, $^{13}\text{C-NMR}$ recorded at $-70\text{ }^\circ\text{C}$; green: After 20 minutes reaction at $-50\text{ }^\circ\text{C}$, $^{13}\text{C-NMR}$ recorded at $-70\text{ }^\circ\text{C}$ with carbon-hydrogen coupling; black: After 60 minutes reaction at $-50\text{ }^\circ\text{C}$, $^{13}\text{C-NMR}$ recorded at $-50\text{ }^\circ\text{C}$).....	166
Figure A.20 $^1\text{H-NMR}$ for the products after the completion of the reaction between palladium complex 4.1 and $^{13}\text{CH}_3\text{I}$	167
Figure A.21 Stacked $^{13}\text{C-NMR}$ of the reaction between bis-NHC-Pd(II)-Me $_2$ and $^{13}\text{CH}_3\text{I}$ in the presence of DMAP (blue: reaction at $-50\text{ }^\circ\text{C}$ for 20 min; green: reaction at $-30\text{ }^\circ\text{C}$ for 20 minutes; gray: reaction at $-30\text{ }^\circ\text{C}$ for 40 minutes; black: reaction at $-30\text{ }^\circ\text{C}$ for 60 minutes).....	168
Figure A.22 $^1\text{H-NMR}$ of 5.11.....	169
Figure A.23 $^1\text{H-NMR}$ of 5.12.....	170
Figure A.24 (a) $^1\text{H-NMR}$ and (b) $^{13}\text{C-NMR}$ of 5.13.....	171
Figure A.25 $^1\text{H-NMR}$ 5.14.....	172
Figure A.26 $^1\text{H-NMR}$ of ^{13}C -labeled bis-NHC-Pd(II)-($^{13}\text{CH}_3$) $_2$ 5.14'.....	173
Figure A.27 $^{13}\text{C-NMR}$ of ^{13}C -labeled bis-NHC-Pd(II)-($^{13}\text{CH}_3$) $_2$ 5.14' (32 scans).....	174
Figure A.28 Stacked $^1\text{H-NMR}$ spectrum of the reaction between bis-NHC-Pd-Me $_2$ (complex 4.1) and dioxygen. (blue: complex 4.1 in THF- d_8 ; black: after addition of oxygen for 2 hours)...	175
Figure A.29 The reaction between PhI(OTFA) $_2$ and bis-NHC-Pd(II)-(CH_3) $_2$ 5.14 to generate bis-NHC-Pd(II)-(CH_3)-(OTFA) and CH_3OOCF_3 as well as bis-NHC-Pd(II)-(OTFA) $_2$ and ethane..	176
Figure A.30 (a) $^1\text{H-NMR}$ of 6.17 (b) Expended aromatic area.....	177
Figure A.31 $^1\text{H-NMR}$ of 7.9 (generated by the reaction between bis-NHC-Pd(II)-Me $_2$ 5.14 and chlorine).....	178
Figure A.32 $^1\text{H-NMR}$ of porphyrin TCPP.....	179
Figure A.33 $^1\text{H-NMR}$ of 9.1.....	180
Figure A.34 $^1\text{H-NMR}$ of 9.2.....	180

Figure A.35	$^1\text{H-NMR}$ of 9.3.....	181
Figure A.36	$^1\text{H-NMR}$ of 9.4.....	181
Figure A.37	$^1\text{H-NMR}$ of 9.5.....	182
Figure A.38	$^1\text{H-NMR}$ of 9.6.....	183
Figure A.39	$^1\text{H-NMR}$ of ligand I.....	184
Figure A.40	(a) $^1\text{H-NMR}$ and (b) $^{13}\text{C-NMR}$ of ligand II.....	185
Figure B.1	(a) ESI^+ Mass spectroscopy of the bis-NHC-Pd(IV)-Cl ₄ 7.9 with stepwise fragmentation. (b) Centroided Mass spectrum for [M-Cl] ion.....	187
Figure B.2	ESI^+ Mass spectroscopy of 9.4.....	188
Figure B.3	ESI^+ Mass spectroscopy of 9.5.....	189
Figure B.4	ESI^+ Mass spectroscopy of ligand I.....	190
Figure B.5	ESI^+ Mass spectroscopy of porphyrin TCPP.....	191

List of Tables

Table 1.1 Representative C-H bond dissociation energies	2
Table 1.2 catalytic conversion of methane into methanol	17
Table 1.3 B3LYP/6-311+G(d,p) calculated free energies (kcal/mol) for the replacement of halogen ligands by trifluoroacetic acid	18
Table 3.1 Selected bond lengths and bond angles of the tripod-bis-NHC-Pd(II)-I ₂ complex 25 .	47
Table 4.1 Second-order rate constants for oxidative addition of MeI to [MMe ₂ (bpy)] in acetone	61
Table 7.1 Selected bond length and bond angle of the bis-NHC-Pd(IV)-Cl ₄ complex.....	108
Table 9.1 Experimental data including SAR values of nanoparticles synthesized by NanoScale/KSU: H: 5.0 kA m ⁻¹ , frequency 366 kHz (sine wave pattern).....	120
Table C.1 Crystal data and structure refinement for 3.25.....	192
Table C.2 Crystal data and structure refinement for 7.9'.....	193

Acknowledgements

First of all, I would like to thank my major professor, Dr. Stefan Bossmann for his guidance, instruction and support during my Ph. D study. His enthusiastic commitment and optimistic attitude to research will have a great influence on my future career. His kindness and encouragement will be always remembered.

I would like to thank Dr. Stefan Kraft, under whose guidance and direction the palladium chemistry was carried out.

I would like to thank all my Ph. D committee members Dr. Christer Aakeröy, Dr. Duy Hua, Dr. Keith Hohn, Dr. Christopher Levy, Dr. Deryl Troyer, for their valuable time and input. I appreciate Dr. Kirby Chapman for being the outside chairperson for the examining committee of my final defense.

I appreciate the collaboration with Dr. Deryl Troyer, Dr. Victor Chikan, and NanoScale Corporation on the nanoparticle-cancer-research project. Special thanks to Mr. Sivasai Balivada and Dr. Raja Shekar Rachakatla who carried out the mice experiment; thanks to Mr. Raj Kumar Dani who helped in the hyperthermia experiment and Dr. Xiaoxuan Leaym who prepared the nanoparticles.

I'm grateful to the faculty and staff members in the chemistry department for their help in the past five and half years. Special thanks to Ms. Katrin Bossmann for her help during my thesis preparation; Dr. John Desper for single crystal structure characterization; Mr. Jim Hodgson for glassware repairs; Mr. Ron Jackson for fixing my vacuum pumps. Thanks to previous NMR manager Dr. Tanya Young, Mr. Alvaro Herrera and current NMR manager Dr. Leila Maurmann for their help with NMR characterization. Thanks to Ms. Earline Dikeman for her help and encouragement. Thanks to Dr. Jun Li and his family for their help and friendship!

Thanks to my group members, past and present, it is because all of you that research work in the lab become more pleasant!

Thanks to my parents for their understanding, support and unfailing love!

Thanks to my wife Tingting for her love!

Thanks to my son Enoch for bringing me joy everyday!

Chapter 1 Introduction

1.1 What is C-H bond activation?

C-H bond activation is often referred to as one of the “Holy Grails” in chemistry.¹ It is my understanding of the concept of the “Holy Grail” in Western culture has been used for centuries to describe a highly prestigious, but rather elusive goal. In the chemical context of this work carbon-hydrogen bond activation can be defined as cleavage of the σ -C-H bond and further reaction without the requirement of overcoming large activation energies. This concept is described in an article by A. E. Shilov: What is the activation of an ordinary σ -bond? It is reasonable to propose that to activate an σ -bond, such as a C-H bond is to increase the reactivity of this bond towards a reagent. As a consequence, the bond is capable of splitting to produce two “particles” in place of one initial species. In many cases, this rupture of a saturated bond is actually a consequence of its activation, and it would be more correct to refer specifically to the “splitting of the C-H bond in these situations.”²

The main result of “activation” of a C-H bond is the replacement of a strong bond (thermodynamically stable) with a weaker (thermodynamically less stable) bond. These weaker bonds permit the further functionalization of molecules much more easily than C-H bonds.

What is the rationale behind the research on C-H-bond activation? Aliphatic hydrocarbons are ubiquitous in nature, but their lack of chemical reactivity in defined reactions (other than combustion, cracking and the generation of synthesis gas)³ has prevented their direct conversion into valuable chemical products. Therefore, strong motivation for my research has been derived from the prospect that C-H activation could enable the conversion of cheap and abundant alkanes into valuable functionalized organic compounds.

What are the principle challenges of C-H bond activation? As already pointed out, the C-H bond energies are usually high and the bond energies of the new bonds that are formed in place of the C-H bond are always lower as is demonstrated in Table 1.1.⁴ This causes the severe problem that it is difficult to control selectivity of the C-H bond activation reaction: the functionalized products are usually more reactive than the starting materials, so the initially formed reaction products will rather act as reaction intermediate and will be further reacted

instead of the starting materials, because that is thermodynamically much easier! Only especially designed catalytic systems do not allow further reactions after the first step has taken place. The strategy to design such a catalyst is to lower the activation barrier for the first steps, the breaking of the C-H bond and the formation of the new C-X-bond, but to significantly increase the activation barrier for all further reactions. To date, only a few catalytic systems can provide these very special reaction conditions.

Table 1.1 Representative C-H bond dissociation energies⁴

Bond type	Bond dissociation energy (kcal/mol)
H-CH ₃	105
H-CH ₂ R	98-101
H-CHR ₂	95-99
H-R ₃	93-95
H-CH=CH ₂	104-111
H-CH ₂ CH=CH ₂	86
H-C≡CH	132-133
H-CH ₂ -C≡CH	89
H-C ₆ H ₅	111-113
H-CH ₂ C ₆ H ₅	88-90
H-CH ₂ OH	94-96
H-C(=O)R	86-88
H-CH ₂ C(=O)R	92-98
H-CH ₂ CO ₂ H	97-99

1.2 Transition Metal Mediated Aromatic C-H Bond Activation

In the middle of 1960s, it was demonstrated that transition metal complexes are capable of inserting into aromatic C-H bonds through the participation of the π orbitals. In 1965, Chatt and Davidson reported that the di-(1,2-bisdimethylphosphinoethane)ruthenium(0) complex $[\text{Ru}(0)(\text{dmpe})_2]$ **1.2** was generated by reduction of trans-dichlorodi-(1,2-bisdimethylphosphinoethane)ruthenium(II) complex $[\text{Ru}(\text{II})(\text{dmpe})_2\text{Cl}_2]$ **1.1**. One C-H bond of naphthalene was activated by the $\text{Ru}(0)(\text{dmpe})_2$ complex **1.2** to form the cis-hydrido-(2-naphthyl)di-(1,2-bisdimethylphosphinoethane)ruthenium(II) complex $[\text{Ru}(\text{II})\text{H}(2\text{-C}_{10}\text{H}_7)(\text{dmpe})_2]$ **1.3** (Figure 1.1).⁵ This is the first reported example of “C-H bond activation” of an aromatic hydrocarbon by a transition metal complex.

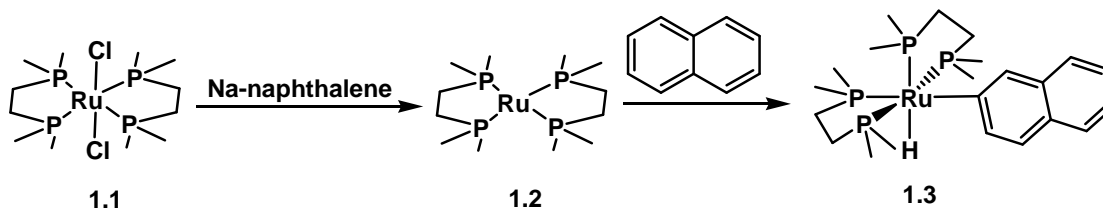


Figure 1.1 $\text{Ru}(0)(\text{dmpe})_2$ complex mediated C-H bond activation of naphthalene.⁵

In 1967, Garnett and Hodges reported the incorporation of deuterium in benzene and benzene derivatives mediated by Na_2PtCl_4 in a $\text{D}_2\text{O}/\text{CD}_3\text{CO}_2\text{D}$ mixture.⁶ It was found that the degree of exchange is not markedly influenced by the electronic character of the substituents, which implies the H-D exchange process is not acid catalyzed. The authors proposed that the benzene coordinated to platinum to form a π -complex intermediate, then the H-D exchange may either go through reversible rearrangement of the π -bonded complex to a six-coordinated hydrido complex or a reversible electrophilic displacement of a proton from the π -bonded complex (Figure 1.2).⁷

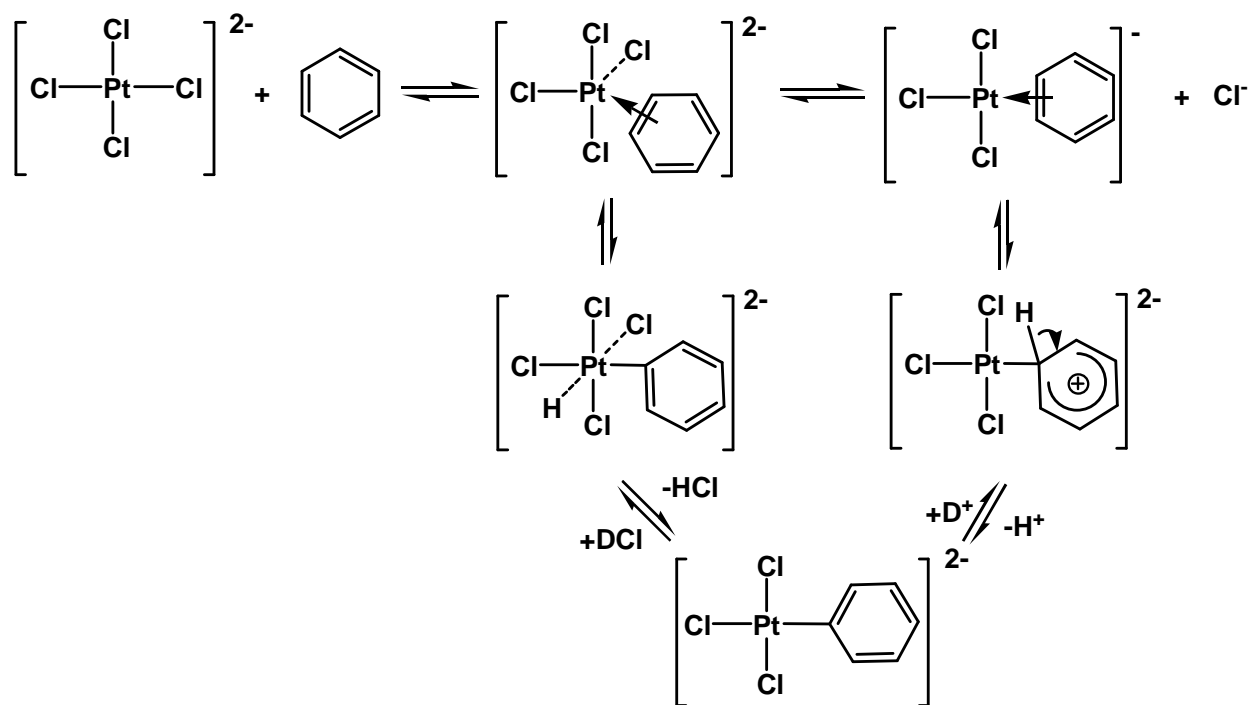


Figure 1.2 Proposed mechanisms for the platinum(II) mediated aromatic H-D exchange.⁷

1.3 Transition Metal Mediated Alkane C-H Bond Activation

Alkanes are the major constituents of natural gas and petroleum. The inertness of alkanes toward other reagents is reflected by their other name, ‘paraffin’, which means not enough affinity. This chemical inertness arises from constituent of atoms of alkanes all being held together by strong and localized C-C and C-H bonds, so that the molecules have no empty orbitals of low energy or filled orbitals of high energy that could participate in chemical reactions.^{2,8}

Despite this inertness of alkanes, it has been demonstrated in the early 1980s that organotransition-metal complexes are capable of inserting into alkane C-H bonds. In 1982, Bergman’s group reported that when dihydrido-trimethylphosphino-pentamethylcyclopentadienyliridium(III) complex $[(\text{Me}_5\text{C}_5)(\text{H})_2(\text{Me}_3\text{P})\text{Ir}(\text{III})]$ **1.4** was irradiated by UV light in alkanes such as cyclohexane and neopentane, oxidative addition of C-H bond of alkanes on the iridium center was observed.⁹ The authors suggested that these reaction proceed by loss of H_2 from complex **1.4** to form the coordinatively unsaturated trimethylphosphino-pentamethylcyclopentadienyliridium(I) species $(\text{Me}_5\text{C}_5)(\text{Me}_3\text{P})\text{Ir}(\text{I})$ **1.5** (Figure 1.3). When the

reaction was carried out in a 50:50 mixture of cyclohexane and neopentane, the products of hydridocyclohexanotrimethylphosphino-pentamethylcyclopentadienyliridium(III) complex **1.6** and hydridoneopentanotrimethylphosphino-pentamethylcyclopentadienyliridium(III) complex **1.7** were formed in a 0.88 ratio, indicating insertion favors a primary over secondary C-H bond.

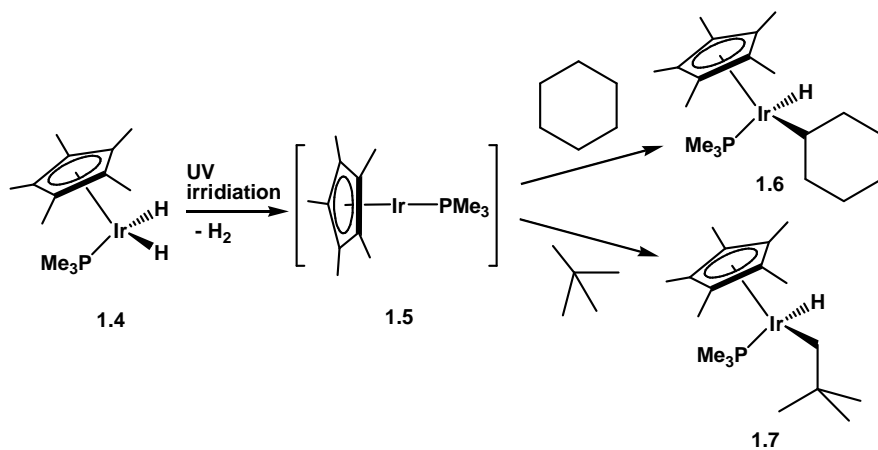


Figure 1.3 Iridium complex **1.4** mediated C-H bond activation of alkanes.⁹

Consistent results were reported by Graham that irradiation of dicarbonylpentamethylcyclopentadienyliridium(I) complex [(Me₅C₅)(CO)₂Ir(I)] **1.8** by UV light in cyclohexane and neopentane led to the oxidative addition of C-H bond of the alkanes to the iridium center (Figure 1.4).¹⁰

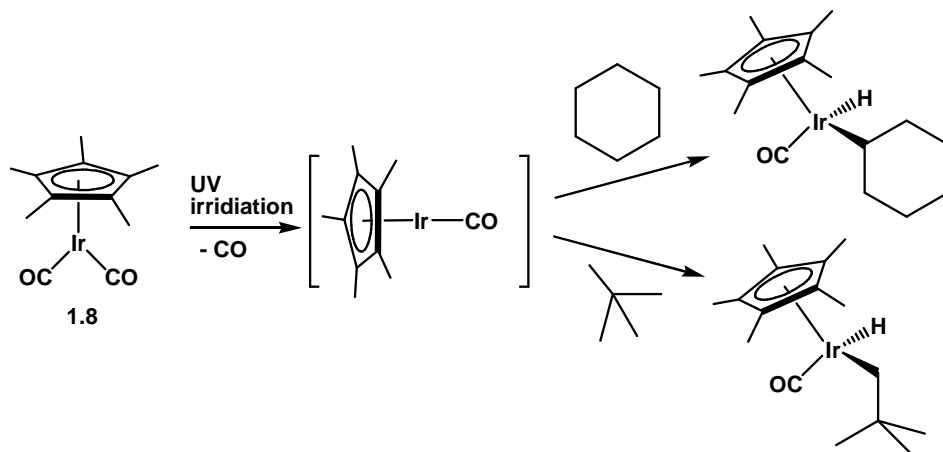


Figure 1.4 Iridium complex **1.8** mediated C-H bond activation of alkanes.¹⁰

In 1983, Jones reported that when dihydrido-trimethylphosphino-pentamethylcyclopentadienylrhodium(III) complex $[(\text{Me}_5\text{C}_5)(\text{H})_2(\text{Me}_3\text{P})\text{Rh}(\text{III})]$ **1.9** was irradiated by UV light in liquid propane at $-55\text{ }^\circ\text{C}$, the oxidative addition of one terminal propane C-H bond to rhodium complex **1.9** occurred to form the hydrido-(1-propano)-trimethylphosphino-pentamethylcyclopentadienylrhodium(III) complex $[(\text{Me}_5\text{C}_5)(\text{H})(1\text{-C}_3\text{H}_7)(\text{Me}_3\text{P})\text{Rh}(\text{III})]$ **1.10** (Figure 1.5).¹¹ All these results showed that the inertness of alkanes had been overestimated to some extent. They can react with certain organotransition-metal complexes facily under relatively mild conditions.

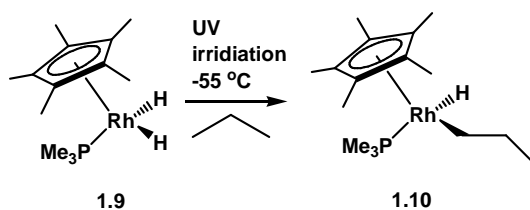


Figure 1.5 Rhodium complex **1.9** mediated C-H bond activation of propane.¹¹

1.4 Transition Metal Catalyzed Methane Oxidation

Methane and ethane constitute over 95% of the natural gas; however, the utilization of methane is limited by the fact that most of the world's established natural gas resource locations are remote, in sites where there is little or no local demand. Exploitation of such a resource is impeded by the high cost of both gas transportation and the current methods for converting hydrocarbon gas into more readily transportable liquid. The available conversion methods are highly energy consuming, involving production of synthesis gas (carbon monoxide and hydrogen) from methane and water at high temperature and under moderate pressure, followed by conversion to desired products (Figure 1.6).¹²

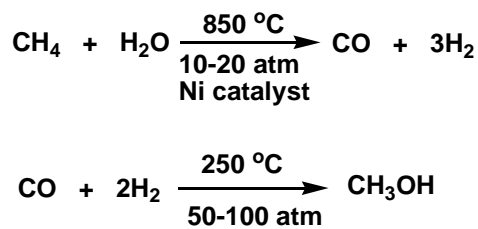


Figure 1.6 Syn-gas method to convert methane to methanol.¹²

Several transition metal complexes that catalyze direct oxidation of methane to methanol derivatives are discussed in the following section.

1.4.1 The Shilov System

In 1969, Shilov and co-workers reported that 2.5 mol% deuterium incorporation was found for methane by heating in a solution of 30% CH₃COOD and 30% HCl in D₂O at 100 °C for 6 hours in the presence of K₂PtCl₄.¹³ Without catalyst, this reaction is known to be possible only at a temperature about 1000 °C. More than 26 mol% deuterium incorporation into ethane was achieved after 9 hours at 150 °C in the same system. This was the first reported homogenous system to activate σ-C-H bonds in an alkane.

In 1972, Shilov and coworkers observed the formation of oxidized alkane products by addition of H₂[PtCl₆] into solutions of K₂[PtCl₄] in D₂O/CH₃COOD (Figure 1.7).¹⁴ It was found that the Pt(II) salt is the catalyst but stoichiometric amounts of K₂[PtCl₆], which acts as the oxidant are required for catalytic reaction to occur.

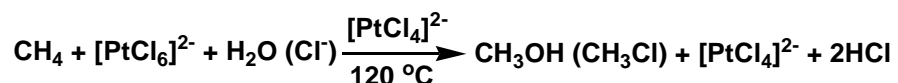


Figure 1.7 Pt(II) mediated methane oxidation.¹⁴

In 1983, the Shilov group proposed a three-step mechanism for the alkane oxidation cycle (Figure 1.8).¹⁵ In the first step the alkane C-H bond is activated by Pt(II) to generate an alkylplatinum(II) intermediate. In the second step the alkylplatinum(II) intermediate is oxidized by [PtCl₆]²⁻ to form an alkylplatinum(IV) species. In the third step the functionalized product is liberated and the Pt center is reduced back to Pt(II) either by reductive elimination from the Pt(IV) species or nucleophilic attack at the Pt-C bond by an external nucleophile (H₂O or Cl⁻).

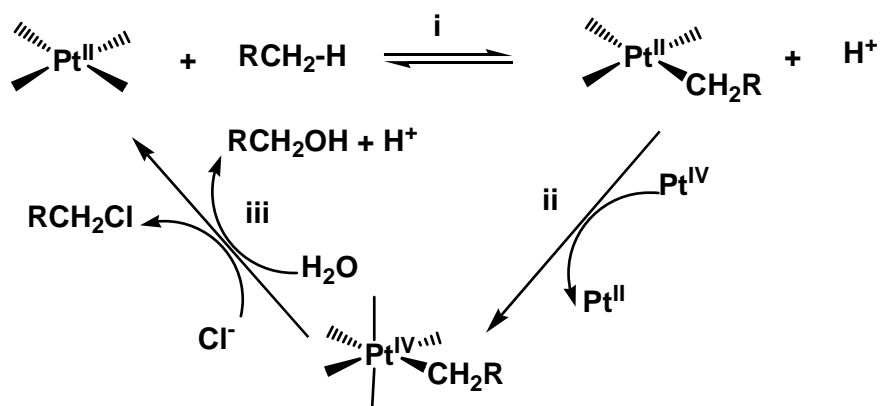


Figure 1.8 Proposed mechanism for the methane oxidation in Shilov System.¹⁵

Despite the impracticality of using an expensive platinum compound as a stoichiometric oxidant, the Shilov system remains to date one of few catalytic systems that accomplish selective alkane functionalization under mild conditions. This catalytic system has received considerable attention from several research groups and convincing experimental results have been obtained to identify the features of each individual reaction step.¹⁶

In the product forming step, two different mechanisms have been postulated: a nucleophilic (S_N2) pathway and a concerted reductive elimination pathway (Figure 1.9).¹⁶

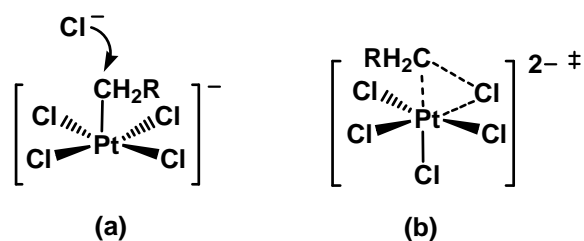


Figure 1.9 Proposed S_N2 pathway (a) and concerted pathway (b) in the product forming step.¹⁶

The Bercaw group provided the most definitive supporting evidence for the S_N2 type reaction in the products forming step. *erythro*- and *threo*- $[\text{PtCl}_5\text{CHDCHDOH}]^{2-}$ were produced by oxidation of isotope-labeled *Zeise's salt* $[\text{PtCl}_3(\text{trans- and cis-CHD=CHD})]^-$ with $[\text{PtCl}_6]^{2-}$ in water. Treatment of the erythro isomer **1.11** with chloride gave primarily *threo*- ClCHDCHDOH **1.12** ($^3J_{\text{HH}} = 6 \text{ Hz}$), upon conversion to 2,3-dideuterioethylene oxide **1.13**, $85 \pm 5\%$ of the *cis*-

isomer was obtained (Figure 1.10). Opposite results were produced when starting with the threo-isomer. This sequence clearly showed the inversion of stereochemistry in the product forming step, which is consistent with a S_N2 mechanism.^{17,18}

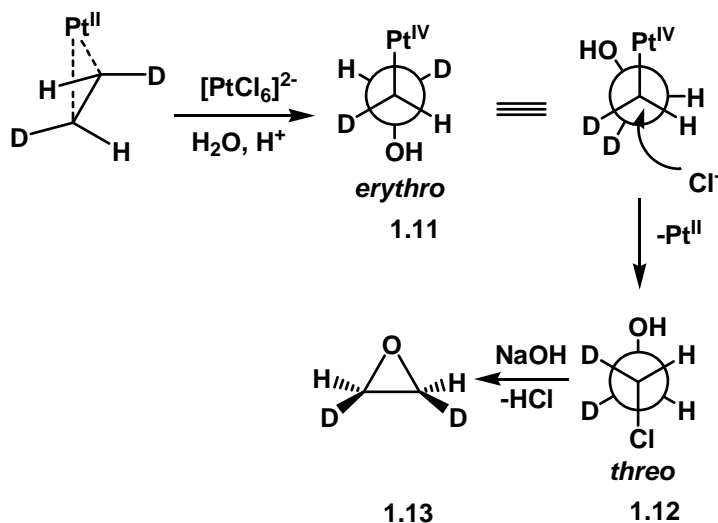


Figure 1.10 Evidence for the S_N2 pathway in the product forming step for the Shilov System.¹⁷

Another important aspect of the mechanism is the oxidation of the alkylplatinum(II) intermediate to alkylplatinum(IV). Two possible mechanisms have been considered: inner-sphere two-electron transfer from $RPt(II)$ to $Pt(IV)$ or alkyl transfer from $RPt(II)$ to $Pt(IV)$ (Figure 1.11). If the former mechanism prevails, then it is possible to circumvent the usage of expensive platinum(IV) as oxidant, whereas the latter demands the presence of platinum(IV).

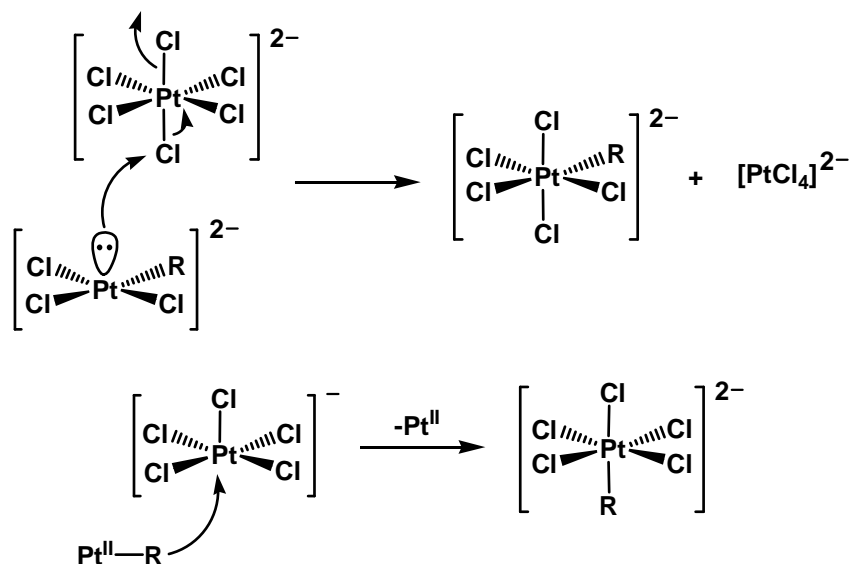


Figure 1.11 Two possible pathways for oxidation of the alkylpalladium(II) intermediate by $[\text{PtCl}_6]^{2-}$.¹⁹

Oxidation of *Zeise's salt* by $[\text{PtCl}_6]^{2-}$ was used as a mechanistic model experiment to distinguish between these two possible oxidation pathways.¹⁹ It was found that in the course of oxidation of *Zeise's salt*, an alkylplatinum(II) intermediate is formed. When isotopically labeled $\text{Na}_2[^{195}\text{PtCl}_6]$ was used as oxidant, the $^1\text{H-NMR}$ spectrum of the product showed the expected intensity of ^{195}Pt satellites for the $\text{Pt-CH}_2\text{CH}_2\text{OH}$ peak (33% of the total peak area, equal to the natural abundance of the ^{195}Pt) (Figure 1.12). This experiment clearly indicated that the oxidation of R-Pt(II) intermediate by $[\text{PtCl}_6]^{2-}$ proceeds by electron transfer, not alkyl transfer.

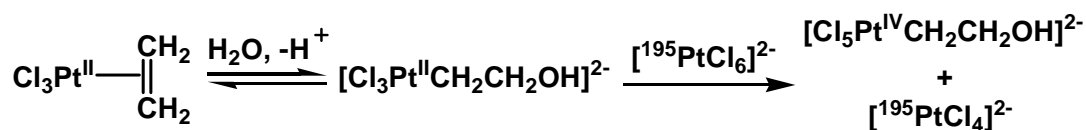


Figure 1.12 Oxidation of *Zeise's salt* by $[\text{PtCl}_6]^{2-}$.¹⁸

Based on these important results, the Bercaw group addressed “*there is accordingly no inherent mechanistic reason why Pt(IV) could not be replaced by another suitable oxidant, as long as it is capable of oxidizing the alkylplatinum(II) intermediate to alkylplatinum(IV) without fully oxidizing $[\text{PtCl}_x(\text{H}_2\text{O})_{4-x}]^{2-x}$ to Pt(IV).*”¹⁸ A lot of efforts have been directed to find a

replacement oxidant that is less expensive than $[\text{PtCl}_6]^{2-}$ or a method to regenerate $[\text{PtCl}_6]^{2-}$. A list of oxidants including SO_3 , Cl_2 , H_2O_2 , O_2 /heteropolyacids and O_2 /Cu(II) were investigated to carry out this transformation, but only little success was obtained.²⁰⁻²⁴ The reaction was also investigated under electrochemical conditions with catalytic amount of Pt(II), only a limited number of turnover was achieved.²⁵

Two different mechanisms have been considered in the C-H bond activation step of the Shilov system. 1) The C-H bond is cleaved by oxidative addition to Pt(II) yielding an alkyl(hydrido)platinum(IV) complex and then deprotonated. 2) The C-H bond is broken by deprotonation of an intermediate Pt(II)-alkane σ -adduct (Figure 1.13).²⁶

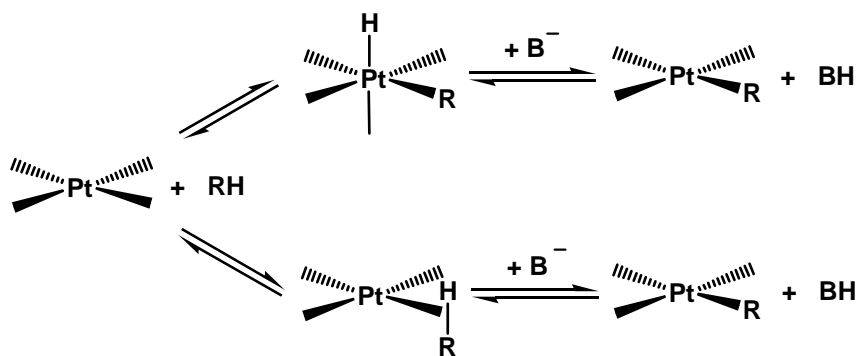


Figure 1.13 Two possible pathways for alkane C-H bond activation by Pt(II).²⁵

Because it is difficult to study the C-H bond activation directly, protonolysis of alkylplatinum complexes which is the microscopic reverse of methane oxidation was studied to gain the mechanistic information.²⁶ Labinger and Bercaw examined the reaction between methylchlorotetramethylethylenediamineplatinum(II) complex (tmeda)PtMeCl **1.14** and HCl, the oxidative addition product hydridomethyldichlorotetramethylethylenediamineplatinum(IV) intermediate [(tmeda)PtMeHCl₂] **1.15** was detected at -78°C, and at -60 °C, the Pt(IV) **1.15** undergoes reductive elimination to give methane and dichlorotetramethylethylenediamineplatinum(II) complex [(tmeda)PtCl₂] **1.16** as products (Figure 1.14).

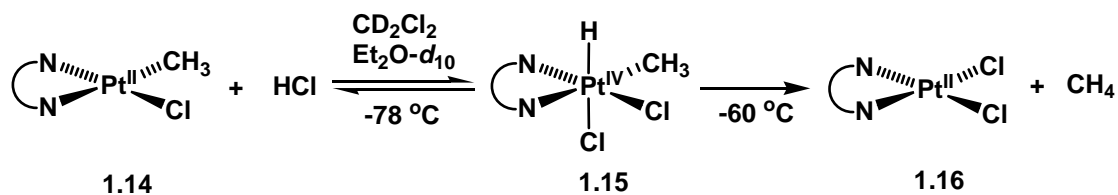


Figure 1.14 Oxidative addition of HCl to (tmeda)Pt(II)(CH₃)Cl complex.²⁶

When CH₃OD was used as solvent, deuterium exchange into the coordinated methyl groups was observed at -40 °C. The multiple deuterium incorporation into methane suggested the reversible formation of Pt(II)-alkane σ adduct (Figure 1.15).

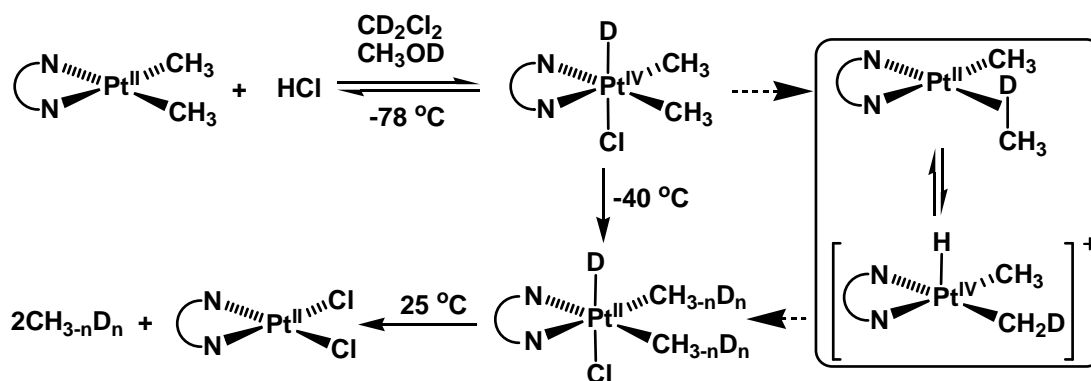


Figure 1.15 Possible pathway for multiple deuterium incorporation into methane.²⁵

These experimental results implicated that both a Pt(II)-alkane σ -adduct and a alkylhydridoplatinum(IV) species can be the intermediates of the C-H bond activation reaction.

Different ligands supported Pt complexes were used as catalysts to study the elementary steps that constitute the oxidation of alkanes to alcohols. Four individual steps have been established in one or more cases during platinum-catalyzed C-H activation reactions: 1) electrophilic C-H bond activation of alkane at Pt(II),²⁷ 2) oxidation of alkyl Pt(II) to alkyl Pt(IV),²⁷ 3) nucleophilic cleavage R-Pt bond to form ROH and 4) ligand exchange to regenerate the original catalyst (Figure 1.16).^{16b} The current challenge is to find a complex which can accomplish all four steps efficiently and in concert.

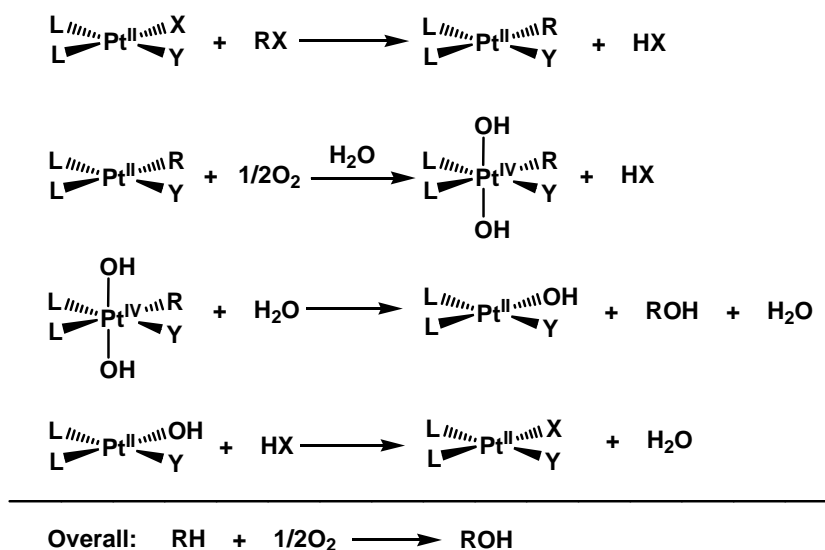
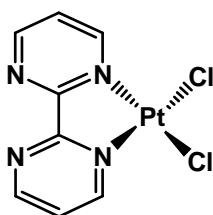
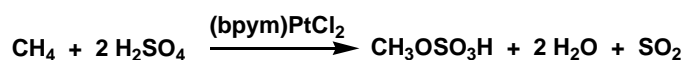


Figure 1.16 Four individual steps of the platinum catalyzed C-H bond activation.^{15b}

1.4.2 The Catalytic System

In 1998, R. A. Periana and coworkers in *Catalytica Advanced Technology Inc.* reported that in fuming sulfuric acid, methane could be selectively converted to methyl bisulfate catalyzed by dichloro(η^2 -{2,2'-bipyrimidine})platinum(II) complex [(bpym)PtCl₂] at 220 °C (Figure 1.17). Impressively, a 72% one-pass yield at 81% selectivity, based on methane, was achieved.²⁰



Structure of (bpym)PtCl₂

Figure 1.17 (bpym)PtCl₂ catalyzed methane oxidation in concentrated sulfuric acid.^{19a}

A remarkable feature of the methane oxidation system is that the system is catalytic in Pt complex and utilizes SO₃ as oxidant. The functionalized product methyl bisulfate can be

hydrolyzed to methanol, and in principle the SO₂ formed during the reaction can be re-oxidized by O₂ to SO₃ (Figure 1.18). All these characteristics make this system potentially practical.

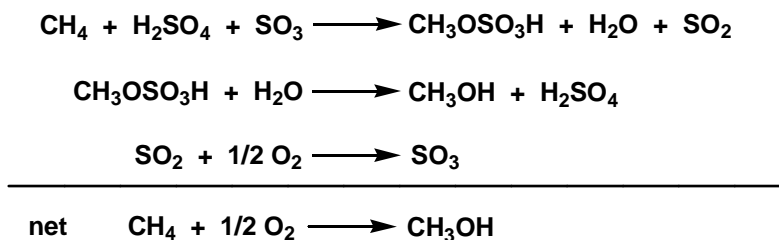


Figure 1.18 Process scheme for the net oxidation of methane to methanol.^{19a}

The bipyrimidine ligand possesses high affinity for Pt(II). It is found that loss of the *bpym* ligand from the Pt center is reversible even under strong acidic and oxidizing conditions. Platinum metal can be dissolved in hot 96% H₂SO₄ in the presence of *bpym* ligand to produce a homogenous solution of (*bpym*)Pt(HSO₄)₂. This “self-assembling” function prevents the deposition of insoluble (PtCl₂)_n during the reaction process and increases the catalyst’s lifetime. Under the strong acidic reaction condition, the ligand may become protonated. Protonation will withdraw electron density from the platinum through the σ-bonding framework of the bidiazine ligand thereby enhancing its electrophilicity.

When the reaction was carried out in D₂SO₄ below 150 °C, multiple H/D exchange can be observed with gas-phase methane, suggesting the involvement of σ-methane intermediate, but no H/D exchange into the methyl group of methyl bisulfate is observed when methyl bisulfate is added in the catalytic system. This is because of the strong electron withdrawing effect of the bisulfate group, which inhabits the electrophilic reaction between the platinum complex and the C-H bond of the methyl bisulfate. The deactivating effect of the bisulfate group is of crucial importance in that it not only leads to desired selectivity, but also prevents undesired over-oxidation to CO₂.

It is believed that under the strong acidic conditions, the catalyst (*bpym*)PtCl₂ undergoes ligand exchange to form a cationic [(*bpym*)PtCl(Sol)]⁺ species **1.17** (Sol = H₂SO₄). Dissociation

of the solvent ligand will lead to a highly electrophilic, coordinatively unsaturated 14-electron T-shaped $[(\text{bpym})\text{PtCl}]^+$ species which can coordinate with methane to form a Pt(II) σ -methane intermediate **1.18**. A three-step catalytic cycle was proposed for the methane oxidation reaction: in the first step, C-H bond activation of methane occurs from the Pt(II) σ -methane intermediate **1.18** either by oxidative cleavage, with deprotonation from a platinum(IV) methyl hydride, or by electrophilic substitution, with loss of proton from Pt(II) σ -methane intermediate **1.18** to form the $(\text{bpym})\text{Pt}(\text{II})(\text{CH}_3)\text{Cl}$ species **1.19**; in the second step, the $(\text{bpym})\text{Pt}(\text{II})(\text{CH}_3)\text{Cl}$ species **1.19** is oxidized to $(\text{bpym})\text{Pt}(\text{IV})(\text{CH}_3)\text{Cl}(\text{OSO}_3\text{H})_2$ species **1.20** by SO_3 ; in the third step, functionalized product methyl bisulfate is released and the catalyst is regenerated (Figure 1.19).

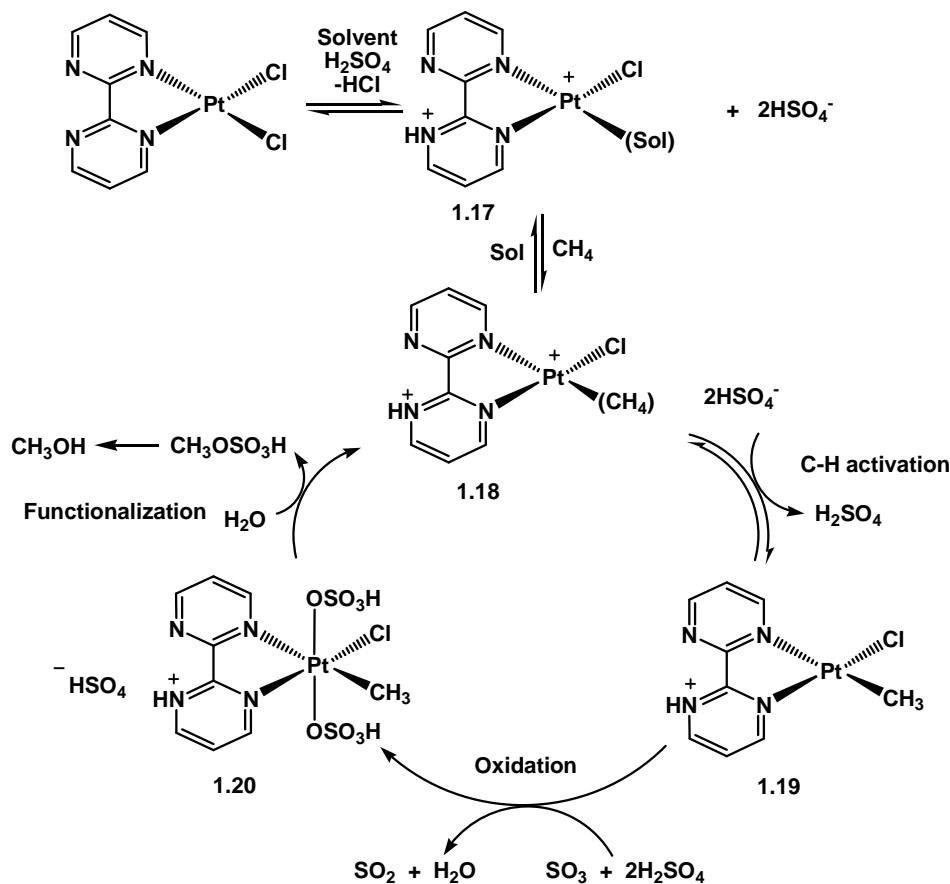


Figure 1.19 Proposed mechanism for the methane oxidation for the Catalytica System.^{20b}

With regard to yields, selectivity and catalyst turnover numbers, the Catalytica system achieved the best results for catalytic methane oxidation and it made the most significant advance in Shilov type chemistry. However, there are some drawbacks in this system. Firstly, this system needs concentrated sulfuric acid as reaction media which is highly corrosive and difficult to handle. Secondly, methyl bisulfate, the product of the methane oxidation, is of little direct use and need to be converted to more useful compound, such as methanol. The hydrolysis of methyl bisulfate will lead to undesired diluted sulfuric acid as side product. Its concentration requires a lot of energy due to the high dilution entropy and the enthalpy of water-binding by sulfuric acid.⁸

1.4.3 The NHC-Pd System by Strassner

In 2002, Strassner and co-workers reported the catalytic conversion of methane to methyl trifluoroacetate by using N-heterocyclic carbene (NHC) palladium(II) complexes as catalysts (Figure 1.20).²⁹ The reactions were carried out in a mixture of trifluoroacetic acid and trifluoroacetic acid anhydride at a methane pressure of 20-30 bar at 80-100 °C, and with potassium peroxodisulfate as an oxidant. Under optimized condition, a TON (turnover number) of 30 relative to NHC-Pd catalyst was reached.

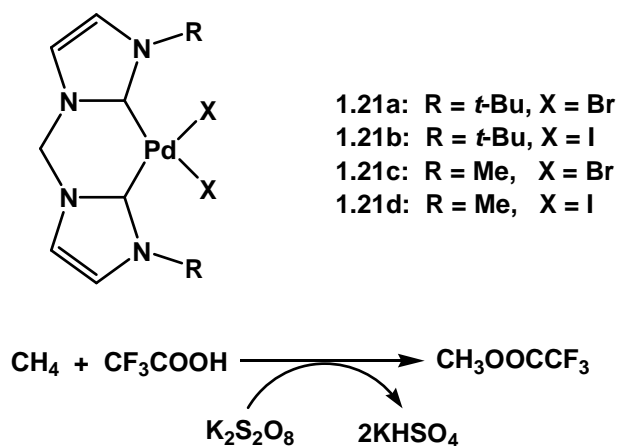


Figure 1.20 NHC-Pd(II) complexes catalyzed methane oxidation.²⁹

It was found that the counterions of the NHC-Pd complexes played an important role in the catalytic process (Table 1.2). In contrast to their bromide analogs (entry 1 and entry 3), the iodide complexes of the palladium N-heterocyclic carbene catalysts were totally inactive (entry 2 and entry 4).

Table 1.2 catalytic conversion of methane into methanol.²⁹

Entry	Catalyst	Yield ^[a] [%]
1	1.21a	519
2	1.21b	0
3	1.21c	980
4	1.21d	0
5	1.21c	3000 ^[b]

[a] By GC analysis, relative to palladium. $T = 80\text{ }^{\circ}\text{C}$, $t = 24\text{ h}$, $p(\text{CH}_4) = 20\text{ bar}$.

[b] By GC analysis, relative to palladium. $T = 90\text{ }^{\circ}\text{C}$, $t = 14\text{ h}$, $p(\text{CH}_4) = 30\text{ bar}$.

As a possible reaction pathway was proposed that the first step of the reaction is the replacement of the anions by trifluoroacetic acid (Figure 1.21), followed by coordination of the methane, electrophilic substitution, oxidation and reductive elimination of $\text{CF}_3\text{COOCH}_3$. At the beginning the authors thought that the initial halogen exchange with trifluoroacetate might make the difference. However, DFT calculations showed that the energy difference between the trifluoroacetate exchange with bromide and iodide ligands is only 5.6 kcal/mol (Table 1.3). This value is too small to explain the inactivity of the NHC-Pd-I₂ catalysts. Another possible reason is that the basicity of iodide is lower than that of bromide, which makes it difficult to protonate the halide ligand off to create a free coordination site, therefore iodine takes up the coordination site for methane.³⁰

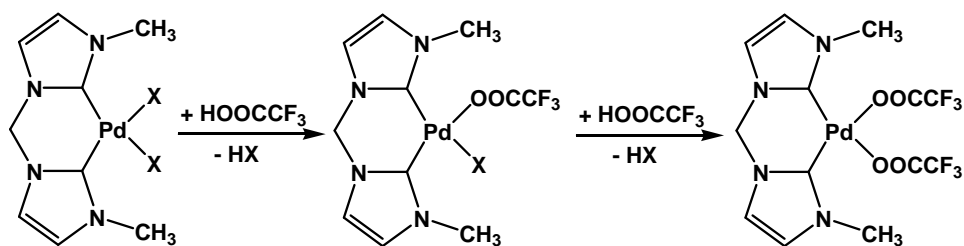


Figure 1.21 Stepwise replacement of halogen with trifluoroacetate.³⁰

Table 1.3 B3LYP/6-311+G(d,p) calculated free energies (kcal/mol) for the replacement of halogen ligands by trifluoroacetic acid.³⁰

Halogen	First replacement	Second replacement	Overall reaction
F	-2.8	+1.2	-1.6
Cl	+11.1	+3.5	+14.7
Br	+14.1	+6.3	+20.4
I	+16.8	+9.2	+26.0

This novel NHC-Pd catalyzed methane oxidation system has the following advantages: first of all, the reaction can be carried out under much milder conditions compared to the Catalytica System. Secondly, potassium peroxodisulfate can be used as an oxidant, which is much cheaper than platinum(IV) salt which is required as an oxidant in the Shilov system. Thirdly, the methane oxidation product of this NHC-Pd(II) catalyzed C-H bond activation process is a methyl trifluoroacetate ester, which can easily be removed from the reaction mixture by distillation and hydrolyzed to produce methanol. The recovered acid and remaining methane can be transferred back to the reaction system. Therefore, it is possible to run it as a cyclic process. The strong electron withdraw trifluoroacetate group also can protect the product from over-oxidation. Last but not the least, the NHC-Pd complexes exhibited extraordinary thermal stability in the presence of strong oxidant in strong acidic medium. This character makes them ideal candidate catalysts for C-H bond activation reactions, because the strong acid can be used

to protect the methane oxidation product against over-oxidation by forming an ester, and the strong oxidants are almost a necessity for catalytic C-H bond activation reactions.

Surprisingly, there are no further mechanistic studies over this promising C-H bond activation system.

1.5 Research Goals

As it has been discussed, the *bis*-NHC-Pd(II) complexes catalyzed methane oxidation system is one of the only a few reported catalytic systems that can directly convert methane to methanol derivatives. To further improve this unique catalytic system, a better understanding of the details of the reaction mechanism is required. Consequently, the goals of the first part of my thesis was to gain mechanistic insight of the *bis*-NHC-Pd(II) complex-catalyzed methane oxidation process. My research has mainly focused on: 1) Synthesis of *bis*-NHC-Pd(II) complexes; 2) Testing these NHC-Pd(II) complexes in C-H bond activation reactions; 3) Studying the oxidative addition and reductive elimination pathways from the *bis*-NHC ligand stabilized palladium species.

Because the reaction conditions are relatively mild, and the catalysts, *bis*-NHC-Pd complexes are well established, it is possible to monitor the reaction by means of $^1\text{H-NMR}$ and $^{13}\text{C-NMR}$ spectroscopy. We expect to isolate or observe key intermediates of the C-H bond activation reaction, through which determine the active catalyst. Furthermore, by investigating the features of the oxidative addition to the *bis*-NHC-Pd species and reductive elimination from the *bis*-NHC-Pd species, valuable information related to the C-H bond activation and following functionalization is expected.

References

1. (a) Bard, A. J.; Whitesides, G. M.; Zare, R. N.; McLafferty, F. W. "Holy Grails of Chemistry," *Acc. Chem. Res.* **1995**, 28, 91. (b) Arndtsen, B. A.; Bergman, R. G.; Mobley, T. A.; Peterson, T. H. "Selective intermolecular carbon-hydrogen bond activation by synthetic metal complexes in homogeneous solution," *Acc. Chem. Res.* **1995**, 28, 154-162.
2. Shilov, A. E.; Shul'pin G. B. "Activation of C-H bond by metal complexes," *Chem. Rev.* **1997**, 97, 2879-2932.
3. Arnold, J. H.; Keith, P. C. "Synthesis of liquid fuels from natural gas," *Progress in Petroleum technology* (Chapter 12), **1951**, 120-137.
4. Labinger, J. A. "Selective alkane oxidation: hot and cold approaches to a hot problem," *Journal of Molecular Catalysis A: Chemical* **2004**, 220, 27-35.
5. Chatt, J.; Davidson, J. M. "The tautomerism of arene and ditertiary phosphine complexes of ruthenium(0), and the preparation of new types of hydrido-complexes of ruthenium(II)," *J. Chem. Soc.* **1965**, 843-855.
6. Garnett, J. L.; Hodges, R. J. "Homogenous metal-catalyzed exchange of aromatic compounds. A new general isotopic hydrogen labeling procedure," *J. Am. Chem. Soc.* **1967**, 89, 4546-4547.
7. Hodges, R. J.; Garnett, J. L. "The kinetics of hydrogen isotope exchange in benzene using a homogeneous platinum catalyst," *J. Phys. Chem.* **1968**, 72, 1673-1682.
8. Labinger, J. A.; Bercaw, J. E. "Understanding and exploiting C-H bond activation," *Nature* **2002**, 417, 507-514.
9. Janowicz, A. H.; Bergman, R. G. "C-H activation in completely saturated hydrocarbons: direct observation of $M + R-H \rightarrow M(R)(H)$," *J. Am. Chem. Soc.* **1982**, 104, 352-354.
10. Hoyano, J. K.; Graham, W. A. G. "Oxidative addition of the carbon-hydrogen bonds of neopentane and cyclohexane to a photochemically generated iridium(I) complex," *J. Am. Chem. Soc.* **1982**, 104, 3723-3725.
11. Jones, W. D.; Feher, F. J. "Alkane carbon-hydrogen bond activation by homogeneous rhodium(I) compounds," *Organometallics* **1983**, 2, 562-563.

12. (a) Keim, W. "Synthesis gas, feedstock for chemicals," *ACS Symposium Series; In Industrial Chemicals via C1 Processes*. **1987**, 1-16. (b) Gradassi, M. J.; Green, N. W. "Economics of natural gas conversion process," *Fuel Proc. Technol.* **1995**, *42*, 65-83.
13. Gol'dshleger, N. F.; Tyabin, M. B.; Shilov, A. E.; Shteinman, A. A. *Zh. Fiz. Khim.* **1969**, *43*, 2174; *Russ. J. Phys. Chem.* **1969**, *43*, 1222 (English translation).
14. Gol'dshleger, N. F.; Es'kova, V. V.; Shilov, A. E.; Shteinman, A. A. *Zh. Fiz. Khim.* **1972**, *46*, 785.
15. Kushch, L. A.; Lavrushko, V. V.; Misharin, Y. S.; Moravsky, A. P.; Shilov, A. E. *Nouv. J. Chim.* **1983**, *7*, 729.
16. (a) Stahl, S. S.; Labinger, J. A.; Bercaw, J. E. "Homogeneous oxidation of alkanes by electrophilic late transition metals," *Angew. Chem. Int. Ed.* **1998**, *37*, 2180-2192. (b) Goldberg, K. I.; Goldman, A. S. "Activation and functionalization of C-H bonds," *ACS Symposium Series 885*, Oxford University Press, 2004.
17. Luinstra, G. A.; Labinger, J. A.; Bercaw, J. E. "Mechanistic and stereochemistry for nucleophilic attack at carbon of platinum(IV) alkyls: Model reactions for hydrocarbon oxidation with aqueous platinum chlorides," *J. Am. Chem. Soc.* **1993**, *115*, 3004-3005.
18. Luinstra, G. A.; Wang, L.; Stahl, S.; Labinger, J. A.; Bercaw, J. E. "C-H activation by aqueous platinum complexes: A mechanistic study," *J. Organomet. Chem.* **1995**, *504*, 75-91.
19. Luinstra, G. A.; Wang, L.; Stahl, S. S.; Labinger, J. A.; Bercaw, J. E. "Oxidation of Zeise's salt by $[\text{PtCl}_6]^{2-}$: A mechanistic model for hydrocarbon oxidation," *Organometallics* **1994**, *13*, 755-756.
20. (a) Periana, R. A.; Taube, D. J.; Gamble, S.; Taube, H.; Satoh, T.; Fujii, H. "Platinum catalysts for the high yield oxidation of methane to methanol derivatives," *Science* **1998**, *280*, 560-564. (b) Xu, X.; Fu, G.; Goddard, W. A., III; Periana, R. A. "Selective oxidation of CH_4 to CH_3OH using the Catalytica (bpym)PtCl₂ catalyst: a theoretical study." *Studies in Surface Science and Catalysis* **2004**, *147*, (Natural Gas Conversion VII), 499-504. (c) Periana, Roy A.; Mironov, Oleg; Taube, Doug; Bhalla, Gaurav; Jones, C. J. "Catalytic, oxidative condensation of CH_4 to CH_3COOH in one step via CH activation," *Science* (Washington, DC, United States) **2003**, *301*(5634), 814-818. (d) Kua, J.; Xu, X.; Periana, R. A.; Goddard, W. A., III. "Stability and thermodynamics of the PtCl₂ type catalyst for activating methane to methanol: A computational study," *Organometallics* **2002**, *21*(3), 511-525.

21. Horváth, I. T.; Cook, R. A.; Millar, J. M.; Kiss, G. "Low-temperature methane chlorination with aqueous platinum chlorides in the presence of chlorine," *Organometallics*, **1993**, *12*, 8
22. DeVries, N.; Roe, D. C.; Thorn, D. L. "Catalytic hydroxylation using chloroplatinum compound," *J. Mol. Catal. A: Chemical* **2002**, *189*,17-22.
23. Geletii, Y. V.; Shilov, A. E. *Kinet. Catal.* **1983**, *24*, 413.
24. Lin, M.; Shen, C.; Garcia-Zayas, E. A.; Sen, A. "Catalytic Shilov chemistry: Platinum chloride-catalyzed oxidation of terminal methyl groups by dioxygen," *J. Am. Chem. Soc.* **2001**, *123*, 1000-1001.
25. Freund, M. S.; Labinger, J. A.; Lewis, N. S.; Bercaw, J. E. "Electrocatalytic functionalization of alkanes using aqueous platinum salts," *J. Mol. Catal.* **1994**, *87*, 11-15.
26. Stahl, S. S; Labinger, J. A.; Bercaw, J. E. "Exploring the mechanism of aqueous C-H activation by Pt(II) through model chemistry: Evidence for the intermediacy of alkylhydridoplatinum(IV) and alkane σ -adducts," *J. Am. Chem. Soc.* **1996**, *118*, 5961-5976.
27. Heyduk, A. F.; Driver, T. G.; Labinger, J. A.; Bercaw, J. E. "Kinetic and thermodynamic preferences in aryl vs benzylic C-H bond activation with cationic Pt(II) complexes," *J. Am. Chem. Soc.* **2004**, *126*, 15034-15035.
28. Rostovtsev V. V.; Labinger, J. A.; Bercaw, J. E.; Lasseter, T. L.; Goldberg, K. I. "Oxidation of dimethylplatinum(II) complexes with dioxygen," *Organometallics*, **1998**, *17*, 4530-4531.
29. Muehlhofer, M.; Strassner, T.; Herrmann, W. A. "New catalyst systems for the catalytic conversion of methane into methanol." *Angew. Chem. Int. Ed.* **2002**, *41*, 1745-1747.
30. Strassner, T.; Muehlhofer, M.; Zeller, A.; Herdtweck, E.; Herrmann, W. A. "The counterion influence on the CH-activation of methane by palladium(II) biscarbene complexes-structure, reactivity and DFT calculations," *Journal of Organometallic Chemistry* **2004**, *689*, 1418-1424.

Chapter 2 NHC-Pd Complexes-mediated Aryl C-H Bond Activation

Study

2.1 Possible Reaction Pathways of the NHC-Pd Catalyzed Methane Oxidation Reaction.

It must be noted again that the discussion of the reaction mechanism in the original paper by T. Strassner was not specific.^{1,2} In relation to the previous discussed “Shilov System”³ and the “Catalytica System”,⁴ at least three distinctly different reaction pathways should be taken into consideration.

The first pathway can be described as the Pd(II)-Pd(0)-Pd(II) cycle: In the first step a cationic [NHC-Pd(II)-(OOCF₃)]⁺ species is generated after ligand-exchange. C-H bond activation occurs at a cationic Pd(II) center to form the NHC-Pd(II)-Me-(OOCF₃) complex. In the second step, the product is then released either by direct reductive elimination or external (S_N2 type)-nucleophilic attack. In the third step, the catalyst is regenerated by oxidation of NHC-Pd(0) to NHC-Pd(II) to complete the catalytic cycle (Figure 2.1).

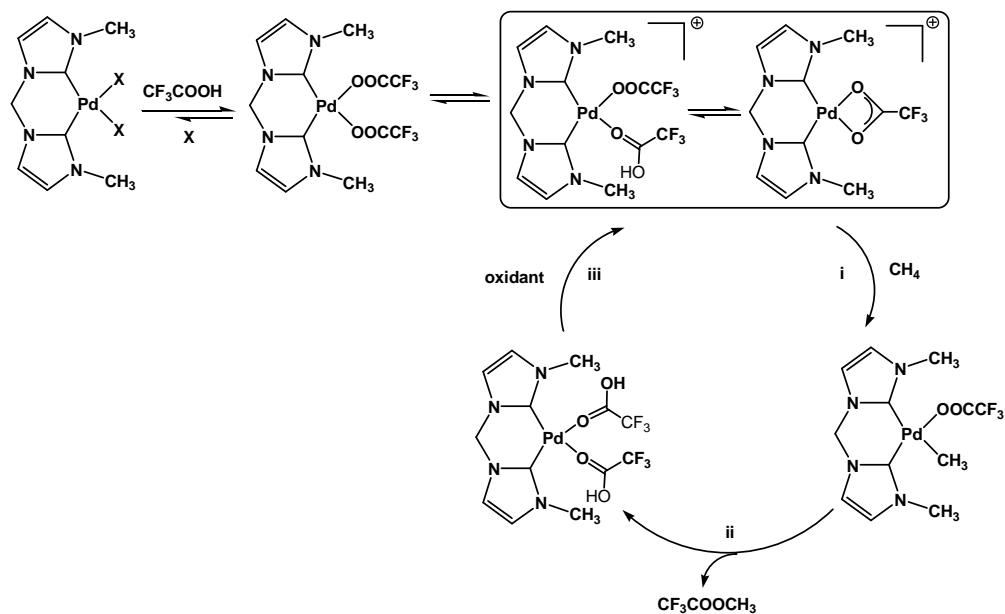


Figure 2.1 Possible methane oxidation pathway I for the Strassner System.

The second possible pathway is similar to the “Shilov system”: In the first step, after ligand exchange, methane C-H bond activation occurs at a cationic Pd(II) center to form a NHC-Pd(II)-Me-(OOCF₃) species. In the second step, the NHC-Pd(II)-Me-(OOCF₃) species is oxidized to NHC-Pd(IV)-Me-(OOCF₃)-Y₂, (where Y = OOCF₃ or OSO₃H); In the third step, the product is released from the NHC-Pd(IV) center and palladium catalyst is regenerated (Figure 2.2).

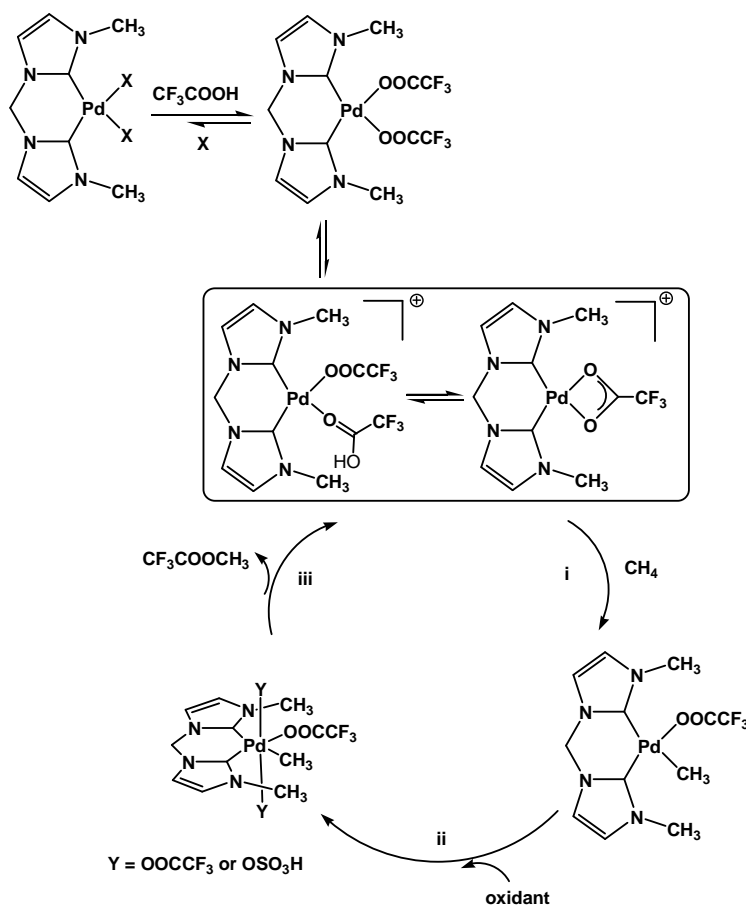


Figure 2.2 Possible methane oxidation pathway II for the Strassner System.

The third pathway differs from pathways one and two: In the first step, the catalyst is oxidized to a NHC-Pd(IV)-(OOCF₃)₂-Y₂ species (Y = OSO₃H or OOCF₃); In the second step, a cationic NHC-Pd(IV) species is generated by ligand dissociation; In the third step, C-H bond activation occurs at the Pd(IV) center to generate a NHC-Pd(IV)-Me species. In the fourth step

of this reaction cycle, the product is released from the Pd(IV) center and Pd(II) species is regenerated; In the final step, NHC-Pd(II)-(OOCF₃)₂ is reformed after ligand exchange. (Figure 2.3)

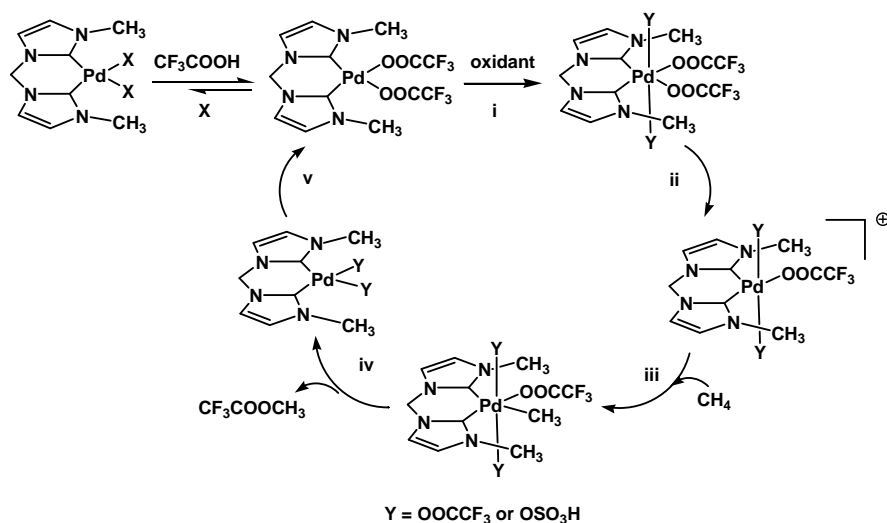


Figure 2.3 Possible methane oxidation pathway III for the Strassner System.

2.2 NHC-Pd Complex Mediated Aryl H-D Exchange

H-D exchange is usually used as a diagnostic proof that the C-H bond activation has occurred.^{5,6,7} I have started my studies of this system by testing whether the NHC-Pd(II) complexes can initiate H-D exchange.

2.2.1 Synthesis of NHC-Pd(II) Complexes

The NHC-Pd(II) complexes were synthesized according to literature reported methods.^{8,9,10} The *bis*-imidazolium dibromide salt **2.1** was obtained by refluxing 1-methylimidazole and dibromomethane in toluene for 12 hours with 73.3% yield.⁸ Treatment of the *bis*-imidazolium dibromide salt **2.1** with Pd(OAc)₂ in DMSO at elevated temperature leads to the formation of the palladium complex *bis*-NHC-Pd(II)-Br₂ **2.2** with 78% yield.⁹ *Bis*-NHC-Pd-

(OOCF₃)₂ **2.3a** and *bis*-NHC-Pd-(OOCCH₃)₂ **2.3b** were synthesized by abstraction of the bromide with AgOOCF₃ and AgOOCCH₃ respectively (Figure 2.4).²

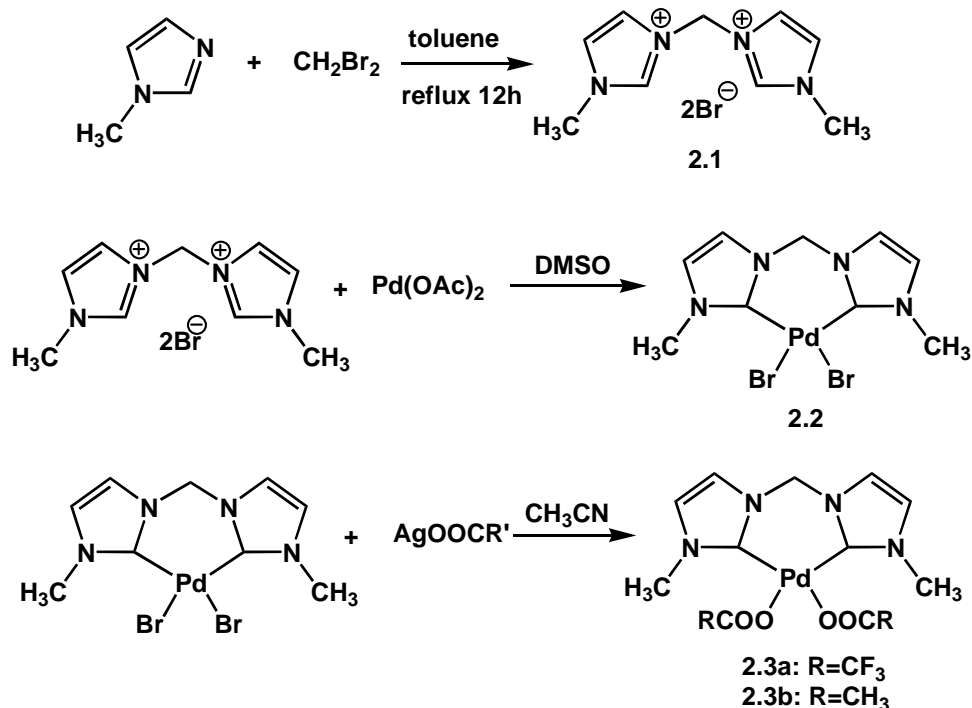


Figure 2.4 Synthesis of *bis*-NHC-Pd(II) complexes.

2.2.2 H-D Exchange Study

At the beginning, H-D exchange was carried out using NHC-Pd-Br₂ as catalyst, toluene as substrate and deuterated trifluoroacetic acid as solvent. Toluene was chosen as a substrate because, firstly, compared to methane, it is much easier to study by NMR spectroscopy; secondly, it provides the opportunity to evaluate whether the catalyst has the ability to differentiate aromatic C-H bond from benzylic C-H bond in the course of C-H bond activation.

The *bis*-NHC-Pd(II)-Br₂ complex **2.2** and toluene (mole ratio of 1/4) were added to 0.70 mL of deuterated trifluoroacetic acid in a J-Young NMR tube. The reaction system was degassed by three consecutive freeze-pump and thaw cycles and then protected under N₂. The NMR tube was put in an 80 °C oil bath and the H-D exchange process was monitored by ¹H-NMR spectroscopy. It was found that the H-D exchange happened at both the *para* and *ortho* positions of toluene. No deuterium incorporation into the *meta* position and the methyl group of toluene was detected. After heating at 80 °C for 20 hours, 60.1% *para*-H and 39.2% *ortho*-H were

substituted with deuterium (Figure 2.5). A control experiment was carried out under same conditions except without adding *bis*-NHC-Pd-Br₂ complex **2.2** as catalyst. No deuterium incorporation into the aromatic ring and methyl group was discerned.

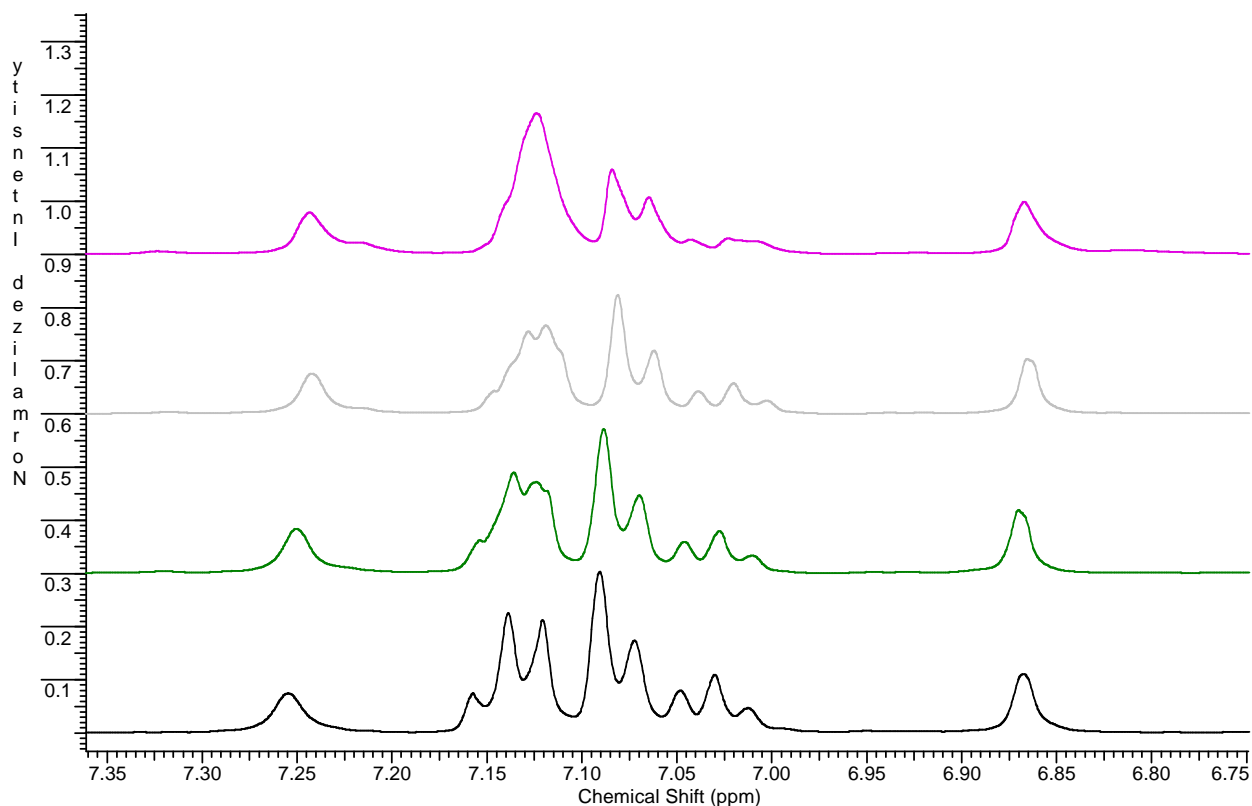


Figure 2.5 Stacked ¹H-NMR of the *bis*-NHC-Pd(II)-Br₂ mediated toluene H-D exchange reaction in CF₃COOD (expanded aromatic area, the spectrum was recorded every 5 hours).

It is my working hypothesis that the aromatic H-D exchange process, as mediated by the *bis*-NHC-Pd(II)-Br₂ complex, proceeds according pathways described in Figure 2.6. In the first step, a cationic species [*bis*-NHC-Pd-(OOCF₃)]⁺ **2.4** is generated after ligand exchange (Br vs OOCF₃) in the acidic medium. In the second step, toluene coordinates to the cationic Pd center by its π -system to form an intermediate **2.5**. In the third step, C-H bond activation occurs either by deprotonation of *bis*-NHC-Pd(II) σ -intermediate **2.6** or deprotonation from oxidative addition type *bis*-NHC-Pd(IV)-hydrido intermediate **2.7** to form aryl *bis*-NHC-Pd(II) **2.8**. In the fourth step, deuterated toluene is released either by direct deuteration of the C-Pd bond of intermediate

2.8 or deuteration of the Pd-center to form a *bis*-NHC-Pd(IV) species **2.9**, and consecutive reductive elimination of deuterated toluene leads then to *bis*-NHC-Pd(II).

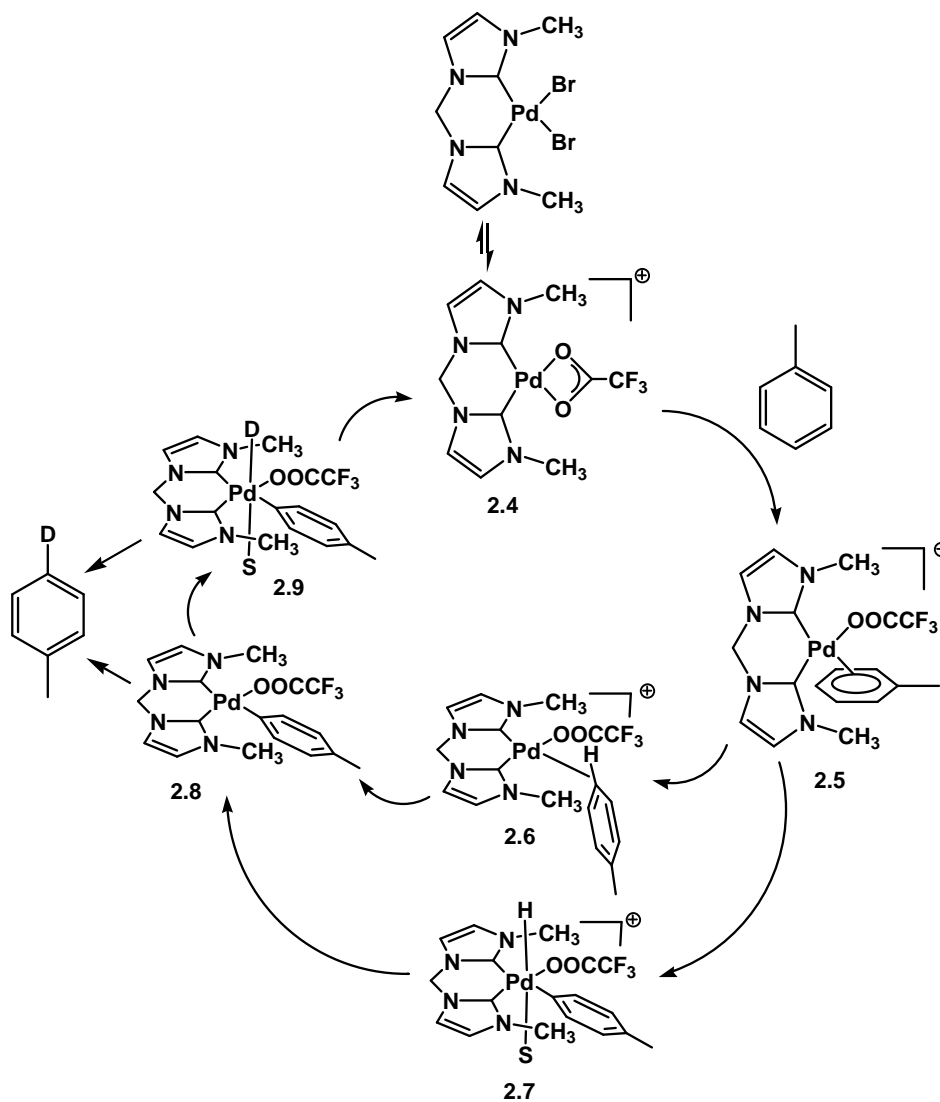


Figure 2.6 Possible pathways for the *bis*-NHC-Pd(II)-Br₂ complex mediated aromatic H-D exchange reaction.

A question in need to be answered is the apparent selectivity of the *bis*-NHC-Pd-Br₂ complex mediated aromatic H-D exchange process. If the proposed mechanism is valid, there should be deuterium incorporation into the *meta* position of toluene, because it is more

accessible to the Pd center than the *ortho* position when steric effect is taken into consideration. However, no deuterium incorporation into the *meta* position was observed.

Another possible pathway is the acid catalyzed H-D exchange. After ligand exchange, small amount of DBr (pKa = -9) was introduced into the reaction system; the strong acid could act as a catalyst to promote the H-D exchange reaction. In this pathway, the *para* and *ortho* positions of toluene are more prone to H-D exchange because they are the more electron-rich sites. To gain more insight into the mechanism, the *bis*-NHC-Pd-(OOCCF₃)₂ complex **2.3a** was synthesized and used as catalyst to mediate the H-D exchange reaction. Under the same conditions, no deuterium incorporation into toluene was observed. This result gave strong supportive evidence that the earlier H-D exchange was catalyzed by acid.

When *para*-xylene was used as substrate instead of toluene, H-D exchange happened at the same rate in the presence or absence of the *bis*-NHC-Pd-(OOCCF₃)₂ complex at 80 °C. It is reasonable to explain that *para*-xylene is more electron rich than toluene, so the trifluoroacetic acid itself is strong enough to catalyze the H-D exchange process (pKa value of CF₃COOH is -0.25). The difference between the electron negativity of toluene and *p*-xylene was demonstrated in a research paper by R. G. Pearson¹⁰, in which the absolute electron negativity of toluene and *p*-xylene were calculated to be 3.9 and 3.7 respectively.

In applying these results, I came to the conclusion that the aromatic H-D exchange in deuterated trifluoroacetic acid is an acid catalyzed process. The *bis*-NHC-Pd(II)-(OOCCF₃)₂ complex and its dissociated cationic form [*bis*-NHC-Pd(II)-OOCCF₃]⁺ may not be the catalytically active species in the C-H bond activation of hydrocarbons! Under the strong oxidation condition of the Strassner's system, one can speculate that high oxidation state palladium species such as [NHC-Pd(IV)-(OOCCF₃)_{4-x}]^{x+} may form and then can act as the real catalyst in the methane C-H bond activation process.

Soon after this finding in 2005,¹¹ Peter Chen reported a method to prepare the cationic [*bis*-NHC-Pd(II)-(OOCCF₃)]⁺ species by treating NHC-Pd(II)-(OOCCF₃)₂ with *p*-toluenesulfonic acid in methylene chloride. This species was isolated and tested for C-H bond activation of benzene in CF₃COOD.¹² Even after heating at 120 °C for 24 hours, no deuterium incorporation into benzene was observed (Figure 2.7). This result provided further evidence that the *bis*-NHC-Pd(II) is not the active species to mediate C-H bond activation.

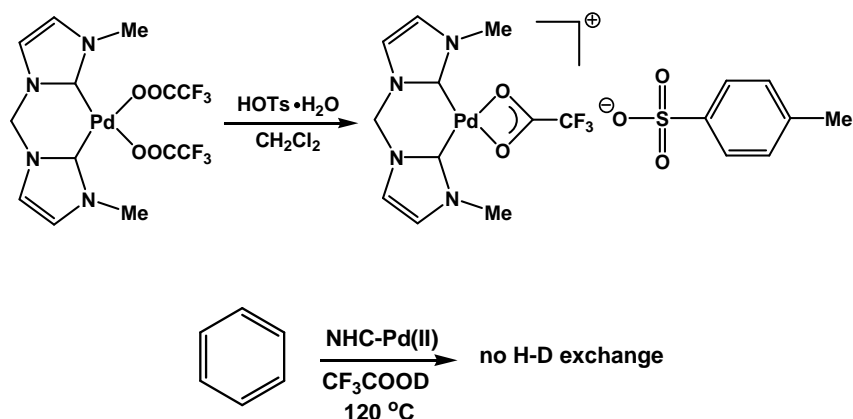


Figure 2.7 Test of cationic *bis*-NHC-Pd(II) species for aromatic H-D exchange reaction.¹²

2.3 Study of *Bis*-NHC-Pd(II) Mediated C-H Bond Activation in the Presence of Potassium Peroxodisulfate

In the Strassner system, trifluoroacetic acid and trifluoroacetic acid anhydride (volume ratio of 6/1) were used as reaction medium, potassium peroxodisulfate was used as oxidant. The same reaction conditions were used to carry out the C-H bond activation of toluene using the *bis*-NHC-Pd(II)-Br₂ complex as catalyst. 5.0 mg of the *bis*-NHC-Pd(II)-Br₂ complex was dissolved in 0.60 mL of deuterated trifluoroacetic acid in a J-Young NMR tube. Upon adding 0.10 mL of trifluoroacetic acid anhydride, all the peaks of the palladium complex were shifted up-field by more than 1 ppm. 20 mg of potassium peroxodisulfate was added to the NMR tube and the mixture was sonicated for 5 minutes, ¹H-NMR spectra was recorded to monitor the reaction after the undissolved potassium peroxodisulfate suspension slowly precipitated to the bottom of the NMR tube. No reaction was observed. Subsequently 5.0 mg of toluene was added to the NMR tube by means of a GC syringe, and the NMR tube was again put in the sonicator at 50 °C. The reaction was kept at 50 °C and monitored hourly by ¹H-NMR. The toluene peaks disappeared slowly and new peaks corresponding to para-substituted toluene increased slowly. After 8 hours, all of the toluene was converted to the new species. In the course of the reaction, no change for the resonances of the catalyst was observed. The mass spectrum showed that the molecular weight of the para-substituted toluene was 172, which matches the molecular weight of *p*-toluenesulfonic acid. This result was really surprising because C-H bond activation of toluene

was expected to happen under the oxidation conditions, similar to the methane oxidation to methyl trifluoro-acetate, *p*-methylphenyl trifluoro-acetate was expected to be the product of this reaction. The absence of the expected product implied that there was no C-H bond activation happening! Even if C-H bond activation would have happened, the trifluoro-acetate group could not have been delivered to toluene.

The formation of *p*-toluenesulfonic acid could be explained by a following hypothetical sequence: in the first step, potassium peroxydisulfate dissociates to form $\text{SO}_3\text{H}^\bullet$ radical; in the second step, the radical react with toluene resulted in the *p*-toluenesulfonic acid as product (Figure 2.8).

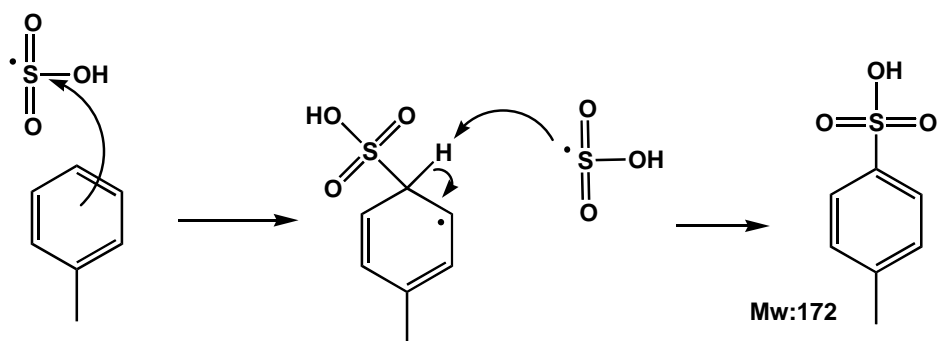


Figure 2.8 The hypothetical sequence for the formation of *p*-toluenesulfonic acid.

2.4 Discussion of the Experimental Findings

The inertness of the *bis*-NHC-Pd(II) complexes towards aromatic C-H bond of toluene was completely unexpected. *N*-heterocyclic carbenes are electron rich σ -donor ligands. The strong electron donating effect was evidenced by the observed IR frequency of the NHC-metal-CO complexes.¹³ For example, in the model Rh complex $\text{Rh}(\text{CO})\text{Cl}(\text{L})_2$, the CO stretching frequencies are sensitive to the electron density of the metal. The stronger electron donating ligand will lead to a more electron rich metal center, which in turn enhances the metal to CO π -backdonating effect. The metal to CO π -backdonating can weaken the bond strength of carbon monoxide because it increases the electron density of the anti-bonding orbital of carbon monoxide (Figure 2.9). The weakened bond will have a lower stretching frequency in the IR absorption.

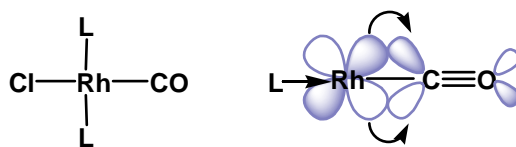
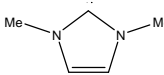
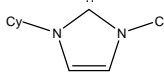


Figure 2.9 Demonstration of the π -backdonating effect.¹³

From the data in Table 2.1, it can be seen that *N*-heterocyclic carbenes induce a significant higher electron density at the rhodium center than the standard phosphine ligands PMe_3 , PCy_3 , and PPh_3 .

Table 2.1 C-O stretching frequencies of *trans*- $\text{RhL}_2(\text{CO})\text{Cl}$ complexes.¹³

$\text{Rh}(\text{CO})\text{Cl}(\text{L})_2$	$\nu(\text{CO}) \text{ (cm)}^{-1}$
	1924
	1929
PCy_3	1939
PMe_3	1957
PPh_3	1983

Because the nitrogen atoms donate their lone pair electrons to the unoccupied p orbital of the carbene through a π -resonance interaction, the π -acceptor ability of *N*-heterocyclic carbene is negligible.¹⁴

Referring to the Shilov system, C-H bond activation involves electrophilic displacement of a proton on the alkane by $\text{Pt}(\text{II})$. However, in the Strassner system, the palladium center is quite electron-rich, because it is *bis*-chelated to the strong electron-donating *N*-heterocyclic carbene ligands. Furthermore, this electron-richness of the metal center is enhanced by the fact that there is very little metal to ligand backbonding effect due to the poor π -acceptor ability of *N*-heterocyclic carbene ligands. The lack of electrophilicity of the palladium center in the *bis*-NHC- $\text{Pd}(\text{II})$ complexes might be the reason that they cannot mediate the C-H bond activation reaction. On the other hand, under oxidizing conditions, the strong electron donating NHC ligand favors

the formation of *bis*-NHC-Pd(IV) species. The *bis*-NHC-Pd(IV) species will be more electrophilic than the *bis*-NHC-Pd(II) species, and it could act as catalyst for the C-H bond activation of methane.

2.5 Experimental

2.5.1 Synthesis of 1, 1'-Dimethyl-3,3'-methylene-diimidazolium dibromide (2.1).

In a 30 mL sealable Schlenk flask 2.00 g (24.4 mmol) methyl imidazole and 2.12 g (12.2 mmol) dibromomethane were dissolved in 10 mL THF and heated to 130 °C for 16 hours. After cooling to room temperature the resulting precipitate was filtered off and washed twice with 10 mL THF. The product was dried under vacuum, yielding 3.32 g (73.3%) of a white powder.

¹H-NMR (δ_{H} ; 400 Hz, DMSO-*d*₆): 3.91 (s, 6H, CH₃), 6.78 (s, 2H, CH₂), 7.82 (s, 2H, NCH), 8.11 (s, 2H, NCH), 9.57 (s, 2H, NCHN).

2.5.2 Synthesis of (1, 1'-Dimethyl-3,3'-methylene-diimidazoline-2,2'-diylidene) palladium(II) dibromide (2.2).

In a 50 mL sealable Schlenk flask 1.00 g (2.90 mmol) of 1, 1'-dimethyl-3,3'-methylene-diimidazolium dibromide and 0.66 g (2.9 mmol) of Pd(OAc)₂ were dissolved 20 mL DMSO. The reaction mixture was stirred at room temperature for 30 minutes and then at 50 °C for 4 hours, after which the reaction mixture was stirred at 90 °C for further 2 hours. DMSO was removed under vacuum at 80 °C to give a yellow solid, which was washed twice with 5 mL portions of dichloromethane to give the product as a pale yellow solid (1.00 g, 78%). ¹H-NMR (δ_{H} ; 400 Hz, DMSO-*d*₆): 3.90 (s, 6H, CH₃), 6.27 (s, 2H, CH₂), 7.33 (s, 2H, NCH), 7.59 (s, 2H, NCH).

2.5.3 Synthesis of (1, 1'-Dimethyl-3,3'-methylene-diimidazoline-2,2'-diylidene) palladium(II) bis(trifluoroacetate) (2.3a).

In a 20 mL sealable Schlenk flask 150 mg (0.34 mmol) of 1, 1'-Dimethyl-3,3'-methylene-diimidazoline-2,2'-diylidene) palladium(II) dibromide and 149 mg (0.68 mmol) silver trifluoroacetate were suspended in 5 mL acetonitrile and the reaction mixture was stirred at 60 °C for 8 hours. The solution was filtered off and the solvent was removed under vacuum to give a

white solid (0.12 g, 69.2%). $^1\text{H-NMR}$ (δ_{H} ; 400 Hz, $\text{DMSO-}d_6$): 3.76 (s, 6H, CH_3), 6.33 (s, 2H, CH_2), 7.40 (s, 2H, NCH), 7.67 (s, 2H, NCH).

2.5.4 Synthesis of (1, 1'-Dimethyl-3,3'-methylene-diimidazoline-2,2'-diylidene) palladium(II) diacetate (2.3b).

1, 1'-Dimethyl-3,3'-methylene-diimidazoline-2,2'-diylidene) palladium(II) diacetate was synthesized by abstract bromo ligands with silver acetate under same condition with the synthesis of bis(trifluoroacetate) palladium(II) complex. $^1\text{H-NMR}$ (δ_{H} ; 400 Hz, $\text{DMSO-}d_6$): 1.74 (s, 6H, CH_3 of acetate), 3.75 (s, 6H, CH_3), 6.20 (s, 2H, CH_2), 7.27 (s, 2H, NCH), 7.55 (s, 2H, NCH).

2.5.5 Bis-NHC-Pd-Br₂ complex 2.2 mediated H-D toluene exchange

In a J-Young NMR tube, 10 mg 1, 1'-dimethyl-3,3'-methylene-diimidazoline-2,2'-diylidene) palladium(II) dibromide and 8.3 mg toluene (mole ratio 1:4) were dissolved in 0.7 mL deuterated trifluoroacetic acid. The NMR tube was heated in an 80 °C oil bath and the H-D exchange reaction was monitored by ^1H NMR spectroscopy at 25 °C every 2 hours. In the $^1\text{H-NMR}$ spectrum the resonances of the *bis*-NHC-Pd(II)-Br₂ complex showed as the following: $^1\text{H-NMR}$ (δ_{H} ; 400 Hz, CF_3COOD): 3.90 (s, 6H, CH_3), 5.94 (d, 1H, $J = 12.5$ Hz, CH_2), 6.56 (d, 1H, $J = 12.5$ Hz, CH_2), 6.87 (s, 2H, NCH), 7.25 (s, 2H, NCH). Resonances for toluene showed as following: $^1\text{H-NMR}$ (δ_{H} ; 400 Hz, CF_3COOD): 2.24 (s, 3H, CH_3), 7.03 (t, 1H, $J = 7.42$ Hz, *p*-H), 7.09 (d, 2H, , $J = 7.42$ Hz, *o*-H), 7.14 (t, 2H, , $J = 7.42$ Hz, *m*-H). The reaction process was monitored by integrations of the three sets of resonance of the benzene ring using the NHC methyl group as an internal standard. (Detailed $^1\text{H-NMR}$ spectrum was showed in Figure A. 5)

2.5.6 Control experiment of toluene H-D exchange

The control experiment of toluene H-D exchange reaction was carried out by dissolving 8.3 mg toluene in CF_3COOD in a J-Young NMR tube and heated to 80 °C. The process of the H-D exchange reaction was monitored every 2 hours by $^1\text{H-NMR}$ at room temperature. (Detailed $^1\text{H-NMR}$ spectrum was showed in Figure A. 6)

2.5.7 *Bis*-NHC-Pd-(OOCCF₃)₂ complex 2.3a mediated toluene H-D exchange

The *bis*-NHC-Pd(II)-(OOCCF₃)₂ mediated toluene H-D exchange reaction was carried out under same condition than described in section 2.5.5 except using *bis*-NHC-Pd(II)-(OOCCF₃)₂ as catalyst.

2.5.8 *Bis*-NHC-Pd-(OOCCF₃)₂ complex 2.3a mediated *p*-xylene H-D exchange

10 mg *bis*-NHC-Pd(II)-(OOCCF₃)₂ complex and 7.8 mg *p*-xylene were dissolved in 0.7 mL CF₃COOD in a J-Young NMR tube and heated to 80 °C. The H-D exchange reaction at room temperature was monitored every hour by ¹H-NMR. (Detailed ¹H-NMR spectrum was showed in Figure A. 7)

2.5.9 Control experiment of *p*-xylene H-D exchange study

The control experiment was carried out under the same condition that described in 2.5.8 except without adding of the *bis*-NHC-Pd(II)-(OOCCF₃)₂ as catalyst. (Detailed ¹H-NMR spectrum was showed in Figure A. 8)

2.5.10 *Bis*-NHC-Pd(II)-Br₂ complex 2.2 mediated C-H bond activation of toluene in the presence of potassium peroxodisulfate.

5.0 mg of the *bis*-NHC-Pd(II)-Br₂ complex 2.2 was dissolved in 0.60 mL of deuterated trifluoroacetic acid in a J-Young NMR tube and to which 0.10 mL of trifluoroacetic acid anhydride was added by means of a syringe. ¹H-NMR showed that all the peaks of the palladium complex were shifted up-field by more than 1 ppm. 20 mg of potassium peroxodisulfate was added to the NMR tube and the mixture was sonicated at 50 °C followed by adding 5 mg of toluene via a GC syringe. The reaction was kept at 50 °C and monitored hourly by ¹H-NMR. (Detailed ¹H-NMR spectrum was showed in Figure A. 9)

References

1. Muehlhofer, M.; Strassner, T.; Herrmann, W. A. "New catalyst systems for the catalytic conversion of methane into methanol," *Angew. Chem. Int. Ed.* **2002**, *41*, 1745-1747.
2. Strassner, T.; Muehlhofer, M.; Zeller, A.; Herdtweck, E.; Herrmann, W. A. "The counterion influence on the CH-activation of methane by palladium(II) biscarbene complexes-structure, reactivity and DFT calculations," *Journal of Organometallic Chemistry* **2004**, *689*, 1418-1424.
3. Gol'dshleger, N. F.; Es'kova, V. V.; Shilov, A. E.; Shteinman, A. A. *Zh. Fiz. Khim.* **1972**, *46*, 785.
4. Periana, R. A.; Taube, D. J.; Gamble, S.; Taube, H.; Satoh, T.; Fujii, H. "Platinum catalysts for the high yield oxidation of methane to methanol derivatives," *Science* **1998**, *280*, 560-564.
5. Garnett, J. L.; Hodges, R. J. "Homogenous metal-catalyzed exchange of aromatic compounds. A new general isotopic hydrogen labeling procedure," *J. Am. Chem. Soc.* **1967**, *89*, 4546-4547.
6. Hodges, R. J.; Garnett, J. L. "The kinetics of hydrogen isotope exchange in benzene using a homogeneous platinum catalyst," *J. Phys. Chem.* **1968**, *72*, 1673-1682.
7. Gol'dshleger, N. F.; Tyabin, M. B.; Shilov, A. E.; Shteinman, A. A. *Zh. Fiz. Khim.* **1969**, *43*, 2174; *Russ. J. Phys. Chem.* **1969**, *43*, 1222 (English translation).
8. Claramunt, R. M.; Elguero, J.; Meco, T. "*N*-polylazolylméthanes. III.. Synthèse et étude rmn du proton des dérivés du méthylène-1,1' diimidazole et du méthylène-1,1' dibenzimidazole," *J. Heterocycl. Chem.* **1983**, *20*, 1245-1249.
9. Herrmann, W. A.; Schwarz, J.; Gardiner, M. G. "High-yield synthesis of sterically demanding *bis*(*N*-heterocyclic carbene) complexes of palladium," *Organometallics* **1999**, *20*, 4082-4089.
10. Pearson, R. G. "Absolute electronegativity and hardness: applications to organic chemistry," *J. Org. Chem.* **1989**, *54*, 1423-1430.
11. Wang, H.; Kraft, S. "Synthesis of Pd(II) *N*-Heterocyclic Carbene Complexes and the Regioselective Remote Intramolecular C-H Bond Activation," Poster Presentation,

- 40th Midwest Regional Meeting of the American Chemical Society, Joplin, MO, United States, October 26-29, 2005.
12. Slotweg, J. C.; Chen, P. "Cationic palladium *bis*-carbene carboxylate complexes," *Organometallics* **2006**, 25 (25), 5863-5869.
 13. Köcher, C.; Herrmann, W. A. "Heterocyclic carbene. One-pot synthesis of rhodium and iridium carbene complexes," *Journal of Organometallic Chemistry* **1997**, 532, 261-265.
 14. (a) Herrmann, W. A.; Köcher, C. "*N*-heterocyclic carbenes" *Angew. Chem. Int. Ed. Engl.* **1997**, 36, 2162-2187. (b) Herrmann, W. A. "*N*-heterocyclic carbene: A new concept in organometallic catalysis," *Angew. Chem. Int. Ed. Engl.* **2002**, 41, 1290.

Chapter 3 Study of NHC-Pd(IV) Species

3.1 Introduction

Although organoplatinum(IV) complexes¹ have been known since 1907 and many organoplatinum complexes have been isolated and extensively studied,^{2,3,4,5} organopalladium(IV) complexes are still very rare.

The first successful synthesis and isolation of Pd(IV) complexes was accomplished in 1975, bidentate nitrogen-donor ligands stabilized organometallic Pd(IV) complexes $\text{Cl}_2(\text{C}_6\text{F}_5)_2\text{Pd(IV)(L-L)}$ **3.2** were prepared by oxidative addition of chlorine to the corresponding bis(pentafluorophenyl)palladium(II) complexes, $(\text{C}_6\text{F}_5)_2\text{Pd(II)(L-L)}$ **3.1**, (L-L are en, bipy and phen) (Figure 3.1).⁶

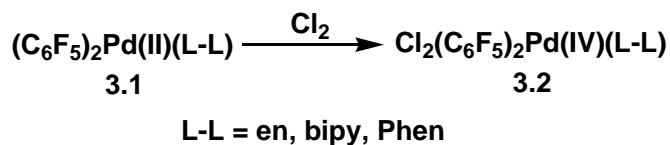


Figure 3.1 Oxidation of Pd(II) complexes to Pd(IV) complexes by chlorine.⁶

In 1980, Stille reported the synthesis of the dimethyl (TRANSPHOS) palladium(II) complex **3.3**. (TRANSPHOS = 2,11-bis(diphenyl-phosphinomethyl)benzo[c]phenanthrene) Because the two methyl groups are in *trans*-position to each other, this complex would not undergo reductive elimination at 100 °C in $\text{DMSO-}d_6$.⁷ The addition of methyl iodide to dimethyl(TRANSPHOS)palladium(II) in $\text{DMSO-}d_6$ solution at room temperature produced ethane! This result gave compelling evidence for the formation of a Pd(IV) intermediate **3.4** (Figure 3.2).⁸

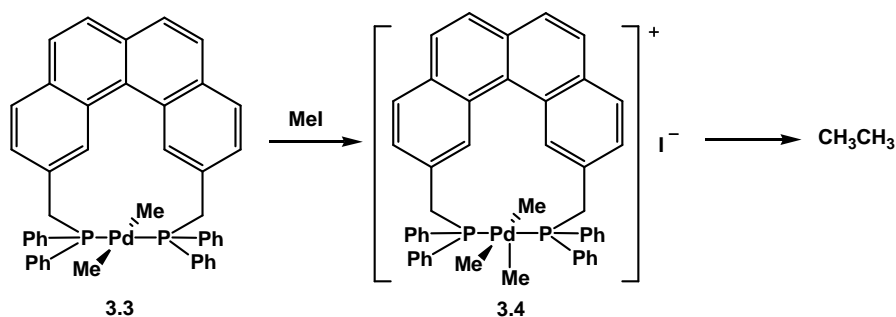


Figure 3.2 Reductive elimination of ethane from a Pd(IV) intermediate.⁸

The Cauty group reported the synthesis of Pd(IV) complexes **3.6** and **3.7** by oxidative addition of $(\text{O}_2\text{CPh})_2$, $(\text{EPh})_2$ ($\text{E}=\text{S}, \text{Se}$) to *bis*-pyridine ligand stabilized palladium(II) dimethyl (bipy)Pd(II)(Me)₂ complex **3.5** (Figure 3.3).⁹

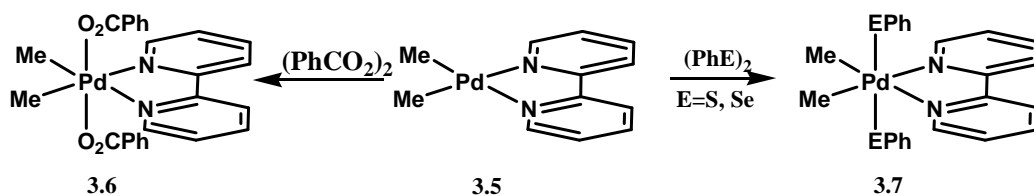


Figure 3.3 *Bis*-pyridine ligand stabilized Pd(IV) complexes formation.⁹

Tris(pyrazol-1-yl)borate ligand supported palladium(IV)cyclopentane complexes **3.9** and **3.10** were obtained by oxidative addition of organohalides to diorganopalladium(II) complex **3.8** (Figure 3.4).¹⁰

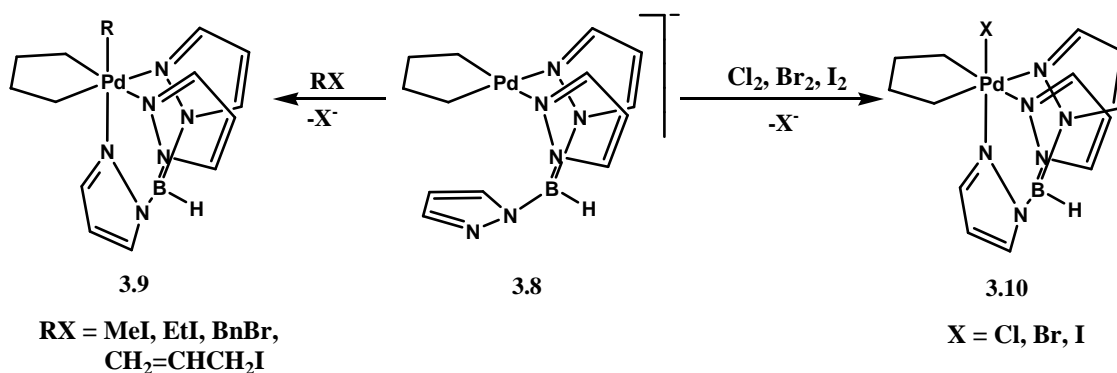


Figure 3.4 Tris(pyrazol-1-yl)borate ligand supported palladium(IV)cyclopentane complexes formation.¹⁰

In 2005, the Sanford group reported the synthesis of *bis*-(phenyl-pyridine) palladium(IV) bisbenzoate complexes **3.11** (Figure 3.5).¹¹ These Pd(IV) complexes were stabilized by two rigid cyclometalated pyridine ligands, and the electronic properties can be manipulated by the *para*-substitution of the benzoate parts. These complexes enabled the first detailed mechanistic investigation of C-O bond-forming reductive elimination from a Pd(IV) metal center.

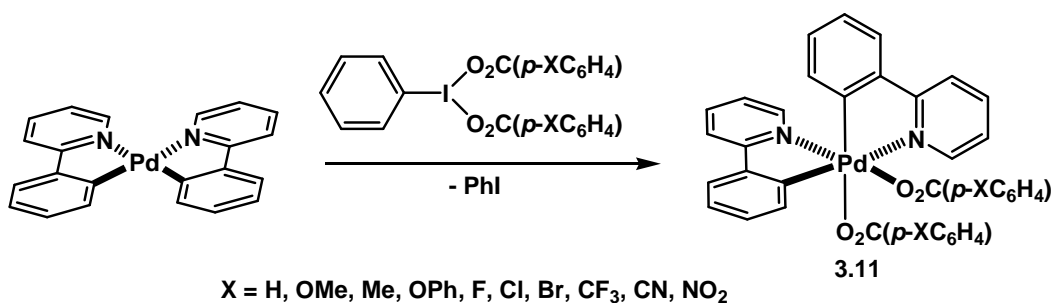


Figure 3.5 Phenylpyridine ligand supported Pd(IV) complexes formation.¹¹

Inspired by all these examples of successful Pd(IV) research, Dr. Kraft and I had decided to direct our efforts to synthesize and characterize NHC-Pd(IV) species. Ideally we wanted to isolate the NHC-Pd(IV) species, study their reactivity towards C-H bonds, and further study the C-O, C-C bond forming reductive elimination from NHC-Pd(IV) species.

3.2 Oxidation of *Bis*-NHC-Pd(II)-(OOCCH₃)₂ and *Bis*-NHC-Pd(II)-(OOCCF₃)₂

Bis-NHC-Pd(II)-(OOCCF₃)₂ **2.3a** and *bis*-NHC-Pd(II)-(OOCCH₃)₂ **2.3b** were synthesized by treating *bis*-NHC-Pd(II)-Br₂ **2.2** with AgOOCCF₃ and AgOOCCH₃ respectively as have been described in **Chapter 2**. Compare with the *bis*-NHC-Pd(II)-Br₂ complex **2.2**, the NHC-Pd(II) di-acetate complexes are more soluble. For example, the *bis*-NHC-Pd(II)-Br₂ complex only can be dissolved in DMSO, DMF and trifluoroacetic acid, while the *bis*-NHC-Pd(II) di-acetate complexes can be dissolved in much less polar solvents such as THF, acetonitrile and methylene chloride etc. Different oxidants such as PhI(OAc)₂, PhI(OTFA)₂ and benzoylperoxide(PhCO₂)₂ were used to oxidize the *bis*-NHC-Pd(II)-(OOCR)₂ complexes **2.3a** and **2.3b**. Various solvents and different temperatures were surveyed, however, no reaction to the

bis-NHC-Pd(II)-(OOCR)₂ was observed. It should be noted that the oxidants decayed over time. Therefore, the attempt to observe or isolate *bis*-NHC-Pd(IV)-tetracarboxyl species failed.

3.3 Oxidation of *bis*-NHC-Pd(II)-Br₂ with Br₂

Another approach to obtain *bis*-NHC-Pd(IV)-tetracarboxyl species is by the reaction of *bis*-NHC-Pd(IV)-Br₄ with silver carboxyl salt. It had been reported the bromine can be used as an oxidant to oxidize Pd(II) complexes to Pd(IV) complexes.¹⁰ The oxidation of *bis*-NHC-Pd(II)-Br₂ with bromine was carried out in acetonitrile. The *bis*-NHC-Pd(II)-Br₂ complex is not soluble in acetonitrile, after adding one equivalent of bromine to the suspension of *bis*-NHC-Pd(II)-Br₂ in acetonitrile, a clear orange solution formed immediately. When the same reaction was carried out in deuterated acetonitrile, ¹H-NMR spectrum broadened substantially. After removing the solvent under vacuum, the obtained solid was re-dissolved in deuterated DMSO, interestingly, exactly the same ¹H-NMR spectrum as of *bis*-NHC-Pd(II)-Br₂ was obtained. It is our hypothesis that the change of the solubility could be due to the oxidation of NHC-Pd(II)-Br₂ to NHC-Pd(IV)-Br₄, which undergoes ligand exchange with acetonitrile to form a more soluble solvent-ligated cationic [NHC-Pd(IV)-Br₃-(CH₃CN)]⁺ species **3.12** (Figure 3.6). However, this process appears to be reversible. When the solvent is removed under vacuum, the NHC-Pd(IV) species undergoes reductive elimination to form NHC-Pd(II) again. Four equivalents of AgOAc were added to convert the proposed *bis*-NHC-Pd(IV)-Br₄ to *bis*-NHC-Pd(IV)-(OAc)₄, but this reaction failed and no product suitable for NMR characterization was isolated. The attempt to obtain single crystals of *bis*-NHC-Pd(IV)-Br₄ by slow diffusion of ether into acetonitrile containing an excess of bromine and *bis*-NHC-Pd(II)-Br₂ also failed. The precipitate obtained was a powder instead of crystals that could be analyzed by X-ray crystallography. The ¹H-NMR spectrum of the powder showed the characteristic peaks of *bis*-NHC-Pd(II)-Br₂.

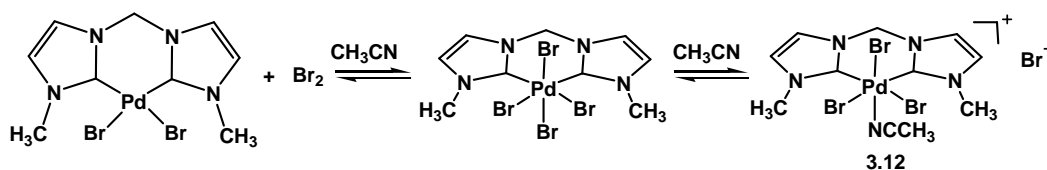
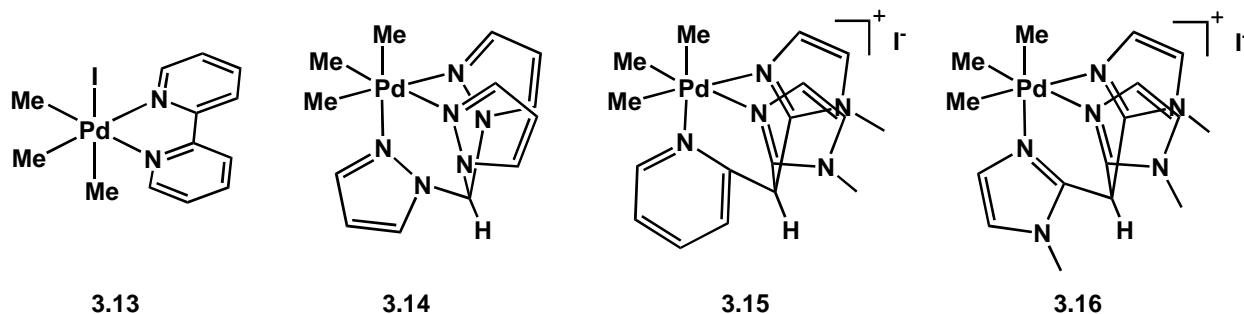


Figure 3.6 Proposed reversible reaction between *bis*-NHC-ligated Pd(II) and Pd(IV)

3.4 Synthesis of Tripodal NHC-Pd Complexes

3.4.1 Examples of Pd(IV) Complexes that Are Stabilized with Tripod Ligands

In a study of the synthesis and characterization of ligand stabilized Pd(IV) complexes, A. J. Canty and coworkers found that in complexes containing the *fac*-Pd(Me)₃ unit, tripodal nitrogen donor ligands result in more stable complexes than the related bidentate ligands;¹² for example, the tri(pyrazo-1-yl)methane ligand stabilized palladium(IV) trimethyl complex [PdMe₃{(pz)₃CH}]I **3.14** is stable at room temperature, but the 2, 2'-bipyridyl ligand supported palladium(IV) complex PdMe₃(bpy) **3.13** requires storage at -20 °C to avoid reductive elimination of ethane to form PdMe(bpy). It was also found that the stability of the Pd(IV) species increased with stronger donor ability of the ligands. For example, the ligands donor ability increases with order of pz < py < imi, complex **3.14** showed a trace of ethane in CDCl₃ after 4 hours at room temperature, but the complexes **3.15** and **3.16** could be heated at 60 °C for 1 hour without any indication of decomposition (Figure 3.7).



Scheme 3.7 Stronger donor ligand stabilize Pd(IV) species better.¹²

3.4.2 Tripod Ligand Design and Synthesis

Inspired by the successful preparation of tripod ligands stabilized Pd(IV) complexes, we want to design a tripod ligand which contains *bis*-chelating NHC-platforms with a pending arm. After oxidation of the Pd(II) to Pd(IV) complex, the coordination geometry changed from square

planar to octahedral. The side arm can lock up an axial site of Pd(IV) and stabilize the Pd(IV) complex. This concept is shown in Figure 3.8.

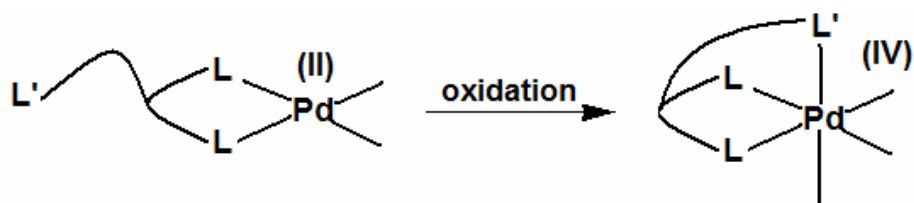


Figure 3.8 Tripod ligand design.

Pyrimidine has been proved to be excellent ligand to bind to platinum even in strongly acidic media, as for instance in the Catalytica methane oxidation system.¹³ Moreover, pyrimidine is rather inert to oxidation, therefore it has a great advantage over other ligands such as alkyl- or aryl-phosphines, because ligand degradation in the presence of strong oxidants is far less likely. In consideration of the simplicity of the ¹H-NMR spectrum, 4,6-dimethyl pyrimidine was chosen as the side arm ligand. The two methyl groups can be used as an indicator for coordination of pyrimidine to the Pd, because before coordination, the two methyl groups are in a symmetrical environment and only one peak will be expected in the ¹H-NMR spectrum; after coordination, the two methyl groups are in a unsymmetrical environment, one close to the Pd and another away from the Pd, so two set of peaks will be expected in the ¹H-NMR spectrum.

The tripod ligand was synthesized according to the Figure 3.9: In the first step, 2-bromo-4,6-dimethyl pyrimidine was treated with BuLi in THF at -78 °C and then react with 1,3-dichloroacetone.¹⁴ The α -chloro-epoxide **3.17** was obtained with a yield of 43.0%. In the second step, the α -chloro-epoxide **3.17** was treated with two equivalent of sodium imidazole salt in DMF to yield pyrimidine *bis*-imidazole alcohol **3.18** in 46.5% yield.¹⁵ In the third step, the hydroxyl group was protected with TIPS to produce **3.19**.¹⁶ The introduction of the bulky TIPS group to the ligand will help the coordination of pyrimidine to the palladium center because it will force the pyrimidine ligand to be close to the palladium center. In the last step, the two imidazoles were methylated with MeI to yield the tripod pyrimidine *bis*-imidazolium ligand **3.20** with a yield of 96.0%.

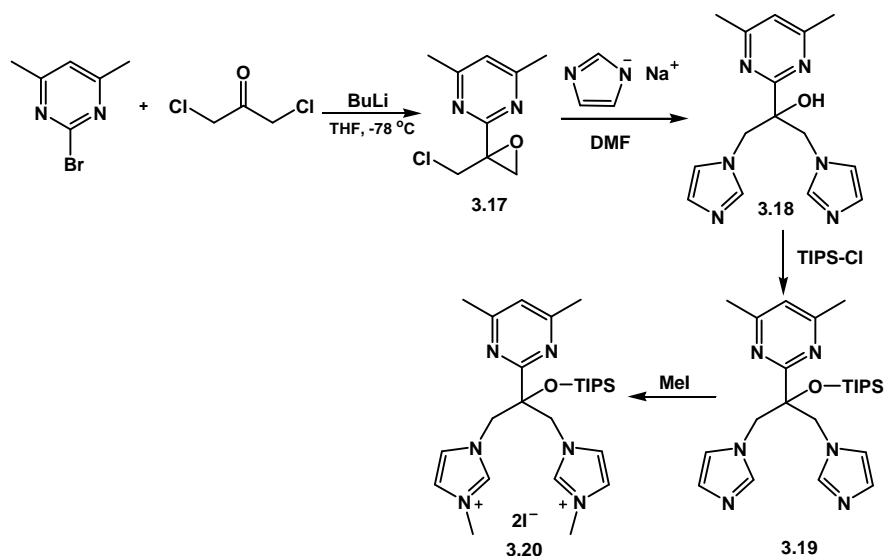


Figure 3.9 Synthesis of the tripodal ligand.

3.4.3 Synthesis of Tripod *bis*-NHC-Pd(II) Complexes.

The aim of this work was the synthesis the tripod-*bis*-NHC-Pd(II)-Me₂ complex **3.22**. It was anticipated that oxidative addition of alkyl halides such as MeI and benzyl bromide to the complex **3.22** will lead to a cationic pyrimidine coordinated *bis*-NHC-Pd(IV)-(pym)-Me₂-R species **3.23** (Figure 3.10). As already pointed out, the introduction of the pyrimidine side arm ligand can significantly increase the stability of the Pd(IV) species, so that we can isolate and characterize the tripodal Pd(IV) species **3.23** and furthermore study the reductive elimination pathway from the Pd(IV) species.

To our disappointment, it proved to be impossible, to synthesize the tips-protected-tripodal *bis*-NHC-Pd(II) complex **3.21**. The classic Herrmann method¹⁷ was applied: Pd(OAc)₂ was used as base to deprotonate the 2-hydrogens of imidazole at elevated temperature to generate the *bis*-N-heterocyclic carbene in situ, which was expected to coordinate the Pd(II) to form *bis*-NHC-Pd(II) complex. But unfortunately, once the heating was applied, the color of the solution turned from orange to black, a lot of black (apparently metallic) palladium appeared within two minutes. After removal of the palladium black by filtration, the filtrate was concentrated to dryness. The ¹H-NMR spectrum was complicated and hard to interpret, most likely due to the presence of several products. One possible reason for the observed behavior is the presence of

the bulky TIPS group that makes it difficult for the two NHC ligands to coordinate to the palladium center, as previously expected. The two NHCs could have turned away from each other and coordinate to palladium with another two units of the tripod ligand.

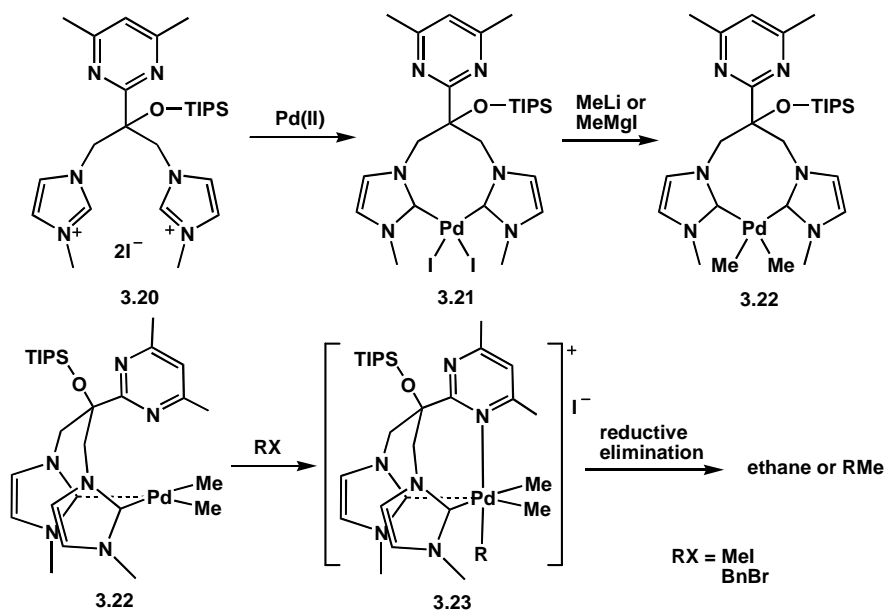


Figure 3.10 Proposed approach to tripodal ligand stabilized Pd(IV) species.

The “less congested” ligand **3.24** was used to react with Pd(OAc)₂ in the same manner, and although a lot of palladium black precipitated out, we did obtain the tripodal-*bis*-NHC-Pd(II)-I₂ complex **3.25** after purification with column chromatography (using CHCl₃/CH₃OH = 20/1 solvent mixture as mobile phase) with a 28% yield (Figure 3.11).

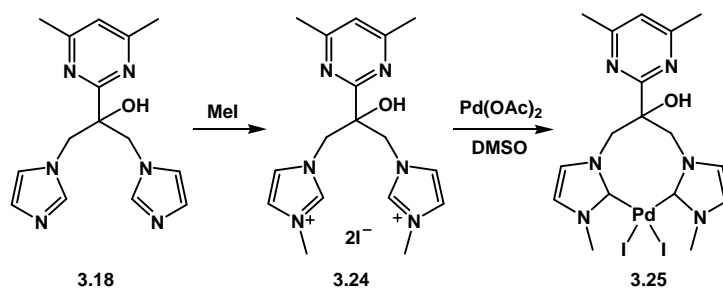


Figure 3.11 Synthesis of tripodal *bis*-NHC-Pd(II)-I₂ complex **3.25**.

Single crystals were obtained by slowly diffusing of methanol into a diluted DMSO solution of the tripodal *bis*-NHC-Pd(II)-I₂ complex **3.25**. Subsequent X-ray analysis revealed complex **3.25** to be monomeric with the dicarbene ligand chelating to the palladium(II) center in a *cis* fashion with a boat-like conformation (from the Pd center) and a chair-like conformation (from side of the pyrimidine-unit and hydroxyl bonded tertiary carbon) being observed for the eight-membered C₅N₂Pd ring. The remaining two coordination sites of the distorted square-planar coordinated palladium center are occupied by iodide anions. In addition, a H-bond is observed between the proton of the hydroxyl group and the oxygen of the DMSO solvent (Figure 3.12). Selected bond lengths and bond angles are listed in Table 3.1.

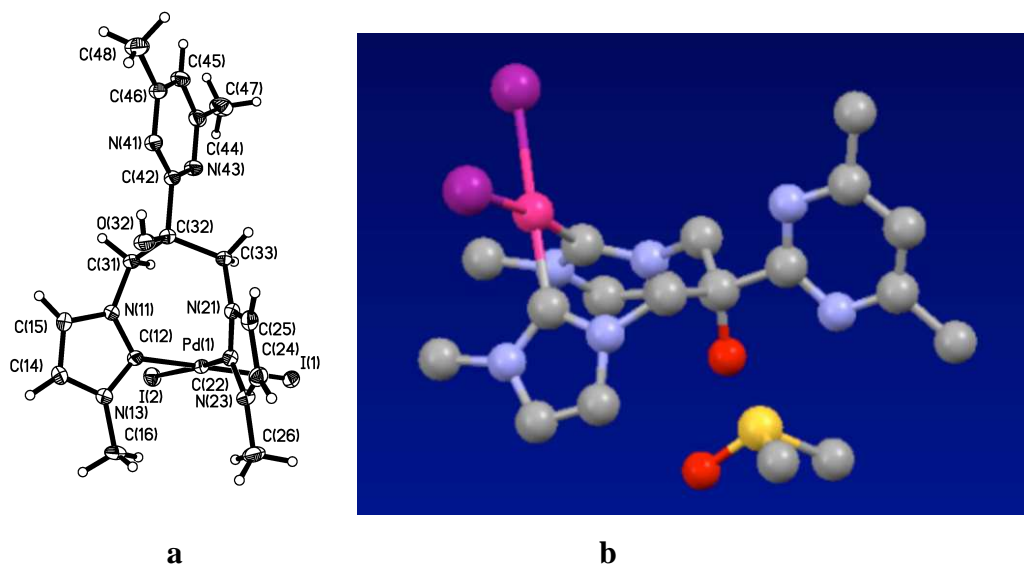


Figure 3.12 X-ray structure of complex **3.25** (a: Thermal ellipsoid plot drawn at the 50% probability level; b: The hydrogen atoms are omitted for clarity reasons).

Table 3.1 Selected bond lengths and bond angles of the tripod-*bis*-NHC-Pd(II)-I₂ complex **3.25**.

Length (Å)		Angle (deg)	
Pd(1)-C(22)	1.968(2)	C(22)-Pd(1)-C(12)	82.54(9)
Pd(1)-C(12)	1.977(2)	C(22)-Pd(1)-I(2)	170.32(6)
Pd(1)-I(2)	2.6530(2)	C(12)-Pd(1)-I(2)	87.83(6)
Pd(1)-I(1)	2.6622(3)	C(22)-Pd(1)-I(1)	90.98(6)
N(11)-C(12)	1.352(3)	C(12)-Pd(1)-I(1)	173.27(6)
N(11)-C(15)	1.388(3)	I(2)-Pd(1)-I(1)	98.612(8)
N(11)-C(31)	1.457(3)	C(12)-N(11)-C(15)	110.39(18)
C(12)-N(13)	1.343(3)	C(12)-N(11)-C(31)	125.48(18)
N(13)-C(14)	1.381(3)	C(15)-N(11)-C(31)	124.13(18)
N(13)-C(16)	1.457(3)	N(13)-C(12)-N(11)	105.56(18)
C(14)-C(15)	1.345(3)	N(13)-C(12)-Pd(1)	126.90(15)
N(21)-C(22)	1.358(3)	N(11)-C(12)-Pd(1)	127.36(16)
N(21)-C(25)	1.388(3)	C(12)-N(13)-C(14)	110.39(18)
N(21)-C(33)	1.465(3)	C(12)-N(13)-C(16)	124.92(19)
C(22)-N(23)	1.348(3)	C(14)-N(13)-C(16)	124.68(19)
N(23)-C(24)	1.380(3)	C(15)-C(14)-N(13)	107.4(2)
N(23)-C(26)	1.468(3)	C(15)-C(14)-H(14)	126.3
C(24)-C(25)	1.351(3)	N(13)-C(14)-H(14)	126.3
C(31)-C(32)	1.544(3)	C(14)-C(15)-N(11)	106.30(19)
C(32)-O(32)	1.415(3)	N(11)-C(31)-C(32)	113.57(17)
C(32)-C(42)	1.532(3)	C(42)-C(32)-C(31)	107.47(17)
C(32)-C(33)	1.537(3)	O(32)-C(32)-C(42)	109.64(17)
		O(32)-C(32)-C(31)	108.97(18)
		O(32)-C(32)-C(33)	109.75(17)

Different oxidants such as $\text{PhI}(\text{OAc})_2$ and $\text{PhI}(\text{OTFA})_2$, bromine and chlorine were used to react with the tripod-*bis*-NHC-Pd(II)-I₂ complex **3.25**, but no Pd(IV) species was observed. The hypervalent-iodine reagent gave no reaction, and the bromine and chlorine cause all the ¹H-NMR resonances of the Pd(II) complex became very broad and could not be resolved.

3.5 Discussion of the Experimental Findings

Although the goal to observe or isolate NHC-ligand stabilized Pd(IV) species was not achieved, valuable information was obtained from this study. First of all, from literature reported methods, almost all the isolated Pd(IV) species are stabilized with bidentate or tridentate ligands, furthermore, most of them contain strong σ -donating alkyl ligands such as methyl ligand. The N-heterocyclic carbene ligand is strong electron-donating ligand which should be able to stabilize high oxidation state palladium species. The reaction between *bis*-NHC-Pd(II)-Br₂ and bromine provided very promising sign of formation of Pd(IV) species. The newly designed tripod ligand **3.20** which contained *bis*-NHC and pyrimidine side arm was synthesized successfully, but the synthesis of the palladium complex with this ligand failed, mostly due to the steric effect of the bulky TIPS group. The oxidation of complex **3.25** was not successful. All these information implied that in order to stabilize palladium(IV) species, more electron-donating ligands such as methyl group should be introduced to the palladium center.

3.6 Experimental

3.6.1 Synthesis of the α -chloro-epoxide **3.17**

In a 50 mL Schlenk flask, 1.08 g (5.77 mmol) of 2-bromo-4,6-dimethylpyrimidine was dissolved in 25 mL dry THF and cooled to -78 °C in a dry ice-acetone bath. 3.6 mL 1.6 M *n*-butyl-lithium (5.77 mmol) hexane solution was added and the reaction mixture was stirred for 5 minutes, to which a solution of 0.74 g (5.77 mmol) of 1,3-dichloroacetone in 4 mL THF was added dropwise under the protection of continuous nitrogen flow. The reaction mixture was stirred at -78 °C for 20 minutes. Then the cooling bath was removed and the temperature was slowly raised to 0 °C. The solvent was removed in high vacuum using a liquid nitrogen trap. 100 mL hexane was added to the residue, which was stirred for 5 minutes, 10 mL KOH-saturated methanol solution was added; a dark oil formed immediately. The hexane phase was transferred to a separatory funnel and washed three times with 15 mL of water and once with 15 mL of brine. After drying with anhydrous MgSO₄, the solvent was removed in vacuum to give 0.49 g (43%) of a clear oil as product. ¹H-NMR (δ_{H} ; 400 Hz, CD₃Cl): 2.49 (s, 6H, CH₃), 3.25 (d, 1H, J

= 5.86 Hz, ClCH₂), 3.49 (d, 1H, J = 5.86 Hz, ClCH₂), 4.29 (s, 2H, OCH), 6.97 (s, 1H, aromatic H). ¹³C-NMR (δ_H; 400 Hz, CD₃Cl): 23.97, 45.32, 53.84, 59.42, 119.30, 163.80, 167.16.

3.6.2 Synthesis of the *bis*-imidazole alcohol **3.18**

To a solution of 222 mg α-chloro-epoxide **3.17** (1.12 mmol) in 5 mL DMF, 222 mg (2.46 mmol) of sodium imidazole salt was added and the reaction mixture was stirred at room temperature for 8 hours. A brown solution formed and the TLC showed that all of the epoxide was consumed. After removal of DMF in vacuum, the residue was dissolved in 15 mL methylene chloride, to which, 1.5 mL 2N HCl ether solution was added. A brown precipitate formed immediately. The precipitate was collected by filtration and then re-dissolved in 10 mL water and washed three times with 3 mL of methylene chloride. 5 mL saturated NaHCO₃ solution was added, and the water phase was extracted three times with 10 mL of methylene chloride. The combined organic phase was dried with anhydrous MgSO₄, and then the solvent was removed to give 155 mg (46.5%) white solid as product. ¹H-NMR (δ_H; 400 Hz, CD₃Cl): 2.40 (s, 6H, CH₃), 4.24 (d, 2H, J = 14.05 Hz, NCH₂), 4.55 (d, 2H, J = 13.66 Hz, NCH₂), 5.36 (s, 1H, OH), 6.71 (s, 2H, NCH), 6.84 (s, 2H, NCH), 6.88 (s, 1H, aromatic H), 7.23 (s, 2H, NHN). ¹³C-NMR (δ_H; 400 Hz, CD₃Cl): 23.67, 53.43, 119.10, 120.13, 128.59, 137.99, 165.35, 167.12.

3.6.3 Tips-protection of hydroxyl group to form **3.19**

4 mg (0.17 mmol) NaH was added to a solution of 50 mg (0.17 mmol) pyrimidine-*bis*-imidazole **3.18** in 5 mL dry THF and stirred at room temperature for 10 minutes, to which 33 mg (0.17 mmol) of triisopropylsilyl chloride was added. The reaction mixture was stirred at room temperature for 16 hours. After removal of the solid by filtration, THF was evaporated under reduced pressure. 26.7 mg (35%) product was obtained after purification with column chromatography (mobile phase: CHCl₃/CH₃OH = 20/1). ¹H-NMR (δ_H; 400 Hz, CD₃Cl): 0.93-1.00 (broad multiplet, 21H, tips CH₃ and CH), 2.51 (s, 6H, CH₃), 4.49 (d, 2H, J = 14.34 Hz, NCH₂), 4.62 (d, 2H, J = 14.34 Hz, NCH₂), 6.72 (s, 2H, NCH), 6.99 (s, 2H, NCH), 7.05 (s, 1H, aromatic H), 7.30 (s, 2H, NHN).

3.6.4 Tips-protected *bis*-imidazolium diiodide 3.20

To a solution of 20 mg (0.044 mmol) tips-protected pyrimidine-*bis*-imidazole **3.19** in 5 mL of DMSO, 31 mg (0.22 mmol) MeI was added and the reaction mixture was stirred at room temperature for 24 hours. The DMSO solvent was removed under reduced pressure to yield 31mg (96%) white solid as product. ¹H-NMR (δ_{H} ; 400 Hz, DMSO-*d*₆): 0.90-0.92 (d, 18H, tips CH₃), 1.02-1.11 (broad multiplet, 3H, tips-CH), 2.45 (s, 6H, CH₃), 3.85 (s, 6H, NCH₃), 4.79-4.87 (dd, 4H, J = 14.05 Hz, NCH₂), 7.39 (s, 2H, NCH), 7.40 (s, 1H, aromatic H), 7.68 (s, 2H, NCH), 8.88 (s, 2H, NHN).

3.6.5 Synthesis of tripod-*bis*-imidazolium diiodide 3.24

To a solution of 50 mg (0.17 mmol) pyrimidine-*bis*-imidazole **3.18** in 8 mL acetonitrile, 238 mg (1.7 mmol) of MeI was added and the reaction mixture was stirred at room temperature for 10 hours. Upon removal of the solvent under reduced pressure, 92 mg (95%) of product was obtained as a white solid. ¹H-NMR (δ_{H} ; 400 Hz, DMSO-*d*₆): 2.46 (s, 6H, CH₃), 3.83 (s, 6H, NCH₃), 4.56 (d, 2H, J = 14.05 Hz, NCH₂), 4.76 (d, 2H, J = 14.05 Hz, NCH₂), 6.32 (s, 1H, OH), 7.32 (s, 1H, aromatic H), 7.38 (s, 2H, NCH), 7.61 (s, 2H, NCH), 8.96 (s, 2H, NHN). ¹³C-NMR (δ_{H} ; 400 Hz, CD₃Cl): 23.67, 53.43, 119.10, 120.13, 128.59, 137.99, 165.35, 167.12.

3.6.6 Synthesis of tripod-*bis*-NHC-Pd(II)-I₂ complex 3.25

To a solution of 90 mg (0.15 mmol) ligand **3.24** in 4 mL DMSO, 35 mg (0.15 mmol) of Pd(OAc)₂ was added and the reaction mixture was stirred at room temperature for 2 hours, the color of the solution changed from dark red to slightly red during this period of time. The reaction mixture was further stirred at 60 °C for 5 hours and then at 90 °C for 2 hours. A black precipitate was formed during that time. The solvent was removed under reduced pressure at 80 °C and the residue was purified by column chromatography (mobile phase: CHCl₃/CH₃OH = 20/1 solvent mixture) to give 30 mg (28%) product as a white solid. ¹H-NMR (δ_{H} ; 400 Hz, DMSO-*d*₆): 2.55 (s, 6H, CH₃), 3.87 (s, 6H, NCH₃), 4.21 (d, 2H, J = 14.29 Hz, NCH₂), 5.35 (d, 2H, J = 14.29 Hz, NCH₂), 5.96 (s, 1H, OH), 7.25 (s, 4H, NCH), 7.37 (s, 1H, aromatic H).

References

1. Pope, W. J.; Peachey, S. J. "A new class of organo-metallic compounds. Preliminary notice. Trimethylplatinimethyl hydroxide and its salt," *Proc. Chem. Soc., London* **1907**, 23, 86-87.
2. Monaghan P. K.; Puddephatt R. J. "Oxidation of dimethylplatinum(II) complexes with alcohols: Synthesis and characterization of alkoxoplatinum(IV) complexes," *Organometallics* **1984**, 3 (3), 444-449.
3. Levy C. J.; Vittal J. J.; Puddephatt R. J. "Synthesis and characterization of group 14-platinum(IV) complexes," *Organometallics* **1996**, 15 (8), 2108-2117.
4. Puddephatt R. J. "Platinum(IV) hydride chemistry," *Coordination Chemistry reviews* **2001**, 157-185.
5. Zhang, F.; Prokopchuk, E. M.; Broczkowski, M. E.; Jennings, M. C.; Puddephatt, R. J. "Hydrido(dimethyl)platinum(IV) complexes with bis(pyridine) ligands: The effect of chelate ring size on reactivity," *Organometallics* **2006**, 25, 1583-1591.
6. Uson, R.; Fornies, J.; Navarro, R. "Dichloro-bis(pentafluorophenyl)(chelate) complexes of palladium(IV)," *J. Organomet. Chem.*, **1975**, 96, 307-312.
7. Gillie, A.; Stille, J. K. "Mechanisms of 1,1-reductive elimination from palladium," *J. Am. Chem. Soc.*, **1980**, 102, 4933-4941.
8. Moravskiy, A.; Stille, J. K. "Mechanisms of 1,1-reductive elimination from palladium: elimination of ethane from dimethylpalladium(II) and trimethylpalladium(IV)," *J. Am. Chem. Soc.*, **1981**, 103, 4182-4186.
9. (a) Canty, A. J. "Development of organopalladium(IV) chemistry: fundamental aspects and systems for studies of mechanism in organometallic chemistry and catalysis," *Acc. Chem. Res.*, **1992**, 25, 83-90.
(b) Canty, A. J.; Jin, H.; Skelton, B. W.; White, A. H. "Oxidation of Complexes by $(O_2CPh)_2$ and $(ER)_2$ (E = S, Se), Including Structures of $Pd(CH_2CH_2CH_2CH_2)(SePh)_2(bpy)$ (bpy = 2,2'-Bipyridine) and $MMe_2(SePh)_2(L_2)$ (M = Pd, Pt; L_2 = bpy, 1,10-Phenanthroline) and C...O and C...E Bond Formation at Palladium(IV)," *Inorg. Chem.*, **1998**, 37, 3975.
10. Canty, A. J.; Jin, H.; Roberts, A. S.; Skelton, B. W.; White, A. H. "Oxidation of diorganopalladium(II) complexes by water and halogens: Reactions involving methyl

group transfer and structural studies of hydrogen-bonded adducts formed by aryl alcohols with the pallada(IV)cyclopentane complex $\text{Pd}(\text{CH}_2\text{CH}_2\text{CH}_2\text{CH}_2)(\text{OH})\{(\text{pz})_3\text{BH}\}$ ($[(\text{pz})_3\text{BH}]^- = \text{Tris}(\text{pyrazol-1-yl})\text{borate}$),” *Organometallics* **1996**, *15*, 5713.

11. Dick, A. R.; Kampf, J. W.; Sanford, M. S. “Unusually stable palladium(IV) complexes: Detailed mechanistic investigation of C–O bond-forming reductive elimination,” *J. Am. Chem. Soc.* **2005**, *127*, 12790-12791.
12. (a) Brown, D. G.; Byers, P. K.; Canty, A. J. “Synthesis of the stable organopalladium(IV) complexes $[\text{fac-PdRMe}_2(\text{tripod})]\text{X}$ and selective reductive elimination of ethane from $(\eta\text{-1-allyl})\text{palladium(IV)}$ complexes to form $(\eta\text{-3-allyl})\text{palladium(II)}$ complexes,” *Organometallics* **1990**, *9*, 1231-1235.
(b) Canty, A. J.; Jin, H.; Roberts, A. S.; Skelton, B. W.; Traill, P. R.; White, A. H. “Synthesis and characterization of ambient temperature stable organopalladium(IV) complexes, including aryl-, $\eta\text{-1-allyl-}$, ethylpalladium(IV), and pallada(IV)cyclopentane complexes. Structures of the poly(pyrazol-1-yl)borate complexes $\text{PdMe}_3\{(\text{pz})_3\text{BH}\}$ and $\text{PdMe}_3\{(\text{pz})_4\text{B}\}$ and three polymorphs of $\text{PdMe}_2\text{Et}\{(\text{pz})_3\text{BH}\}$,” *Organometallics* **1995**, *14* (1), 199-206.
13. Periana, R. A.; Taube, D. J.; Gamble, S.; Taube, H.; Satoh, T.; Fujii, H. “Platinum catalysts for the high yield oxidation of methane to methanol derivatives,” *Science* **1998**, *280*, 560-564.
14. Chen, S; Fang, J. “An improved method for the addition reactions of 1,3-dichloroacetone with combined organolithium-cerium trichloride reagents,” *Journal of the Chinese Chemical Society* (Taipei, Taiwan) **2003**, *50*(4), 927-930.
15. Arnold, P. L.; Scarisbrick, A. C.; Blake, A. J.; Wilson, C. “Chelating alkoxy-N-heterocyclic carbene complexes of silver and copper,” *Chem. Commun.* **2001**, *22*, 2340-2341.
16. Ogilvie, K. K.; Thompson, E. A.; Quilliam, M. A.; Westmore, J. B. “Selective protection of hydroxyl groups in deoxynucleosides using alkylsilyl reagents,” *Tetrahedron Letters* **1974**, 2865-2868.
17. Herrmann, W. A.; Schwarz, J.; Gardiner, M. G. “High-yield syntheses of sterically demanding bis(N-heterocyclic carbene) complexes of palladium,” *Organometallics* **1999**, *20*, 4082-4089

Chapter 4 Direct Observation of Trimethyl *Bis*-NHC-Pd(IV) Species

4.1 The Principle of Microscopic Reversibility

In a reversible reaction, the mechanism in one direction is exactly the reverse of the mechanism in the other direction. This is called the principle of Microscopic Reversibility (Figure 4.1).¹ To understand the mechanism of C-H bond activation, it is desirable to have the opportunity to directly observing the oxidative addition of a C-H bond to isolable metal complexes. But this is normally impossible, because the oxidative addition products $M(R)(H)$ are thermodynamically unstable, compared to the reactants. However, important mechanistic information can be obtained from the thermodynamically favorable reductive elimination reaction from the metal complex, which is the microscopic reverse of the C-H bond activation.² Therefore, *bis*-NHC-Pd(Me)₂ complexes were synthesized to study the reductive elimination behavior of these complexes under oxidative conditions. Our aim was to isolate or/and observe the intermediates of the reaction by monitoring the reaction at various temperatures via ¹H-NMR and ¹³C-NMR spectroscopy. Based on the principle of Microscopic Reversibility, valuable mechanistic information could be obtained with respect to the C-C and C-X (X=O, Cl) bond forming process which may involve high-oxidation state Pd(IV) intermediates.

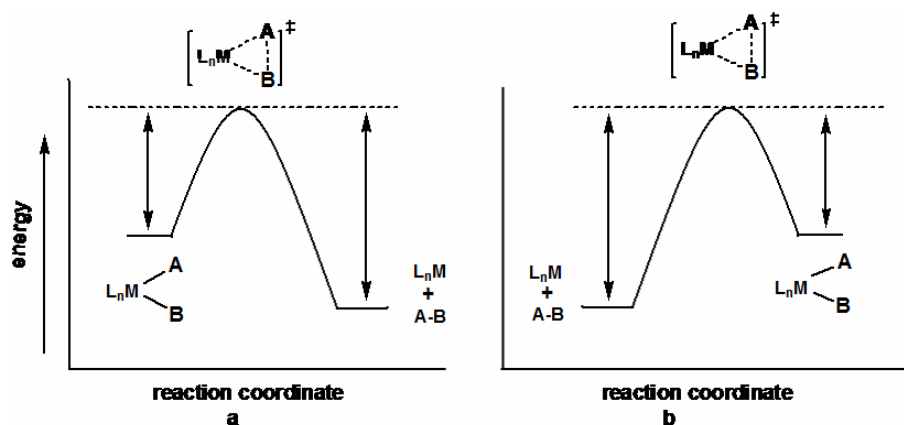


Figure 4.1 Energy diagram of a reversible reaction (a: reductive elimination; b: oxidative addition).¹

4.2 Synthesis of a *Bis*-NHC-Pd-Me₂ Complex

The synthesis of a *bis*-NHC-Pd-Me₂ complex **4.1** was first attempted by treating *bis*-NHC-Pd-Br₂ complex **2.2** (synthesis of this complex was described in Chapter 2) with MeLi in THF at -78 °C (Figure 4.2).³ The palladium complex **2.2** was not soluble in THF at the beginning of the reaction. A clear solution formed once the reaction was completed. But the removal of LiBr from the reaction mixture was problematic. It was found that traces of water are capable of totally destroying the *bis*-NHC-Pd(II)-Me₂ complex **4.1**, resulting in a black precipitate. If the *bis*-NHC-Pd(II)-Me₂ complex was exposed to air for 30 minutes, a black precipitate was formed as well. Based on this observation, it is my working hypothesis that oxygen can trigger the reductive elimination of ethane from *bis*-NHC-Pd(II)-Me₂ complex.

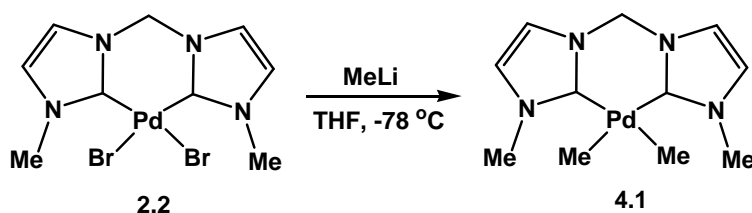


Figure 4.2 Synthesis of *bis*-NHC-Pd(II)-Me₂ complex using MeLi.

To eliminate the side effect caused by oxygen and water, the reaction was carried out in a nitrogen filled glove-box. The Grignard reagent MeMgBr was used instead of MeLi to introduce methyl groups to the palladium by a transmetalation reaction (Figure 4.3).⁴ It was found that the reaction was completed after 1 hour at room temperature. Again the removal of MgBr₂ caused some concerns in the beginning, because it is very soluble in THF and can form an adduct with THF, and if it is not completely separated from the *bis*-NHC-Pd(II)-Me₂ complex, rather large THF peaks will show up in the ¹H-NMR spectrum even after the sample had been dried under high vacuum for 24 hours. After numerous failures to isolate pure *bis*-NHC-Pd(II)-Me₂ complex, it was found that 1,4-dioxane is the perfect solvent to use to separate the MgBr₂ salt from the *bis*-NHC-Pd-Me₂ complex. Furthermore, the MeMgBr reagent will undergo transmetalation by itself in 1,4-dioxane to form Me₂Mg and MgBr₂, which are both not soluble in 1,4 dioxane. This special effect of 1,4-dioxane make it possible to obtain pure *bis*-NHC-Pd-Me₂ complex even

when the reaction was carried out with excess of Grignard reagent. After the reaction was completed in 1 hour, THF solvent was removed in vacuum. Pre-dried 1,4-dioxane was added to the residue solid and stirred at room temperature for 5 min, then the white solid was separated by filtering through a short pad of pre-dried celite. The filtrate was concentrated in vacuum, and pure *bis*-NHC-Pd(II)-Me₂ complex was obtained with a 90% yield.

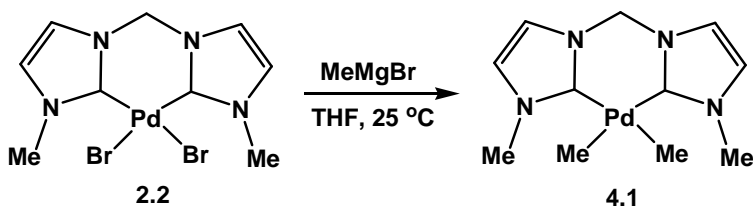


Figure 4.3 Synthesis of *bis*-NHC-Pd(II)-Me₂ complex using MeMgBr.

4.3 Oxidative Addition of MeI to *Bis*-NHC-Pd-Me₂ Complex

Inspired by the successful examples of observation, isolation and characterization of Pd(IV) complexes by oxidative addition of MeI to the dimethyl Pd(II) complexes,^{3a,5,6} the investigation of oxidative addition of MeI to *bis*-NHC-Pd(II)-Me₂ complex was carried out. 8.0 mg of the *bis*-NHC-Pd(II)-Me₂ complex **4.1** was added to a J-Young NMR tube and 0.60 mL pre-dried deuterated THF-*d*₈ was added by vacuum transfer. The ¹H-NMR spectrum showed the characteristic up-field resonance of the palladium coordinated methyl groups at -0.32 ppm.^{3a} After cooling the sample to -70 °C, 2 equivalents of MeI in 0.1 mL THF-*d*₈ stock solution were added. The sample was carefully shaken to disperse the MeI thoroughly at -70 °C and then quickly inserted into a pre-cooled NMR probe (-70 °C). The reaction process was monitored by NMR at various temperatures.

Both the oxidative addition and the reductive elimination products were observed when the temperature was raised to -50 °C. The oxidative addition of MeI to the *bis*-NHC-Pd-Me₂ complex resulted in a trimethyl *bis*-NHC-Pd(IV) species as intermediate. Even though the amount of this intermediate was very small, all its resonances could be clearly assigned. The two singlet peaks appeared at 1.17 ppm and 1.29 ppm with the integration ratio of 2 to 1, corresponding to the equatorial methyl groups and axial methyl group on the Pd(IV) species; and the singlet peak at 4.01 ppm was corresponding to the methyl groups on the NHC ligand; and the

two peaks at 7.11 ppm and 7.33 ppm were corresponding to 4-,5-protons of the imidazole ring; the CH₂-bridge signal was not apparent. It is very likely that it was concealed under the CH₂-bridge signals of the starting material and/or the reductive elimination product. From the integration of the ¹H-NMR spectrum, the amount of this intermediate *bis*-NHC-Pd(IV)-Me₃ species kept almost constant as long as there was some of the starting material *bis*-NHC-Pd-Me₂ complex left. The decrease of the intensity of the *bis*-NHC-Pd(II)-Me₂ signals (characteristic peak for the Pd-Me₂ at -0.30 ppm) was accompanied by the increase of the intensity of the reductive elimination products *bis*-NHC-Pd(II)-Me-I (characteristic peak for the Pd-Me-I at 0.28 ppm) and ethane (0.84 ppm). The reaction was completed in 1 hour at -50 °C and the clean NHC-Pd(II)-Me-I complex was formed. The stacked ¹H-NMR spectrum along the reaction process at -50 °C was demonstrated in Figure 4.4, and the time interval between two spectra is 10 min.

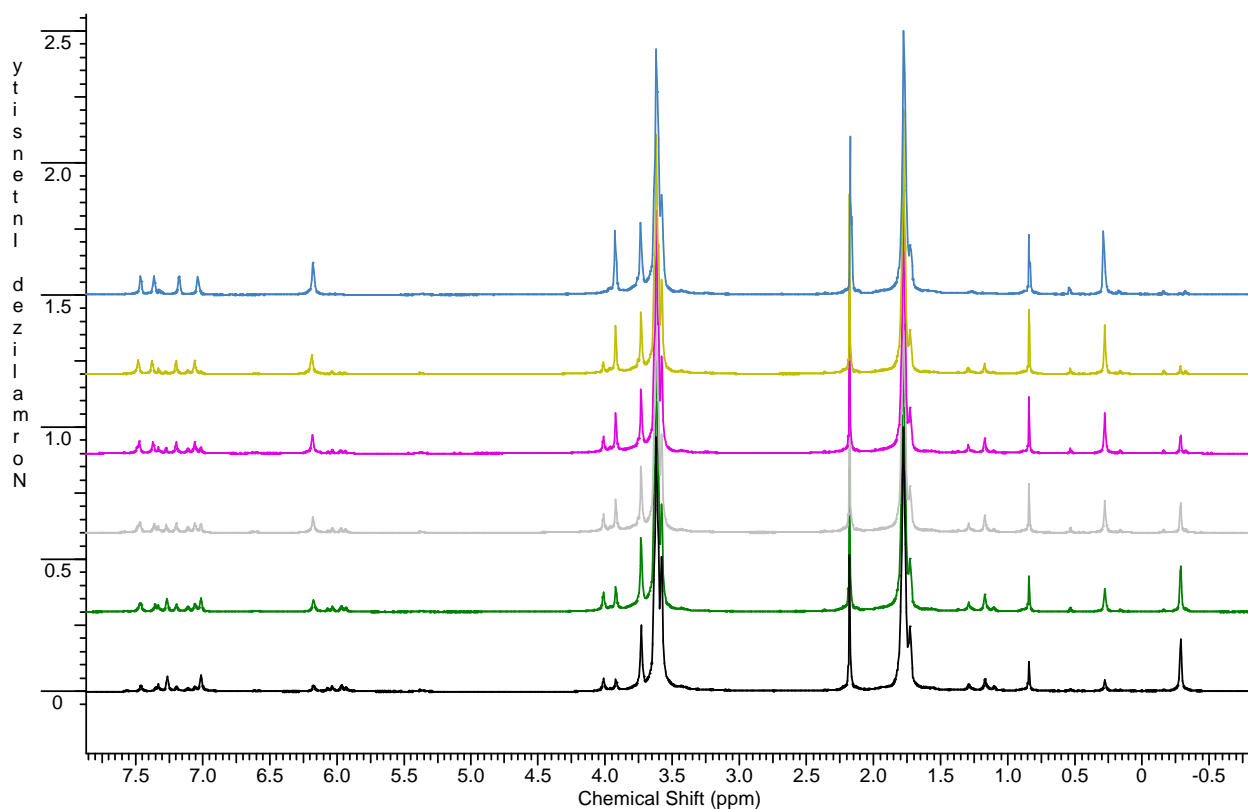


Figure 4.4 Stacked ¹H-NMR spectra recorded during the reaction process between *bis*-NHC-Pd(II)-(CH₃)₂ complex **4.1** and MeI at -50 °C in 10 min intervals.

Based on the information obtained from the VT $^1\text{H-NMR}$ study, a reasonable reaction pathway can be drawn as described in Figure 4.5. In the first step of the reaction, oxidative addition of MeI to the *bis*-NHC-Pd(II)- $(\text{CH}_3)_2$ complex **4.1** yield either a neutral (species **4.2**) or cationic (species **4.3**) trimethyl *bis*-NHC-Pd(IV) intermediate. In the second step, reductive elimination occurs from the Pd(IV) intermediate to form ethane and *bis*-NHC-Pd(II)-Me-I complex **4.4**.

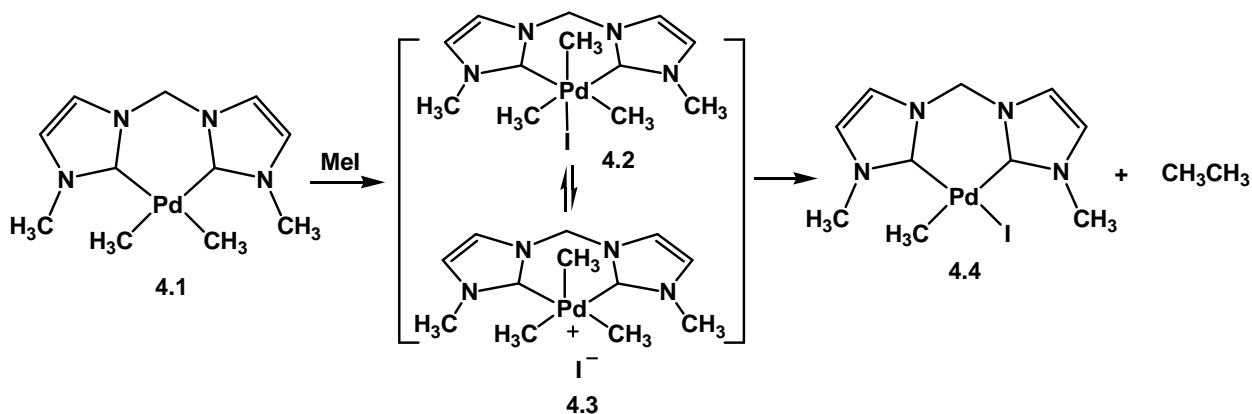


Figure 4.5 Proposed reaction pathway between *bis*-NHC-Pd(II)- $(\text{CH}_3)_2$ complex **4.1** and MeI.

4.4 Oxidative Addition of $^{13}\text{CH}_3\text{I}$ to *Bis*-NHC-Pd-Me₂ Complex

To further prove the presence of a trimethyl *bis*-NHC-Pd(IV) species during the oxidative addition of MeI to the *bis*-NHC-Pd(II)-Me₂ complex **4.1**, ^{13}C labeled methyl iodide was used. The oxidative addition reaction between $^{13}\text{CH}_3\text{I}$ and *bis*-NHC-Pd(II)-Me₂ was initiated at $-70\text{ }^\circ\text{C}$ and slowly warmed up to $-50\text{ }^\circ\text{C}$ within 20 minutes. To preserve the intermediate, the temperature was re-cooled to $-70\text{ }^\circ\text{C}$ and the intermediate was characterized by $^{13}\text{C-NMR}$ spectroscopy. Five major peaks were observed in the $^{13}\text{C-NMR}$ spectrum: the most intense peak at -23.16 ppm was assigned to $^{13}\text{CH}_3\text{I}$, the peak at -8.97 ppm was assigned to the unsymmetrical *bis*-NHC-Pd(II)- $^{13}\text{CH}_3\text{-I}$ complex produced after the reductive elimination of ethane from the intermediate trimethyl *bis*-NHC-Pd(IV) species; the peak at 7.46 ppm was assigned to the reductive elimination product $^{13}\text{CH}_3\text{CH}_3$; the two peaks at 12.03 ppm and 16.97 ppm were tentatively assigned to the ^{13}C labeled methyl group of the trimethyl *bis*-NHC-Pd- $^{13}\text{CH}_3(\text{CH}_3)_2$

intermediates, one for the methyl group in axial position and the other for the methyl group in equatorial position, though it is not clear which signal belong to which methyl group. It need to be mention that there was a tiny peak at 13.42 ppm which could not be assigned, but when the ^{13}C -NMR was run with C-H coupling, this tiny peak did not show any coupling pattern. Therefore, it is assigned to a ^{13}C - labeled impurity. The temperature was slowly brought to $-50\text{ }^{\circ}\text{C}$, and the two peaks at 12.03 ppm and 16.97 ppm disappeared after 40 minutes at $-50\text{ }^{\circ}\text{C}$. The two peaks assigned to $\text{Pd-}^{13}\text{CH}_3\text{-I}$ and $^{13}\text{CH}_3\text{CH}_3$ preserved, and an increase in the intensity of these two peaks was observed. Due to the change of temperature, a up-field shift (7.46 ppm to 7.20 ppm for $^{13}\text{CH}_3\text{CH}_3$ and -8.97 ppm to -9.40 ppm for $\text{bis-NHC-Pd(II)-}^{13}\text{CH}_3\text{-I}$) of these two peaks was observed. The stacked ^{13}C -NMR spectra, which were recorded during the process of this reaction is shown in Figure 4.6.

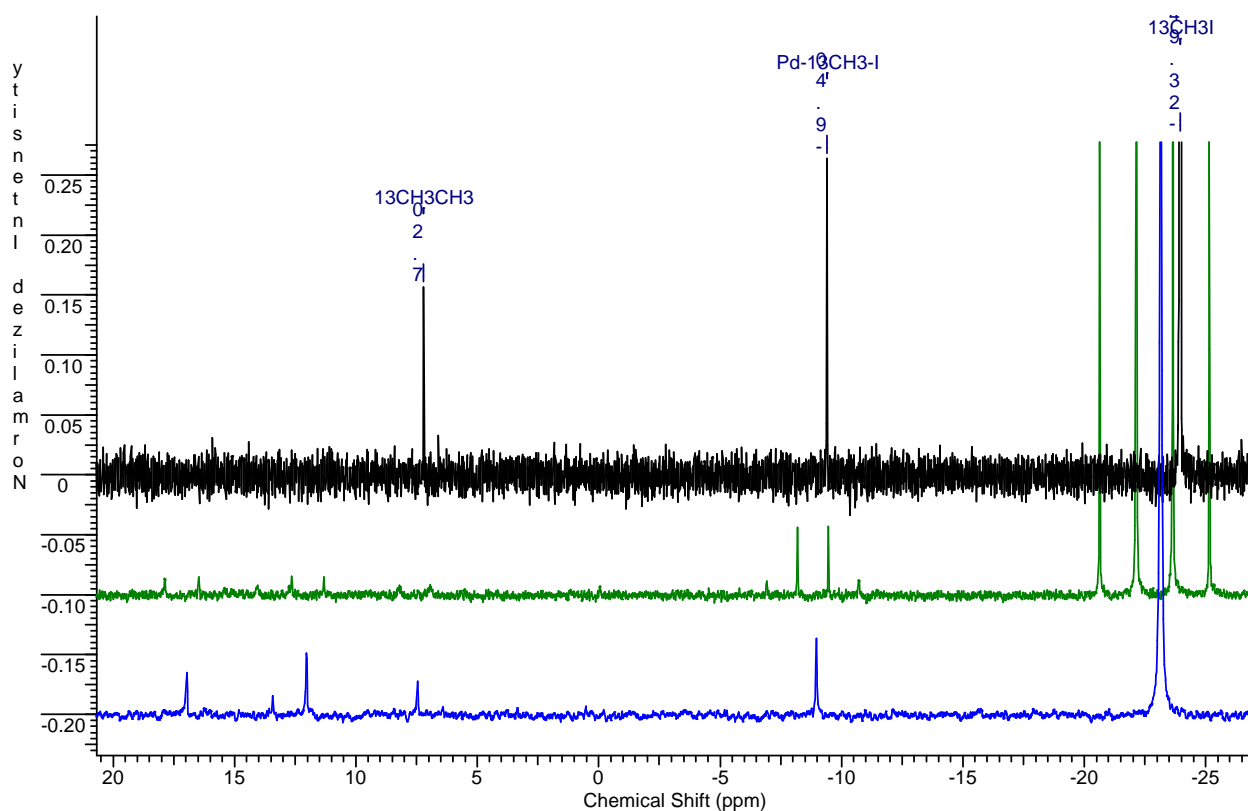


Figure 4.6 Stacked ^{13}C -NMR of the reaction between $\text{bis-NHC-Pd(II)-Me}_2$ complex and $^{13}\text{CH}_3\text{I}$ (blue: After 20 minutes reaction at $-50\text{ }^{\circ}\text{C}$, ^{13}C -NMR recorded at $-70\text{ }^{\circ}\text{C}$; green: After 20 minutes reaction at $-50\text{ }^{\circ}\text{C}$, ^{13}C -NMR recorded at $-70\text{ }^{\circ}\text{C}$ with carbon-hydrogen coupling; black: After 60 minutes reaction at $-50\text{ }^{\circ}\text{C}$, ^{13}C -NMR recorded at $-50\text{ }^{\circ}\text{C}$).

In the ^1H -NMR spectrum, a mixture of CH_3CH_3 (major peak at 0.84 ppm) and $^{13}\text{CH}_3\text{CH}_3$ (two triplet satellites at 0.69 ppm and 0.99 ppm with $J_{\text{C-H}}$ coupling constant of 119.2 Hz) as well as *bis*-NHC-Pd(II)-(CH₃)-I (major peak at 0.31 ppm) and *bis*-NHC-Pd(II)-($^{13}\text{CH}_3$)-I (two singlet satellites at 0.15 ppm and 0.47 ppm with $J_{\text{C-H}}$ coupling constant of 128.2 Hz) were clearly observed (Figure 4.7). The results obtained from this experiment provided more supportive information for the formation of the transient trimethyl *bis*-NHC-Pd(IV) intermediate produced from the oxidative addition of MeI to *bis*-NHC-Pd(II)-Me₂ complex.

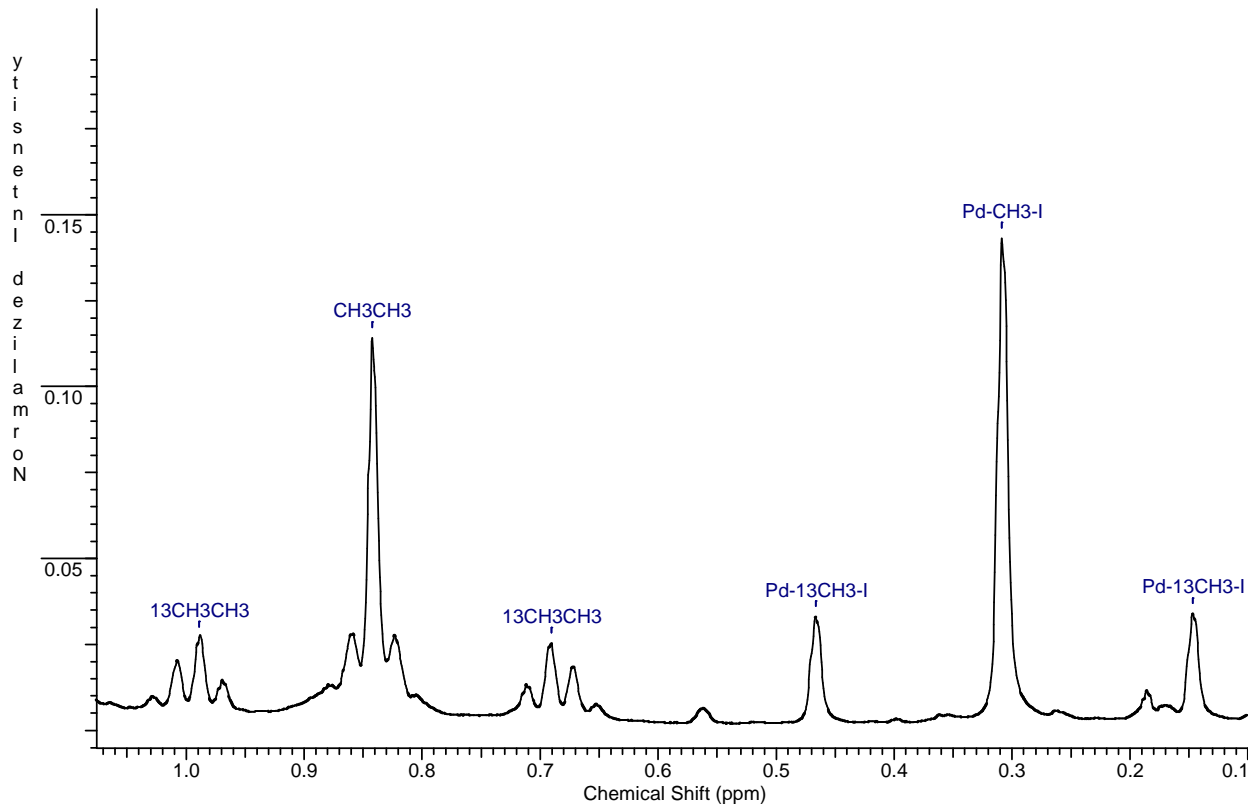


Figure 4.7 ^1H -NMR for the products after reductive elimination from the Pd(IV) species.

4.5 Mechanistic Discussion of the Oxidative Addition of MeI to the *Bis*-NHC-Pd(II)-Me₂ Complex and the Reductive Elimination from the Trimethyl *Bis*-NHC-Pd(IV) Species

4.5.1 Pathway for the Oxidative Addition

It has been established that the oxidative addition of MeI to square planar d⁸ complexes follows a S_N2 mechanism. For example, oxidative addition of MeI to bpy-Pt(II)-Me₂ complex **4.5** at -40 °C in CD₃CN resulted in a cationic species **4.6**, upon warming, cationic species **4.6** decayed to a pure neutral complex **4.7** (Figure 4.8). The initial oxidative addition was shown to be *trans* by using CD₃I as reagent and the scrambling of CH₃ and CD₃ groups occurred faster for the cationic species **4.6** than for neutral complex **4.7**.⁷

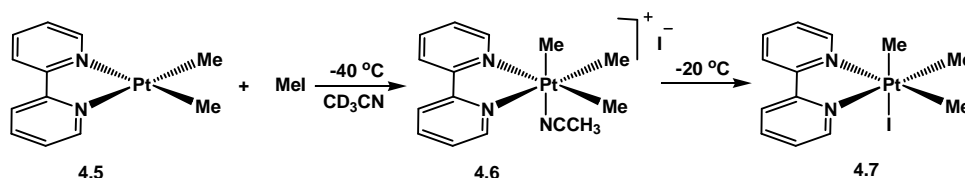


Figure 4.8 Oxidation of bpy-Pt(II)-Me₂ complex with methyl iodide.⁷

The same reaction was performed for the palladium analog bpy-Pd(II)-Me₂ complex **4.8**.⁸ The neutral complex **4.9** and the cationic species **4.10** were obtained with a ratio of 3:1. When the temperature was increased, the NMR-resonances of the methyl groups in the cationic species **4.10** became broad and coalesced at -5 °C, but the bpy resonance for the cationic species **4.10** and all the resonances for the neutral bpy-Pd-Me₃-I complex **4.9** remained sharp. This result indicated that intramolecular methyl groups scrambling occurred in the cationic species **4.10**, but not in the neutral complex **4.9** (Figure 4.9).

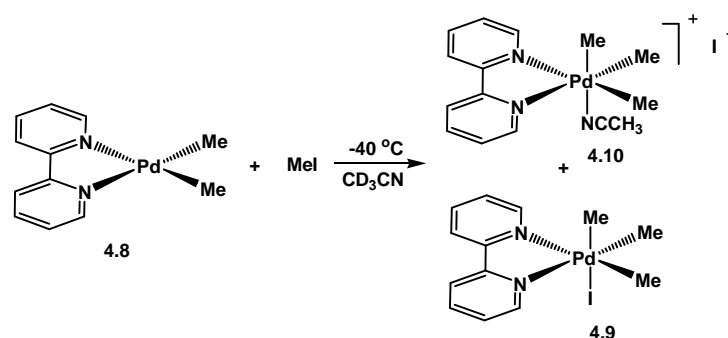


Figure 4.9 Oxidation of bpy-Pd(II)-Me₂ complex with methyl iodide.⁸

Kinetic studies of both [PdMe₂(bpy)] and [PtMe₂(bpy)] in the presence of excess MeI were carried out by Canty's group using UV-kinetics.⁸ Both of these two oxidative addition reactions followed second-order kinetics, (first-order for each reagent). The large negative ΔS^\ddagger values that have been determined in these experiments strongly supported the assumption of S_N2 mechanism for the oxidative addition in both cases (Table 4.1).

Table 4.1 Second-order rate constants for oxidative addition of MeI to [MMe₂(bpy)] in acetone (table redraw from reference 8 without permission).⁸

M	T, °C	k ₂ , L mol ⁻¹ s ⁻¹	E _a , kJ mol ⁻¹	ΔS [‡] (20 °C) J K ⁻¹ mol ⁻¹
Pd	3.0	1.75 ± 0.05		
Pd	10.3	2.25 ± 0.06		
Pd	20.0	3.23 ± 0.08		
Pd	30.0	4.65 ± 0.10	25.3 ± 0.6	-148 ± 2
Pt	-7.5	14 ± 1		
Pt	3.6	22 ± 1		
Pt	20	40 ± 1	24.9 ± 0.1	-129 ± 1

It is our mechanistic paradigm that the oxidative addition of MeI to the *bis*-NHC-Pd(II)-Me₂ complex also follows the S_N2 mechanism. Only one intermediate was observed in the course of the reaction at -50 °C, and so far we could not determine whether it is a neutral *bis*-NHC-

Pd(IV)-Me₃-I complex or a cationic [*bis*-NHC-Pd(IV)-Me₃-THF]⁺I⁻ species. But, according to the finding described in the literature, the most likely intermediate is a cationic species. Our argument is, when ¹³CH₃I was used as a reagent, two distinct resonances for the axial and equatorial methyl groups of the *bis*-NHC-Pd(IV)-Me₃ species were observed in the ¹³C-NMR spectrum, which indicated that the intramolecular scrambling of ¹³CH₃ and CH₃ had occurred even at -50 °C. Based on the results obtained by Puddephatt and Canty, the methyl groups scrambling occurred faster in the cationic [(byp)PtMe₃] species⁷ and only in the cationic [(bpy)PdMe₃] species.⁸ Therefore, it is straightforward to conclude that the observed intermediate is the cationic [*bis*-NHC-Pd(IV)-Me₃-THF]⁺ species.

4.5.2 Pathway for Reductive Elimination

The reductive elimination from a five-coordinated cationic d⁶ complex has been well studied.^{3a,9} In 2005, the Goldberg group synthesized a series of cationic trimethylpyridine*bis*-(diphenylphosphinoethane)platinum(IV) { *fac*-[(dppe)Pt(IV)Me₃(4-NC₅H₄X)][OTf] } complexes, in which 4-NC₅H₄X are uncharged 4-substituted pyridine derivatives (X=NH₂, Me, Ph, and CN). The dependence of the reductive elimination of ethane on the electronic properties of the platinum-bound nitrogen donor was studied.¹⁰ It was found that the reaction is considerably faster for more electron-withdrawing substituents than for electron-donating substituents. In the Hammett plot showed in Figure 4.10, a positive ρ -value of 1.9 was obtained, indicating that the electron-withdrawing groups decrease the donor ability of the pyridine, thus facilitating the release of the pyridine ligands. This favors the formation of penta-coordinated intermediates.

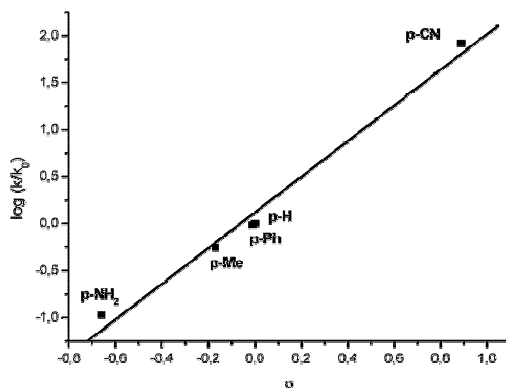


Figure 4.10 Hammett plot for electronic effects on reductive elimination (Figure taken from reference 10 without permission).¹⁰

These results support the proposed reaction mechanism for the reductive elimination reaction. The reductive elimination of ethane proceeds by a two step pathway: in the first step, the reversible dissociation of the pyridine derivative occurs from the cationic complex to generate a five-coordinated Pt(IV) intermediate; in the second step, irreversible and therefore, rate-determining elimination of ethane occurs from the penta-coordinate Pt(IV) intermediate (Figure 4.11).

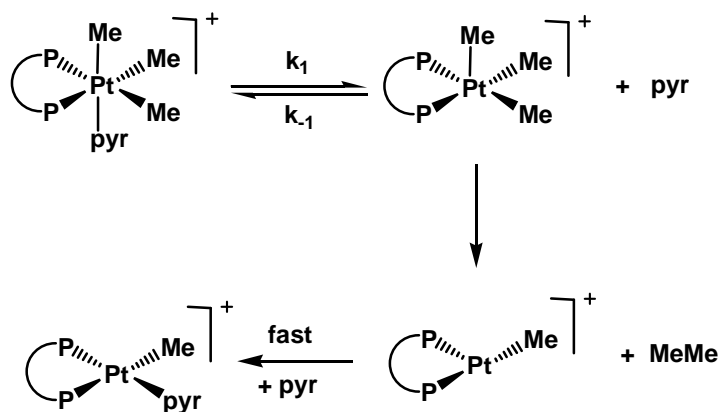


Figure 4.11 Proposed reaction mechanism for the reductive elimination reaction.¹⁰

On the basis of these literature findings, we propose that the reductive elimination of ethane from the $[bis\text{-NHC-Pd(IV)-Me}_3\text{-THF}]^+$ proceeds via a penta-coordinated Pd(IV) species. Because THF is a very weak coordinate solvent, it can easily dissociate from the six-fold-coordinated $[bis\text{-NHC-Pd(IV)-Me}_3\text{-THF}]^+$ intermediate to form a penta-coordinated $[bis\text{-NHC-Pd(IV)-Me}_3]^+$ species. In fact, the reductive elimination of ethane in THF- d_8 is so fast that only a very small amount of transient $[bis\text{-NHC-Pd(IV)-Me}_3\text{-THF}]^+$ intermediate was observed in the $^1\text{H-NMR}$ spectrum at $-50\text{ }^\circ\text{C}$, and it disappeared as soon as the $bis\text{-NHC-Pd(II)-Me}_2$ was consumed. To further verify our proposed mechanism of the reductive elimination, the oxidative addition of $^{13}\text{CH}_3\text{I}$ to $bis\text{-NHC-Pd(II)-Me}_2$ complex in the presence of 10 equivalent of DMAP was carried out. A stacked $^{13}\text{C-NMR}$ spectrum is showed in Figure 4.12. Two new resonances for the axial and equatorial methyl groups of the $[bis\text{-NHC-Pd(IV)-Me}_3]$ intermediate were observed at 8.73 ppm and 17.50 ppm in the $^{13}\text{C-NMR}$ spectrum at $-50\text{ }^\circ\text{C}$. It is worth mentioning that there is a large up-field shift for the axial methyl resonance compared with that of the reaction without addition of DMAP (8.73 ppm to 12.03 ppm). The dramatic change in chemical shift reflected the change of the chemical environment for the axial methyl group in the $[bis\text{-$

NHC-Pd(IV)-Me₃]⁺ intermediate, which is a good indication that DMAP coordinated to the palladium center to form a [*bis*-NHC-Pd(IV)-Me₃-DMAP]⁺T intermediate. The reductive elimination of ethane from this Pd(IV) intermediate was very slow at -50 °C, but when the temperature was raised to -30 °C, the reaction finished in one hour. In the ¹³C-NMR, a resonance at -2.86 ppm for the mono-methyl Pd(II) species resulting from the reductive elimination reaction was observed. There is a dramatic down-field shift compared to that of the reaction without addition of DMAP (-9.40 ppm). It is our working hypothesis that instead of a neutral Pd(II) complex, a cationic [*bis*-NHC-Pd(II)-Me-DMAP]⁺ species has formed after the reductive elimination.

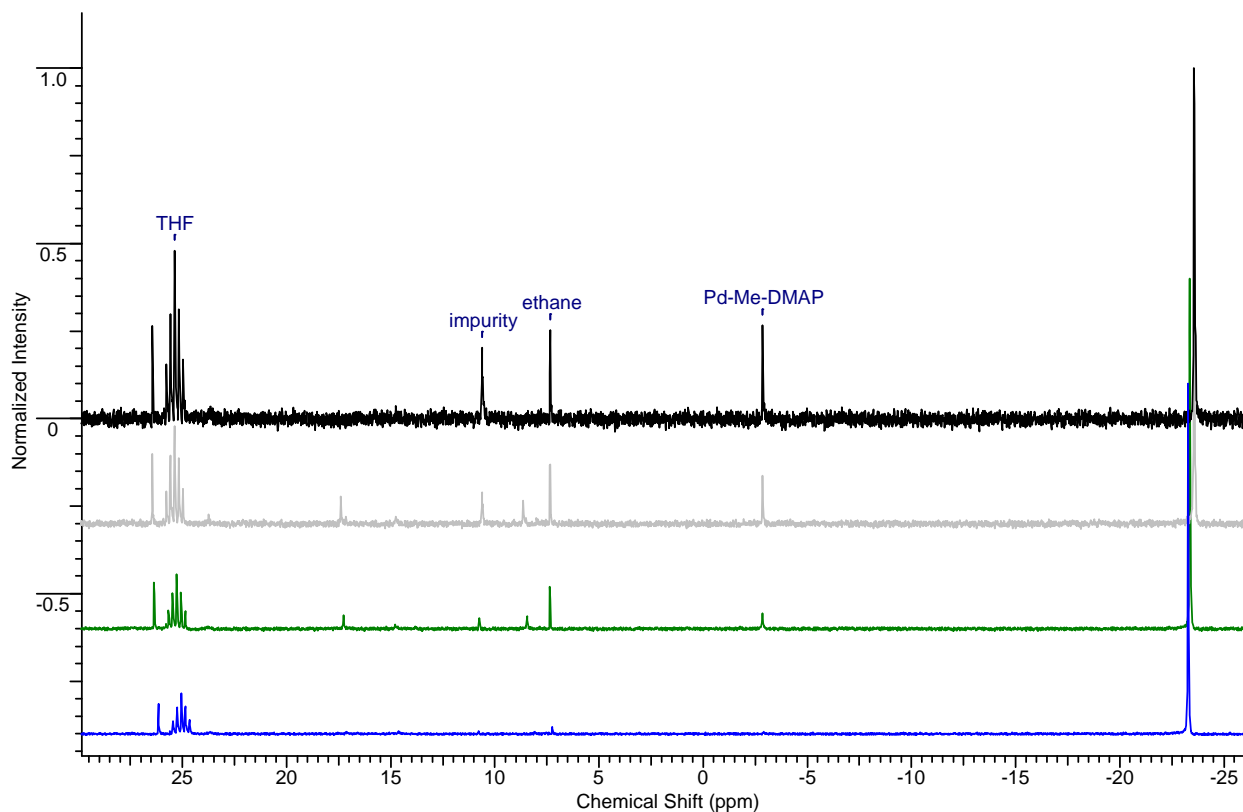


Figure 4.12 Stacked ¹³C-NMR of the reaction between *bis*-NHC-Pd(II)-Me₂ and ¹³CH₃I in the presence of DMAP (blue: reaction at -50 °C for 20 min; green: reaction at -30 °C for 20 minutes; gray: reaction at -30 °C for 40 minutes; black: reaction at -30 °C for 60 minutes)

4.6 Experimental

4.6.1 Synthesis of *bis*-NHC-Pd(II)-(CH₃)₂ complex 4.1

In a nitrogen filled glove-box, 1.2 mL 0.50 M MeMgBr ether solution was added to a suspension of 120 mg *bis*-NHC-Pd(II)-Br₂ complex **2.2** in 10 mL dry THF. The reaction mixture was stirred at room temperature for 1 hour, a clear colorless solution formed. After removal of the solvent under reduced pressure, 5 mL pre-dried 1,4-dioxane was added to the solid residue and stirred at room temperature for 5 min. The undissolved white solid was removed by filtering through a short pad of dry celite and the filter-cake was washed with 1 mL portion of dry THF for three times. The filtrate was concentrated to dryness. 76.3 mg (90.2% yield) product was obtained as a white solid. ¹H-NMR (δ_H; 400 Hz, THF-*d*₈): -0.32 (s, 6H, Pd-CH₃), 3.72 (s, 6H, N-CH₃), 5.92 (d, 1H, *J* = 12.82 Hz, N-CH₂), 6.08 (d, 1H, *J* = 12.82 Hz, N-CH₂), 7.06 (d, 2H, *J* = 1.83 Hz, N-CH), 7.27 (d, 2H, *J* = 1.83 Hz, N-CH).

4.6.2 VT-NMR study of the reaction between *bis*-NHC-Pd(II)-(CH₃)₂ complex 4.1 and CH₃I

8.0 mg (0.025 mmol) *bis*-NHC-Pd(II)-Me₂ complex was dissolved in 0.60 mL pre-dried THF-*d*₈ in a J-Young NMR tube, after cooling to -70 °C, 2 equivalents of MeI in 0.10 mL THF-*d*₈ stock solution were added by means of a syringe under nitrogen protection. The NMR tube was carefully shaken to disperse the MeI thoroughly in the sample at -70 °C, and then quickly inserted into a pre-cooled NMR probe (-70 °C). The reaction process was carefully monitored by ¹H-NMR at various temperatures. (The detailed NMR spectrum of the intermediate is shown in the appendix **A.17**).

4.6.3 VT-NMR study of the reaction between *bis*-NHC-Pd(II)-(CH₃)₂ and ¹³CH₃I

8.0 mg (0.025 mmol) *bis*-NHC-Pd(II)-Me₂ complex was dissolved in 0.60 mL pre-dried THF-*d*₈ in a J-Young NMR tube, after cooling to -70 °C, 2 equivalents of ¹³C labeled MeI in 0.10 mL THF-*d*₈ stock solution were added by means of a syringe under nitrogen protection. The NMR tube was carefully shaken to disperse the MeI thoroughly in the sample at -70 °C, and then quickly inserted into a pre-cooled -70 °C NMR probe. The reaction process was carefully monitored by ¹³C-NMR at various temperatures.

4.6.4 VT-NMR study of the reaction between *bis*-NHC-Pd(II)-(CH₃)₂ and ¹³CH₃I in the presence of DMAP

8.0 mg (0.025 mmol) *bis*-NHC-Pd(II)-Me₂ complex was dissolved in 0.50 mL pre-dried THF-*d*₈ in a J-Young NMR tube, after cooling to -70 °C, 2 equivalents of ¹³C labeled MeI in 0.10 mL THF-*d*₈ stock solution and 10 equivalents of DMAP in 0.10 mL THF-*d*₈ stock solution were added by means of a syringe under nitrogen protection. The NMR tube was carefully shaken to disperse the MeI thoroughly in the sample at -70 °C, and then quickly inserted into a pre-cooled -70 °C NMR probe. The reaction process was carefully monitored by ¹³C-NMR at various temperatures.

References

1. Tolman, R. C. "The Principles of Statistical Mechanics," **1938**. Oxford University Press, London, UK.
2. Stahl, S. S.; Labinger, J. A.; Bercaw, J. E. "Exploring the mechanism of aqueous C-H activation by Pt(II) through model chemistry: Evidence for the intermediacy of alkylhydridoplatinum(IV) and alkane σ -adducts," *J. Am. Chem. Soc.* **1996**, *118*, 5961-5976.
3. (a) de Graaf, W.; Boersma, J.; Smeets, W. J. J.; Spek, A. L.; van Koten, G. "Dimethyl(N,N,N',N')-tetramethylethanediamine)palladium(II) and dimethyl[1,2-bis(dimethylphosphino)ethane]palladium(II): Synthesis, X-ray crystal structures, and thermolysis, oxidative-addition, and ligand-exchange reactions," *Organometallics* **1989**, *8*, 2907-2917.
(b) Byers, P. K.; Canty, A. J. "Synthetic routes to methylpalladium(II) and dimethylpalladium(II) chemistry and the synthesis of new nitrogen donor ligand system," *Organometallics* **1990**, *9*, 210-220.
(c) Canty, A. J.; Jin, H.; Roberts, A. S.; Skelton, B. W.; White, A. H. "Oxidation of diorganopalladium(II) complexes by water and halogens: reactions involving methyl group transfer and structural studies of hydrogen-bonded adducts formed by aryl alcohols with the palladium(IV)cyclopentane complex $\text{Pd}(\text{CH}_2\text{CH}_2\text{CH}_2\text{CH}_2)(\text{OH})\{(\text{pz})_3\text{BH}\}$ ($[(\text{pz})_3\text{BH}]^- = \text{tris}(\text{pyrazol-1-yl})\text{borate}$)," *Organometallics* **1996**, *15*, 5713-5722.
4. Pope, W. J.; Peachey, S. J. "A new class of organo-metallic compounds. Preliminary notice. Trimethylplatinimethyl hydroxide and its salt," *Proc. Chem. Soc., London* **1907**, *23*, 86-87.
5. Byers, P. K.; Canty, A. J.; Skelton, B. W.; White, A. H. "The oxidative addition of iodomethane to $[\text{PdMe}_2(\text{bpy})]$ and X-ray structure of the organopalladium(IV) product $\text{fac-}[\text{PdMe}_3(\text{bpy})\text{I}]$ ($\text{bpy} = 2,2'$ -bipyridyl)," *J. Chem. Soc., Chem. Commun.* **1986**, 1722-1724.
6. Gillie, A.; Stille, J. K. "Mechanisms of 1,1-reductive elimination from palladium," *J. Am. Chem. Soc.* **1980**, *102*, 4933-4941.

7. Crespo, M.; Puddephatt, R. J. "Cationic intermediates in oxidative addition reactions of alkyl halides to d8 complexes: Evidence for the S_N2 mechanism," *Organometallics* **1987**, *6*, 2548-2550.
8. Byers, P. K.; Canty, A. J.; Crespo, M.; Puddephatt, R. J.; Scott, J. D. "Reactivity and mechanism in oxidative addition to palladium(II) and reductive elimination from palladium(IV) and an estimate of the palladium methyl bond energy," *Organometallics* **1988**, *7*, 1363-1367.
9. Canty, A. J.; Hoare, J. L.; Davies, N. W.; Traill, D. R. "Synthesis and decomposition behavior of pallada(IV)cyclopentane complexes," *Organometallics* **1998**, *17*, 2046-2051.
10. Procelewska, J.; Zahl, A.; Liehr, G.; van Eldik, R.; Smythe, N. A.; Williams, B. S.; Karen I. Goldberg, K. I. "Mechanistic information on the reductive elimination from cationic trimethylplatinum(IV) complexes to form carbon-carbon Bonds," *Inorg. Chem.*, **2005**, *44*(22) 7732-7742.

Chapter 5 Dioxygen Triggered C-C Bond Formation and C-O Bond Formation from the *Bis*-NHC-Pd(II)-Me₂ Complex

5.1 Introduction

From a practical standpoint, dioxygen is undoubtedly the most attractive reagent for hydro-carbon oxidation reactions.¹ The most notable example is the Wacker process which has been used in industry for than 40 years to oxidize ethylene to acetaldehyde, using PdCl₂ and CuCl₂ as catalysts and dioxygen as oxidant to regenerate the catalysts (Figure 5.1).^{2,3,4}

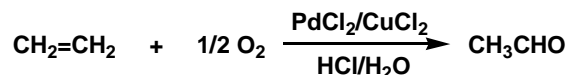


Figure 5.1 Wacker process.²

Stoichiometric reaction between dioxygen and well-defined platinum and palladium complexes were reported by different research groups.^{5,6,7,8,9}

5.1.1 Examples of Reaction between Dioxygen and Pt(II) Complexes

Goldberg and Bercaw reported the oxidation of dimethylplatinum(II) complexes with dioxygen in 1998.⁵ It was found that in methanol, di-nitrogen based ligands (bpy, phen and tmeda) stabilized (N-N)Pt(II)(CH₃)₂ complexes **5.1** can be oxidized to (N-N)Pt(IV)(OCH₃)(OH)(Me)₂ complexes **5.2**, and 0.5 equivalent of molecular O₂ was consumed per atom of platinum(II). The resulting Pt(IV) complexes were stable at room temperature and no reductive elimination of ethane was observed (Figure 5.2).

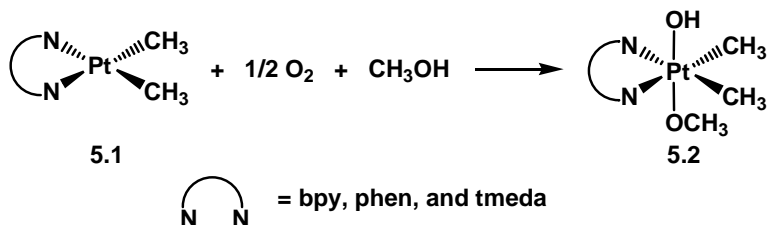


Figure 5.2 Oxidation of Pt(II) complexes to Pt(IV) complexes by dioxygen.⁵

Further mechanistic studies carried out in Bercaw's group revealed that the oxidation of (tmeda)Pd(II)(CH₃)₂ to (tmeda)Pt(IV)(OH)(OCH₃)(CH₃)₂ by dioxygen in methanol proceeds via a two-step mechanism. In the first step, (tmeda)Pt(CH₃)₂ reacts with dioxygen to yield a hydroperoxoplatinum(IV) intermediate (tmeda)Pt(OOH)(OCH₃)(CH₃)₂ **5.3**. In the second step, the intermediate (tmeda)Pt(OOH)(OCH₃)(CH₃)₂ reacts with a second equivalent of (tmeda)Pt(II)(CH₃)₂ to yield 2 equivalents of (tmeda)Pt(II)(OCH₃)(OH)(CH₃)₂ as final product (Figure 5.3).⁶

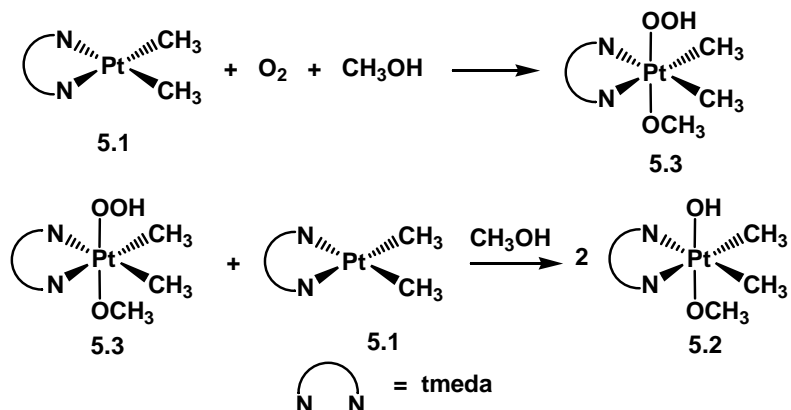


Figure 5.3 A two-step mechanism for the oxidation (tmeda)Pd(II)Me₂ to (tmeda)Pt(IV)Me₂(OH)(OCH₃) by dioxygen.⁶

The authors proposed that the interaction of dioxygen with (N-N)Pt(II)(CH₃)₂ complexes resulted in either η^1 - or η^2 - (N-N)Pt(IV)(CH₃)₂ dioxygen complexes **5.4** and **5.5**. Protonation of the dimethylplatinum(IV) dioxygen complex gave the intermediate (tmeda)Pt(OOH)(OCH₃)(CH₃)₂ species **5.3** (Figure 5.4). It is noteworthy that the strong σ -donating methyl ligands of the dimethylplatinum(II) complex showed a pronounced effect on the reactivity towards dioxygen, whereas (tmeda)Pt(CH₃)₂ is readily oxidized by dioxygen, no oxidation takes place with (tmeda)Pt(CH₃)Cl, (tmeda)PtCl₂ or (tmeda)Pt(C₆H₅)₂.

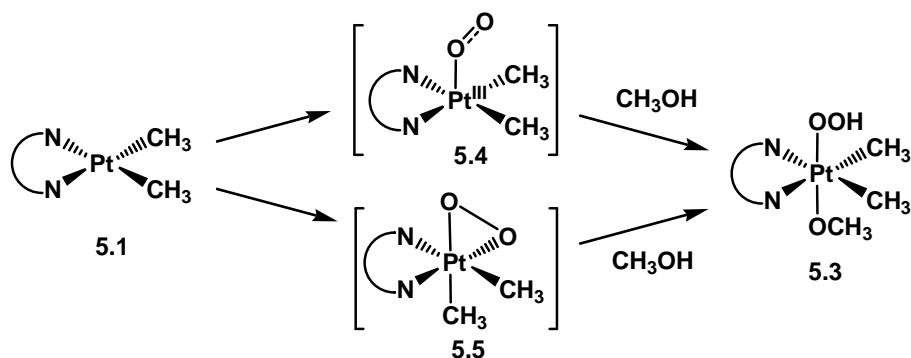


Figure 5.4 Proposed two pathways for the interaction of dioxygen with Pt(II) complexes.⁶

5.1.2 Examples of Reaction between Dioxygen and Pd(0), Pd(II) complexes.

In 2004, Stahl's group reported the synthesis of the η^2 -peroxo (IMes)₂Pd(O₂) complex **5.7** by the reaction of (IMes)₂Pd(0) complex **5.6** with dioxygen at -78 °C in toluene.⁷ This complex was fully characterized by ¹H-, ¹³C-NMR spectroscopy and IR spectroscopy. The structure of this complex was definitely established by X-ray crystallography. The hydroperoxopalladium(II) complex **5.8** was formed rapidly when one equivalent of acetic acid was added to a toluene solution of complex **5.7** at room temperature (Figure 5.5).

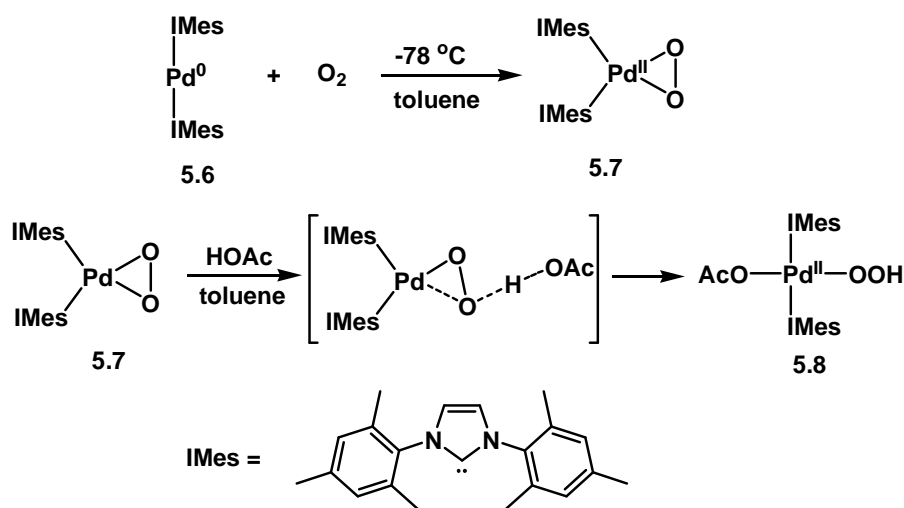


Figure 5.5 The oxidation of (IMes)₂Pd(0) with dioxygen to form η^2 -peroxo (IMes)₂Pd(O₂) complex, and protonation of this complex to form the hydroperoxopalladium(II) complex.⁷

Further studies revealed that the hydroperoxopalladium(II) complex **5.8** could also be prepared by dioxygen insertion into a Pd(II)-hydride species **5.9**, which was quantitatively generated by the reaction of one equivalent of acetic acid with (IMes)₂Pd(0) complex **5.6** (Figure 5.6).⁸

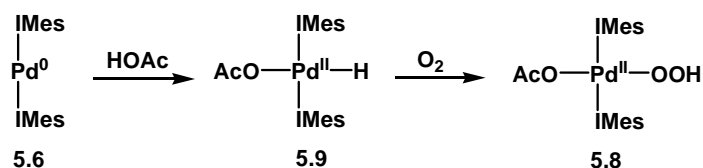


Figure 5.6 Dioxygen insertion into a Pd-H bond.⁸

One of the possible mechanisms for the reaction of dioxygen with a Pd(II)-hydride to produce a Pd(II)-hydroperoxide was proposed by Stahl et al, as Pd(IV)-peroxo pathway (Figure 5.7). In the first step, oxidative addition of dioxygen to the Pd(II) center can yield an η^2 -peroxo-Pd(IV) intermediate **5.10**. In the second step, reductive elimination of an O-H bond from the η^2 -peroxo-Pd(IV) intermediate can lead to the hydroperoxide product. The authors argued that the access to Pd(IV) oxidation state could be facilitated by the presence of strong electron-donating NHC ligands.⁹

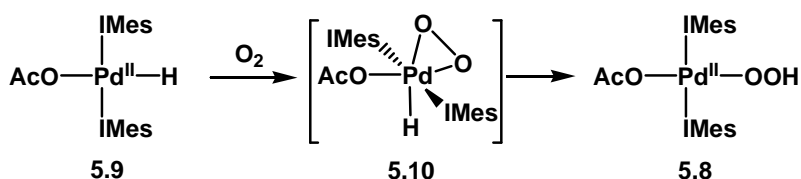


Figure 5.7 One of the proposed pathways for the dioxygen insertion into Pd-H bond.⁹

5.2 Synthesis of 1,1'-Di(n-butyl)-3,3'-Methylene-4-Diimidazolin-2,2'-Diyldene Palladium(II) Dimethyl Complex

I have found that the *bis*-NHC-Pd(II)-Br₂ complex **2.2** can be dissolved in only polar solvents such as DMSO and DMF. The *bis*-NHC-Pd(II)-Me₂ complex **4.1** can be dissolved in THF, but the solubility of the *bis*-NHC(Me)₂-Pd(II)-Me-I complex **4.4** resulted from the

reductive elimination of ethane is not good in THF, and with the progress of the reaction, this species precipitates out from the solution. To improve the solubility, a *n*-butyl side chain was introduced to the *bis*-NHC ligand. 1-*n*-butyl imidazole **5.11** was obtained with over 90% yield by treating imidazole with excess of KOH powder in THF first, and then with *n*-BuBr. The *bis*-imidazolium salt **5.12** was obtained with 78% yield by heating neat 1-*n*-butyl-imidazole and dibromomethane at 130 °C for 24 hours in a sealed tube. The *bis*-NHC-Pd(II)-Br₂ complex **5.13** was synthesized according literature reported method with 83% yield.¹⁰ This complex is soluble in THF, CH₃CN, and slightly soluble in CHCl₃ and CH₂Cl₂. The *bis*-NHC-Pd(II)-Me₂ complex **5.14** was synthesized by the reaction of the *bis*-NHC-Pd(II)-Br₂ **5.13** with MeMgBr in THF with 82.1% yield, and it is soluble in THF, CH₃CN, CH₂Cl₂. The synthesis of the *bis*-NHC-Pd(II)-Me₂ complex **5.14** is outlined in Figure 5.8.

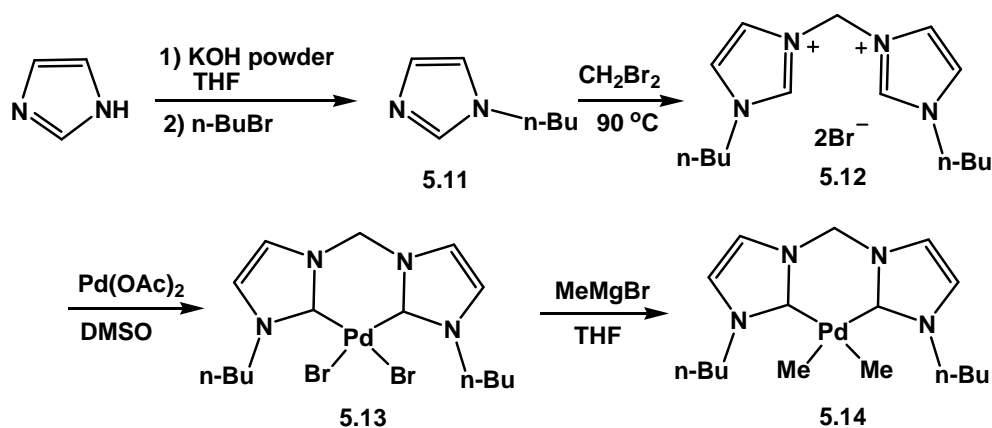


Figure 5.8 Synthesis of the *bis*-NHC-Pd(II)-Me₂ complex **5.14**.

5.3 Oxygen Triggered C-C Bond Formation

In a nitrogen filled glovebox, 10 mg *bis*-NHC-Pd(II)-Me₂ complex **5.14** was dissolved in 0.6 mL pre-dried CD₃CN in a J-Young NMR tube. After degassing the sample by three consecutive freeze, pump and-thaw cycles, 1 atm. of pre-dried O₂ was introduced into the NMR tube at -20 °C. After carefully shaking in the cooling bath, the NMR tube was inserted in a NMR probe, which was pre-cooled to -20 °C. The reaction was monitored by ¹H-NMR at various temperatures. It was found that at -20 °C, the dimethylpalladium complex is stable in the presence of O₂. When the temperature was raised to 20 °C, the integration of the resonance for

the methyl groups on the palladium center at -0.32 ppm started to decrease, and simultaneously, all the $^1\text{H-NMR}$ resonances for the ligand become broad. The reaction was completed within 2 hours, and a lot of white precipitate was formed in the NMR tube, and the ethane resonance, which was masked by the resonance of the methyl group of the n-butyl side chain appeared at 0.85 ppm. Then the solvent was removed under vacuum. The residue in the NMR tube was re-dissolved in pre-dried DMSO and a small amount of palladium black was filtered off. $^1\text{H-NMR}$ showed that a symmetric *bis*-NHC-Pd species had formed. To avoid the masking effect of the ethane resonance by the butyl side chain, a separated reaction was carried out using *bis*-NHC-Pd(II)-Me₂ complex **4.1** as starting material. 8 mg of complex **4.1** was dissolved in dry 0.6 mL dry THF-*d*₈ in a J-Young NMR tube and treated with dry dioxygen. The $^1\text{H-NMR}$ clearly showed that upon reaction, the palladium containing species precipitated out and only ethane could be observed in the spectrum as a reductive elimination product.

Although no intermediate was observed by $^1\text{H-NMR}$ spectroscopy during the reaction, the reductive elimination of ethane gave strong indication that a η^2 -peroxo *bis*-NHC-Pd(IV)-(CH₃)₂-(O₂) intermediate **5.15** had formed via oxidation of *bis*-NHC-Pd(II)-(CH₃)₂ complex **5.14** with dioxygen. The combination of the chelated strong electron-donating *bis*-N-heterocyclic-carbene ligand with the strong σ -donating methyl ligand could indeed facilitate the formation of the Pd(IV) species. The reductive elimination of ethane from this Pd(IV) species resulted in a η^2 -peroxo *bis*-NHC-Pd(II)-(O₂) complex **5.16** (Figure 5.9).

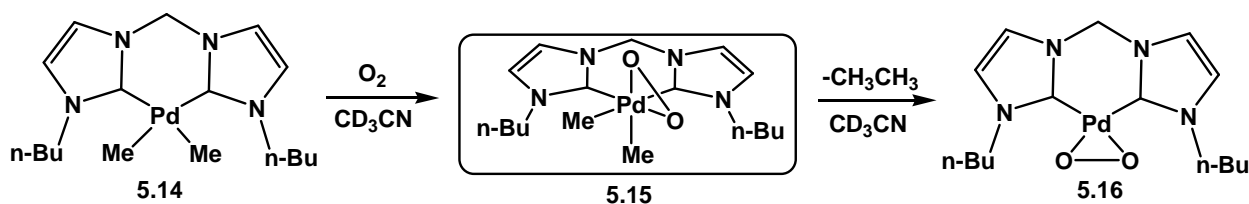


Figure 5.9 Proposed pathway for the reaction between the Pd(II) dimethyl complex **5.14** and dioxygen.

5.4 Oxygen Triggered C-C Bond Formation and C-O Bond Formation in the Presence of Water

In a nitrogen filled glove-box, 10 mg *bis*-NHC-Pd(II)-Me₂ complex **5.14** was dissolved in 0.60 mL pre-dried CD₃CN in a J-Young NMR tube. After degassed for three consecutive freeze, pump and-thaw cycles, the sample was cooled down to -20 °C. 0.05 mL CD₃CN which contained 1% of water (H₂O) was added under the protection of nitrogen (1 equivalent of H₂O relative to the palladium dimethyl complex). Then, 1 atm. of pre-dried O₂ was introduced into the NMR tube at -20 °C, and the sample was carefully swirled in the cooling bath. The NMR tube was inserted into a pre-cooled NMR probe (-20 °C) and the reaction was monitored at various temperatures. It was found that at 20 °C, the *bis*-NHC-Pd(II)-Me₂ complex **5.14** slowly decomposed and a proton resonance for methanol at 3.26 ppm appeared. During the reaction, two new up-field shifted methyl group resonances were observed at -0.23 ppm and -0.12 ppm, and with the progress of the reaction, these two peaks slowly disappeared. This observation gave strong indication that transient methylpalladium(IV) intermediates had formed during the reaction. The reaction was completed within 40 minutes, and by the end of the reaction, all the resonances for the *bis*-NHC ligand became broad, and the ethane resonance, which was masked by the resonance of the methyl group of the n-butyl side-chain appeared at 0.85 ppm. A small amount of methane at 0.20 ppm was also observed due to the protonation of the methyl groups on the palladium by water. The stacked ¹H-NMR spectrum is showed in Figure 5.10. A lot of black precipitate (metallic palladium) was formed in the NMR tube upon the completion of the reaction. After removing CD₃CN under vacuum, 0.80 mL DMSO-*d*₆ was added to the residue and palladium black was filtered off. The ¹H-NMR of the residue was too complicated to be resolved.

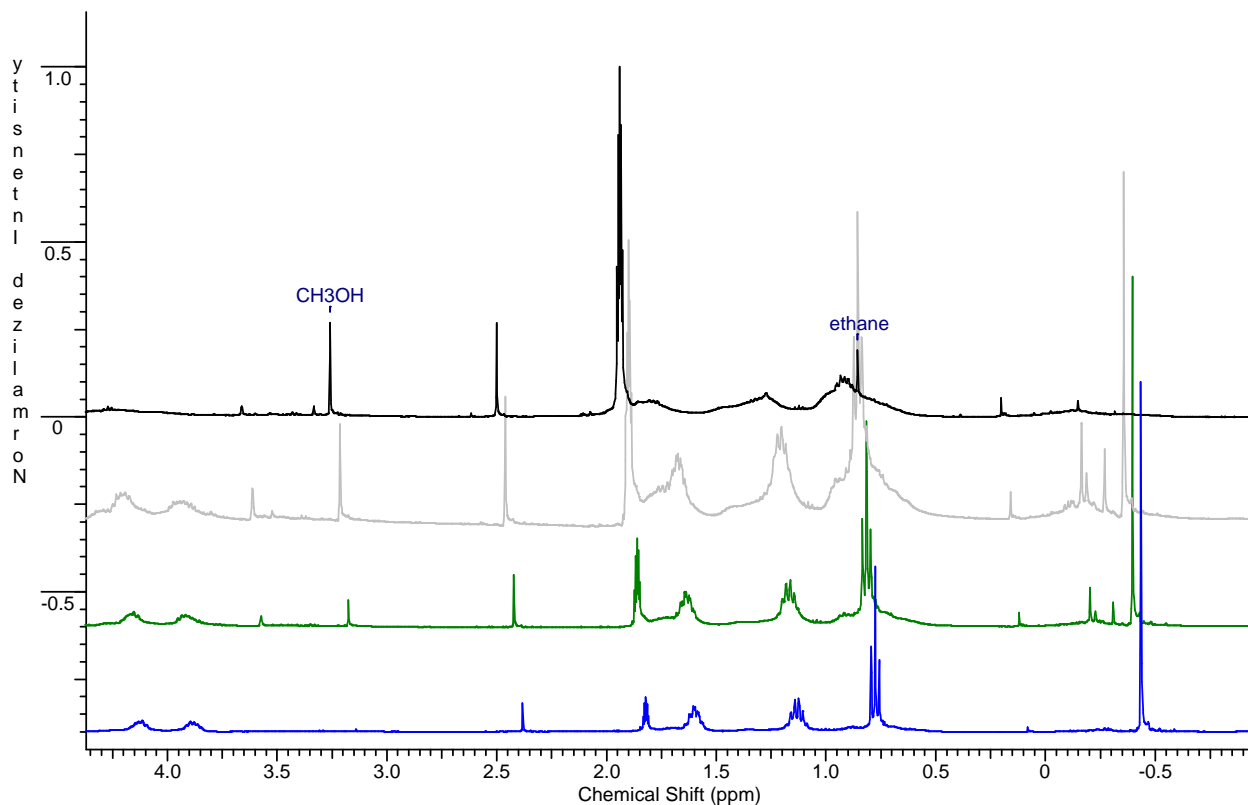


Figure 5.10 Stacked ^1H -NMR spectrum for the reaction between the palladium(II) dimethyl complex **5.14** with dioxygen in the presence of H_2O .

To further verify the formation of methanol and ethane, the ^{13}C labeled *bis*-NHC-Pd(II)-($^{13}\text{CH}_3$)₂ complex was synthesized by reacting the *bis*-NHC-Pd(II)-Br₂ complex **5.13** with $^{13}\text{CH}_3\text{MgI}$. In the ^1H -NMR spectrum, two up-field shifted resonances at -0.47 ppm and -0.17 ppm for the palladium coordinated methyl groups were observed. Although these two peaks look like two singlets, they are actually belonging to a doublet with a characteristically large ^{13}C -H coupling constant (123.64 Hz), (detailed ^1H -NMR showed in appendix). After treating with O_2 and H_2O under the same conditions as in the previous experiment, this complex decomposed slowly and a doublet for $^{13}\text{CH}_3\text{OH}$ between 3.08 ppm and 3.43 ppm with ^{13}C -H coupling constant of 139.42 Hz (Figure 5.11) together with a doublet for $^{13}\text{CH}_3^{13}\text{CH}_3$ between 0.70 ppm and 1.00 ppm with ^{13}C -H coupling constant of 121.56 Hz (Figure 5.12) were observed. The result from this experiment clearly showed that both C-O bond and C-C bond formation occurred during the reaction of *bis*-NHC-Pd(II)-(CH_3)₂ complex **5.14** with dioxygen in the presence of water.

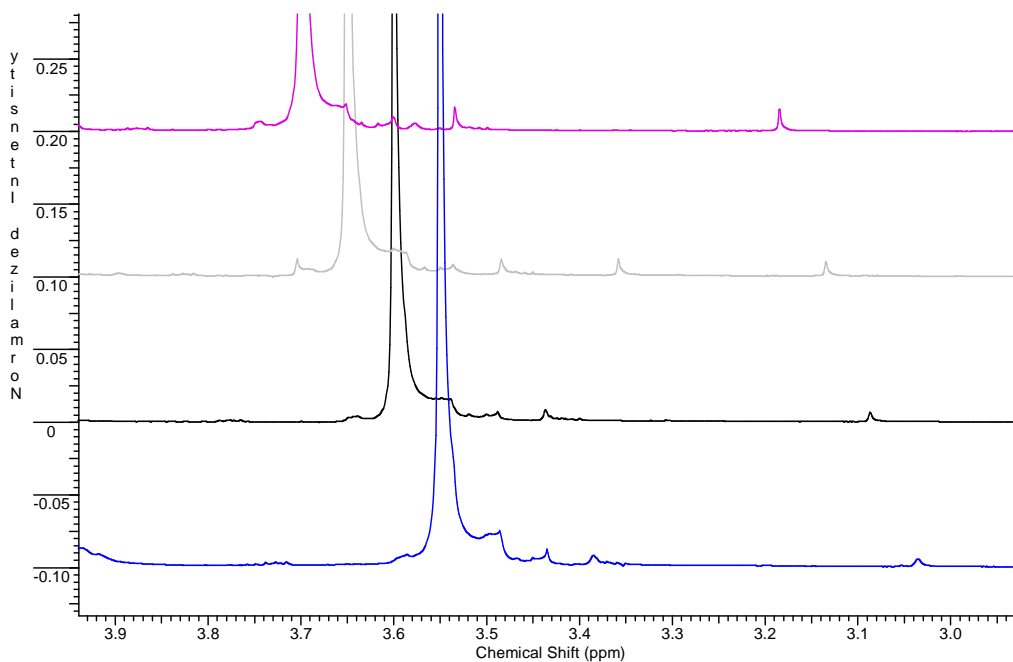


Figure 5.11 Expanded methanol region for the reaction between the *bis*-NHC-Pd(II)-($^{13}\text{CH}_3$) $_2$ complex and dioxygen in the presence of H_2O .

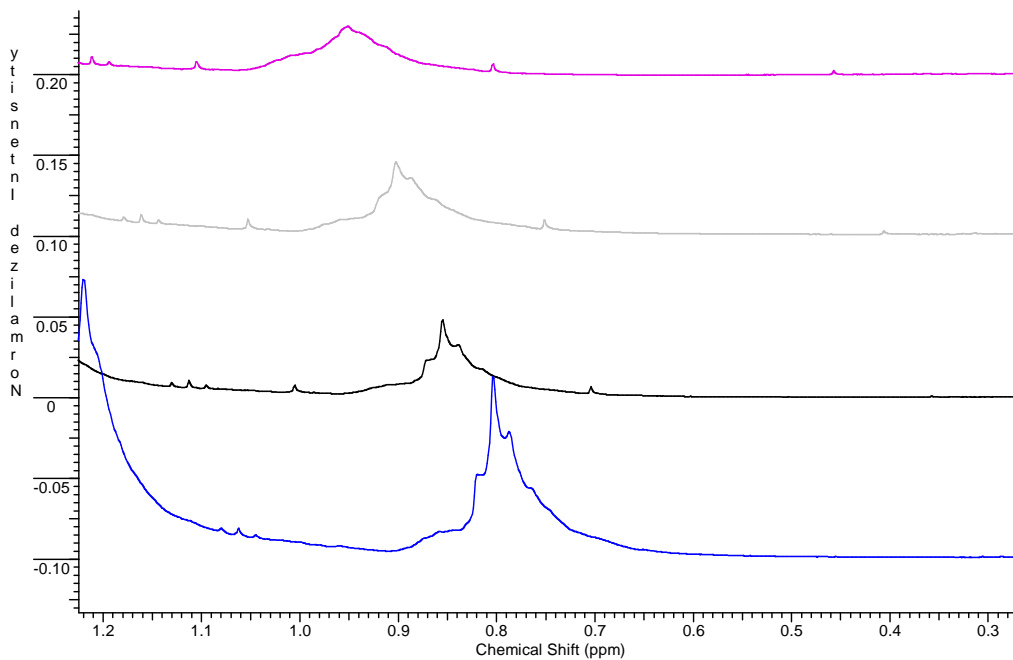


Figure 5.12 Expanded ethane region for the reaction between the *bis*-NHC-Pd(II)-($^{13}\text{CH}_3$) $_2$ complex and dioxygen in the presence of H_2O .

There are at least two reaction pathways as described in Figure 5.13 that should be taken into consideration. In the first pathway, dioxygen reacts with palladium(II) dimethyl complex **5.14** to form a η^2 -peroxo *bis*-NHC-Pd(IV)-(CH₃)₂-(O₂) intermediate **5.15**, from which, the ethane formation goes through a intramolecular C-C bond forming reductive elimination process, and similar to the Shilov system, the methanol formation goes through a S_N2 type external water attacking of the methyl group of the Pd(IV) intermediate process to produce complex **5.17** as product. In the second pathway, protonation of the η^2 -peroxo *bis*-NHC-Pd(IV)-(CH₃)₂-(O₂) intermediate **5.15** leads to the formation of *bis*-NHC-Pd(IV)-(OH)-(OOH)-(CH₃)₂ intermediate **5.18**, and from which, competitive C-O and C-C reductive elimination occurs to form methanol and ethane as well as palladium(II) complexes **5.19** and **5.17**.

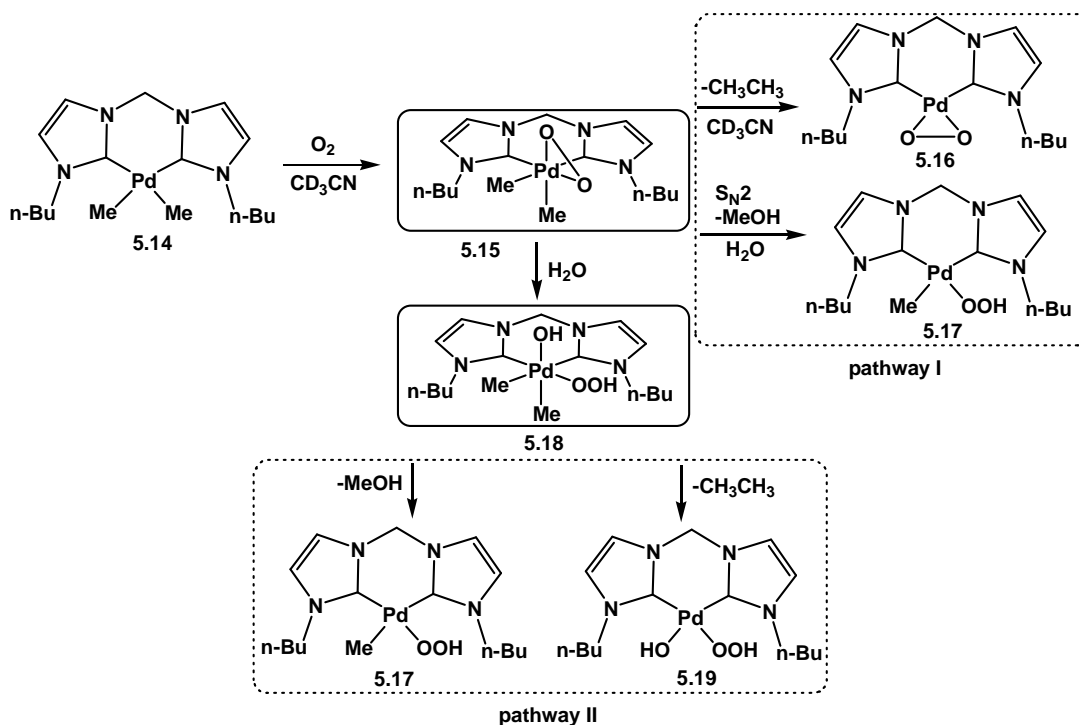


Figure 5.13 Two proposed pathways for the reaction between the palladium(II) dimethyl complex **5.14** with dioxygen in the presence of H_2O .

This experiment provided unprecedented supportive information that with the facilitation of strong electron-donating ligands, such as N-heterocyclic carbenes and strong σ -donating methyl ligands, high oxidation state of Pd(IV) can be achieved by using dioxygen as an oxidant. Furthermore, both C-C bond and C-O bond formation, possibly involving reductive elimination

from this Pd(IV) species or S_N2 type external attacking of methyl groups bonded to the Pd(IV) species were observed. To understand this intriguing system in more detail, careful mechanistic studies have to be carried out in the future.

5.5 Experimental

5.5.1 Synthesis of n-butyl imidazole 5.11.

To a solution of 6.8 g imidazole in 50 mL dry THF, 30 g KOH powder was added. After stirring at room temperature for 3 hours, the excess KOH was removed by filtration. 13.6 g n-butylbromide was added to the filtrate and the reaction mixture was stirred at room temperature for another 12 hours. The solvent was removed under reduced pressure. 11.6 g (93.5%) product was obtained as clear oil after removing the white precipitate (KBr) by filtration. ¹H-NMR (δ_{H} ; 400 Hz, DMSO-*d*₆): 0.88 (t, 3H,), 1.20 (sextet, 2H), 1.67 (quintet, 2H), 3.94 (t, 2H), 6.87 (t, 1H), 7.15 (t, 1H), 7.60 (s, 1H).

5.5.2 Synthesis of 1,1'-di-n-butyl-3,3'-methylenediimidazolium dibromide 5.12.

2.0 g n-butylimidazole and 1.70 g dibromomethane were stirred in a sealed tube at 130 °C for 24 hours. The produced solid was washed with hexane and dried under high vacuum. 2.70 g (78%) white powder was obtained. ¹H-NMR (δ_{H} ; 400 Hz, CDCl₃): 0.98 (t, 6H,), 1.39 (sextet, 4H), 1.95 (quintet, 4H), 4.27 (t, 4H), 7.51 (t, 2H), 7.58 (s, 2H), 9.26 (t, 2H), 11.14 (s, 2H).

5.5.3 Synthesis of (1,1'-di-n-butyl-3,3'-methylenediimidazoline-2,2'-diylidene)palladium(II) dibromide 5.13.

A stirred DMSO solution (5 mL) of 1,1'-di-n-butyl-3,3'-methylenediimidazolium dibromide (188 mg) and Pd(OAc)₂ (100 mg) was heated at 50 °C for 4 hours, after which the solution was refluxed for another 20 minutes, the solvent was removed under high vacuum at 80 °C, after washing the residue with cold methylene chloride, 195 mg (83%) product was obtained as a pale yellow powder. ¹H-NMR (δ_{H} ; 400 Hz, DMSO-*d*₆): 0.88 (t, 6H,), 1.19 (sextet, 4H), 1.75 (quintet, 2H), 4.03 (m, 2H), 4.83 (broad singlet, 2H), 6.28 (s, 2H), 7.39 (s, 2H), 7.59 (s, 2H). ¹³C-NMR (δ_{H} ; 200 Hz, DMSO-*d*₆): 13.44, 19.06, 32.54, 49.97, 62.52, 121.28, 121.97.

5.5.4 Synthesis of (1,1'-di-n-butyl-3,3'-methylenediimidazoline-2,2'-diylidene)palladium(II) dimethyl **5.14**.

To a THF solution (10 mL) of (1,1'-di-n-butyl-3,3'-methylenediimidazoline-2,2'-diylidene)palladium(II) dibromide (53.0 mg), 0.40 mL 0.5 M MeMgBr ether solution was added and the reaction mixture was stirred at room temperature for 1 hour. Solvents were removed under reduced pressure. 5 mL of pre-dried 1,4-dioxane was added to the residue and stirred at room temperature for 5 minutes. The white solid was removed by filtering through a short pad of dry celite, and the filtrate was concentrated to dryness in high vacuum. 32.3 mg (82.1%) product was obtained as a white solid. $^1\text{H-NMR}$ (δ_{H} ; 400 Hz, CD_3CN): -0.32 (s, 6H), 0.90 (t, 6H), 1.24 (sextet, 4H), 1.72 (quintet, 2H), 4.02 (m, 2H), 4.23 (m, 2H), 5.77 (d, 1H), 5.99 (d, 1H), 6.92 (d, 2H), 7.14 (d, 2H).

5.5.5 Synthesis of (1,1'-di-n-butyl-3,3'-methylenediimidazoline-2,2'-diylidene)palladium(II) di(^{13}C -methyl) **5.14'**.

This compound was synthesized by the same procedure as in 5.5.4 except using ^{13}C -labeled $^{13}\text{CH}_3\text{MgI}$ (which was prepared by reacting $^{13}\text{CH}_3\text{I}$ with Mg in ether). A product was isolated as a white solid with a 76% yield. $^1\text{H-NMR}$ (δ_{H} ; 400 Hz, CD_3CN): between -0.47 and -0.16 (d, $J_{\text{C-H}} = 123.37$ Hz, 6H), 0.90 (t, 6H), 1.24 (sextet, 4H), 1.72 (quintet, 2H), 4.02 (m, 2H), 4.23 (m, 2H), 5.77 (d, 1H), 5.99 (d, 1H), 6.92 (d, 2H), 7.14 (d, 2H).

5.5.6 Reaction between *bis*-NHC-Pd(II)-Me₂ complex **5.14** and O₂

In a nitrogen filled glovebox, 10 mg *bis*-NHC(Bu)₂-Pd(II)-Me₂ complex **5.14** was dissolved in 0.6 mL pre-dried CD_3CN in a J-Young NMR tube. After degassing the sample by three consecutive freeze, pump and-thaw cycles, 1 atm. of pre-dried O₂ was introduced into the NMR tube at -20 °C. After carefully shaking in the cooling bath, the NMR tube was inserted in a NMR probe, which was pre-cooled to -20 °C. The reaction was monitored by $^1\text{H-NMR}$ at various temperatures.

5.5.7 Reaction between *bis*-NHC-Pd(II)-Me₂ complex **5.14** and O₂ in the presence of H₂O

In a nitrogen filled glove-box, 10 mg *bis*-NHC-Pd(II)-Me₂ complex **5.14** was dissolved in 0.60 mL pre-dried CD_3CN in a J-Young NMR tube. After degassed for three consecutive freeze,

pump and-thaw cycles, the sample was cooled down to $-20\text{ }^{\circ}\text{C}$. $0.05\text{ mL CD}_3\text{CN}$ which contained 1% of H_2O was added under the protection of nitrogen (1 equivalent of H_2O relative to the palladium dimethyl complex). Then, 1 atm. of pre-dried O_2 was introduced into the NMR tube at $-20\text{ }^{\circ}\text{C}$, and the sample was carefully swirled in the cooling bath. The NMR tube was inserted into a pre-cooled NMR probe ($-20\text{ }^{\circ}\text{C}$) and the reaction was monitored at various temperatures.

References

1. Stahl, S. S. "Palladium oxidase catalysis: Selective oxidation of organic chemicals by direct dioxygen-coupled turnover," *Angew. Chem. Int. Ed.* **2004**, *43*, 3400-3420.
2. Smidt, J.; Hafner, W.; Jira, R.; Sedlmeier, J.; Sieber, R.; Rüttinger R.; Hojer, H. "Katalytische Umsetzungen von Olefinen an Platinmetall-Verbindungen Das Consortium-Verfahren zur Herstellung von Acetaldehyd," *Angew. Chem.* **1959**, *71*, 176-182.
3. Jira, R. in *Applied homogeneous catalysis with organometallic compound, Vol. 1*, 2nd ed. (Eds.:B. Cornils, W. A. Herrmann), Wiley-VCH, Weinheim, **2002**, pp. 386-405.
4. Moiseev, I. I.; Vargaftik, M. N. in *homogeneous catalysis with organometallic compound, Vol. 1*, 2nd ed. (Eds.:B. Cornils, W. A. Herrmann), Wiley-VCH, Weinheim, **2002**, pp.406-417.
5. Rostovtsev, V. V.; Labinger, J. A.; Bercaw, J. E.; Lasseter, T. L.; Goldberg, K. I. "Oxidation of dimethylplatinum(II) complexes with dioxygen," *Organometallics* **1998**, *17*, 4530-4531.
6. Rostovtsev, V. V.; Henling, L. M.; Labinger, J. A.; Bercaw, J. E. "Structural and mechanistic investigations of the oxidation of dimethylplatinum(II) complexes by dioxygen," *Inorg. Chem.* **2002**, *41*, 3608-3619.
7. Konnick, M. M.; Guzei, L. A.; Stahl, S. S. "Characterization of peroxo and hydroperoxo intermediates in the aerobic oxidation of N-heterocyclic-carbene-coordinated palladium(0)," *J. Am. Chem. Soc.* **2004**, *126*, 10212-10213.
8. Konnick, M. M.; Gandhi, B. A.; Guzei, L. A.; Stahl, S. S. "Reaction of molecular oxygen with Pd^{II}-hydride to produce a Pd^{II}-hydroperoxide: Acid catalysis and implications for Pd-catalyzed aerobic oxidation reactions," *Angew. Chem. Int. Ed.* **2006**, *45*, 2904-2907.
9. Konnick, M. M.; Stahl, S. S. "Reaction of molecular oxygen with a Pd^{II}-hydride to produce a Pd^{II}-hydroperoxide: Experimental evidence for an HX-reductive-elimination pathway," *J. Am. Chem. Soc.* **2008**, *130*, 5753-5762
10. Herrmann, W. A.; Schwarz, J.; Gardiner, M. G. "High-Yield Syntheses of Sterically Demanding Bis(N-heterocyclic carbene) Complexes of Palladium," *Organometallics* **1999**, *20*, 4082-4089.

Chapter 6 $\text{PhI}(\text{OAc})_2$ and $\text{PhI}(\text{OTFA})_2$ Triggered C-C Bond and C-O Bond Formation from *Bis*-NHC-Pd(II)- $(\text{CH}_3)_2$ Complex

6.1 Introduction

Hypervalent iodine reagent such as PhIO , $\text{PhI}=\text{NTs}$, PhICl_2 and $\text{PhI}(\text{OAc})_2$ ¹ have been applied to stoichiometrically react with Pd-aryl complexes. These reactions generally result in clean and high yielding functionalization/cleavage of the Pd-C bond. Detailed mechanistic study revealed that, in many cases, these transformation proceed via Pd(IV) intermediates.²

The reaction between PhIO and cyclometalated Pd(II) complex led to the insertion of an oxygen atom into the Pd-C bond (Figure 6.1).^{3,4} Similarly, the reaction between $\text{PhI}=\text{NTs}$ and cyclometalated Pd(II) complex resulted in the insertion of NTs into the Pd-C bond (Figure 6.2).⁵ It was proposed that both these two transformations involved Pd(IV) intermediates such as Pd(IV)-oxo species **6.1** and Pd(IV)-imido species **6.5** resulted from oxidation of the Pd(II) complexes with hypervalent iodine reagents, and the collapse of the intermediates to afford the insertion products.

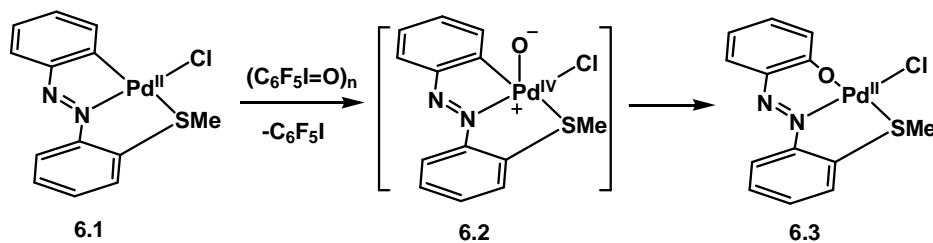


Figure 6.1 O insertion into a Pd^{II}-C bond with $(\text{C}_6\text{F}_5\text{I}=\text{O})_n$.³

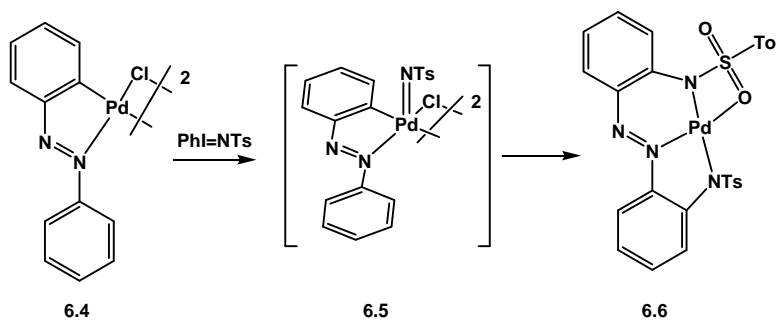


Figure 6.2 Double amination of palladacycle **6.4**.⁵

The chlorination of Pd(II)-C bonds with PhICl_2 is another transformation that has been extensively explored, and there are strong evidences showed that the chlorination reactions proceed via C-Cl bond forming reductive elimination from Pd(IV) intermediates. For example, the reaction between pincer Pd(II) complex **6.7** and PhICl_2 afforded a Pd(IV) intermediate **6.8**,⁶ which can be characterized by $^1\text{H-NMR}$ spectroscopy at room temperature. This species decomposed over several minutes to give the C-Cl bond forming product **6.9** (Figure 6.3).

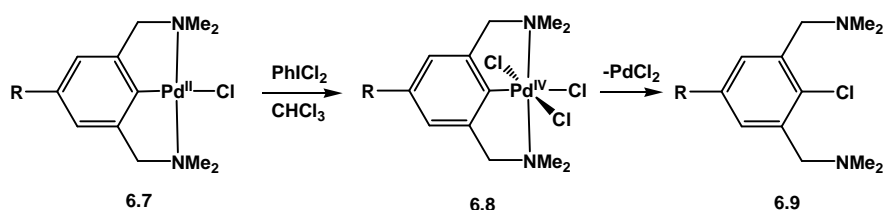


Figure 6.3 Oxidation of Pd^{II} to Pd^{IV} with PhICl_2 .⁶

The Sanford group demonstrated the stable palladium(IV) carboxylate complex $(\text{phpy})_2\text{Pd}(\text{IV})(\text{O}_2\text{CPh})_2$ [$\text{phpy} = 2\text{-phenylpyridine}$] **6.11** can be isolated by the reaction of $(\text{phpy})_2\text{Pd}(\text{II})$ **6.10** with $\text{PhI}(\text{O}_2\text{CPh})_2$. Upon heating to $60\text{ }^\circ\text{C}$, this complex underwent clean C-O bond forming reductive elimination to yield the oxygenated product (Figure 6.4). The mechanistic study showed this process occurred from a five-coordinate intermediate resulted from pre-dissociation of one arm of the phenylpyridine ligand.⁷

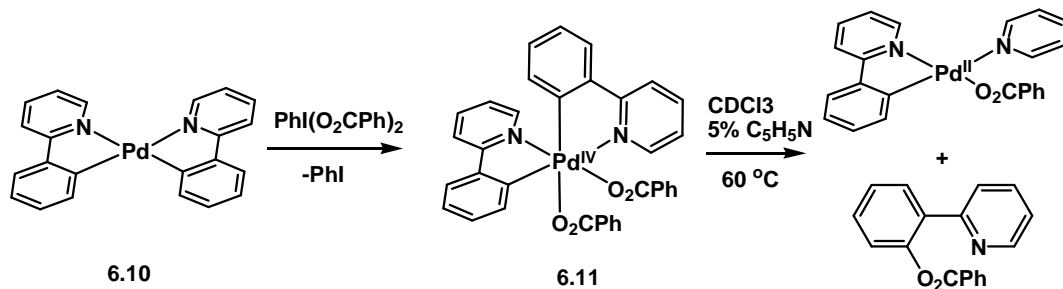


Figure 6.4 Oxidation of Pd^{II} to Pd^{IV} with $\text{PhI}(\text{O}_2\text{CPh})_2$.⁷

6.2 $\text{PhI}(\text{OAc})_2$ Triggered C-C Bond Formation from $\text{Bis-NHC-Pd(II)-(CH}_3)_2$ Complex

In a nitrogen filled glove-box, 5 mg $\text{bis-NHC-Pd(II)-(CH}_3)_2$ complex **5.14** was dissolved in 0.60 mL pre-dried CD_3CN in a J-Young NMR tube. After degassing by three consecutive freeze, pump and-thaw cycles, the sample was cooled to $-40\text{ }^\circ\text{C}$. A solution of one equivalent of $\text{PhI}(\text{OAc})_2$ in 0.10 mL dry CD_3CN was added via a syringe under the protection of nitrogen. The NMR tube was carefully swirled in the cooling bath and quickly inserted into a pre-cooled NMR probe ($-40\text{ }^\circ\text{C}$). The reaction was monitored at various temperatures. At $-40\text{ }^\circ\text{C}$, only the C-C reductive elimination product ethane was observed (0.85 ppm). Stacked $^1\text{H-NMR}$ spectrum for this reaction is showed in Figure 6.5. With the progress of the reaction, the resonances for the bis-NHC-Pd species became broad due to the lower solubility of the complex at lower temperature. Upon warming up to $25\text{ }^\circ\text{C}$, resonances for a symmetrical bis-NHC-Pd species appeared, which have been identified as $\text{bis-NHC-Pd}(\text{OAc})_2$ by comparing with a standard sample obtained by reaction of bis-NHC-Pd-Br_2 with AgOAc .

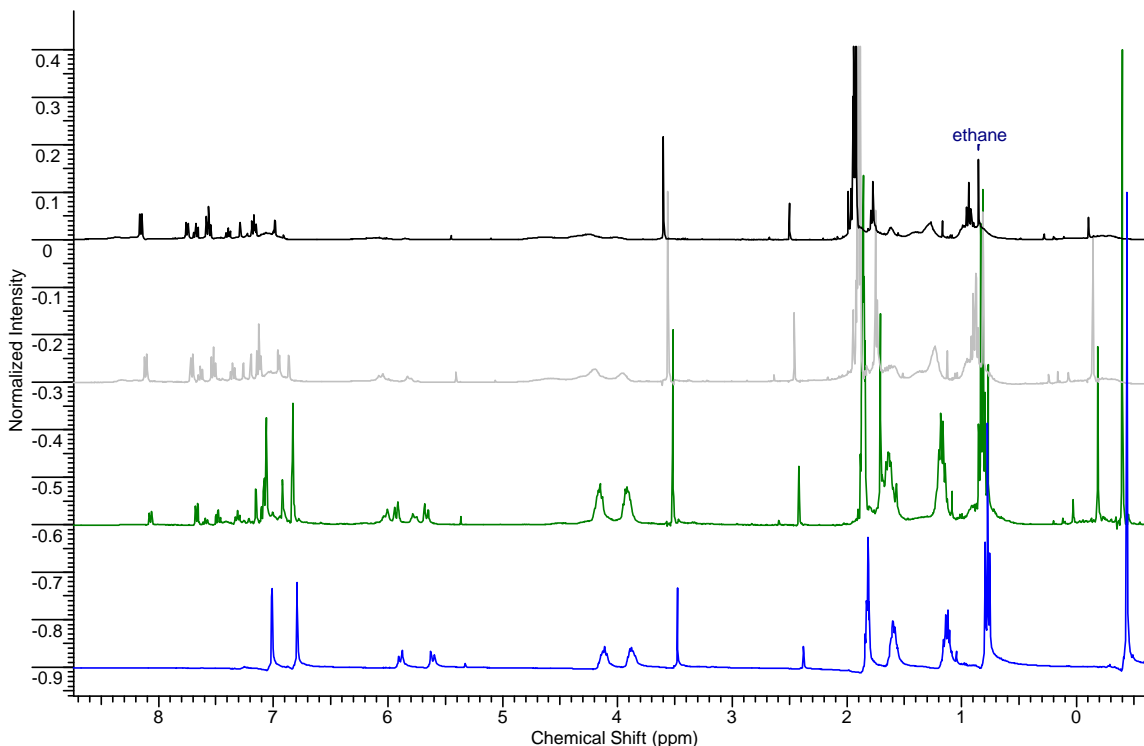


Figure 6.5 Stacked $^1\text{H-NMR}$ spectrum for the reaction between $\text{bis-NHC-Pd(II)-(CH}_3)_2$ complex **5.14** and $\text{PhI}(\text{OAc})_2$.

Based on this reaction result, it is our working hypothesis that the *bis*-NHC-Pd(II)-(CH₃)₂ complex **5.14** was oxidized by PhI(OAc)₂ to form a *bis*-NHC-Pd(IV)-(CH₃)₂-(OAc)₂ intermediate **6.12**, followed by C-C reductive elimination to give ethane and *bis*-NHC-Pd(II)-(OAc)₂ **6.13** as products (Figure 6.6).

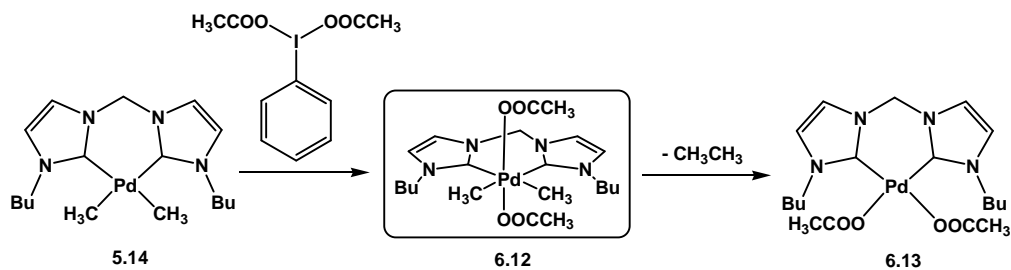


Figure 6.6 Proposed reaction pathway between *bis*-NHC-Pd(II)-Me₂ and PhI(OAc)₂.

6.3 PhI(OTFA)₂ Triggered C-C Bond and C-O Bond Formation from *Bis*-NHC-Pd(II)-(CH₃)₂ Complex

Compared with PhI(OAc)₂, PhI(OTFA)₂ exhibits better solubility in common organic solvents. Therefore, Dr. Kraft and I have decided to investigate the reaction between PhI(OTFA)₂ and *bis*-NHC-Pd(II)-(CH₃)₂.

In a nitrogen filled glove-box, 10 mg *bis*-NHC-Pd(II)-(CH₃)₂ complex **5.14** was dissolved in 0.60 mL pre-dried CD₃CN in a J-Young NMR tube. After degassing by three consecutive freeze, pump and-thaw cycles, the sample was cooled to -40 °C. A solution of one equivalent of PhI(OTFA)₂ in 0.10 mL dry CD₃CN was added via a syringe under the protection of nitrogen. The NMR tube was carefully swirled in the cooling bath and quickly inserted into a pre-cooled NMR probe (-40 °C). The reaction was monitored at various temperatures. It was found that at -40 °C, both C-C and C-O reductive elimination products ethane (0.85 ppm) and methyl trifluoroacetate (3.95 ppm) were observed. The reaction was completed within 5 minutes. The resonance at 0.11 ppm was assigned to the methyl group of the unsymmetrical *bis*-NHC-Pd(II)-CH₃-(OTFA) resulted from the C-O reductive elimination reaction. The dioxane residue was used as an internal standard to calculate the relative rate of the C-C vs C-O reductive elimination. In the original sample before adding oxidant, the integration of the dioxane (3.60 ppm) was 0.95 when the methyl resonance (-0.32 ppm) was set to 6. Keeping the integration of dioxane at 0.95 after

the reaction, the integration of the methyl of *bis*-NHC-Pd-(CH₃)-(OTFA) was found to be 1.45. This result showed that the relative rate of the C-C vs C-O reductive elimination is 1/1 under this reaction condition.

¹H-NMR also showed that the *bis*-NHC-Pd(II)-(CH₃)-(OTFA) species is stable at room temperature, as soon as a solution of 0.50 equivalent of PdI(OTFA)₂ in CD₃CN was added, it was quickly converted to *bis*-NHC-Pd(II)-(OTFA)₂ and gave one equivalent of CH₃OCCF₃. A stacked ¹H-NMR spectrum for the reaction between *bis*-NHC-Pd(II)-(CH₃)₂ and PhI(OTFA)₂ is showed in Figure 6.7.

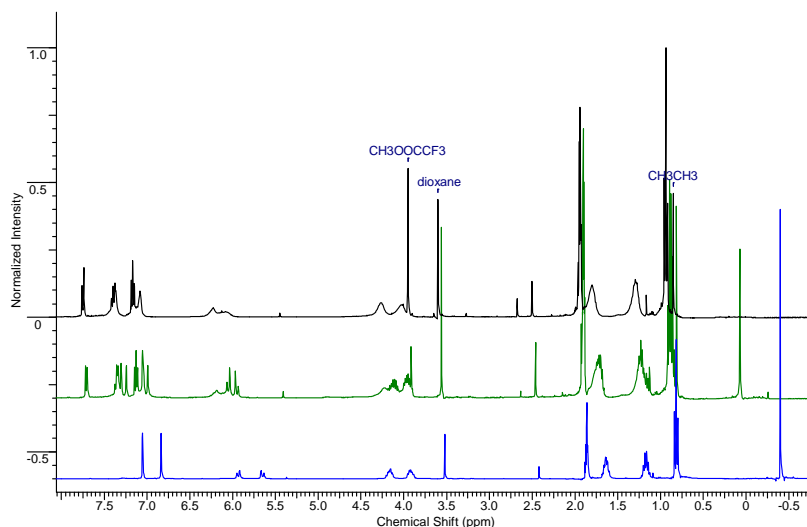


Figure 6.7 Stacked ¹H-NMR spectrum for the reaction between *bis*-NHC-Pd(II)-(CH₃)₂ and PhI(OTFA)₂. (blue: *bis*-NHC-Pd(II)-(CH₃)₂ at -40 °C; green: adding 1 equivalent of PhI(OTFA)₂ at -40 °C for 5 minutes; black: after adding 0.50 equivalent of PhI(OTFA)₂ at room temperature).

In order to confirm the formation of both ethane and methyl trifluoroacetate, the ¹³C labeled dimethylpalladium(II) complex *bis*-NHC-Pd(II)-(¹³CH₃)₂ was synthesized and used as starting material to react with PhI(OTFA)₂. At -40 °C, the ¹H-NMR clearly showed the disappearance of the doublet between -0.52 ppm and -0.22 ppm with the large ¹³C-H coupling constant of 123.69 Hz, which was assigned to the methyl groups of the dimethylpalladium(II) complex. Three sets of doublets were observed after the reaction at -40 °C: The one between -0.11 ppm and 0.21 ppm with ¹³C-H coupling constant of 128.03 Hz was assigned to the methyl group of the unsymmetrical *bis*-NHC-Pd(II)-(¹³CH₃)-(OTFA) complex; the one between 0.67 ppm and 0.97 ppm with ¹³C-H coupling constant of 120.50 Hz was assigned to the ¹³C labeled

ethane; and the one between 3.72 ppm and 4.10 ppm with ^{13}C -H coupling constant of 152.50 Hz was assigned to the ^{13}C labeled methyl group of methyl trifluoroacetate. A stacked ^1H -NMR spectrum for the reaction between *bis*-NHC-Pd(II)-($^{13}\text{CH}_3$) $_2$ complex and $\text{PhI}(\text{OTFA})_2$ is showed in Figure 6.8. In the ^{13}C -NMR, the starting material ^{13}C labeled dimethylpalladium(II) complex **5.14** showed one peak at -5.34 ppm. After the reaction at -40 °C, the peak at -5.34 ppm disappeared and three new peaks showed up. The peak at -7.06 ppm was assigned to the ^{13}C labeled methyl group of the *bis*-NHC-Pd(II)-($^{13}\text{CH}_3$)-(OTFA); the peak at 7.06 was assigned to $^{13}\text{CH}_3^{13}\text{CH}_3$; and the peak at 55.68 ppm was assigned to the ^{13}C labeled methyl group of methyl trifluoroacetate. A stacked ^{13}C -NMR spectrum for the reaction between *bis*-NHC-Pd(II)-($^{13}\text{CH}_3$) $_2$ complex and $\text{PhI}(\text{OTFA})_2$ is showed in Figure 6.9. The results from his experiment provided solid evidence that both C-C and C-O bond formed in the reaction between *bis*-NHC-Pd(II)-(CH_3) $_2$ and $\text{PhI}(\text{OTFA})_2$.

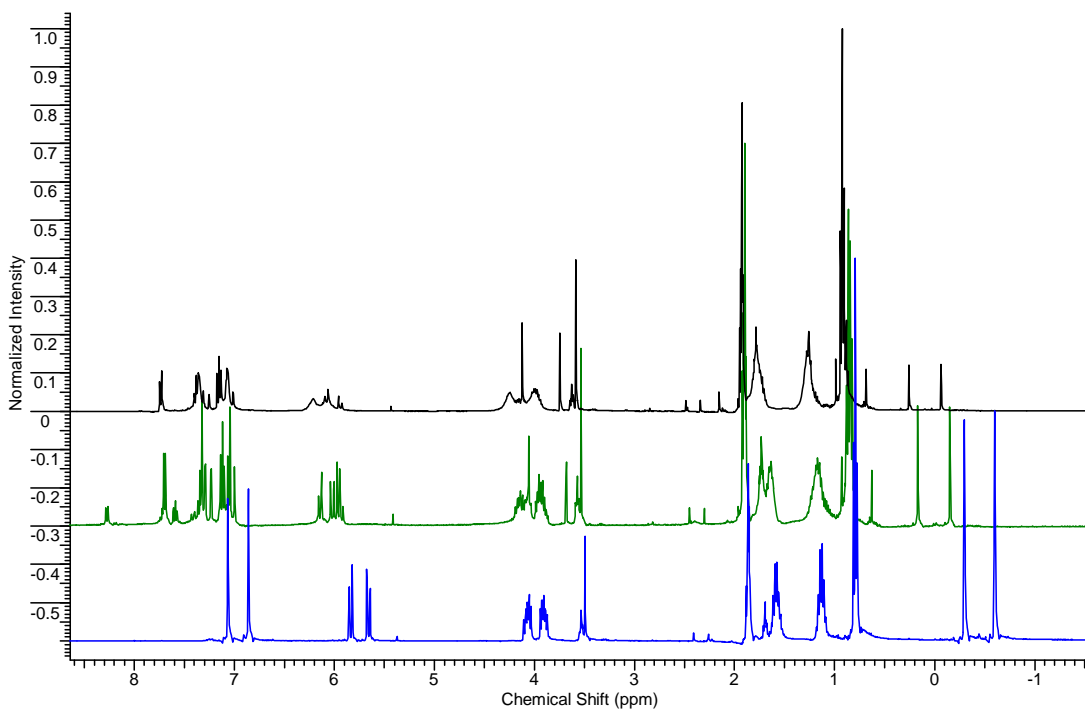


Figure 6.8 Stacked ^1H -NMR spectrum for the reaction between *bis*-NHC-Pd(II)-($^{13}\text{CH}_3$) $_2$ complex and $\text{PhI}(\text{OTFA})_2$. (blue: *bis*-NHC-Pd(II)-($^{13}\text{CH}_3$) $_2$ at -40 °C; green: adding 1 equivalent of $\text{PhI}(\text{OTFA})_2$ at -40 °C for 5 minutes; black: after adding 0.20 equivalent of $\text{PhI}(\text{OTFA})_2$ at room temperature).

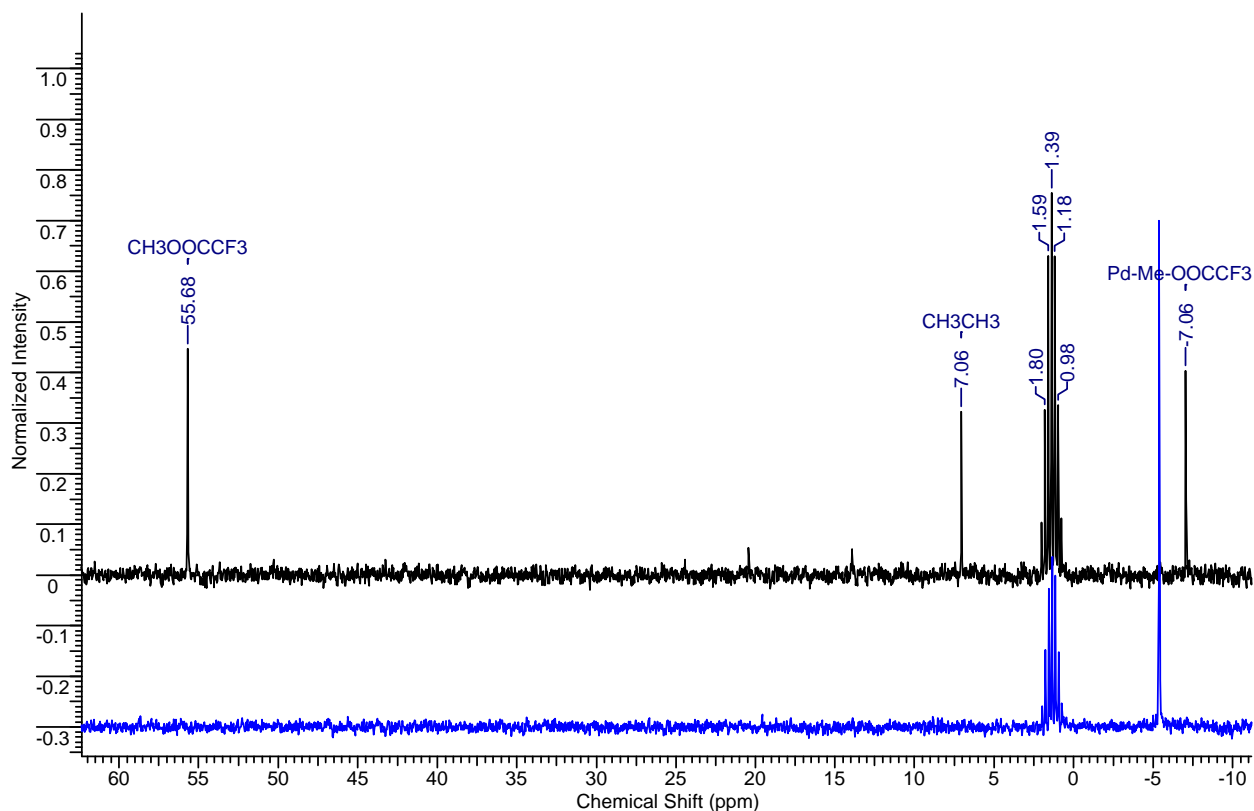


Figure 6.9 Stacked ^{13}C -NMR spectrum for the reaction between *bis*-NHC-Pd(II)-($^{13}\text{CH}_3$) $_2$ complex and $\text{PhI}(\text{OTFA})_2$. (blue: *bis*-NHC-Pd(II)-($^{13}\text{CH}_3$) $_2$ at $-40\text{ }^\circ\text{C}$; black: adding 1 equivalent of $\text{PhI}(\text{OTFA})_2$ at $-40\text{ }^\circ\text{C}$ for 5 minutes).

6.4 Mechanistic Discussion of the $\text{PhI}(\text{OAc})_2$ Triggered C-C Bond Formation vs $\text{PhI}(\text{OTFA})_2$ Triggered C-C and C-O Bond Formation.

For the process of C-C bond formation in both cases, it is our working hypothesis that a *bis*-NHC-Pd(IV)-(CH_3) $_2$ -(OOCR) $_2$ intermediate is formed by oxidation of *bis*-NHC-Pd-(CH_3) $_2$ with hypervalent iodine reagents $\text{PhI}(\text{OOCR})_2$. C-C bond forming reductive elimination from this intermediate releases ethane and generates *bis*-NHC-Pd(II)-(OOCR) $_2$ complexes (Figure 6.10).

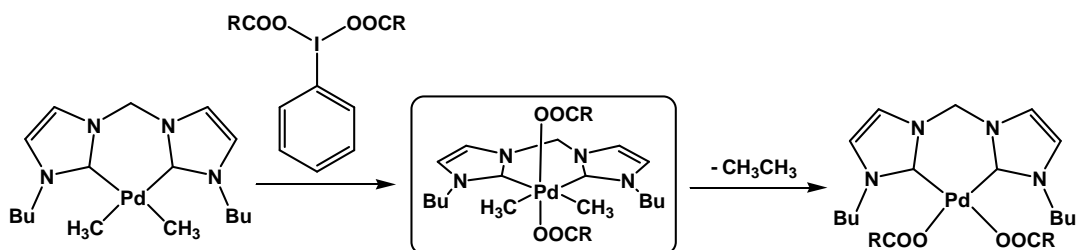


Figure 6.10 Proposed pathway for the C-C bond formation process.

For the C-O bond formation during the reaction between $\text{PhI}(\text{OTFA})_2$ and *bis*-NHC-Pd(II)- $(\text{CH}_3)_2$, at least two reaction pathways should be taken into consideration. In the first pathway, C-O bond formation does not involve a palladium(IV) intermediate. Methyl trifluoroacetate could be formed from the direct attack of the palladium coordinated methyl groups by the OTFA anion, which has been previously dissociated from $\text{PhI}(\text{OTFA})_2$ in solution (Figure 6.11)

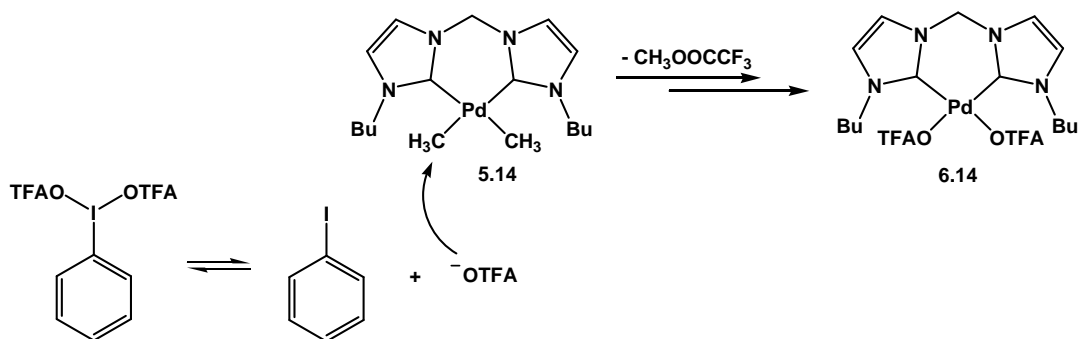


Figure 6.11 Proposed C-O bond formation pathway via external attack.

In the second pathway, the transient *bis*-NHC-Pd(IV)- $(\text{CH}_3)_2$ - $(\text{OTFA})_2$ intermediate **6.15** undergoes competitive C-C bond forming and C-O bond forming reductive elimination to yield ethane and methyl trifluoroacetate as well as palladium(II) complexes **6.14** and **6.16** (Figure 6.12). Similar mechanisms had been proposed by A. J. Canty.⁸

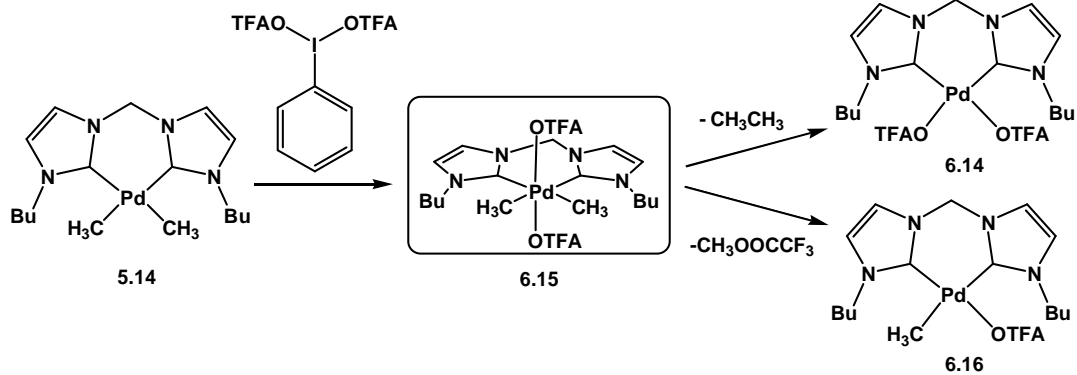


Figure 6.12 Proposed C-O bond formation pathway via reductive elimination from Pd(IV) species.

The first pathway can be easily ruled out. $^1\text{H-NMR}$ showed that the rate of dissociation of the OAc anion from $\text{PhI}(\text{OAc})_2$ is comparable with the rate of dissociation of the OTFA anion from $\text{PhI}(\text{OTFA})_2$ in CD_3CN . If the C-O bond formation is from an external attack of the acetate anion, the OAc anion will lead to a more facile C-O bond formation than the OTFA anion, because it is more electron rich. The absence of methyl acetate suggested that the C-O bond formation is not following this pathway. Experimental support was obtained by treating ^{13}C labeled *bis*-NHC-Pd(II)-($^{13}\text{CH}_3$) $_2$ complex **5.14'** with one equivalent of diisopropylethylammonium trifluoroacetate salt in CD_3CN at $-40\text{ }^\circ\text{C}$. It was found that in the presence of free OTFA anion, there was no formation of methyl trifluoroacetate. Only methane and *bis*-NHC-Pd(II)-($^{13}\text{CH}_3$)-(OTFA) complex **6.16'** were observed, due to the selective protonation of one methyl group from the *bis*-NHC-Pd(II)-($^{13}\text{CH}_3$) $_2$ complex. After warming up to room temperature, one equivalent of $\text{PhI}(\text{OTFA})_2$ was added to the NMR tube, the *bis*-NHC-Pd(II)-($^{13}\text{CH}_3$)-(OTFA) complex **6.16'** was quickly consumed and methyl trifluoroacetate was formed. A stacked $^1\text{H-NMR}$ spectrum for the reaction between the *bis*-NHC-Pd(II)-($^{13}\text{CH}_3$) $_2$ complex and diisopropylethylammonium trifluoroacetate salt and further reaction of the *bis*-NHC-Pd(II)-($^{13}\text{CH}_3$)-OTFA with $\text{PhI}(\text{OTFA})_2$ is shown in Figure 6.13.

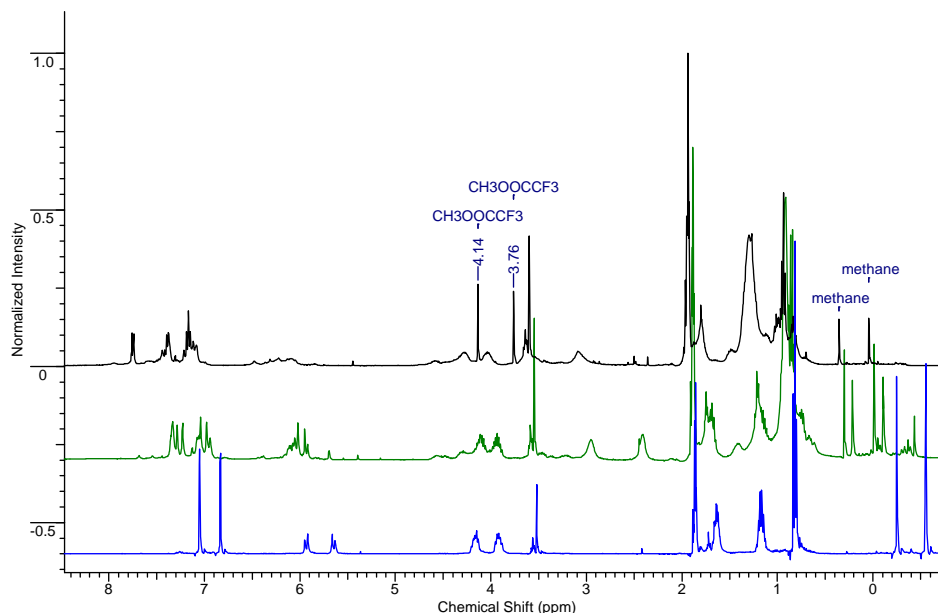


Figure 6.13 Stacked ^1H -NMR spectrum for the reaction between *bis*-NHC-Pd(II)-($^{13}\text{CH}_3$) $_2$ complex and diisopropylethylammonium trifluoroacetate salt, and the further reaction with $\text{PhI}(\text{OTFA})_2$. (blue: *bis*-NHC-Pd(II)-($^{13}\text{CH}_3$) $_2$ at $-40\text{ }^\circ\text{C}$; green: adding 1 equivalent of diisopropylethylammonium trifluoroacetate salt at $-40\text{ }^\circ\text{C}$ for 5 minutes; black: after adding 1.0 equivalent of $\text{PhI}(\text{OTFA})_2$ at room temperature).

This experiment provided strong supportive information that the C-O bond formation is not from the external attack of the methyl groups of *bis*-NHC-Pd(II)-(CH_3) $_2$ complex by the OTFA anion. Therefore, it is far more likely that a palladium(IV) intermediate had been involved in the C-O bond formation process (Figure 6.14).

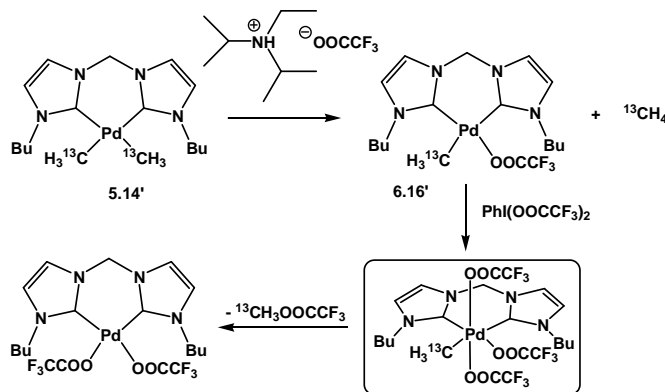


Figure 6.14 Protonation of *bis*-NHC-Pd(II)-(CH_3) $_2$ and further oxidative addition triggered C-O reductive elimination.

One question in need to be answered is: Why there is no C-O bond formation when $\text{PhI}(\text{OAc})_2$ was used as oxidant? One possible reason for our finding is that OAc is a stronger donor ligand than OTFA, because the electron-withdrawing CF_3 group makes OTFA a less electron-donating ligand. OAc binds stronger to the palladium center than OTFA, and it does not undergo C-O reductive elimination. Ideally, we would like to synthesize the *bis*-NHC-Pd(II)-(CH₃)-(OAc) complex and treat it with $\text{PhI}(\text{OTFA})_2$ as oxidant. If the assumption we have made is correct, then only CH_3OCCF_3 should be expected as reaction product. We have attempted several ways to synthesize the *bis*-NHC-Pd(II)-(CH₃)-(OAc) complex, including the protonation of the dimethylpalladium(II) complex with HOAc at low temperature, and abstraction of the iodine ligand from *bis*-NHC-Pd(II)-(CH₃)-I with AgOAc, but unfortunately, we could not observe the formation of this complex. The protonation led to the complete release of methyl groups and the AgOAc method resulted in the decomposition of the *bis*-NHC-Pd(II)-CH₃-I complex to palladium black.

When the *bis*-NHC-Pd(II)-(CH₃)₂ complex was treated with one equivalent of *para*-chlorophenol at -20 °C in CD₃CN, a clean mono-methylpalladium(II) complex *bis*-NHC-Pd(II)-(CH₃)-(4-Cl-C₆H₄O) **6.17** (methyl resonance at -0.08 ppm), as well as methane (resonance at 0.20 ppm) have formed. Upon adding one equivalent of $\text{PhI}(\text{OTFA})_2$, a resonance at 3.95 ppm assigned to methyl trifluoroacetate appeared immediately, and no formation of the hypothetical methyl ether (4-Cl-PhOCH₃) was observed during the reaction (Figure 6.15). A stacked ¹H-NMR spectrum of these two reactions is showed in Figure 6.16. Compared with OTFA, *para*-chlorophenoxido ligand was attached stronger to the palladium center. The result from this experiment showed that only weaker ligand can undergo C-O bond forming reductive elimination from a Pd(IV) center. This finding supports our mechanistic hypothetic explaining of the absence of C-O bond formation when $\text{PhI}(\text{OAc})_2$ was used as oxidant to react with *bis*-NHC-Pd(II)-(CH₃)₂ complex.

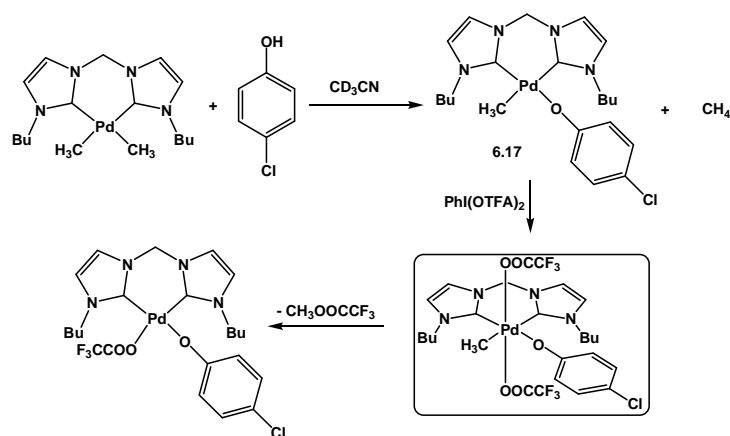


Figure 6.15 Protonation of the *bis*-NHC-Pd(II)-(CH₃)₂ complex with *p*-chlorophenol and the further oxidation of the *bis*-NHC-Pd(II)-(CH₃)-(p-Cl-C₆H₄) with PhI(OTFA)₂.

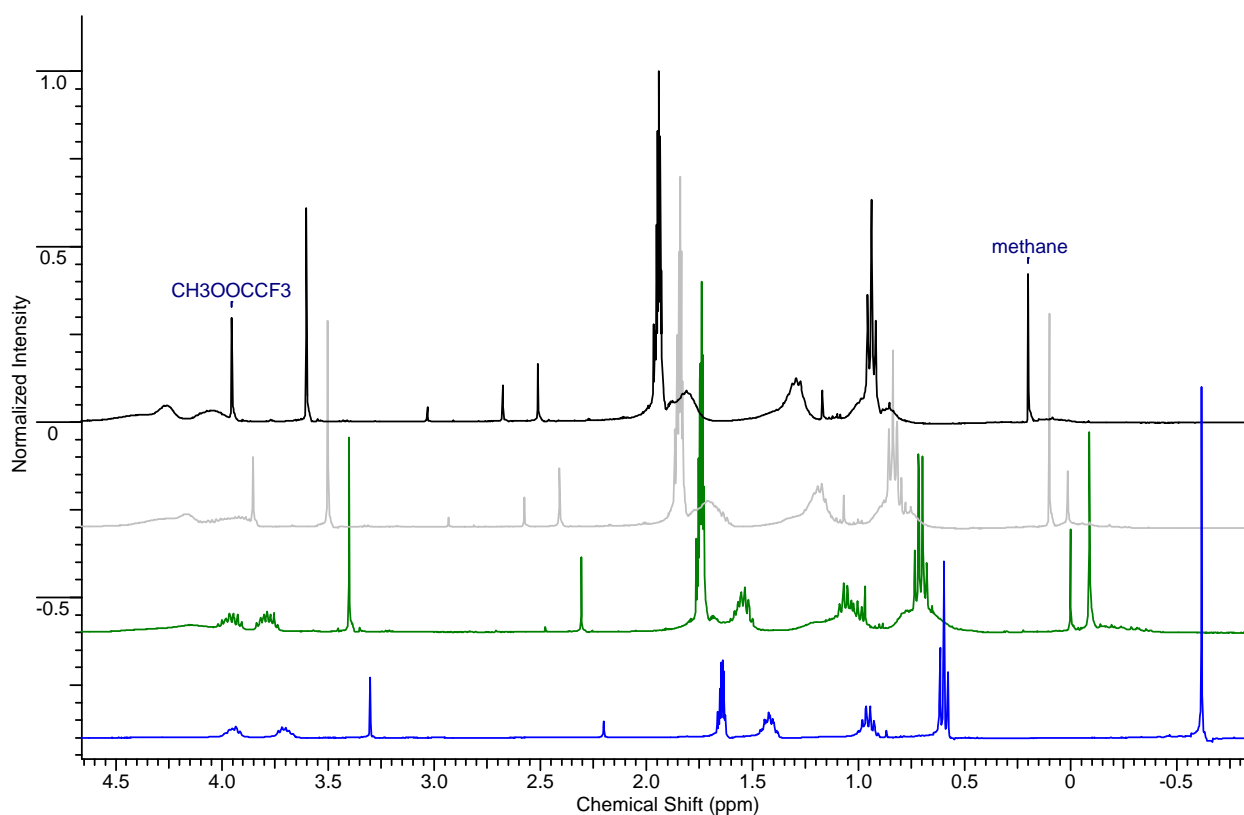


Figure 6.16 Stacked ¹H-NMR spectrum of the protonation of the *bis*-NHC-Pd(II)-(CH₃)₂ complex with *p*-chlorophenol and the further oxidation with PhI(OTFA)₂. (blue: *bis*-NHC-Pd(II)-(CH₃)₂ at -20 °C; green: After adding one equivalent of *p*-chlorophenol for 2 minutes at -20 °C; gray: after adding one equivalent of PhI(OTFA)₂ for 1 minute at room temperature; black: after adding one equivalent of PhI(OTFA)₂ for 5 minutes at room temperature).

6.5 Experimental

6.5.1 The reaction between $\text{PhI}(\text{OAc})_2$ and *bis*-NHC-Pd(II)-(CH₃)₂ complex 5.14.

In a nitrogen filled glove-box, 5 mg *bis*-NHC(Bu)₂-Pd(II)-Me₂ complex was dissolved in 0.60 mL pre-dried CD₃CN in a J-Young NMR tube. After degassing by three consecutive freeze, pump and-thaw cycles, the sample was cooled to -40 °C. A solution of one equivalent of $\text{PhI}(\text{OAc})_2$ in 0.10 mL dry CD₃CN was added via a syringe under the protection of nitrogen. The NMR tube was carefully swirled in the cooling bath and quickly inserted into a pre-cooled NMR probe (-40 °C). The reaction was monitored at various temperatures.

6.5.2 The reaction between $\text{PhI}(\text{OTFA})_2$ and *bis*-NHC-Pd(II)-(CH₃)₂ complex 5.14.

In a nitrogen filled glove-box, 10 mg *bis*-NHC-Pd(II)-Me₂ complex was dissolved in 0.60 mL pre-dried CD₃CN in a J-Young NMR tube. After degassing by three consecutive freeze, pump and-thaw cycles, the sample was cooled to -40 °C. A solution of one equivalent of $\text{PhI}(\text{OTFA})_2$ in 0.10 mL dry CD₃CN was added via a syringe under the protection of nitrogen. The NMR tube was carefully swirled in the cooling bath and quickly inserted into a pre-cooled NMR probe (-40 °C). The reaction was monitored by ¹H-NMR at various temperatures. Because of the formation of both *bis*-NHC-Pd(II)-(OTFA)₂ and *bis*-NHC-Pd(II)-(CH₃)-(OTFA), it is difficult to assign peaks for each species. The new peak at 0.11 ppm is assigned to the methyl coordinated to the palladium center in the *bis*-NHC-Pd(II)-(CH₃)-(OTFA) complex. And the imidazole backbone show the characteristic unsymmetrical structure.

6.5.3 Mono-protonation of *bis*-NHC-Pd(II)-(CH₃)₂ complex with diisopropylethylammonium trifluoroacetate salt and further reaction with $\text{PhI}(\text{OTFA})_2$

In a nitrogen filled glove-box, 10 mg *bis*-NHC-Pd(II)-Me₂ complex was dissolved in 0.50 mL pre-dried CD₃CN in a J-Young NMR tube. After degassing by three consecutive freeze, pump and-thaw cycles, the sample was cooled to -40 °C. A solution of one equivalent of diisopropylethylammonium trifluoroacetate salt in 0.10 mL dry CD₃CN was added via a syringe under the protection of nitrogen. The NMR tube was carefully swirled in the cooling bath and quickly inserted into a pre-cooled NMR probe (-40 °C). The reaction was monitored by ¹H-NMR

at various temperatures. The starting material 5.14 was consumed immediately and methane and *bis*-NHC-Pd(II)-(CH₃)-(OTFA) were produced. After warming up to room temperature, a solution of one equivalent of PhI(OTFA)₂ in 0.10 mL dry CD₃CN was added via a syringe under the protection of nitrogen, and the reaction was monitored by ¹H-NMR. The *bis*-NHC-Pd(II)-(CH₃)-(OTFA) was consumed immediately, and the formation of methyl trifluoroacetate was observed.

6.5.4 Mono-protonation of *bis*-NHC-Pd(II)-(CH₃)₂ complex to form *bis*-NHC-Pd(II)-(CH₃)-(4-Cl-C₆H₄O) complex.

10 mg *bis*-NHC-Pd(II)-(CH₃)₂ complex was dissolved in 0.50 mL CD₃CN, cooled to -20 °C, 1 equivalent of p-chloro-phenol in 0.10 mL of CD₃CN was added by means of syringe under the protection of nitrogen. ¹H-NMR showed the formation of *bis*-NHC-Pd(II)-(CH₃)-(4-Cl-C₆H₄O) in 5 minutes. ¹H-NMR (δ_H; 400 Hz, CD₃CN): -0.08 (s, 3H, Pd-CH₃), 0.82 (t, 3H, CH₃), 0.95 (t, 3H, CH₃), 1.12 (m, 2H, CH₂), 1.28 (m, 2H, CH₂), 1.60 (m, 2H, CH₂), 1.80 (m, 2H, CH₂), 3.79 (m, 1H, CH₂), 3.99 (m, 1H, CH₂), 4.32 (m, 2H, CH₂), 5.86 (d, 1H, CH₂ bridge), 6.18 (d, 1H, CH₂ bridge), 6.66 (d, 2H, aromatic), 6.79 (d, 2H, aromatic), 6.85 (d, 1H, imidazole backbone), 7.02 (d, 1H, imidazole backbone), 7.13 (d, 1H, imidazole backbone), 7.22(d, 1H, imidazole backbone).

6.5.5 The reaction between PhI(OTFA)₂ and *bis*-NHC-Pd(II)-(CH₃)-(4-Cl-C₆H₄O) complex.

One equivalent of PhI(OTFA)₂ in 0.10 mL CD₃CN was added to the NMR tube which contains *bis*-NHC-Pd(II)-(CH₃)-(4-Cl-C₆H₄O) complex (from the previous step) at room temperature. The C-O bond formation was observed.

References

- (a) Wirth, T., Ed. "Hypervalent iodine chemistry, modern developments in organic synthesis," *Topics in Current Chemistry*; Springer: New York, **2003**; Vol. 224.

(b) Zhdankin, V. V.; Stang, P. J. "Recent developments in the chemistry of polyvalent iodine compounds," *Chem. Rev.*, **2002**, *102*, 2523-2584.

(c) Stang, P. J.; Zhdankin, V. V. "Organic polyvalent iodine compounds," *Chem. Rev.*, **1996**, *96*, 1123-1178.

(d) Varvoglis, A. "Chemical transformations induced by hypervalent iodine reagents," *Tetrahedron* **1997**, *53*, 1179-1255.
- Deprez, N, R.; Sanford, M. S. "Reactions of hypervalent iodine reagents with palladium: Mechanisms and applications in organic synthesis," *Inorg. Chem.*, **2007**, *46*, 1924-1935.
- Bhawmick, R.; Biswas, H.; Bandyopadhyay, D. "Oxygen insertion into palladium-arene bonds by iodosylbenzene," *J. Organomet. Chem.* **1995**, *498*, 81-83.
- Kamaraj, K.; Bandyopadhyay, D. "Mechanism of palladium-carbon bond oxidation: Dramatic solvent effect," *Organometallics* **1999**, *18*, 438-446.
- Dick, A. R.; Remy, M. S.; Kampf, J. W.; Sanford, M. S. "Carbon-nitrogen bond-forming Reactions of palladacycles with hypervalent iodine reagents," *Organometallics* **2007**, *26*, 1365-1370.
- Lagunas, M-C.; Gossage, R. A.; Spek, A. L.; van Koten, G. "Synthesis and characterization of the *bis*-Cyclometalating ligand 3,3',5,5'-tetrakis[(dimethylamino)methyl]biphenyl and its use in the preparation of bimetallic M(II), M(IV) (M = Pt, Pd), and mixed-valence Pt(II)-Pt(IV) complexes via a dilithio-derivative. Crystal structure of the Pd dimer [ClPd{2,6-(Me₂NCH₂)₂C₆H₂}]₂," *Organometallics* **1998**, *17*, 731-741.
- Dick, A. R.; Kampf, J. W.; Sanford, M. S. "Unusually stable palladium(IV) complexes: Detailed mechanistic investigation of C-O bond-forming reductive elimination," *J. Am. Chem. Soc.*, **2005**, *127*, 12790-12791.
- (a) Canty, A. J.; Jin, H.; Skelton, B. W.; White, A. H. "Oxidation of complexes by (O₂CPh)₂ and (ER)₂ (E = S, Se), including structures of Pd(CH₂CH₂CH₂CH₂)(SePh)₂(bpy)

(bpy = 2,2'-Bipyridine) and $MMe_2(SePh)_2(L_2)$ ($M = Pd, Pt$; $L_2 = bpy, 1,10$ -Phenanthroline) and C...O and C...E bond formation at palladium(IV)," *Inorg. Chem.*, **1998**, 37, 3975-3981. (b) Canty, A. J.; Denney, M. C. "Carbon-oxygen bond formation at organopalladium centers: The reactions of $PdMeR(L_2)$ ($R = Me, 4$ -tolyl; $L_2 = tmeda, bpy$) with diaroyl peroxides and the involvement of organopalladium(IV) species," *Organometallics* **2004**, 23, 1122-1131. (c) Canty, A. J.; Denney, M. C.; van Koten, G.; Skelton, B. W.; White, A. H. "Carbon-oxygen bond formation at metal(IV) centers: Reactivity of palladium(II) and platinum (II) complexes of [2,6-(dimethylaminomethyl)phenyl-N,C,N] (Pincer) ligand toward iodomethane and dibenzoyl peroxide; Structural of M(II) and M(IV) complexes," *Organometallics* **2004**, 23, 5432-5439.

Chapter 7 Chlorine Triggered C-C Bond Formation Vs C-Cl Bond Formation from *Bis*-NHC-Pd(II)-Me₂ Complex

7.1 Introduction

Although all the oxidation of the *bis*-NHC-Pd(II)-(CH₃)₂ complex chemistry I had carried out implied the formation of Pd(IV) species, up to now, I have not obtained a isolable *bis*-NHC ligand supported Pd(IV) species! I have tried the oxidation reaction of *bis*-NHC-Pd(II)-Br₂ with bromine, as has been showed in **chapter 2**. The result, although not conclusive, implied that a *bis*-NHC-Pd(IV)-Br₄ species had formed, which could not be isolated or characterized, because it readily released bromine to re-form *bis*-NHC-Pd(II)-Br₂ complex.

It was found that the very first several isolated Pd(IV) complexes were obtained by oxidative addition of chlorine to the di-nitrogen ligands supported Pd(II) complexes (Figure 7.1).^{1,2}

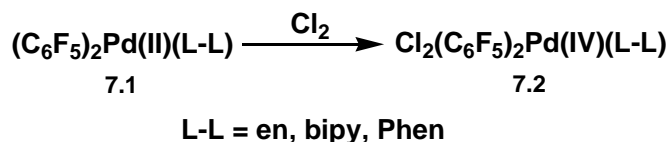


Figure 7.1 Chlorine oxidation of bidentate ligands supported Pd(II) to Pd(IV).¹

In 1993, G. van Koten and co-workers reported the isolation of a stable palladium(IV) complex **7.4** by oxidative addition of chlorine to a terdentate CNN' ligand supported palladium(II) complex **7.3** (Figure 7.2).³

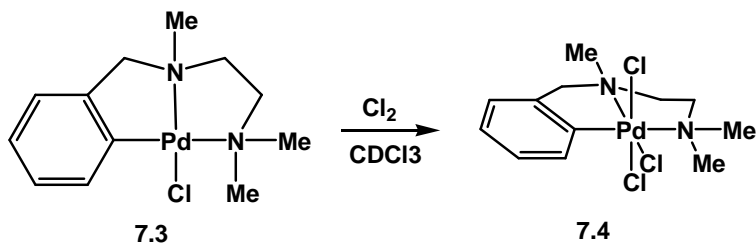


Figure 7.2 Chlorine oxidation of terdentate ligand supported Pd(II) to Pd(IV).³

Inspired by these results, Dr. Kraft and I had decided to investigate using chlorine as an oxidant to react with the *bis*-NHC-Pd(II)-(CH₃)₂ complex.

7.2 Chlorine Triggered C-C Bond and C-Cl Bond Formation at Lower Temperature.

10.0 mg *bis*-NHC-Pd(II)-(CH₃)₂ complex was dissolved in 0.60 mL dry CD₃CN in a J-Young NMR tube, and after degassing by three consecutive freeze, pump and-thaw cycles, 1 atm. of chlorine gas was introduced into the NMR tube at -40 °C, and the reaction was monitored by ¹H-NMR spectroscopy at -40 °C. The resonance for ethane (0.85 ppm) and the resonance for methyl chloride (3.03 ppm) showed up right after addition of chlorine in the ¹H-NMR spectrum. Three new singlet peaks also appeared: the two peaks at 2.24 ppm and 2.27 ppm were tentatively assigned for the equatorial and axial methyl groups of *bis*-NHC-Pd(IV)-(CH₃)₂-Cl₂ intermediate **7.5**., and the one at -0.02 was assigned to the methyl group of *bis*-NHC-Pd(II)-(CH₃)-Cl complex **7.6**. It was found that the starting material *bis*-NHC-Pd(II)-(CH₃)₂ complex was consumed in 30 minutes at -40 °C, and the resonances for the *bis*-NHC-Pd(IV)-(CH₃)₂-Cl₂ intermediate disappeared within 5 minutes after the depletion of the dimethylpalladium(II) complex **5.14**. The *bis*-NHC-Pd(II)-(CH₃)-Cl complex **7.6** was consumed in 20 minutes at -40 °C after the disappearance of the dimethylpalladium(II) complex **5.14**. The reaction process was recorded in a stacked ¹H-NMR spectrum in Figure 7.3. Using solvent residue dioxane as an internal standard, the integrations showed that ethane and methyl chloride formed with a ratio of 2/1 (assuming all the palladium coordinated methyl groups were converted to either ethane or methyl chloride). After completion of reaction, at least two *bis*-NHC-Pd species could be observed in the ¹H-NMR spectrum, and some white precipitation formed in the NMR tube.

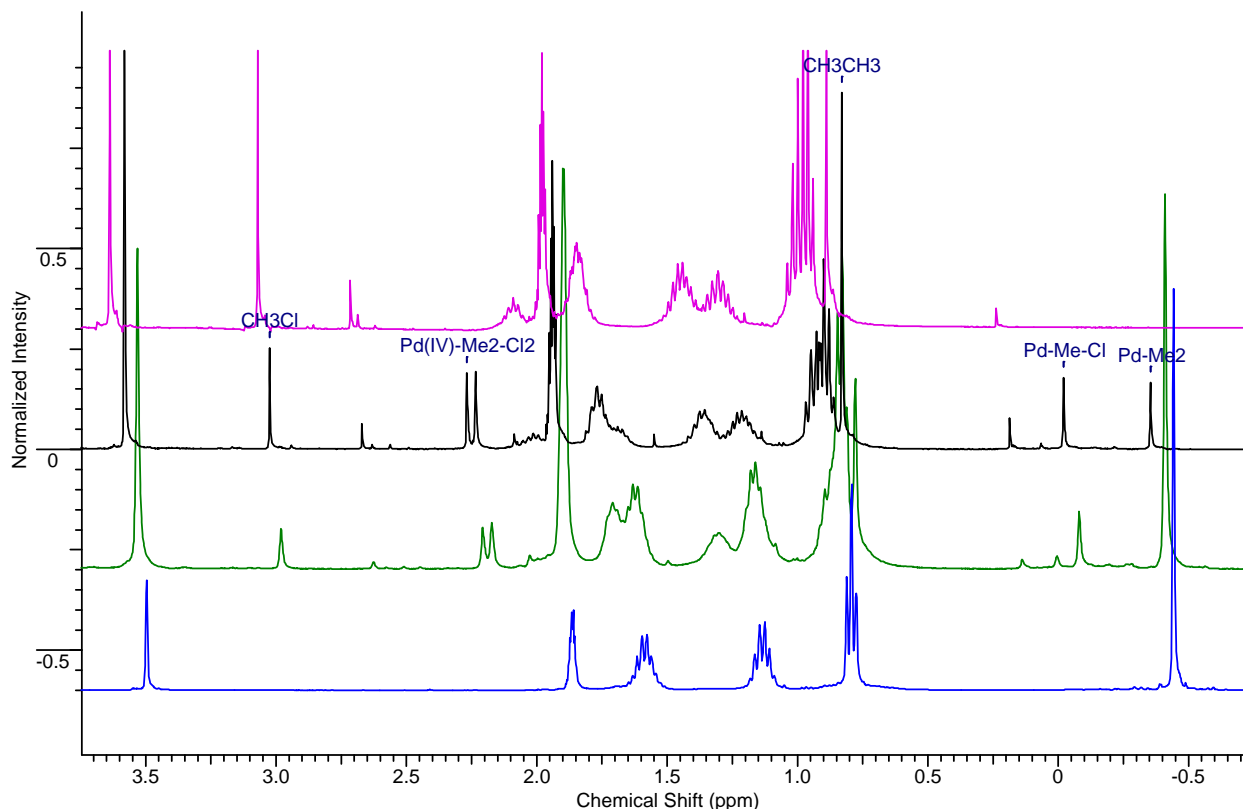


Figure 7.3 Stacked ^1H -NMR spectrum (expanded area to show the methyl chloride and ethane) of the reaction between the *bis*-NHC-Pd(II)- $(\text{CH}_3)_2$ complex **5.14** and chlorine gas at $-40\text{ }^\circ\text{C}$. (blue: *bis*-NHC-Pd(II)- $(\text{CH}_3)_2$ at $-40\text{ }^\circ\text{C}$; the green and black spectrum were recorded after adding chlorine gas with 10 minutes intervals; the pink spectrum was recorded after adding chlorine gas for 50 minutes).

7.3 Chlorine Triggered C-C Bond and C-Cl Bond Formation at Room Temperature.

In order to figure out the identity of the final products, the reaction has been diluted in order to avoid the occurrence of precipitation. 3.0 mg *bis*-NHC-Pd(II)- $(\text{CH}_3)_2$ complex was dissolved in 0.60 mL dry CD_3CN in a J-Young NMR tube, and after degassing by three consecutive freeze, pump and-thaw cycles, 1 atm. of chlorine gas was introduced into the NMR tube at room temperature and the reaction was monitored by ^1H -NMR spectroscopy. It was found that the starting material was consumed immediately, and no intermediates were observed. Both methyl chloride and ethane were produced, and two palladium complexes were present in the spectrum. One of the species disappeared after 5 minutes and the other one remained there

until to the end. The quickly disappearing species could be the *bis*-NHC-Pd(II)-Cl₂ complex **7.7**, which was oxidized by chlorine gas to *bis*-NHC-Pd(IV)-Cl₄ complex **7.9** (Figure 7.4).

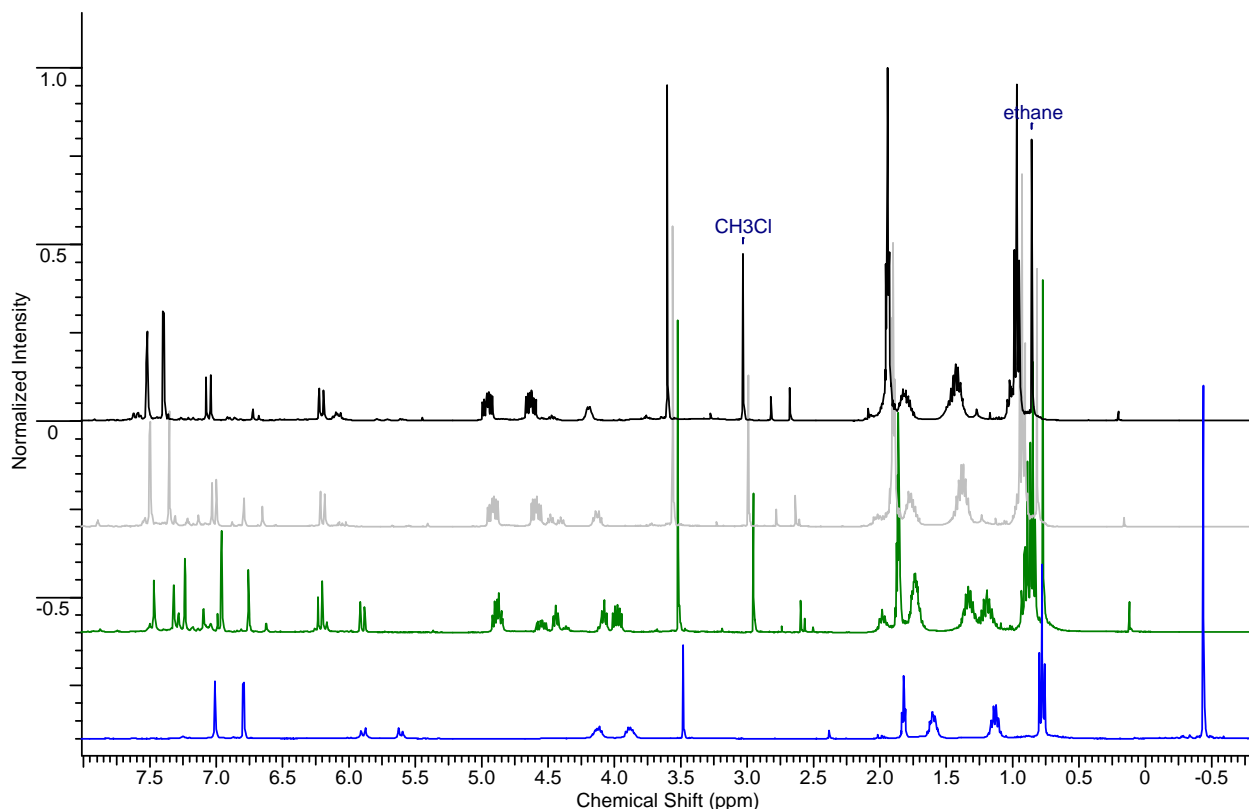


Figure 7.4 Stacked ¹H-NMR spectrum of the reaction between the *bis*-NHC-Pd(II)-(CH₃)₂ complex and chlorine gas at 25 °C. (blue: *bis*-NHC-Pd(II)-(CH₃)₂ at 25 °C; green: right after the addition of chlorine; the other two spectrum were recorded after adding chlorine gas with 5 minutes intervals).

7.4 Mass Spectroscopy Characterization of the Final Product

A drop of solution taken from the NMR tube was used to carry out a Mass spectroscopy characterization. When applying the electrospray ionization method,⁴ a tiny M+H⁺ ion was observed at 507.1 for the *bis*-NHC-Pd(IV)-Cl₄ complex, and the fragmentation ion was observed at 471.3 corresponding to [*bis*-NHC-Pd(IV)-Cl₃]⁺ with major intensity (Figure 7.5). Because the natural abundance of ³⁷Cl is 32.5% that of ³⁵Cl, the [M-Cl]⁺ (471.3, 100.0%), [M-Cl+2]⁺ (473.2, 84.9%), [M-Cl+4]⁺ (475.2, 79.8%), and [M-Cl+6]⁺ (477.2, 26.1%) isotope peaks clearly

demonstrate that the fragmentation ion contains three chlorine atoms. Further fragmentation leads to the formation of $[M-2Cl+H]^+$ ion at 437.1, $[M-3Cl]^+$ ion at 401.2, and $[M-4Cl+H]^+$ at 367.3.

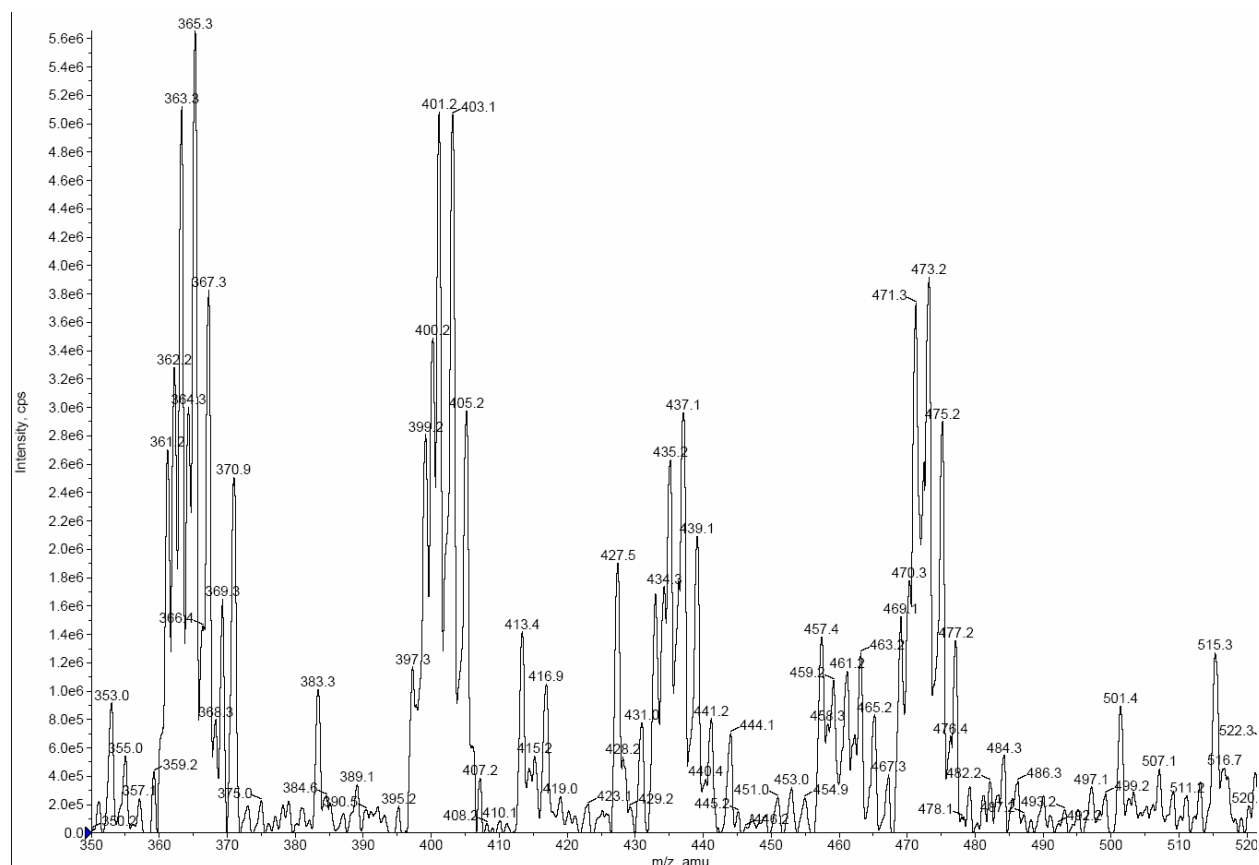


Figure 7.5 ESI⁺ Mass spectroscopy of the *bis*-NHC-Pd(IV)-Cl₄.

7.5 Discussion of The Mechanism of the Reaction between the *Bis*-NHC-Pd(II)-(CH₃)₂ Complex and Chlorine.

Based on the results obtained from the previous two experiments, we were able to propose a mechanism for the Cl₂ triggered C-C bond and C-Cl bond formation from the *bis*-NHC-Pd(II)-(CH₃)₂ complex. In the first step, the dimethylpalladium(II) complex **5.14** was oxidized to a *bis*-NHC-Pd(IV)-(CH₃)₂-Cl₂ intermediate **7.5**. In the second step, both C-C bond and C-Cl bond formation by reductive elimination occurs within the Pd(IV) intermediate. The C-

Cl reductive elimination yields methyl chloride and *bis*-NHC-Pd(II)-(CH₃)-Cl complex **7.6** as reaction products, and the C-C reductive elimination yields ethane and the *bis*-NHC-Pd(II)-Cl₂ complex **7.7** as reaction products. In the third step, the *bis*-NHC-Pd(II)-(CH₃)-Cl complex **7.6** is oxidized by chlorine to the *bis*-NHC-Pd(IV)-(CH₃)-Cl₃ intermediate **7.8**, from which C-Cl reductive elimination occurs again to form methyl chloride and the *bis*-NHC-Pd(II)-Cl₂ complex. In the fourth step, the *bis*-NHC-Pd(II)-Cl₂ complex is oxidized to the *bis*-NHC-Pd(IV)-Cl₄ complex **7.9**. (Figure 7.6)

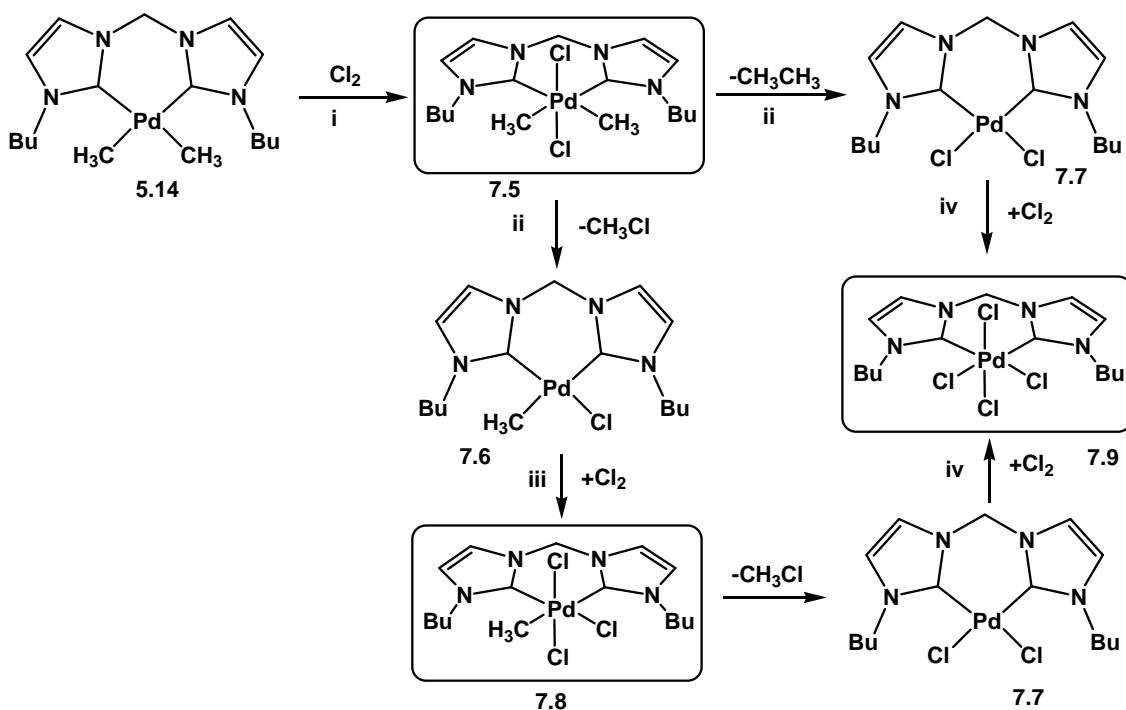


Figure 7.6 Proposed pathway for the reaction between the *bis*-NHC-Pd(II)-(CH₃)₂ complex and chlorine gas.

7.6 The Stability of the *Bis*-NHC-Pd(IV)-Cl₄ in Solution.

The solubility of the formed *bis*-NHC-Pd(IV)-Cl₄ complex **7.9** is very low in CD₃CN, after 2 hours at room temperature, most of the complex precipitated out of solution. CD₃CN was

carefully removed through a long syringe needle, and after drying in high vacuum, the residue was dissolved in 0.60 mL DMF- d_7 . Both *bis*-NHC-Pd(IV)-Cl₄ (**7.9**) and *bis*-NHC-Pd(II)-Cl₂ (**7.7**) were observed in the ¹H-NMR. After 2 hours at room temperature, the resonances for the Pd(IV) species completely disappeared, while the resonances for the *bis*-NHC-Pd(II)-Cl₂ remained unchanged. Using a solvent impurity (THF from the glove-box “vapor”) as internal standard, the peak positions and the integrations clearly indicated that all of the Pd(IV) species was eventually converted to the Pd(II) species (Figure 7.7). When 1 atm. of chlorine gas was bubbled through the solution for 10 seconds, the ¹H-NMR spectrum showed that all of the *bis*-NHC-Pd(II)-Cl₂ complex has been converted to the *bis*-NHC-Pd(IV)-Cl₄ complex (Figure 7.8).

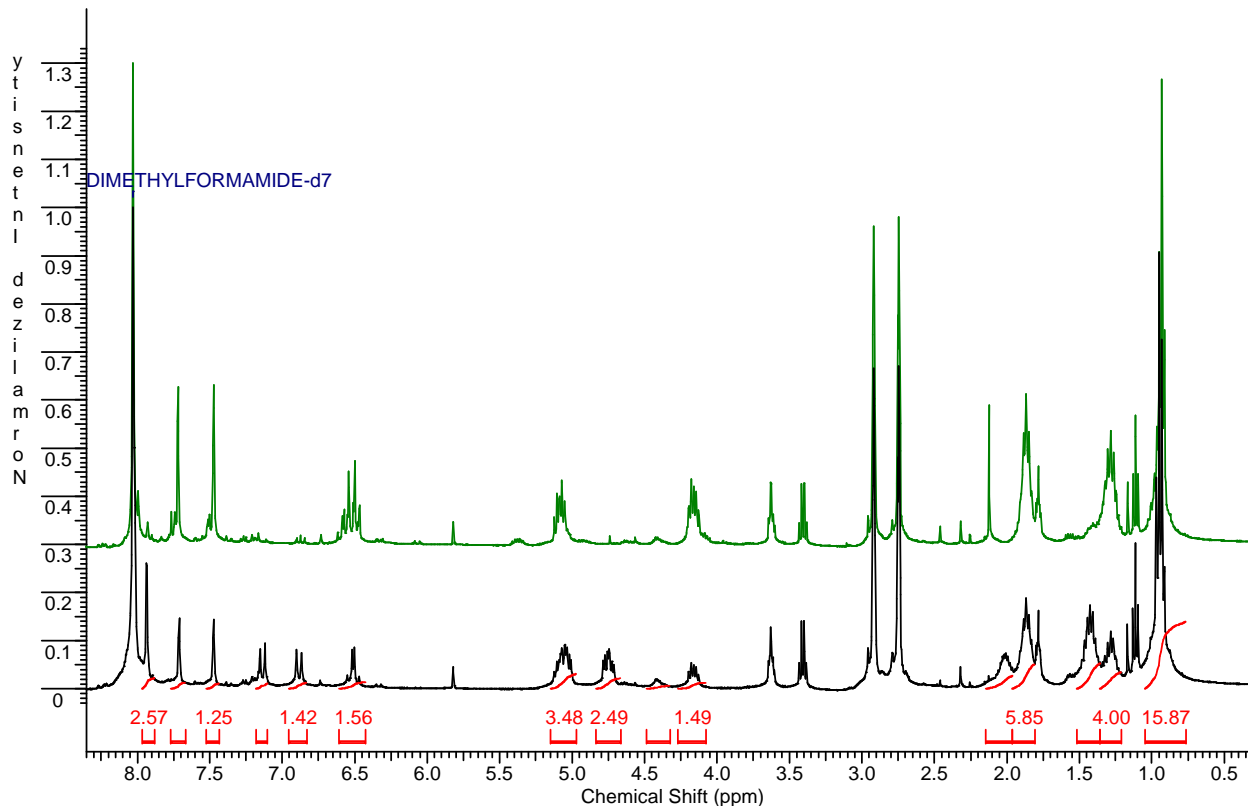


Figure 7.7 The *bis*-NHC-Pd(IV)-Cl₄ complex was reduced back to the *bis*-NHC-Pd(II)-Cl₂ complex in the absence of chlorine.

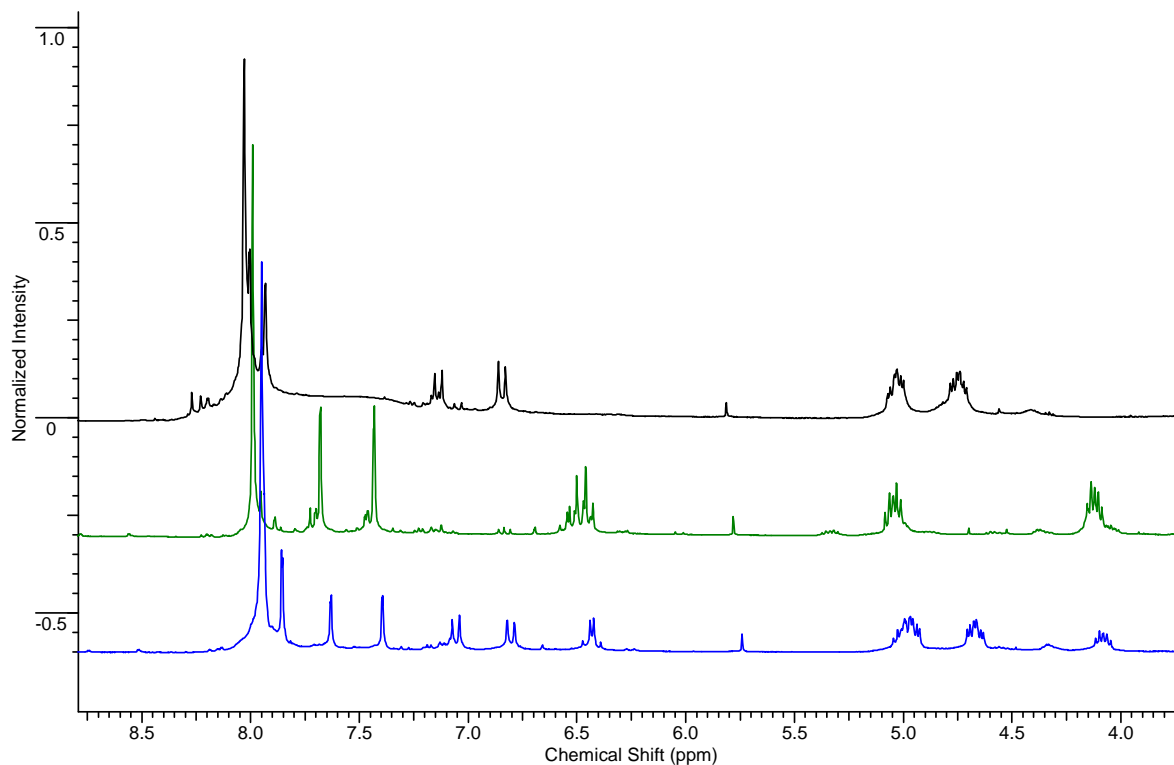


Figure 7.8 The *bis*-NHC-Pd(II)-Cl₂ complex was oxidized back to the *bis*-NHC-Pd(IV)-Cl₄ complex in the presence of chlorine.

From this experiment, we can clearly see that the *bis*-NHC-Pd(IV)-Cl₄ complex is not stable in DMF solution at room temperature. It can slowly dissociate chlorine gas and form the *bis*-NHC-Pd(II)-Cl₂ complex. But in the presence of excess chlorine gas, the *bis*-NHC-Pd(II)-Cl₂ complex can be re-oxidized back to the *bis*-NHC-Pd(IV)-Cl₄ complex (Figure 7.9).

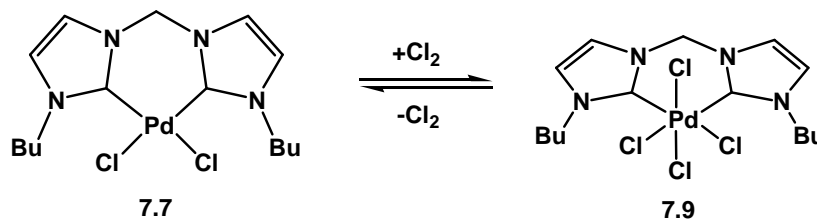


Figure 7.9 Reversible reaction between *bis*-NHC-ligand supported Pd(II) complex and Pd(IV) complex.

7.7 Crystal Structure of a Isolated *Bis*-NHC-Pd(IV)-Cl₄ Complex

Finally, single crystals of a *bis*-NHC-Pd(IV)-Cl₄ complex **7.9'** were obtained by slow vapor diffusion of CH₂Cl₂ into a solution of *bis*-NHC-Pd(II)-Br₂ complex in DMF in a chlorine atmosphere (Figure 7.10). This work was achieved by Scott Mccall, a talented undergraduate student who was working in Dr. Kraft's research lab in 2008. The crystal structure showed that the *bis*-NHC-Pd(IV)-Cl₄ complex to be monomeric with the dicarbene ligand chelating to the palladium(IV) center in a *cis* fashion with a boat-like conformation being observed for the six-membered C₃N₂Pd ring. The remaining four coordination sites of the distorted octahedral coordinated palladium center are occupied by chloride anions. Figure 7.11 showed the discrete molecule structure. Selected bond lengths and bond angles are listed in Table 7.1.

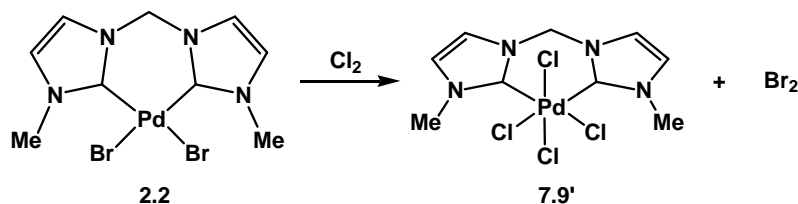


Figure 7.10 Formation of single crystals of a *bis*-NHC-Pd(IV)-Cl₄ complex.

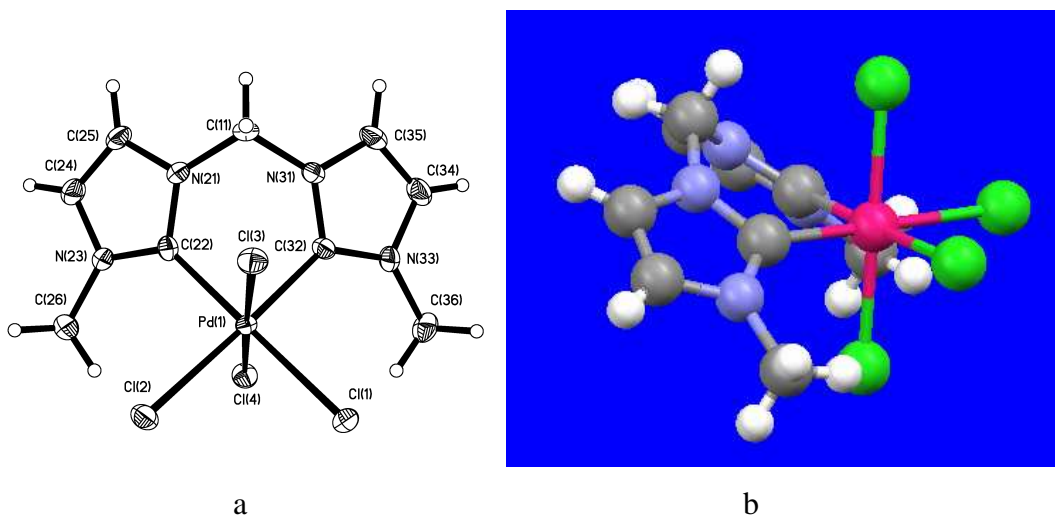


Figure 7.11 X-ray structure of the *bis*-NHC-Pd(IV)-Cl₄ complex (a: Thermal ellipsoid plot drawn at the 50% probability level; b: The boat conformation of the six-membered ring).

Table 7.1 Selected bond length and bond angle of the *bis*-NHC-Pd(IV)-Cl₄ complex

	Length (Å)		Angle (deg)
Pd(1)-C(22)	2.019(4)	C(32)-Pd(1)-Cl(4)	89.76(11)
Pd(1)-C(32)	2.015(4)	C(32)-Pd(1)-C(22)	85.80(15)
Pd(1)-Cl(4)	2.3081(9)	C(22)-Pd(1)-Cl(4)	89.08(11)
Pd(1)-Cl(3)	2.3189(9)	C(32)-Pd(1)-Cl(3)	88.29(11)
Pd(1)-Cl(1)	2.3769(10)	C(22)-Pd(1)-Cl(3)	91.33(10)
Pd(1)-Cl(2)	2.3813(9)	Cl(4)-Pd(1)-Cl(3)	177.97(3)
C(11)-N(31)	1.448(5)	C(32)-Pd(1)-Cl(1)	94.14(11)
C(11)-N(21)	1.456(5)	C(22)-Pd(1)-Cl(1)	179.08(11)
N(21)-C(22)	1.345(5)	Cl(4)-Pd(1)-Cl(1)	91.83(4)
N(21)-C(25)	1.376(5)	Cl(3)-Pd(1)-Cl(1)	87.76(3)
C(22)-N(23)	1.341(5)	C(32)-Pd(1)-Cl(2)	177.36(11)
N(23)-C(24)	1.391(5)	C(22)-Pd(1)-Cl(2)	92.64(10)
N(23)-C(26)	1.463(5)	Cl(4)-Pd(1)-Cl(2)	92.35(3)
C(24)-C(25)	1.343(6)	Cl(3)-Pd(1)-Cl(2)	89.62(3)
N(31)-C(32)	1.350(5)	Cl(1)-Pd(1)-Cl(2)	87.39(3)
N(31)-C(35)	1.385(5)	N(31)-C(11)-N(21)	109.3(3)
C(32)-N(33)	1.341(5)	C(22)-N(21)-C(25)	110.7(3)
N(33)-C(34)	1.391(5)	C(22)-N(21)-C(11)	125.6(3)
N(33)-C(36)	1.469(5)	C(25)-N(21)-C(11)	123.7(3)
C(34)-C(35)	1.337(6)	N(23)-C(22)-N(21)	105.9(3)
		N(23)-C(22)-Pd(1)	131.6(3)
		N(21)-C(22)-Pd(1)	122.5(3)
		C(22)-N(23)-C(24)	109.7(3)
		C(22)-N(23)-C(26)	130.2(3)
		C(24)-N(23)-C(26)	120.1(3)

A Pd(IV) complex with which the comparison can be made is the [Pd(IV)(bipy)Cl₄] complex, which was obtained by oxidative addition of chlorine to the [Pd(II)(bipy)Cl₂] complex.⁵ The crystal structure is shown in Figure 7.12. It was reported that Pd-Cl bond lengths fall in the range 2.289-2.310 Å in [Pd(IV)(bipy)Cl₄], and the mutually *trans* chlorines have significantly longer bonds to Pd (2.302-2.310 Å) than the chlorine atoms *trans* to nitrogen

(2.289-2.290 Å). In contrast to the [Pd(IV)(bipy)Cl₄] complex, the mutually *trans* chlorines have significantly shorter bonds to Pd (2.3081-2.3189 Å) than the chlorine atoms *trans* to the NHC ligand (2.3769-2.3813 Å) in the *bis*-NHC-Pd(IV)-Cl₄ complex. The bond length difference in these two Pd(IV) complexes clearly demonstrated that the NHC ligand possesses much stronger *trans* influence than the bipy ligand.⁶

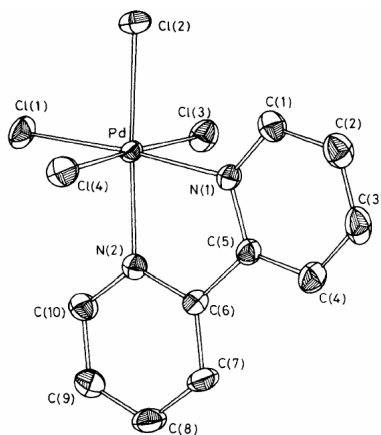


Figure 7.12 Discrete molecule of [Pd(IV)(bipy)Cl₄] excluding H atoms and with 40% probability thermal ellipsoids. (Structure copied from reference 5 without permission).⁵

7.8 Experimental

3.0 mg *bis*-NHC-Pd(II)-(CH₃)₂ complex was dissolved in 0.60 mL dry CD₃CN in a J-Young NMR tube, and after degassing by three consecutive freeze, pump and-thaw cycles, 1 atm. of chlorine gas was introduced into the NMR tube at room temperature and the reaction was monitored by ¹H-NMR spectroscopy. The starting material was consumed immediately. Both CH₃Cl and CH₃CH₃ were produced. The ¹H-NMR showed the resonance for the *bis*-NHC-Pd(IV)-Cl₄ complex **7.9**. ¹H NMR (δ_H; 400 Hz, CD₃CN): 0.95-0.98 (t, 6H, *J* = 7.32Hz, CH₃ of butyl side chain), 1.38-1.48 (broad multiplet, 4H, CH₂ of butyl side chain), 1.76-1.85 (broad multiplet, 4H, CH₂ of butyl side chain), 4.59-4.67 (broad multiplet, 2H, NCH₂ of butyl side chain), 4.92-4.99 (broad multiplet, 2H, NCH₂ of butyl side chain), 6.19-6.22 (d, 1H, *J* = 13.11 Hz, NCH₂), 7.04-7.08 (d, 1H, *J* = 13.11 Hz, NCH₂), 7.41 (d, 2H, *J* = 2.13 Hz, NCH), 7.52 (d, 2H, *J* = 2.13 Hz, NCH).

References

1. Uson, R.; Fornies, J.; Navarro, R. "Dichloro-bis(pentafluorophenyl)(chelate) complexes of palladium(IV)," *J. Organomet. Chem.* **1975**, *96*, 307-312.
2. Uson, R.; Fornies, J.; Navarro, R. "Novel organometallic palladium(IV) complexes," *Synth. React. Inorg. Met. Org. Chem.* **1977**, *7*, 235-241.
3. Alsters, P. L.; Engel, P. F.; Hogerheide, M. P.; Copijn, M.; Spek, A. L.; van Koten, G. "Rigid five- and six-membered C,N,N'-bound aryl, benzyl, and alkyl organopalladium complexes: sp^2 vs sp^3 C-H activation during cyclopalladation and palladium(IV) intermediates in oxidative addition reactions with dihalogens and alkyl halides," *Organometallics* **1993**, *12*, 1831-1844.
4. Fenn, J. B.; Mann, M.; Meng, C. K.; Wong, S. F.; Whitehouse, C. M. "Electrospray ionization for mass spectrometry of large biomolecules," *Science* **1989**, *246*, 64-71.
5. Gray, L. R.; Gulliver, D. J.; Levason, W.; Webster, M. "Co-ordination chemistry of higher oxidation states. Part 4. Palladium(IV) complexes of nitrogen, phosphorus, and arsenic donor ligands. Crystal and molecular structures of $[Pd(bipy)Cl_4]$ and $[Pd\{o-C_6H_4(AsMe_2)_2\}_2Cl_2][ClO_4]_2$," *J. Chem. Soc. Dalton Trans.* **1983**, 133-141.
6. Coe, B. J.; Glenwright, S. J. "Trans-effects in octahedral transition metal complexes," *Coordination Chemistry Reviews* **2000**, *203*, 5-80.

Chapter 8 Conclusion and Future Work of the *Bis*-NHC-Pd(IV) Studies

This work was initiated by the interest of the mechanism of the *bis*-NHC-Pd(II) species mediated C-H bond activation system. Surprisingly, the H-D exchange study showed that the *bis*-NHC-Pd(II) complex was not the active catalyst for the methane oxidation system! This unexpected result directed the remainder of my work on the pathway to study the *bis*-NHC-Pd(IV) chemistry. The oxidative addition of methyl iodide to the *bis*-NHC-Pd(II)-Me₂ complex led to the successful observation of the formation of a transient [*bis*-NHC-Pd(IV)-Me₃] intermediate by both ¹H-NMR and ¹³C-NMR spectroscopy. Dioxygen triggered C-C bond formation and dioxygen triggered C-C and C-O bond formation in the presence of H₂O has provided a strong indication that the *bis*-NHC-Pd(II)-Me₂ complex can be oxidized to a *bis*-NHC-Pd(IV) intermediate by dioxygen. The reaction between the hypervalent iodine reagents and *bis*-NHC-Pd(II)-Me₂ complex gave selectively reductive elimination products, which can act as a model system that is able to provide valuable information of the product forming (functionalization) step of the C-H bond activation system. The reaction between chlorine and the *bis*-NHC-Pd(II)-Me₂ complex resulted in a relatively stable *bis*-NHC-Pd(IV)-Cl₄ complex, which was characterized by ¹H-NMR spectroscopy and mass spectroscopy. The structure of the *bis*-NHC-Pd(IV)-Cl₄ was definitely established by X-ray crystallography (single crystals were obtained by Scott McCall).

In the future, the reaction between dioxygen and the *bis*-NHC-Pd(II)-Me₂ complex deserves a more detailed study. The mechanisms of the palladium-catalyzed selective aerobic oxidation of organic molecules have been proposed to proceed via a Pd(II)/Pd(0) catalytic cycle, in which Pd(II) mediates substrate oxidation and Pd(0) is re-oxidized by dioxygen.^{1,2,3,4} The finding that it is possible that Pd(II) can be oxidized to Pd(IV) by dioxygen may lead to a new insight into the mechanism of the palladium-catalyzed aerobic oxidation reactions. There is no doubt the reactivity of the isolated *bis*-NHC-Pd(IV)-Cl₄ complex toward C-H bonds should be carefully studied. The preliminary stability study indicated that this Pd(IV) species stoichiometrically releases chlorine gas in solution and slowly goes back to the Pd(II) species. This particular character of the Pd(IV) species makes it a potential chlorine storage reagent.

References

1. Stahl, S. S. "Palladium oxidase catalysis: Selective oxidation of organic chemicals by direct dioxygen-coupled turnover," *Angew. Chem. Int. Ed.* **2004**, *43*, 3400-3420.
2. Jensen, D. R.; Schultz, M. J.; Mueller, J. A.; Sigman, M. S. "A well-defined complex for palladium-catalyzed aerobic oxidation of alcohols: Design, synthesis, and mechanistic considerations," *Angew. Chem. Int. Ed.*, **2003**, *42*, 3810-3813.
3. Cornell, C. N.; Sigman, M. S. "Recent progress in Wacker oxidations: Moving toward molecular oxygen as the sole oxidant," *Inorg. Chem.* **2007**, *46*, 1903-1909.
4. Gligorich, K.M.; Sigman, M.S. "Recent advancements and challenges of palladiumII-catalyzed oxidation reactions with molecular oxygen as sole oxidant," *Chem. Commun.*, **2009**, 3854 – 3867.

Chapter 9 Synthesis of Functionalized Bimagnetic Core/Shell Fe/Fe₃O₄ Nanoparticles for the Treatment of Cancer

I would like to acknowledge all the researchers who have worked on this project and made this chapter possible.

Sivasai Balivada, Dr. Raja Shekar Rachakatla, Marla Pyle, Dr. Masaaki Tamura, Dr. Deryl L. Troyer from Department of Anatomy and Physiology, Kansas State University, who designed, performed *in vitro* and *in vivo* experiments and interpreted data.

Raj Kumar Dani, Dr. Viktor Chikan from Department of Chemistry, Kansas State University, who supervised AMF experiments and interpreted AMF data.

Dr. Franklin O. Kroh, Brandon Walker, Dr. Xiaoxuan Leaym, Dr. Olga B. Koper, from NanoScale Corporation, Manhattan, KS., who provided core/shell Fe/Fe₃O₄ nanoparticles.

Thilani N. Samarakoon, Dr. Leila Maurmann from Department of Chemistry, Kansas State University, who carried out the T¹, T² measurement

9.1 Introduction

The application of hyperthermia in cancer treatment has been recently attracted a lot of attention, because it has a lot of synergy with classic treatment techniques, such as chemotherapy. In hyperthermia (also called thermal therapy or thermotherapy), body tissue is exposed to high temperatures (currently up to 45°C). Cancerous tissue has been shown to be more susceptible to heat damage than healthy tissue.¹ It is also of importance that hyperthermia is known to trigger the biosynthesis and consequent release of heat shock proteins from the cancer cells, which can stimulate the immuno-response to cancer. Several methods of hyperthermia are currently under study, including local, regional, and whole-body hyperthermia.²⁻⁵

In local hyperthermia, heat is applied to a defined area, such as a tumor, using a variety of conceptionally different techniques (including microwave, radiofrequency, and ultrasound) that are capable of delivering energy to heat the tumor tissue.⁶

A/C-Magnetic hyperthermia⁷ makes use of nanoparticles that are being delivered to the tumor site either by using the enhanced permeation and retention effect (EPR or passive delivery) caused by rapid angiogenesis in the vicinity of the tumors,^{8,9} or by targeted delivery making use of attached antibodies (ABs) or AB-fragments, or of small attached molecules that can trigger receptors at the surface of tumor cells that facilitate their intake.^{8,10}

Porphyrins are known to trigger highly selective uptake by the cancer cells, because they over-express porphyrin receptors in their cell membranes. They are in need of porphyrins as prosthetic groups in their elevated sugar-metabolism.¹¹ The LDL-receptor (low-density-lipoprotein), which is over-expressed in cancer cells, has the ability to take up porphyrins, either alone and/or by a simultaneous lipid uptake mechanism. The higher the hydrophobicity of a porphyrin, chlorin or bacteriochlorin, the easier can the uptake be facilitated by the LDL-receptor.¹² Besides their rapid uptake by cancer cells, porphyrins, as well as porphyrin-labeled nanoparticles, have a tendency to be taken up by stem cells as well.¹³ Therefore, they may enable killing cancer stem cells by hyperthermia treatment together with the fast growing tumor cells. This would be a significant advantage when compared to classic chemotherapy.

Several examples of the chemical attachment of porphyrins and related compounds to iron oxide nanoparticles exist in the literature.¹⁴⁻¹⁷ All of these references follow the approach of combining photodynamic therapy and hyperthermia. The potential of porphyrin-based fluorescence imaging of tumors and the use of iron oxide nanoparticles as MRI contrast agents has been discussed as well.¹⁸ Although the porphyrins were attached primarily as singlet oxygen photosensitizers, it must be noted that the targeting efficiency is very high and can exceed 50/1 (cancer tissue/healthy tissue),¹⁹ which is significantly better than less than 10/1 for classic chemotherapy.²⁰

Since the pioneering studies of Gordon et al. demonstrating induced intracellular hyperthermia using dextran magnetite nanoparticles in a high frequency magnetic field (such as 100-500 kHz), the advantages of iron oxide based magnetic nanoparticles, such as negligible or low toxicity, biocompatibility, injectability into the blood stream, potentially high level accumulation in the target tumor, make them prime candidates for hyperthermia applications.²¹ However, the specific absorption rates (SAR's) of those early systems were low.

Magnetic nanoparticles absorb the power of an AC magnetic field and transmit it to their surroundings, therefore providing heating (magnetic hyperthermia).^{22,23} The important factor for

magnetic heating experiments is the specific absorption rate or SAR, which is determined by $SAR=C*\Delta T/\Delta t$, where C is the specific heat capacity of the sample and T and t are the temperature and time, respectively. SAR is very sensitive to the material properties. While in multi-domain particles the dominant heating is hysteresis loss due to the movement of domain walls, it is not so in case of small particles. The two main contributing mechanisms of SAR in single domain magnetic nanoparticles are the Brownian (rotation of the entire nanoparticles)²⁴ and Néel (random flipping of the spin without rotation of the particle) relaxations.²⁵ The transition between the two mechanisms occurs between 8-12nm for iron and iron oxides,^{8,26} but it also varies with frequency.²⁷

To date, the frequencies employed in A/C-hyperthermia (63-700 kHz), as well as the amplitudes (3-25 kA m⁻¹) and nanoparticles concentrations vary considerably so that direct comparisons of the SAR's (Specific Absorption Rate) of various magnetic nanoparticles are rather difficult.²⁸ The state-of-the-art of A/C-magnetic hyperthermia using superparamagnetic and paramagnetic iron oxide (nano)particles has been recently summarized in several reviews.^{8,29,30}

Hergt et al. have demonstrated that the SAR of iron oxide nanoparticles (maghemite) can reach values up to more than 400 W g⁻¹ at 410 kHz for particles featuring diameters of more than 15nm, which follow Brownian relaxation.³⁰ The experimentally SAR's for iron oxide nanoparticles, which are below 8nm in diameter and follow Néel relaxation are much smaller (SAR < 20 W g⁻¹). Only a few reports of iron(0) nanoparticles and iron/iron oxide core/shell nanoparticles for hyperthermia applications exists in the literature to date.³¹⁻³⁴ These systems, although up to more than five times more efficient in their specific absorption rates³⁴ and, therefore, in the heating of tumor tissue,³⁵ suffer from rapid oxidation/biocorrosion in vivo. Furthermore, special preparation techniques are required for many of these systems, which make their mass production and handling under clinical conditions less likely.^{32, 34}

9.2 Research Goal

It was our aim to synthesize water-soluble stealth iron/iron oxide core/shell nanoparticles that should be sufficiently stable when injected into the bloodstream or directly into the tumor to

perform as efficient heat transmitters in A/C-hyperthermia experiments. These nanoparticles should feature an inorganic iron/ iron oxide core/shell structure that is smaller than 10nm to permit efficient uptake by cancer cells.^{8,36,37} Superparamagnetic iron possesses a higher magnetic moment and a higher saturation magnetization, which permits both lower concentrations and shorter A/C- heating times during the treatment of patients.³⁸ Iron oxide shell could both protect the iron core from oxidation, and act as Magnetic Resonance Imaging (MRI) contrast reagent to permit the detection of cancer tissue. Dopamine-anchored tetraethylene glycol ligands should be bound to the iron oxide shell of the core/shell nanoparticles to provide further protection against biocorrosion caused by the aqueous environment³⁹ and especially in the presence of thiol-containing proteins/peptides.⁴⁰ The dopamine-anchored tetraethylene glycol ligands should also provide stealth-protection against rapid clearance of the nanoparticles by the reticuloendothelial system.^{7,8} Furthermore, porphyrin TCPP (tetracarboxyphenyl-porphyrin) as targeting ligand should be tethered to the dopamine-anchored tetraethylene glycol to permit active targeting of cancer cells.

9.3 Surface Modification of the Fe/Fe₃O₄ Core/Shell Nanoparticles

9.3.1 Synthesis of the Organic Ligands

The synthesis and characterization of the dopamine-anchored stealth-ligands is described in detail in the experimental section. In short, a protection-deprotection sequence of the primary aliphatic amine group and the phenolic OH-groups permitted the selective reaction of the amine-group with succinic anhydride to generate carboxylic acid,^{41,42} which reacts with tetraethylene glycol to yield a dopamine-anchored tetraethylene glycol ligand **I**.⁴³ The reaction sequence is summarized in Figure 9.1.

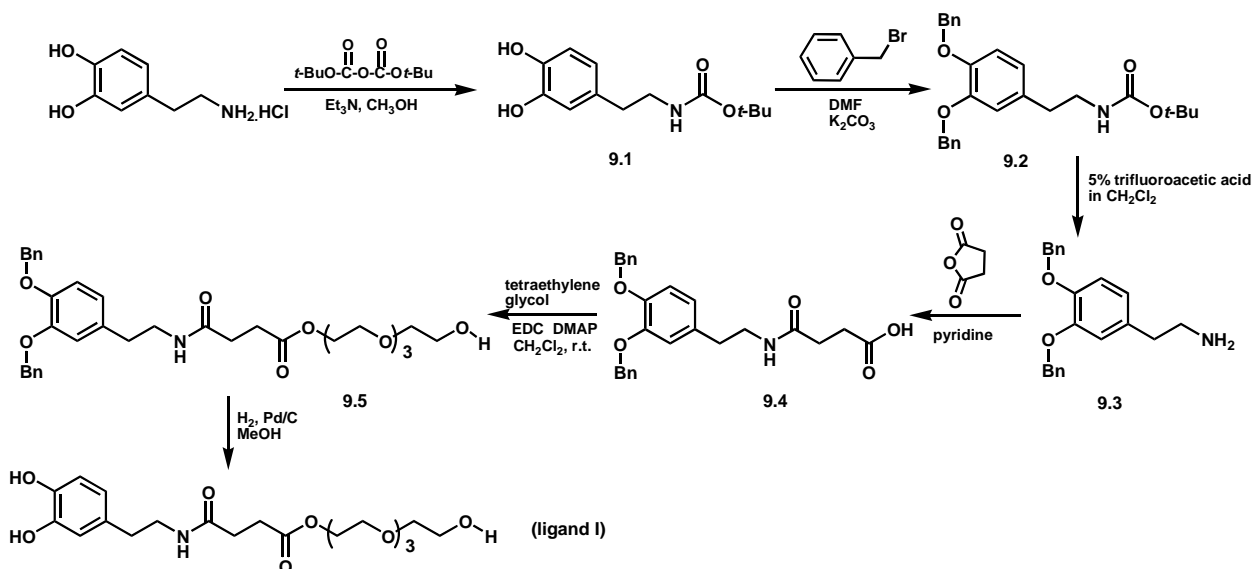


Figure 9.1 Synthesis of dopamine-anchored tetraethylene glycol ligand for the stabilization of $\text{Fe}/\text{Fe}_3\text{O}_4$ -nanoparticles (t-Bu: tertiary butylate, Bn: benzyl, EDC: 1-Ethyl-3-[3-dimethylaminopropyl]carbodiimide, DMAP: 4-Dimethyl-aminopyridine, DMF: Dimethylformamide).^{41,42}

To enhance the solubility of the stealth-protected $\text{Fe}/\text{Fe}_3\text{O}_4$ -nanoparticles, an Fmoc-protected glycine-unit was connected to the dopamine-anchored tetraethylene glycol ligand via an ester bond by using EDC/DMAP.⁴³ Both protection groups, Bn and Fmoc, were removed together by hydrogenation in the presence of catalytic amount of Pd/C and acetonitrile (Figure 9.2).⁴⁴

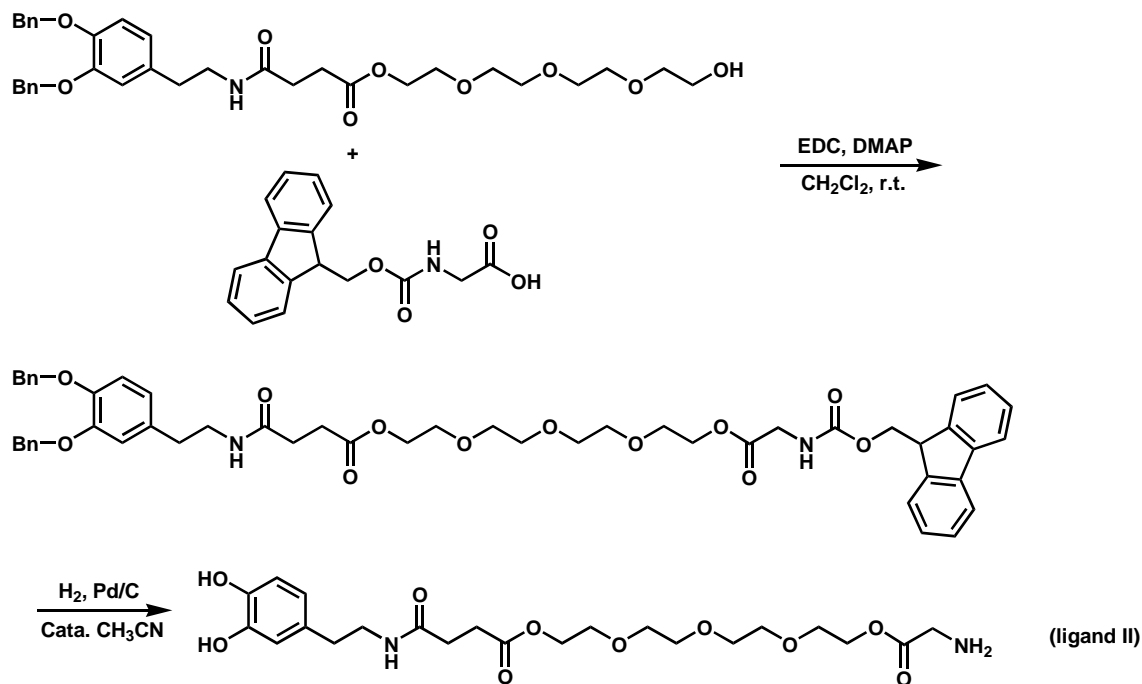


Figure 9.2 Synthesis of “glycine-tipped” dopamine-anchored tetraethylene glycol ligands for the stabilization of Fe/Fe₃O₄-nanoparticles (Bn: benzyl, EDC: 1-Ethyl-3-[3-dimethylaminopropyl]carbodiimide, DMAP: 4-Dimethyl-aminopyridine, Fmoc: Fluorenylmethyloxycarbonyl-).^{43,44}

9.3.2 Tethering the Ligands on the Nanoparticles and Introduction of a TCPP Porphyrin as Targeting Tag

The Fe/Fe₃O₄-nanoparticles were dispersed in THF by sonication and a mixture of dopamine-anchored tetraethylene glycol ligand and glycine-tipped tetraethylene glycol ligand (95/5; mol/mol) was added. The mixture was allowed to react for 60 min.^{42,45} The nanoparticles were then collected by using a strong magnet (0.5T). The excess ligands were removed by repeated washing of the nanoparticles with THF (up to 10 washing-magnetoprecipitation-redispersion cycles). TCPP was co-dissolved in THF and tethered by an amide-bond to the amine-function of the “glycine-tipped” tetraethylene glycol ligands. Since the amines of ligand (II) are not protonized in THF, they will react much faster in an EDC/NHS procedure.⁴⁶ After sonication

for a designated time, the un-reacted porphyrin TCPP and coupling reagents were removed by repeated washing of the nanoparticles with THF (up to 10 washing-magnetoprecipitation-redispersion cycles). The last three redispersion&washing procedures were performed in argon-saturated PBS prior to physical characterization or use in hyperthermia experiments (Figure 9.3).

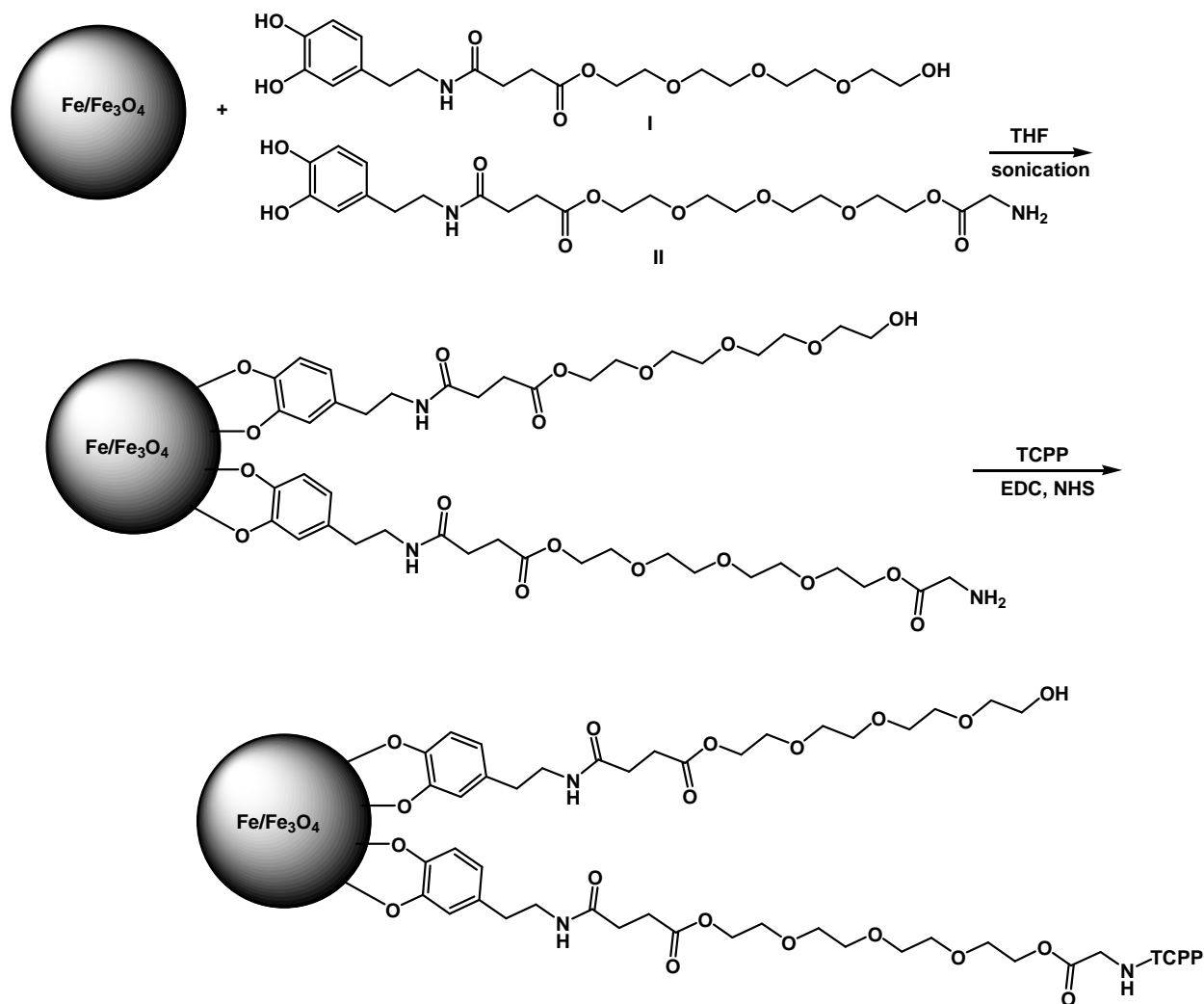


Figure 9.3 Synthesis of dopamine-anchored stealth nanoparticles using two ligands: dopamine-anchored tetraethylene glycol (I) and “glycine-tipped” dopamine-anchored tetraethylene glycol (II). A molar ratio of 95 mol percent (I) and 5 mol percent (II) was used for the organic stealth layers of all $\text{Fe}/\text{Fe}_3\text{O}_4$ core/shell nanoparticles synthesized here. Mesotetrakis-4-(carboxylphenyl)porphyrin was attached by using an EDC/NHS standard protocol in THF (EDC: 1-Ethyl-3-[3-dimethylaminopropyl]carbodiimide, NHS: *N*-Hydroxysuccinimide).^{45,46}

9.4 Magnetic Heating of Nanoparticles

Iron/iron oxide nanoparticles with different iron core sizes and diameters were provided by NanoScale Corporation. After treating with a molar ratio of 95 mol percent ligand I and 5 mol percent ligand II, the solubility of these surface modified nanoparticles were measured; and the heating capability of different sized nanoparticles were evaluated by the hyperthermia apparatus developed by Dr. Chikan of KSU's Chemistry Department (Table 9.1). The hyperthermia apparatus used here has a "heavy duty" induction heater converted to allow measurement of the temperature of a sample. In the setup, a remote fiber optic probe (Neoptix) is used to monitor the temperature change. The frequency is fixed (366 kHz), sine wave pattern); field amplitude is 5 kA/m. The coil diameter is 1 inch, 4 turns continuously water cooled. As it can be seen in Table 9.1, the nanoparticles with iron cores demonstrated a much better heating capacity than the iron oxide nanoparticle. Among all the nanoparticle samples, the one with 5.4 ± 1.1 nm iron core and 7.2 ± 2.8 nm total diameter of the nanoparticle (sample #4) exhibited best heating effect, a specific absorption rate (SAR) of 63.9 was observed.

Table 9.1 Experimental data including SAR values of nanoparticles synthesized by NanoScale/KSU: H: 5.0 kA m^{-1} , frequency 366 kHz (sine wave pattern).^a

Nanoparticle Sample	ΔT_{max} ($^{\circ}\text{C}$)	Fe(0) Core Size (nm)	Diameter of the inorganic NP (nm)	Solubility in H_2O (mg/ml)	SAR (W/g (Fe))
Fe/Fe ₃ O ₄ #1	18	2.1 ± 0.4	5.5 ± 0.8	0.015	24.5
Fe/Fe ₃ O ₄ #2	25	4.1 ± 1.3	6.2 ± 1.4	0.16	47.6
Fe/Fe ₃ O ₄ #3	23	5.3 ± 1.2	7.0 ± 2.2	0.11	46.4
Fe/Fe ₃ O ₄ #4	34	5.4 ± 1.1	7.2 ± 2.8	0.35	63.9
Fe ₃ O ₄ #5	5	/	7.5 ± 2.9	0.38	5.2

a) conc: 0.050 mg mL^{-1} of organically coated stealth NPs (Fe-conc.: $0.0107\text{-}0.1150 \text{ mg mL}^{-1}$, as determined by ICP-fluorescence detection.)

9.5 Light-Absorption and Emission Properties of Fe/Fe₃O₄ Core/Shell Nanoparticles Featuring Chemically Attached Porphyrin Units (TCPP)

The onset of the absorption&scattering peak of the nanoscopic Fe/Fe₃O₄ core/shell nanoparticles can be observed at approx. 320 nm. At higher wavelengths no UV/Vis absorption&scattering is observed. However, when meso-tetrakis(4-carboxyphenyl) porphyrin (TCPP) is chemically linked to the Fe/Fe₃O₄ core/shell nanoparticles, it dominates the UV/Vis-absorption in the visible range. As it can be seen in Figure 9.4, the peak position of the Soret band (extremely intense near-ultraviolet band) are $\lambda = 417\text{nm}$ for TCPP. The absorption coefficients are $4.8 \times 10^5 \text{ M}^{-1} \text{ cm}^{-1}$ for TCPP in principal agreement with the literature.⁴⁷ It is noteworthy that chemical attachment to the bimagnetic Fe/Fe₃O₄ nanoparticles via a dopamine-tetraethylene glycol bridge decreases the absorption coefficient of TCPP by approximately a factor of 2.1. Figure 4 shows the UV/Vis-spectra for two TCPP-doped nanoparticles, which both are based on core/shell nanoparticle sample #4 (see Table 9.1). We have determined the ratios of Fe/Fe₃O₄ to porphyrin are 1:5 and 1:1.2.

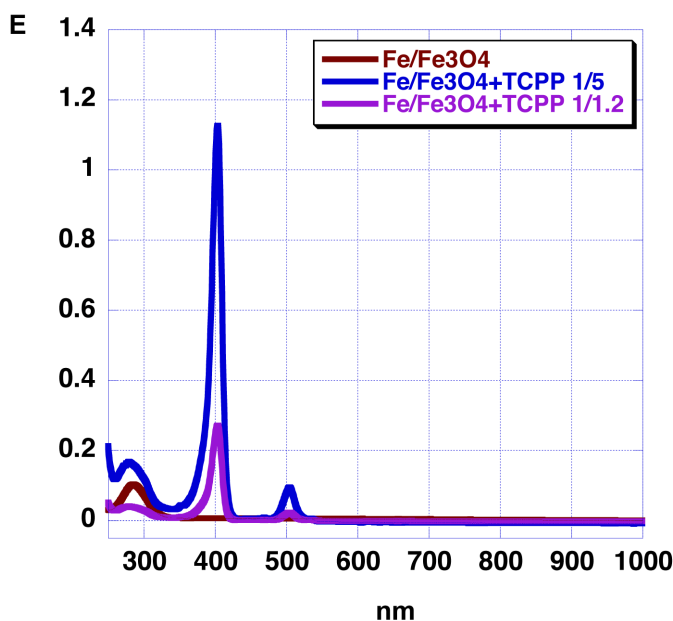


Figure 9.4 UV/Vis-spectra of Fe/Fe₃O₄ core/shell nanoparticles (#4, see Table 1) containing 0, 1.2 and 5 TCPP units per nanoparticle (statistical average) in 0.05M aqueous phosphate buffer (pH=7.2)

The light emission behavior is shown in Figure 9.5: TCPP (non-metalated) and, tethered to the Fe/Fe₃O₄-NPs has two emission bands at $\lambda_1= 654\text{nm}$, $\lambda_2= 718\text{nm}$. The fluorescence quantum yield does not exceed a maximum of $\Phi=0.011$ for the Fe/Fe₃O₄-bound porphyrins, which is approx. 20 times lower than in aqueous solution. Emission from the iron(0)-core is not detectable.

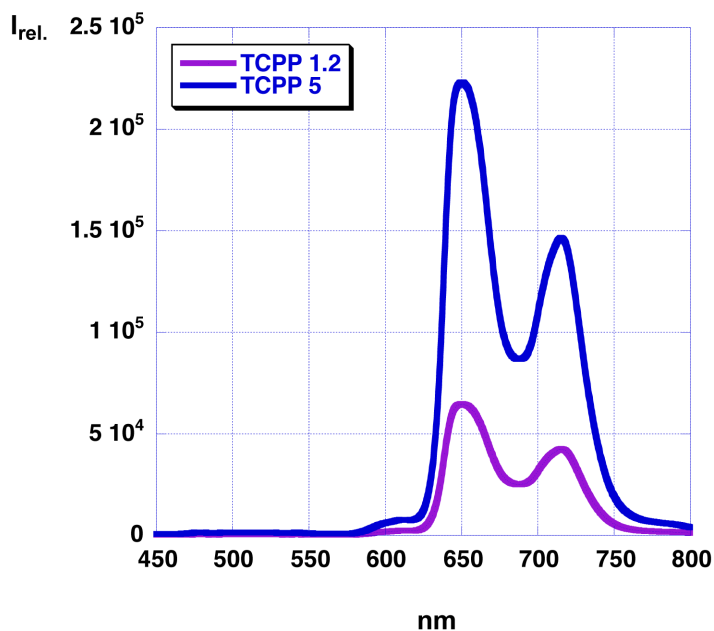


Figure 9.5 Fluorescence emission of Fe/Fe₃O₄ core/shell nanoparticles (#4, see Table 1) 1.2 and 5 TCPP units per nanoparticle (statistical average) in 0.05M aqueous phosphate buffer (pH=7.2); excitation wavelength: 400 nm.

9.6 NMR-Measurement of T¹ and T²-Relaxation Times

Aqueous dispersions of single, stabilized sub-20nm nanocrystals (hydrodynamic size) of iron oxides are classified as ultrasmall particles of iron-oxide (USPIO). Typically, these materials generate positive contrasts in T₁-weighted images and negative contrasts in T₂-weighted images. Typical relaxivities r_1 for aqueous USPIO dispersions are 10-20 mM⁻¹ s⁻¹ for T₁-enhancement and $r_2 = \text{approx. } -100 \text{ mM}^{-1} \text{ s}^{-1}$ for T₂-decrease in clinical MRI fields of 60-100 MHz (1.4 to 2.35 T). The relaxivities r_1 and r_2 are measures of the ability of the agent to enhance/decrease the longitudinal and transversal relaxation of the proton spins in the tissue.⁴⁸

$r_1 = \frac{T_{1,contrast}^{-1} - T_{1,water}^{-1}}{c(Fe)}$	$r_2 = \frac{T_{2,contrast}^{-1} - T_{2,water}^{-1}}{c(Fe)}$
$c(Fe): \text{ mM}, T_1, T_2: \text{ s}$	

In 1996, Feridex® (dextran coating) was introduced as the world's first organ-specific MR imaging agent for detecting and evaluating liver lesions associated with an alteration in the reticuloendothelial system (RES).⁴⁹ Feridex® consists of a γ -Fe₂O₃-core of 4-5nm in diameter and a dextran coating. The ratio $r_2/r_1 = -10.4$ of Feridex® is an important benchmark, which has to be exceeded in any successful future development of simultaneous T₁-positive and T₂-negative MRI contrast agents.

We have determined the concentration dependence of the Fe/Fe₃O₄-nanoparticles (inorganic cores alone and after the stealth-layer has been attached) on the T₁ and T₂-relaxation behavior of ¹H-spins in water employing KSU's 400MHz NMR (Varian, field strength 9.4 T) using standard T₁ and T₂ pulse sequences. These are definitely high field conditions, which are usually off the maximum of proton relaxivity.⁵⁰ Figure 9.6 indicates that the tetraethylene-glycol-stabilized bimetallic nanoparticles increase the T₁-relaxation time. As anticipated, the presence of the tetraethylene glycol layer does not hamper the magnetic effects of the nanoparticle on the surrounding H₂O/D₂O-mixture.⁵⁰ This is a clear advantage of the Fe/Fe₃O₄-nanoparticles, compared with gadolinium-based contrast agents. The maximally observed increase of T¹ is 16 times, which is close to the best results reported in the literature.⁵¹ As Figure 9.7 shows, T² is remarkably decreased (up to a factor of 57) when Fe/Fe₃O₄-nanoparticles are added. The observed significant decrease in T², which is very promising with respect to the use of NanoScale's bimetallic nanoparticles as MRI contrast agents, occurs due to the presence of the superparamagnetic iron(0)-cores in the nanoparticles.⁵² The increase of T² at higher nanoparticle concentrations is again in agreement with the relevant literature.⁵⁰⁻⁵² Note that sample #5, which was obtained by oxidation of sample #4 in air for 14 days prior to the attachment of the stabilizing dopamine-anchored stealth layer, shows a much smaller decrease of T². For instance, at a concentration of 80 $\mu\text{g/mL}$, T²=1.24±0.22 s was measured for Fe_xO_y (composition very close to Fe₂O₃) compared to T²=0.072±0.005 s in the presence of stealth coated Fe/Fe₃O₄. The decrease of T² to values that are significantly below 1 s at high field conditions can be regarded

as experimental proof of the existence of an Fe(0)-core, especially when considering that our Fe/Fe₃O₄-nanoparticles are below 10nm in diameter.

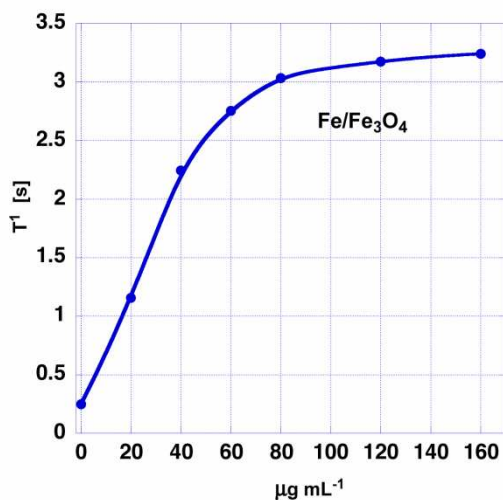


Figure 9.6 T¹-relaxation times of H₂O/D₂O (9/1) at 9.4T in dependence on the concentration of Fe/Fe₃O₄-NPs (#4, see Table 1).

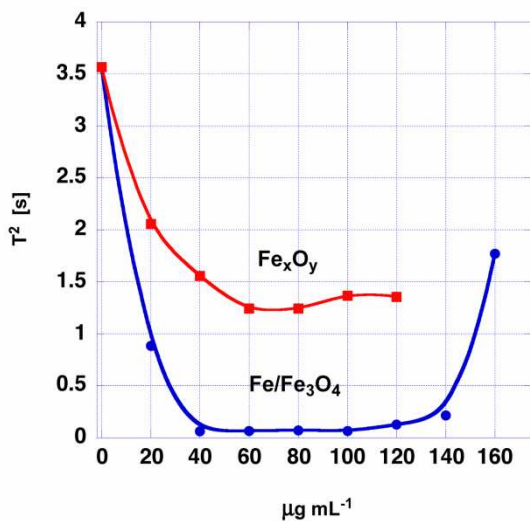


Figure 9.7 T²-relaxation times of H₂O/D₂O (9/1) at 9.4T in dependence on the concentration of NPs (Fe/Fe₃O₄: #4, Fe_xO_y: #5, see Table 1).

In a concentration range from 20 to 80 µg Fe per mL, NanoScale Corporation's new materials achieved a maximal $r_1 = 150 \pm 20 \text{ mM s}^{-1}$ and a $r_2 = (-)4300 \pm 250 \text{ mM s}^{-1}$, $r_2/r_1 = -28$, which is advantageous in T₁-enhancement, T₂-decrease and the ratio of r_2/r_1 . The observed

increase of T^2 and higher concentrations of Fe/Fe₃O₄-nanoparticles can be attributed to the formation of clusters of nanoparticles, which change the physical behavior from superparamagnetic to paramagnetic.^{29,52}

9.7 Hyperthermia Experiments of Charles River Mice Featuring Impregnated B16-F10-Melanomas.

Surface modified core/shell nanoparticle sample #4 in Table 9.1 tethering TCPP (the ratio of Fe/Fe₃O₄ to porphyrin is 1:5) was chosen to carry out the hyperthermia experiment because these nanoparticles exhibited highest heating effect among all the samples. The nanoparticles were administered to B16-F10 melanoma bearing mice either by intratumoral injection or intravenous injection. Tumors were exposed to alternating magnetic field (AMF), and the effects of magnetic hyperthermia were evaluated by measuring the tumor size and tumor weight after AMF exposure.

9.7.1 Cytotoxicity of Magnetic Nanoparticles on B16-F10 cells.

Potential cytotoxic effects of MNPs were studied by incubating cells in differing concentrations of MNPs based on iron concentration. B16-F10 cells were incubated overnight with MNP amounts corresponding to 5, 10, 15, 20, and 25 $\mu\text{g/mL}$ iron. After incubation, the medium was removed and the cells were washed twice with DMEM and cell numbers were counted with Trypan blue staining. This method also allows counting non-viable cells since only they allow the blue stain into the cell. All experiments were run in triplicate and repeated at least twice. B16-F10 cancer cell viability assessment in the presence of varying concentration of MNPs is shown in Figure 9.8. There was a dose-dependent cytotoxicity if the MNPs. A pronounced cytotoxic effect on B16-F10 cells was observed when the concentration of the iron exceeds 10 $\mu\text{g/mL}$.

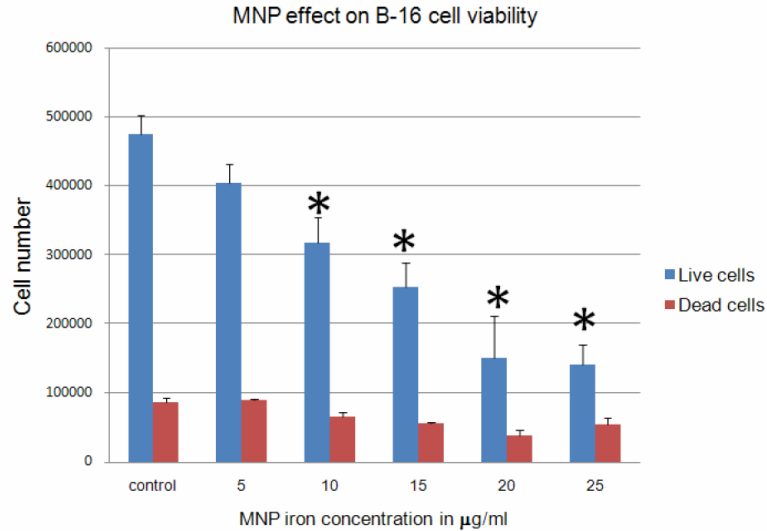


Figure 9.8 *In vitro* cell viability of B16-F10's cultured in medium containing increasing concentration of MNPs, as measured by iron concentration. *Statistically significant (p-value less than 0.05).

9.7.2 Temperature Measurement on Mice

For all *in vivo* experiments, the mice were placed into the induction coil using a specially designed Teflon supporter so that tumors were located exactly in the region of the AMF possessing the highest field density. MNPs containing 100 µg of iron in 100 µl of distilled water were injected into the rear limb muscle of one mouse and the leg was then exposed to AMF for 10 min. A fiber optical temperature probe was inserted intramuscularly at the injection site and the temperature increase was measured during AMF exposure. At the same time, the body temperature was monitored with a separate temperature probe. A temperature increase of 11 °C was observed at the MNPs injection site within 10 min of AMF exposure. There was no increase in core body temperature (Figure 9.9). These data demonstrate specific magnetic hyperthermia.

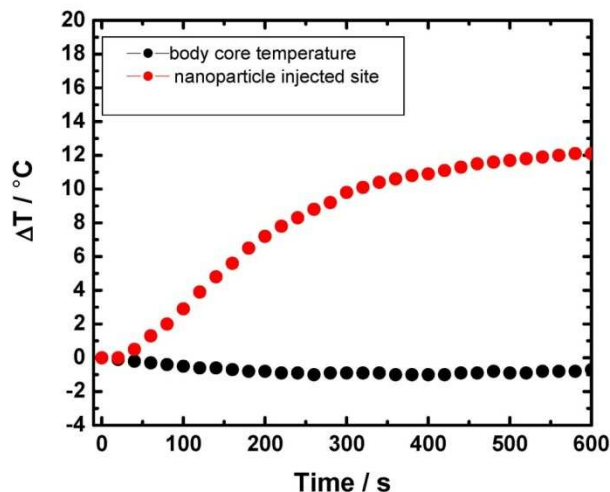


Figure 9.9 Temperature change at MNP injection site and in body core during AMF exposure, measure with a fiber optic temperature probe.

9.7.3 Intratumoral Administration of MNPs with AMF Exposure

Ten female CB57 BL/6 mice were transplanted with 1×10^6 B16F10 melanoma cells suspended in PBS subcutaneously into each rear limb above the stifle. 120 μ L of saline was injected into melanomas on the left leg of all mice and 120 μ L of 1mg Fe/mL MNP (120 μ g iron) was injected into right leg tumors of all mice in three injections on day 4, 5, 6 (total of 360 μ g iron). Both left(saline) and right(MNP) leg tumors of half of the mice(5) were exposed to AMF for 10 minutes soon after injections and remaining five mice left and right leg tumors were not exposed. Based on this there were 4 groups.

Group 1: Intratumoral saline injection, not exposed to AMF (left legs of first five mice).

Group 2: Intratumoral injection of saline, exposed to AMF (left legs of remaining five mice).

Group 3: Intumoral injection of MNPs, not exposed to AMF (right legs of first five mice).

Group 4: Intratumoral injection of MNP, exposed to AMF (right legs of remaining five mice).

After three AMF exposures tumor sizes were measured by using a caliper on day 8 to 14, and tumor volume was calculated by using formula $0.5ab^2$ (a=longest diameter b= smaller diameter). The results were summarized in Figure 9.10. The tumors with administration of MNPs and exposure to AMF showed a significant reduction in tumor volume at 8, 9, 11 and 14 days

($p < 0.1$) compared to the saline treated groups. A decrease in size with only MNPs treatment (without AMF) relative to the saline controls was also noted; however, this decrease was not significant. Since earlier intramuscular injections and optical probe measurements revealed hyperthermia after AMF, the probable cause for tumor attenuation shown here is local hyperthermia.

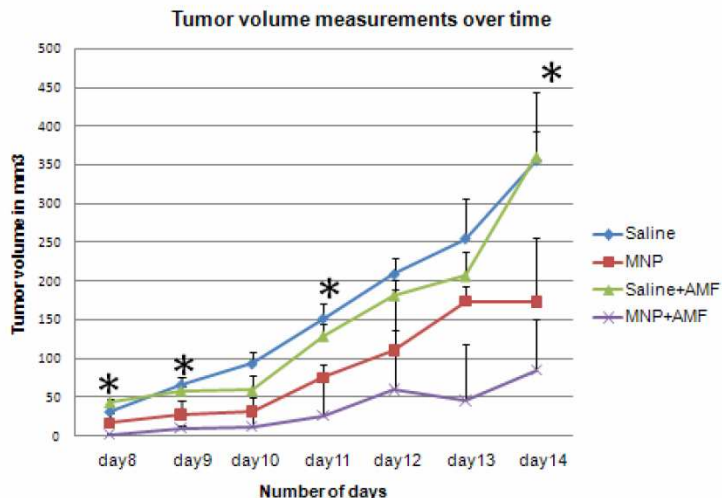


Figure 9.10 Effect on tumor burden of intratumoral injection of MNPs followed by alternating magnetic field (AMF) treatments. Graph depicting average tumor volumes over time of B16-F10 tumor bearing mice which were later injected with either saline or MNP intratumorally and with or without AMF treatments. *Statistically significant (p-value less than 0.1).

9.7.4 Intravenous Administration of MNPs with AMF Exposure

0.35×10^6 B16-F10 melanoma cells were injected subcutaneously into the right legs of 27 mice. Mice were randomly divided into three groups:

Group I, IV injection of MNPs, no AMF treatment.

Group II, IV injection of MNPs, with AMF treatment.

Group III, IV injection of DMEM, no AMF treatment.

On day 6, 9 and 11 after tumor cell transplant, MNPs corresponding to 226 μg of iron were injected intravenously into each mouse in groups I and II. On the same day, DMEM was injected intravenously into group III. For group II, tumors were exposed to AMF for 10 min one day after each intravenous MNPs injection (total of three AMF treatments). Tumor sizes were measured

using a caliper on days 14 and 18, and tumor volume was calculated as described above. On day 18, all mice were euthanized, tumors were excised, and tumor weights were measured. As can be seen in figure 9.11, a significant decrease in tumor weight ($p < 0.1$) was observed in the intravenous MNPs+AMF group, and this attenuation of tumor weight was most likely due to the heat generated by MNPs in tumors. Some tumor weight decrease was also observed in the intravenous MNPs injection but without AMF treatment group.

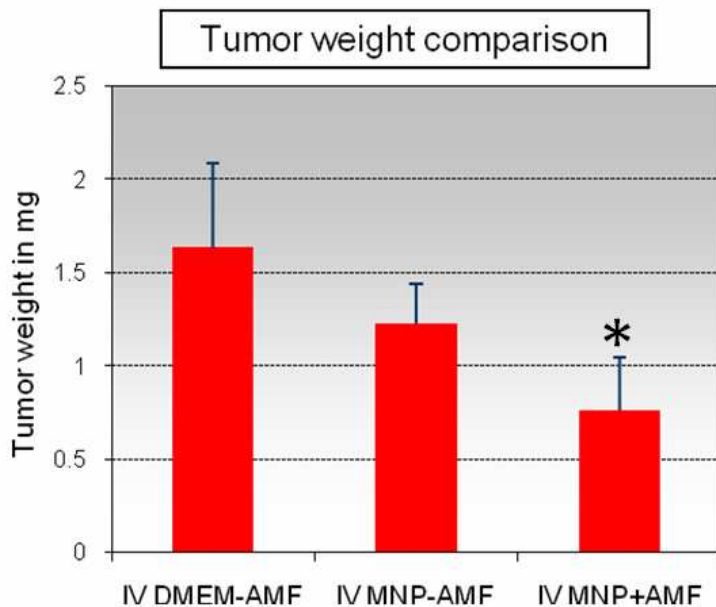


Figure 9.11 Effect of intravenous injection of MNPs and AMF on tumor weight. *Statistically significant (p -value less than 0.1) between control and IV MNPs+AMF groups.

A marked tumor volume decrease was observed for the mice with intravenous MNPs injection and AMF treatment; however, this decrease was not significant (Figure 9.12).

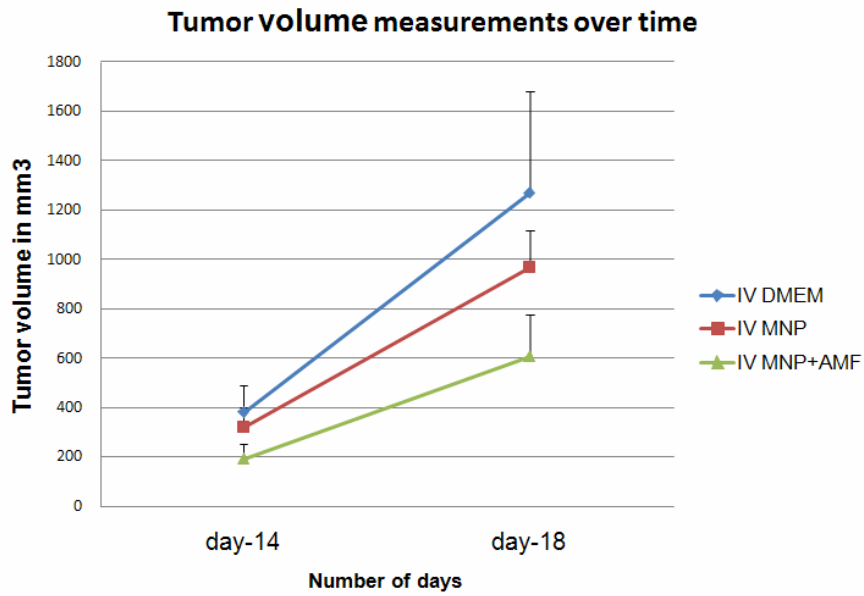


Figure 9.12 Tumor volume comparison of IV MNP+AMF experiment on day 14 and 18.

After AMF treatment, significant amounts of nanoparticles were found in the melanoma tumors (Figure 9.13A), indicating that the tethered porphyrin (TCPP) can act as a “bait” to facilitate the uptake of nanoparticles by tumor cells. Some nanoparticles were also found in lung and liver (Figure 9.13B and 9.13C). Despite this wild spread distribution of nanoparticles *in vivo*, no fatalities of mice due to the blocking of arteries or exposure to AMF were observed.

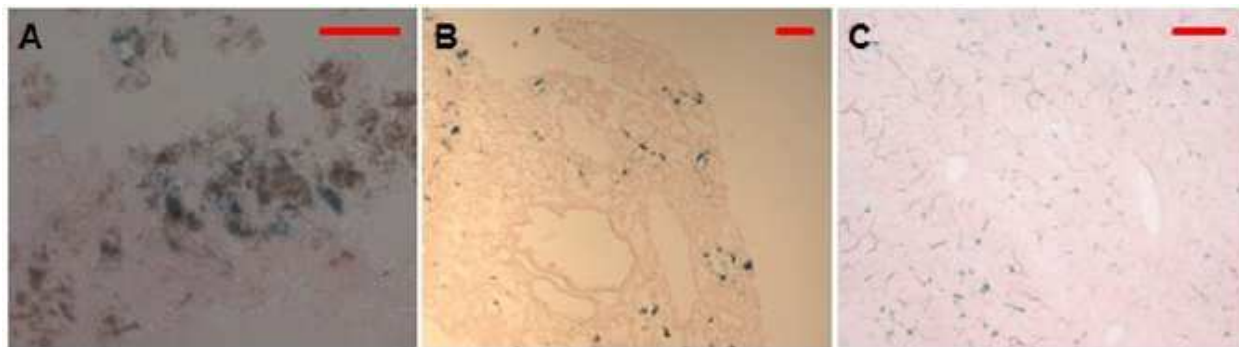


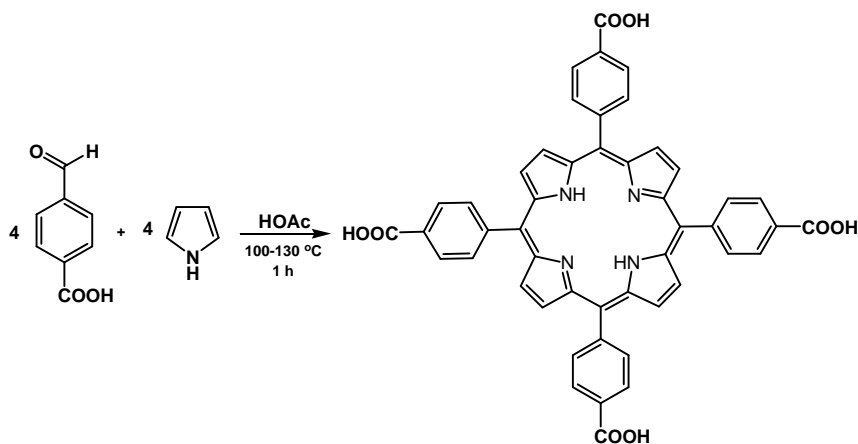
Figure 9.13 Prussian blue staining of tumor section (picture A), lung section (picture B) and liver section (picture C) after *in vivo* experiment.

9.8 Conclusion

We have synthesized Fe/Fe₃O₄ core shell nanoparticles with an organic stealth coating and tethered porphyrin (TCPP) units. The NMR-measurement of T¹ and T²-relaxation times showed a significant enhancement of T¹ relaxation time and a remarkable decrease of T² relaxation time with the increase of the nanoparticle concentration. These results implied that it is very promising with respect to use of this stealth nanoparticles as MRI contrast agents. The mice hyperthermia experiment indicates that the ligands modified nanoparticles administrated intravenously or intratumorally at low concentrations can significantly attenuate B16-F10 melanoma tumors in mice after repetitive short AMF exposure. These results demonstrated that the core/shell Fe/Fe₃O₄ nanoparticles possess high heating capacity in the alternating magnetic field, which permits the small dose and short treatment time during hyperthermia therapy. Furthermore, significant amount of nanoparticles were found in melanoma tumor when the nanoparticles were administrated intravenously, which indicate the porphyrin tethered on the nanoparticles can facilitate the uptake of nanoparticles by tumor cells.

9.9 Experimental

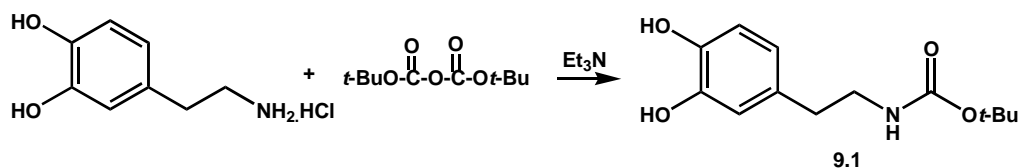
9.9.1. Synthesis of porphyrin (TCPP)⁵³



1.50 g 4-carboxybenzaldehyde was dissolved in 80 mL acetic acid. The solution was warmed to 100 °C and a solution of 0.67 g pyrrole in 10 mL acetic acid was added dropwise in 20 minutes. Upon completion of addition, the solution was warmed up to 130 °C slowly and kept at 130 °C for 1 hour. The mixture was cooled to 80 °C and 100 mL 95% ethanol was added and the

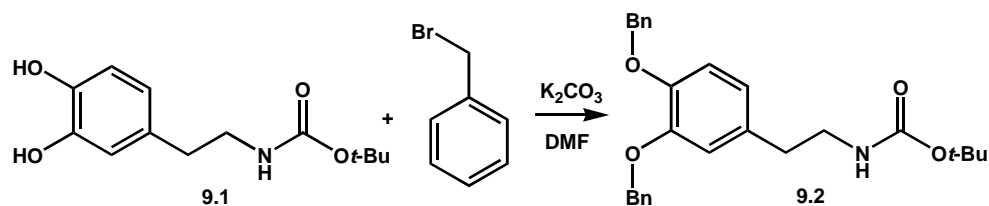
temperature was lowered to room temperature while stirring in 3 hours. Then the mixture was kept in at -15 °C for 24 hours. Purple solid was collected by vacuum filtration. The filter cake was washed with cold 50/50 ethanol/acetic acid (3×5mL) and dried under high vacuum (oil pump) overnight. 0.51g pure product was obtained (25.5% yield). ^1H NMR ($\text{DMSO-}d_6$) δ : -2.94 (s, 2H); 8.35 (d, 8H); 8.39 (d, 8H); 8.86 (s, 8H); 13.31 (s, 4H). ^{13}C NMR ($\text{DMSO-}d_6$) δ : 119.31; 127.90; 130.51; 134.44; 145.42; 167.46. MS-ESI $^+$: m/z 791.2. Molecular weight calculated for 790.2.

9.9.2 Boc-protection of Dopamine.⁴¹



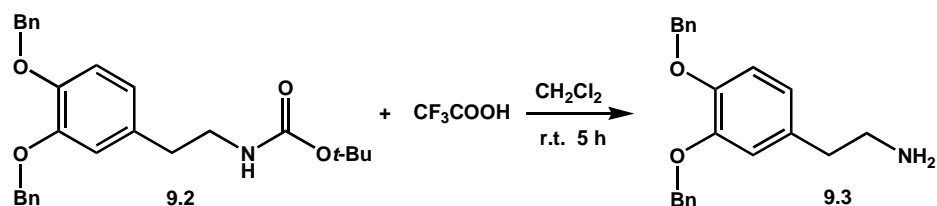
A solution of dopamine (310 mg, 1.63 mmol) in methanol (8 mL) was stirred under N_2 for 5 minutes. TEA (1.8 mmol) was added followed by Boc-anhydride (393 mg, 1.8 mmol). The mixture was stirred under N_2 for 12 hours and the solvent was removed under reduced pressure. The remaining residue was dissolved in 40 mL CH_2Cl_2 and washed with 1 N HCl (3×5 mL) and brine (5 mL). The organic layer was dried over anhydrous Na_2SO_4 . After filtration, the organic phase was kept at -5 °C for 3 hours. A white precipitate came out as product **9.1** and collected by filtration. Overall yield is 85%. ^1H NMR ($\text{DMSO-}d_6$) δ : 1.73 (s, 9H); 2.48 (t, 2H); 3.02 (q, 2H); 6.40 (d, 1H); 6.54 (s, 1H); 6.61 (d, 1H); 6.83 (t, 1H); 6.85 (s, 1H); 6.76 (s, 1H).

9.9.3 Benzyl-protection of Boc-dopamine.⁴²



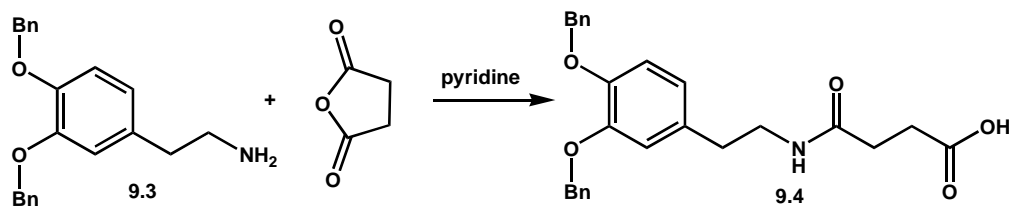
3.47 g Boc-protected dopamine **9.1** was dissolved in 100 mL DMF. 12.6 g K_2CO_3 was added and the system was protected under N_2 . 4.69 g (2 eq.) benzyl bromide was added drop wise. The mixture was stirred at room temperature for 24 hours without light. The solid was removed by filtering through a short pad of celite and the filter-cake was washed with ether (3×100 mL). The combined filtrate and washing solution were washed with ice-water (3×50 mL) and brine (15 mL). The organic layer was dried over anhydrous Na_2SO_4 and concentrated to 150 mL. After setting at $-5\text{ }^\circ\text{C}$ for 5 hours, white precipitate came out as product **9.2** and was collected by vacuum filtration. (overall yield 90%). $^1\text{H NMR}$ ($CDCl_3$) δ : 1.45 (s, 9H); 2.70 (t, 2H); 3.31 (q, 2H); 4.49 (s, 1H); 5.15 (d, 4H); 6.71 (d, 1H); 6.80 (s, 1H); 6.88 (d, 1H); 7.32 (t, 2H); 7.37 (t, 4H); 7.45 (d, 4H).

9.9.4 Deprotect of Boc-group.⁴²



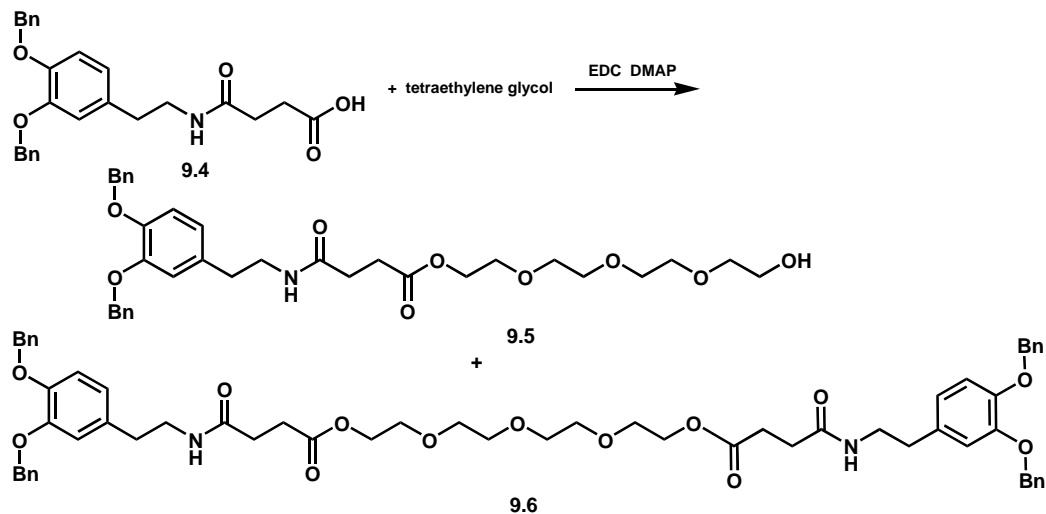
4.3g Bn-Boc-dopamine **9.2** was dissolved in 150 mL 5% TFA CH_2Cl_2 solution and stirred at room temperature for 5 hours. The solvent was removed under vacuum and clear oil was obtained as product **9.3**. (100% yield). $^1\text{H NMR}$ ($CDCl_3$) δ : 2.79 (t, 2H); 3.08 (m, 2H); 5.11 (s, 4H); 6.68 (d, 1H); 6.75 (s, 1H); 6.90 (d, 1H); 7.32 (t, 2H); 7.35 (t, 4H); 7.42 (d, 4H). $^{13}\text{C NMR}$ ($CDCl_3$) δ : 32.90; 41.85; 71.50; 72.00; 115.60; 116.25; 122.30; 127.60; 127.85; 128.35; 128.45; 128.63; 128.85; 136.70; 136.85; 148.45; 149.00; 160.88; 161.20; 161.58; 161.90.

9.9.5 Amide Formation.⁴³



1.43 g Bn-dopamine **9.3** and 0.43 g succinic anhydride (1/1 ratio) were dissolved in 6 mL pyridine. The solution was stirred at room temperature for 5 hours. The solvent was removed by co-evaporation with toluene (toluene 5×5 ml). White solid was obtained and washed with CH₂Cl₂ for 3 times. After drying under vacuum, 1.4 g product **9.4** was obtained. 75% yield. ¹H NMR (DMSO-*d*₆) δ: 2.29 (t, 2H); 2.42 (t, 2H); 2.60 (t, 2H); 3.21 (q, 2H); 5.09 (d, 4H); 6.71 (d, 1H); 6.94 (s, 1H); 6.96 (d, 1H); 7.32 (t, 2H); 7.38 (d, 4H); 7.45 (t, 4H); 7.90 (t, 1H); 12.08 (s, 1H). MS-ESI⁺: *m/z* 434.2. Molecular weight calculated for 433.5.

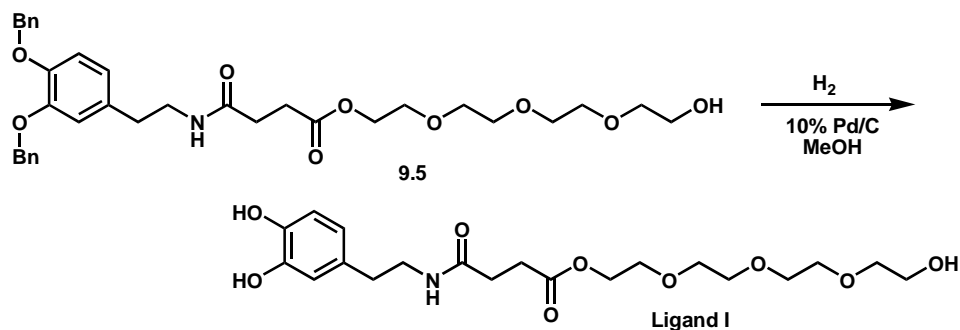
9.9.6 Synthesis of ligand I.⁴⁴



0.964 g dopamine-based carboxylic acid **9.4** and 0.426g EDC (1/1 ratio) were dissolved in 100 mL CH₂Cl₂ and stirred at room temperature for 10 minutes. 0.433 g tetraethylene glycol was added followed by 5 mg DMAP. After stirring for 12 hours at room temperature, the organic

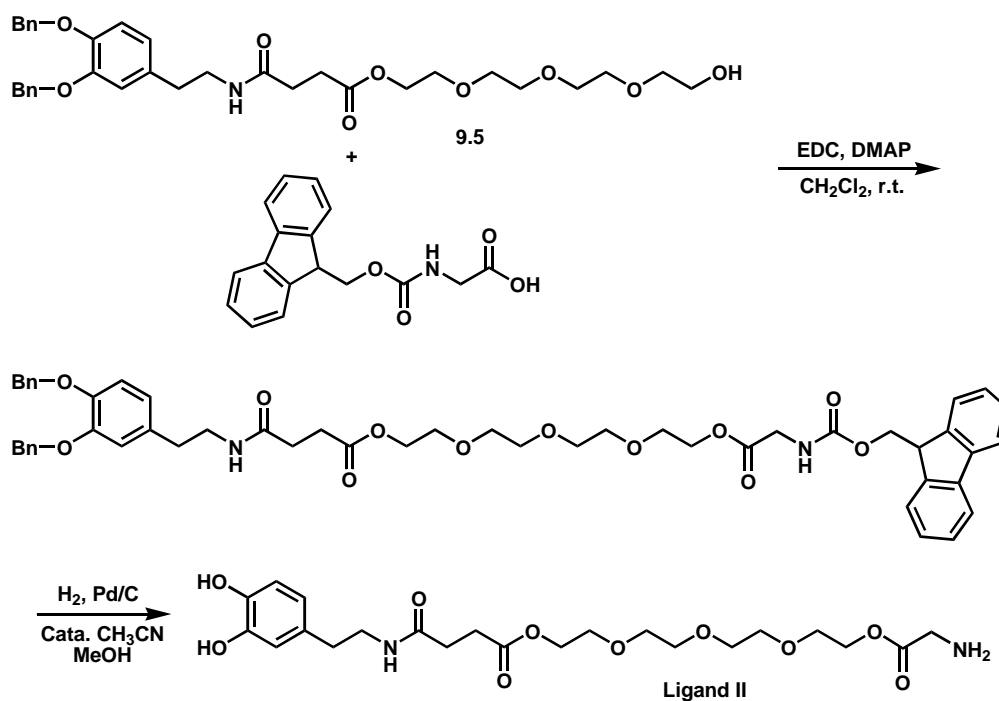
phase was washed with 10% H₃PO₄ solution (3×10 mL), water (3×10 mL) and brine (10 mL). The organic phase was dried over anhydrous Mg₂SO₄. After removing the solvent under vacuum, the residue was loaded on column and eluted with 1/1 acetone/methylene chloride. 0.42 g ideal product **9.5** was obtained. (40% yield). 0.21 g side product **9.6** was isolated. ¹H NMR for **9.5** (CDCl₃) δ: 2.39 (t, 2H); 2.57 (t, 1H); 2.70 (q, 4H); 3.44 (q, 2H); 3.60 (t, 2H); 3.65 (broad 12H); 4.24 (t, 2H); 5.15 (d, 4H); 5.74 (t, 1H); 6.71 (d, 1H); 6.81 (s, 1H); 6.89 (d, 1H); 7.31 (t, 2H); 7.37 (t, 4H); 7.46 (d, 4H). MS-ESI⁺: *m/z* 610.4. Molecular weight calculated for 609.3. ¹H NMR for **9.6** (CDCl₃) δ: 2.37 (t, 4H); 2.67 (m, 8H); 3.42 (q, 4H); 3.63 (s, 8H); 3.67 (t, 4H); 4.22 (t, 4H); 5.15 (d, 8H); 5.70 (t, 2H); 6.70 (d, 2H); 6.80 (s, 2H); 6.88 (d, 2H); 7.31 (t, 4H); 7.36 (t, 8H); 7.45 (d, 8H). MS-ESI⁺: *m/z* 610.4. Molecular weight calculated for 609.3.

De-protection of benzyl groups to produce ligand I.⁴³



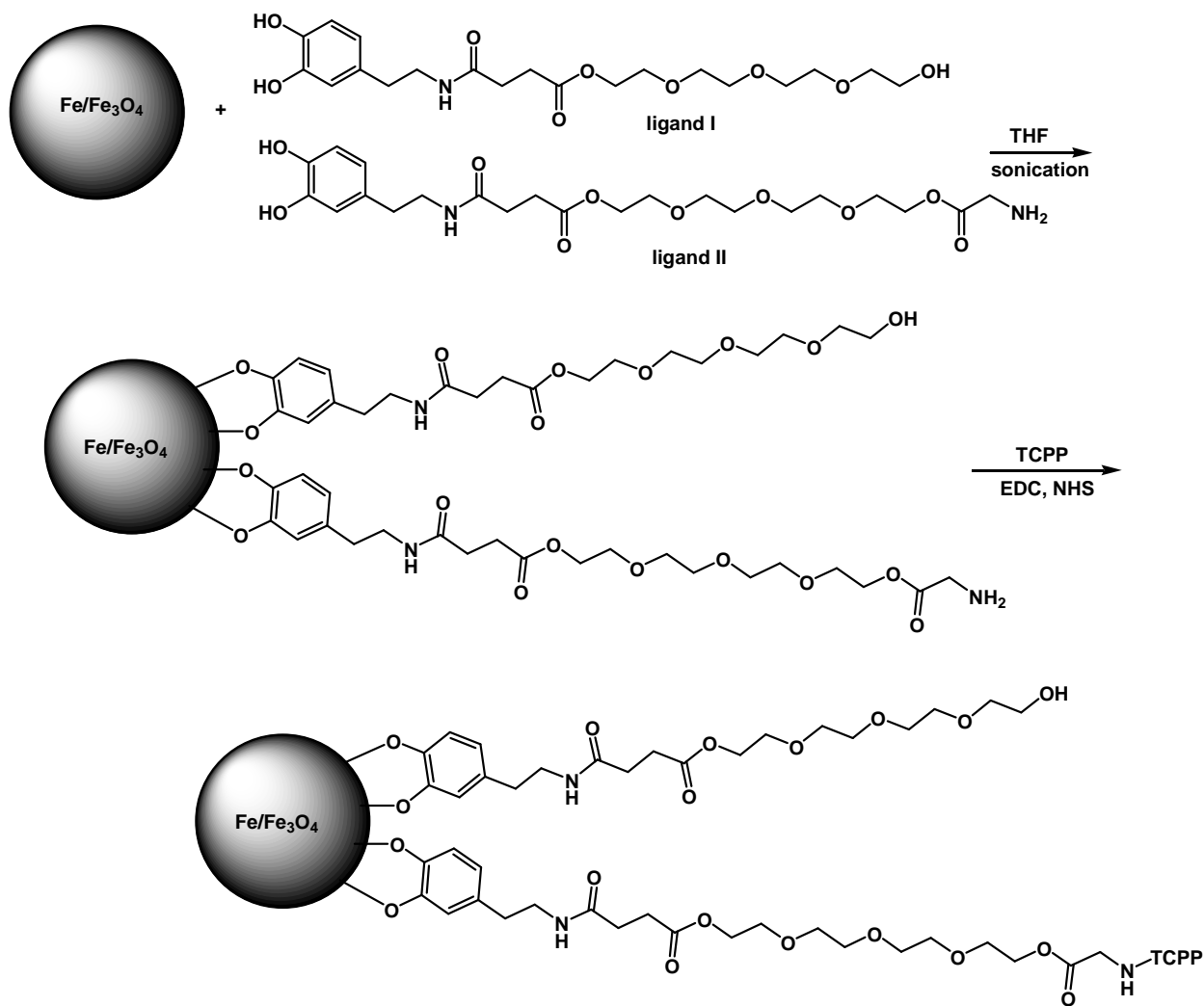
0.34 g Bn-dopamine-based tetraethylene glycol **9.5** was dissolved in 50 mL methanol. 77 mg Pd/C was added under N₂. After evacuating three times, 1 atm. H₂ was applied and the mixture was stirred for 24 hours at room temperature. The catalyst was removed by filtering through a short pad of celite. After removing solvent under vacuum, 0.23 g **ligand I** was obtained as product. (100% yield). ¹H NMR (DMSO-*d*₆) δ: 2.33 (t, 2H); 2.48 (q, 2H); 3.15 (broad multiplet, 4H); 3.41 (t, 2H); 3.49 (t, 2H); 3.51 (broad multiplet, 8H); 3.59 (t, 2H); 4.11 (t, 2H); 6.41 (d, 1H); 6.55 (s, 1H); 6.61 (d, 1H). MS-ESI⁺: *m/z* 430.4. Molecular weight calculated for 429.4.

9.9.7 Synthesis of glycine-tipped ligand (ligand II).^{44,45}



Bn-protected dopamine tetraethylene glycol **9.5** was treated with 1 equiv. of Fmoc-Glycine and 1.2 equiv. of EDC in the presence of catalytic amount of DMAP in methylene chloride. After stirring for 12 hours at room temperature, the organic phase was washed with 10% H₃PO₄ solution (3×10 mL), water (3×10 mL) and brine (10 mL). The organic phase was dried over anhydrous Mg₂SO₄. After removing the solvent under vacuum, a white solid was obtained as pure product with 95% yield. The Bn and Fmoc groups were deprotected at the same time under the H₂-Pd/C condition in the presence of catalytic amount of CH₃CN. After removing the catalyst by filtration, solvent was removed under reduced pressure, clear oil together with some white solid formed. The white solid was removed by washing the mixture with hexane (3×5 mL), after concentration, **ligand II** was obtained as clear oil with 85% yield. ¹H NMR (DMSO-*d*₆) δ: 2.33 (t, 2H); 2.46 (q, 2H); 3.14 (q, 2H); 3.41 (t, 2H); 3.49 (t, 4H); 3.51 (broad multiplet, 8H); 3.59 (t, 2H); 4.10 (t, 2H); 4.57 (t, 2H); 6.43 (d, 1H); 6.55 (s, 1H); 6.61 (d, 1H); 7.90 (t, 1H); 8.62 (s, 1H); 8.73 (s, 1H). ¹³C NMR (DMSO-*d*₆) δ: 28.95, 29.83, 34.73, 60.23, 63.32, 68.30, 69.79, 72.37, 115.48, 115.95, 119.21, 130.22, 143.53, 145.06, 170.44, 172.47.

9.9.8 Modification of Fe/Fe₃O₄ nanoparticles with dopamine-based ligands I and II and introducing of porphyrin (TCPP).^{45,46}



A typical example for preparing surface modified Fe/Fe₃O₄ nanoparticles featuring 5 TCPP per nanoparticle is described here. 50 mg dopamine-based **ligand I** and 3 mg dopamine-based **ligand II** (mole ratio 95/5) were dissolved in 10 mL THF, 20 mg Fe/Fe₃O₄ nanoparticles (# 4 in Table 1) were added, after sonicating for 60 minutes, the nanoparticles were collected by a magnet. The solid was washed with 3 mL portion of THF for 10 washing-magnetprecipitation-re-dispersion cycles. The surface modified nanoparticles were dispersed in 10 mL of THF, 1.5

mg porphyrin (TCPP), 1 mg NHS and 2 mg EDC were added to the suspension and sonicated for 60 minutes. The nanoparticles were collected by a strong magnet and further washed with 3 mL portion of THF for 10 washing-magnetprecipitation-re-dispersion cycles. The solid was dried under vacuum. 17.6 mg nanoparticles were obtained.

References

1. <http://www.cancer.gov/cancertopics/factsheet/Therapy/hyperthermia>
2. van der Zee J. Heating the patient: A promising approach? *Annals of Oncology* **2002**, *13*, 1173–1184.
3. Hildebrandt B, Wust P, Ahlers O, et al. The cellular and molecular basis of hyperthermia. *Critical Reviews in Oncology/Hematology* **2002**, *43*, 33–56.
4. Wust P, Hildebrandt B, Sreenivasa G, et al. “Hyperthermia in combined treatment of cancer,” *The Lancet Oncology* **2002**, *3*, 487–497.
5. Falk MH, Issels RD. “Hyperthermia in oncology,” *International Journal of Hyperthermia* **2001**, *17*(1), 1–18.
6. Kapp DS, Hahn GM, Carlson RW. “Principles of hyperthermia,” In: Bast RC Jr., Kufe DW, Pollock RE, et al., editors. *Cancer Medicine e.5*. 5th ed. Hamilton, Ontario: B.C. Decker Inc., **2000**.
7. Shinkai, M. "Functional magnetic particles for medical application," *J. Biosci. Bioeng.* **2002**, *94*, 606-613.
8. Bossmann, S. H. in "Nanoparticles for Hyperthermia Treatment of Cancer"; Wang, X. Katz, E.; Research Signpost, Trivandrum, Kerala, India, **2009**, pp 171-206.
9. Nie, S.; Xing, Y.; Kim, G. J.; Simons, H. W. "Nanotechnology Applications in Cancer" *Annu. Rev. Biomed. Eng.* **2007**, *9*, 257-88.
10. Yang, L.; Mao, H.; Wang, Y. A.; Cao, Z.; Peng, X.; Wang, X.; Duan, H.; Ni, C.; Yuan, Q.; Adams, G.; Smith, M. Q.; Wood, W. C.; Gao, X.; Nie, S. “Single chain epidermal growth factor receptor antibody conjugated nanoparticles for in vivo tumor targeting and imaging,” *Small* **2009**, *5*, 235-243.
11. Kannagi, R. “Molecular mechanism for cancer -associated induction of sialyl Lewis X and sialyl Lewis A expression-The Warburg effect revisited,” *Glycoconjugate Journal* **2003**, *20*, 353-364.
12. Maziere, J. C.; Santus, R.; Morliere, P.; Reyftmann, J. P.; Candide, C.; Mora, L.; Salmon, S.; Maziere, C.; Gatt, S.; Dubertret, L. “Cellular uptake and photosensitizing properties of

- anticancer porphyrins in cell membranes and low and high density lipoproteins," *J. Photochem. Photobiol.* **1990**, *6*, 61-68.
13. Final Report for the grant CHHSN261200800059C from the Small Business Innovation Research Development Center (SBIR) of the National Cancer Institute (Kroh. F. (PI); Bossmann, S. H.; Troyer, D. L.; Chikan V. (Co-PIs).
 14. Gu, H.; Xu, K.; Yang, Z.; Chang, C. K.; Xu, B. "Synthesis and cellular uptake of porphyrin decorated iron oxide nanoparticles-a potential candidate for bimodal anticancer therapy," *Chem. Commun.* **2005**, *34*, 4270-4272.
 15. Park, S. I.; Lim, J. H.; Kim, J. H.; Yun, H. I.; Kim, C. O. "In vivo and in vitro investigation of photosensitizer-adsorbed superparamagnetic nanoparticles for photodynamic therapy," *IEEE Transactions on Magnetics* **2005**, *41*(10), 4111-4113.
 16. Reddy, G. Ramachandra; Bhojani, Mahaveer S.; McConville, Patrick; Moody, Jonathan; Moffat, Bradford A.; Hall, Daniel E.; Kim, Gwangseong; Koo, Yong-Eun L.; Woolliscroft, Michael J.; Sugai, James V.; Johnson, Timothy D.; Philbert, Martin A.; Kopelman, Raoul; Rehemtulla, Alnawaz; Ross, Brian D. "Vascular targeted nanoparticles for imaging and treatment of brain tumors," *Clinical Cancer Research* **2006**, *12*(22), 6677-6686.
 17. Yang, Z.; Xu, K.; Zhang, B.; Xu, B.; Zhang, X.; Chang, C. K. "Photosensitizer decorated iron oxide nanoparticles: bimodal agent for combined hyperthermia and photodynamic therapy," *Proceedings of SPIE-The International Society for Optical Engineering* **2006**, *6139*(*Optical Methods for Tumor Treatment and Detection: Mechanisms and Techniques in Photodynamic Therapy XV*), 613906/1-613906/10.
 18. Ross, Brian; Rehemtulla, Alnawaz; Koo, Yong-Eun L.; Reddy, Ramachandra; Kim, Gwangseong; Behrend, Caleb; Buck, Sarah; Schneider, Randal J.; Philbert, Martin A.; Weissleder, Ralph; Kopelman, Raoul. "Photonic and magnetic nanoexplorers for biomedical use: from subcellular imaging to cancer diagnostics and therapy," Dep. Radiol., Univ. of Michigan, Ann Arbor, MI, USA. *Proceedings of SPIE-The International Society for Optical Engineering* (2004), *5331*(*Nanobiophotonics and Biomedical Applications*), 76-83.
 19. Moreira, L. M.; dos Santos, F. V.; Lyon, J. P.; Maftoum-Costa, M.; Pacheco-Soares, C.; da Silva, N. S. Photodynamic Therapy : Porphyrins and Phthalocyanines as Photosensitizers., *Australian Journal of Chemistry* **2008**, *61*, 741-754.

20. Donnelly, J. G. Pharmacogenetics in cancer chemotherapy. Balancing toxicity and response., *Therapeutic Drug Monitoring* **2004**, *26*, 231-235.
21. Gordon, R. T.; Hines, J. R.; Gordon, D. Intracellular hyperthermia - a biophysical approach to cancer via intracellular temperature and biophysical alterations. *Med. Hypothesis* **1979**, *5*, 83-102.
22. Jordan, A.; Scholz, R.; Maier-Hauff, K.; Johannsen, M.; Wust, P.; Nadobny, J.; Schirra, H.; Schmidt, H.; Deger, S.; Loening, S.; Lanksch, W.; Felix, R. "Presentation of a new magnetic field therapy system for the treatment of human solid tumors with magnetic fluid hyperthermia." *Journal of Magnetism and Magnetic Materials* **2001**, *225*, 118-126.
23. Jordan, A.; Wust, P.; Fahling, H.; John, W.; Hinz, A.; Felix, R. "Inductive Heating of Ferrimagnetic Particles and Magnetic Fluids - Physical Evaluation of Their Potential for Hyperthermia." *International Journal of Hyperthermia* **1993**, *9*, 51-68.
24. Pakhomov, A. B.; Bao, Y. P.; Krishnan, K, M. "Effects of surfactant friction on Brownian magnetic relaxation in nanoparticle ferrofluids," *Journal of Applied Physics* **2005**, *97*, 10Q305/1-10Q305/3
25. Kotitz, R.; Fannin, P. C.; Trahma, L. "Time-domain study of Brownian and Neel relaxation in ferrofluids," *Journal of Magnetism and Megnetic Materials* **1995**, *149*, 42-46.
26. Huber, D. L. "Synthesis, Properties, and Applications of Iron Nanoparticles," *Small* **2005**, *1*, 482-501.
27. Mornet, S.; Vasseur, S.; Grasset, F.; Duguet, E. "Magnetic nanoparticle design for medical diagnosis and therapy." *Journal of Materials Chemistry* **2004**, *14*, 2161-2175.
28. Vasseur, S. M.; Grasset, F.; Duguet, E. Magnetic nanoparticle design for medical diagnosis and therapy, *J. Mat. Chem.* **2004**, *14*, 2161-2175.
29. Laurent, S.; Forge, D.; Port, M.; Roch, A.; Robic, C.; Elst, L. V.; Muller, R. N. "Magnetic Iron Oxide Nanoparticles: Synthesis, Stabilization, Vectorization, Physicochemical Characterizations, and Biological Applications," *Chem. Rev.* **2008**, *108*, 2064-2110.
30. Hergt, R.; Hiergeist, R.; Zeisberger, M.; Glöckl, G.; Weitschies, W.; Ramirez, L. P.; Kaiser, W. A. "Enhancement of AC-losses of magnetic nanoparticles for heating applications," *Journal of Magnetic Materials*, **2004**, *280*, 359-368

31. Zeng, Q.; Baker, I.; Loudis, J. A.; Liao, Y.; Hoopes, P. J.; Weaver, J. B. "Fe/Fe oxide nanocomposite particles with large specific absorption rate for hyperthermia." *Applied Physics Letters* **2007**, *90*, 233112/1-233112/3.
32. Qiang, Y.; Antony, F.; Sharma, A.; Nutting, J.; Sikes, D.; Meyer, D. Iron/iron oxide core-shell nanoclusters for biomedical applications, *Journal of Nanoparticle Research* **2006**, *8*, 489-496.
33. Sharma, A.; Qiang, Y.; Meyer, D.; Souza, R.; McConaughoy, A.; Muldoon, L.; Baer, D. Biocompatible core-shell magnetic nanoparticles for cancer treatment, *J. Appl. Phys.* **2008**, *103*, 07A308.
34. Mehdaoui, B. M.; Meffre, A.; Lacroix, L.-M.; Carrcy, J.; Lachaize, S.; Respaud, M.; Gaugeon, M.; Chaudret, B. Record heating in magnetic hyperthermia of metallic iron nanocubes and way for further improvements., **2009**, <http://arxiv.org/pdf/0907.4063>,
35. Kettering, M.; Winter, J.; Zeisberger, M.; Bremer-Streck, S.; Oehring, H.; Bergemann, C.; Alexiou, C.; Hergt, R.; Halbhuber, K. J.; Kaiser, W. A.; Hilger, I. Magnetic nanoparticles as bimodal tools in magnetically induced labelling and magnetic heating of tumour cells: an in vitro study, *Nanotechnology* **2007**, *18*, 175101-110.
36. Salata, O. V. Applications of nanoparticles in biology and medicine, *Journal of Nanobiotechnology* **2004**, *2*, 1477-3155-2-3.
37. Weissleder, R.; Kelly, K.; Sun, E. Y.; Shtatkand, T.; Josephson, L. Cell-specific targeting of nanoparticles by multivalent attachment of small molecules, *Nature Biotechnology* **2005**, *23*, 1418-1422.
38. Jordan, A.; Scholz, R.; Wust, P.; Fahling, H.; Felix, R. "Magnetic fluid hyperthermia (MFH): Cancer treatment with AC magnetic field induced excitation of biocompatible superparamagnetic nanoparticles." *Journal of Magnetism and Magnetic Materials* **1999**, *201*, 413-419.
39. Jain, T. K.; Morales, M. A.; Sahoo, S. K.; Leslie-Pelecky, D. L.; Labhasetwar, V. Iron Oxide Nanoparticles for Sustained Delivery of Anticancer Agents, *Molecular Pharmaceutics* **2005**, *2*, 194-205.
40. Winterbourn, C. C. Toxicity of iron and hydrogen peroxide: the Fenton reaction, *Toxicology Letters* **1995**, *82-83*, 969-974 and references quoted therein.

41. Fernández, C.; Nieto, O.; Rivas, E.; Montenegro, G.; Fontenla, J. A.; Fernández-Mayoralas, A. "Synthesis and biological studies of glycosyl dopamine derivatives as potential antiparkinsonian agents," *Carbohydrate Research* **2000**, 327, 353-365.
42. Xu, C.; Xu, K.; Gu, H.; Zhang, R.; Liu, H.; Zhang, X.; Guo, Z.; Xu, B. "Dopamine as A robust anchor to immobilize functional molecules on the iron oxide shell of magnetic nanoparticles," *J. Am. Chem. Soc.* **2004**, 126, 9938-9939.
43. Xu, Z.; Peng, Y.; Ye, T. "The total synthesis and stereochemical revision of yanucamide A," *Organic Letters*, **2003**, 5, 2821.
44. Maegawa, T.; Fujiwara, Y.; Ikawa, T.; Hisashi, H.; Monguchi, Y.; Sajiki, H. "Novel deprotection method of Fmoc group under neutral hydrogenation conditions," *Amino Acids*, **2009**, 36, 493-499.
45. Gu, H.; Xu, K.; Yang, Z.; Chang, C. K.; Xu, B. "Synthesis and cellular uptake of porphyrin decorated iron oxide nanoparticles-a potential candidate for bimodal anticancer therapy," *Chem. Commun.* **2005**, 4270-4272.
46. Sehgal, D.; Vijay, I. K. "A method for the high efficiency of water-soluble carbodiimide-mediated amidation," *Anal. Biochem.* **1994**, 218, 87-91.
47. Clarke, Suzanne E.; Wamser, Carl C.; Bell, Harry E. Aqueous Complexation Equilibria of meso-Tetrakis(4-carboxyphenyl)porphyrin with Viologens : Evidence for 1:1 and 1:2 Complexes and Induced Porphyrin Dimerization. *Journal of Physical Chemistry A*, **2002**, 106, 3235-3242.
48. Meledandri, C. J.; Stolarczyk, J. K.; Ghosh, S.; Brougham, D. F. Nonaqueous Magnetic Nanoparticle Suspensions with Controlled Particle Size and Nuclear Magnetic Resonance Properties, *Langmuir* **2008**, 24, 14159-14165 and references given therein.
49. http://www.medcyclopaedia.com/library/topics/volume_i/e.aspx
50. Levitt, M. H. "Spin Dynamics: Basics of Nuclear Magnetic Resonance"; John Wiley&Sons: New York, 2001; pp 672
51. Shapiro, M. G.; Atanasijevic, T.; Faas, H.; Westmeyer, G. G.; Jasanoff, A. "Dynamic imaging with MRI contrast agents: quantitative considerations." *Magnetic Resonance Imaging* **2006**, 24, 449-462.
52. Miguel, O. B.; Gossuin, Y.; Morales, M. P.; Gillies, P.; Muller, R. N.; Veintemillas-Verdaguer, S. "Comparative analysis of the ¹H-NMR relaxation enhancement produced by

iron oxide and core-shell iron-iron oxide nanoparticles,” *Magnetic Resonance Imaging* **2007**, 25, 1437-1441.

53. Adler, A. D.; Longo, F. R.; Finarelli, J. D.; Goldmacher, J.; Assour, J.; Korsakoff, L. "A simplified synthesis for meso-tetraphenylporphine,” *J. Org. Chem.* **1967**, 32 (2): 476.

Appendix A- ^1H and ^{13}C -NMR Data

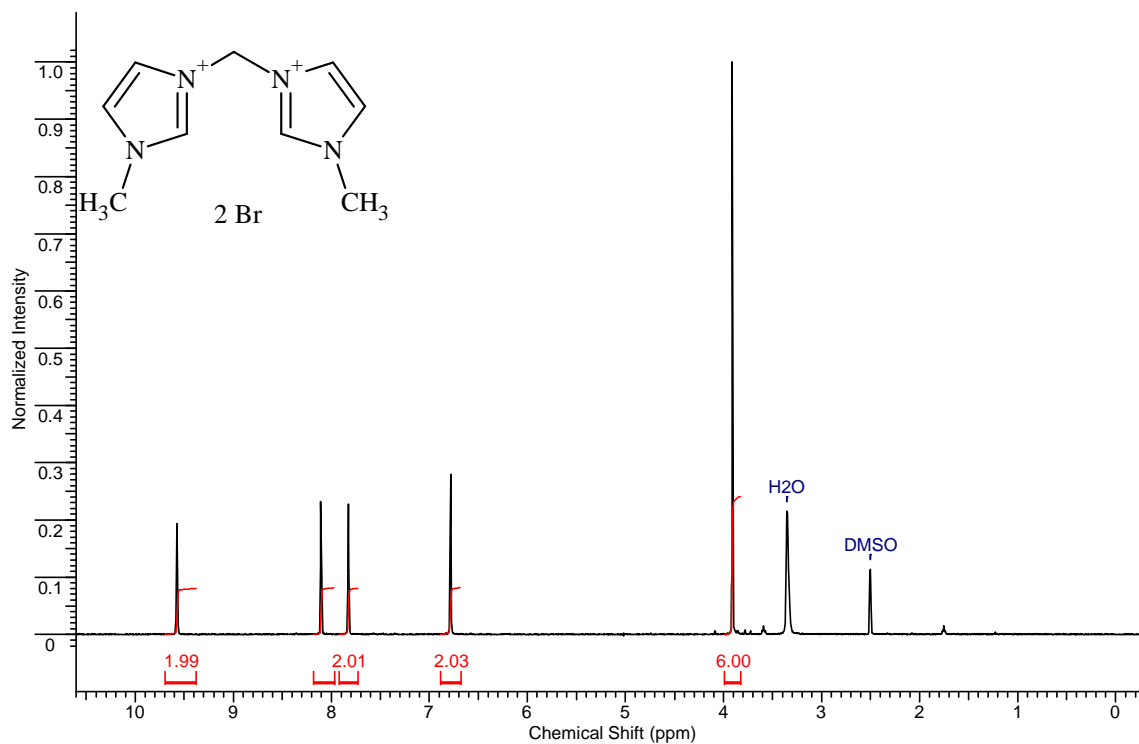


Figure A.1 ^1H -NMR of 2.1 (in $\text{DMSO-}d_6$)

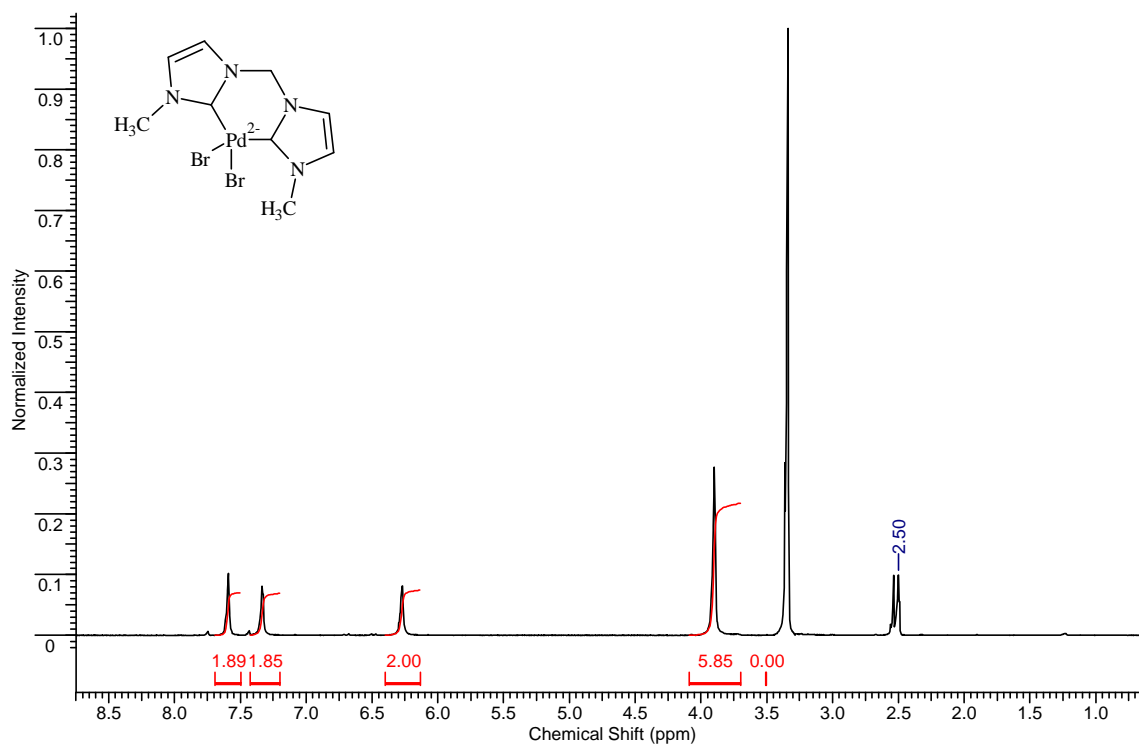


Figure A.2 $^1\text{H-NMR}$ of **2.2** (in $\text{DMSO-}d_6$)

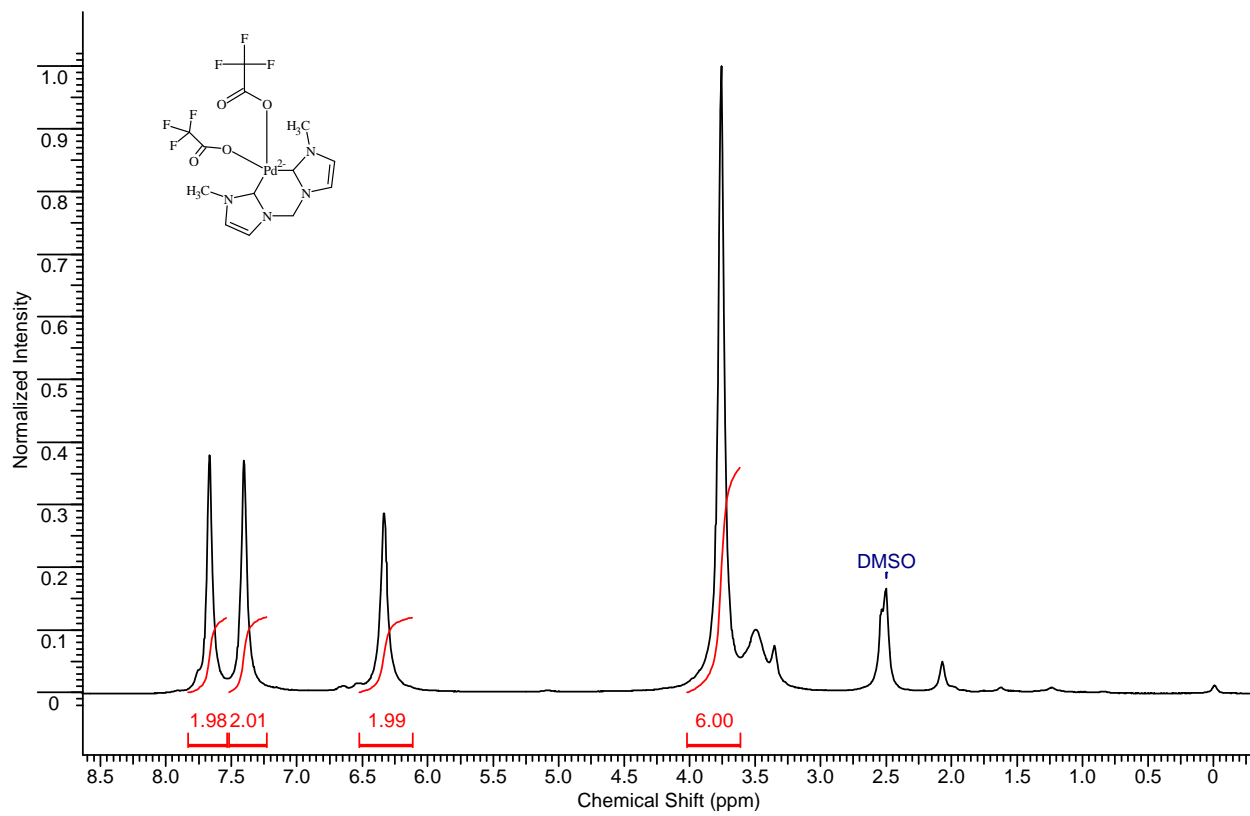


Figure A.3 $^1\text{H-NMR}$ of **2.3a** (in $\text{DMSO-}d_6$)

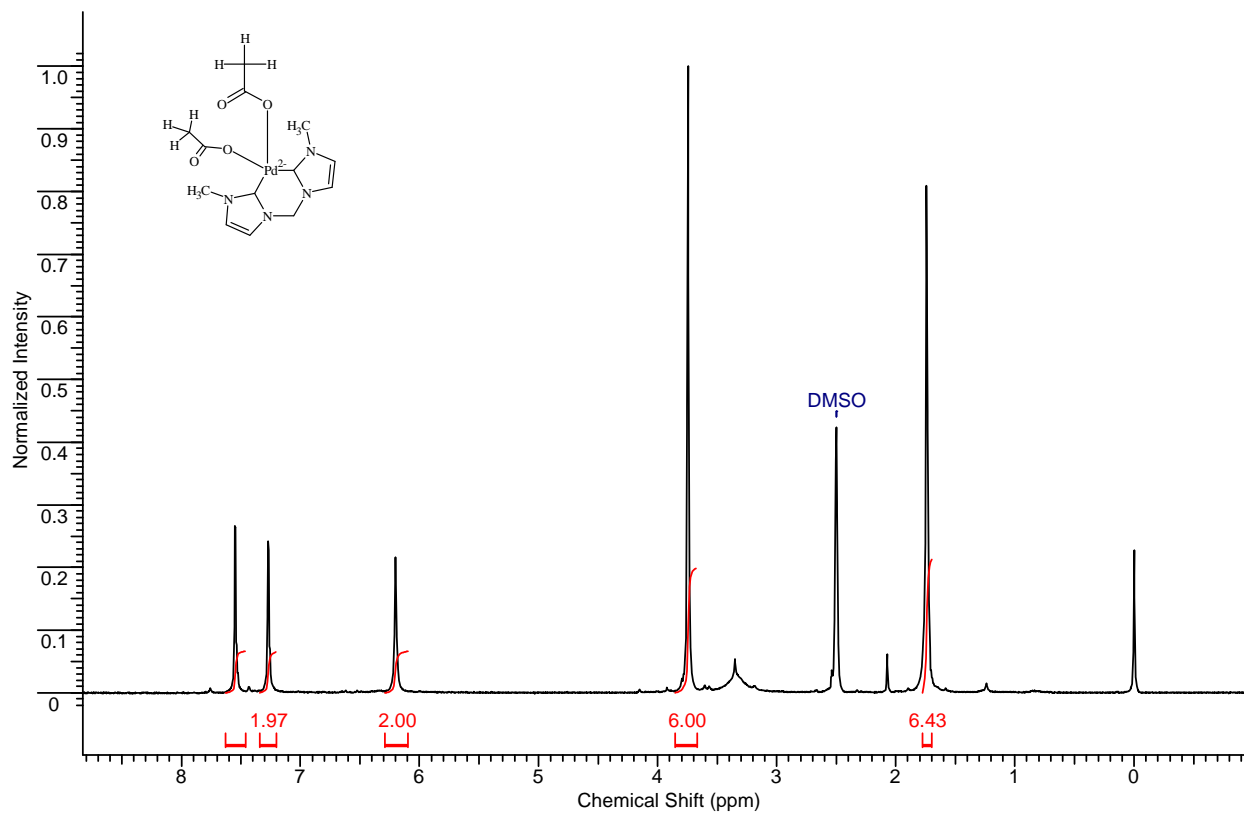
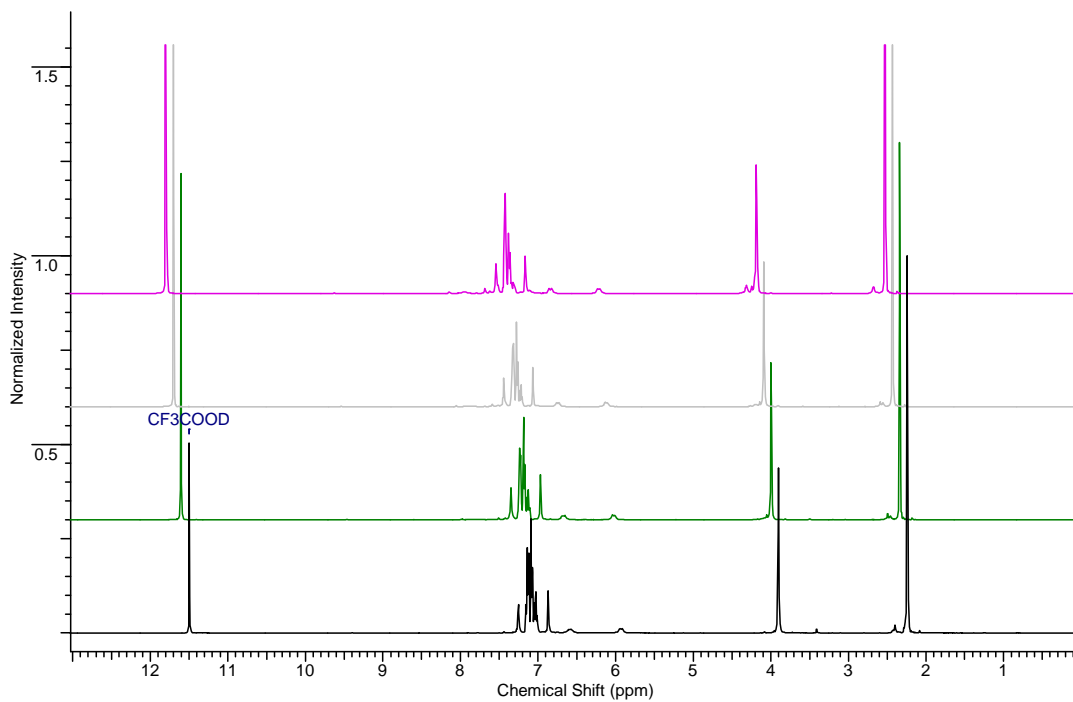
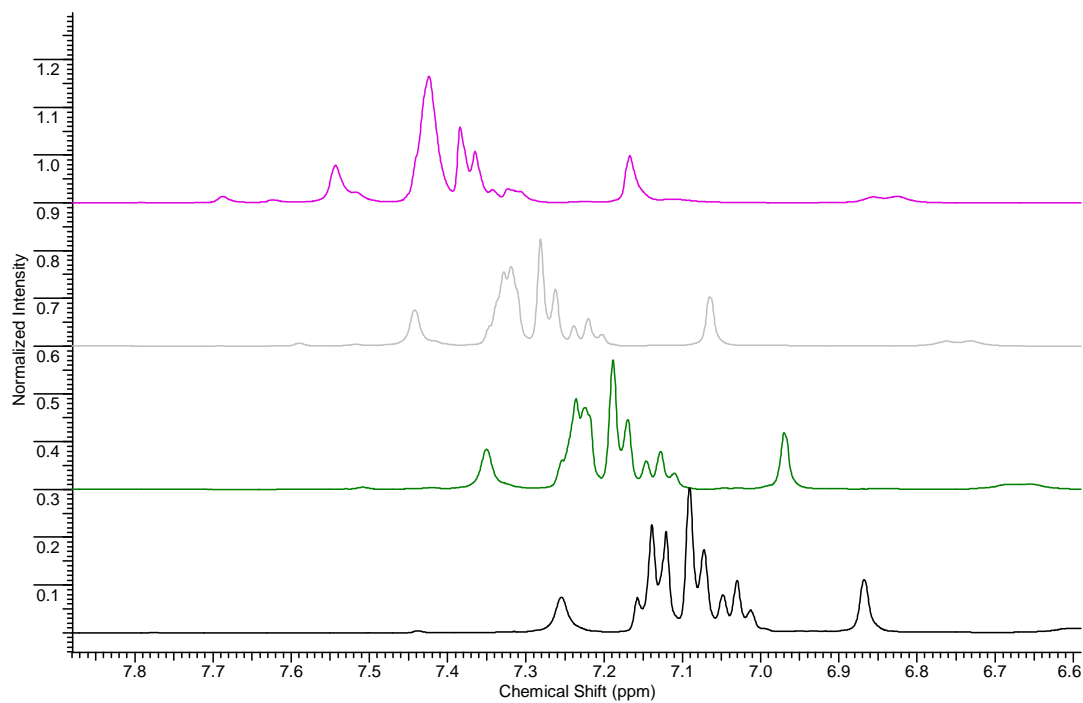


Figure A.4 $^1\text{H-NMR}$ of **2.3b** (in $\text{DMSO-}d_6$)

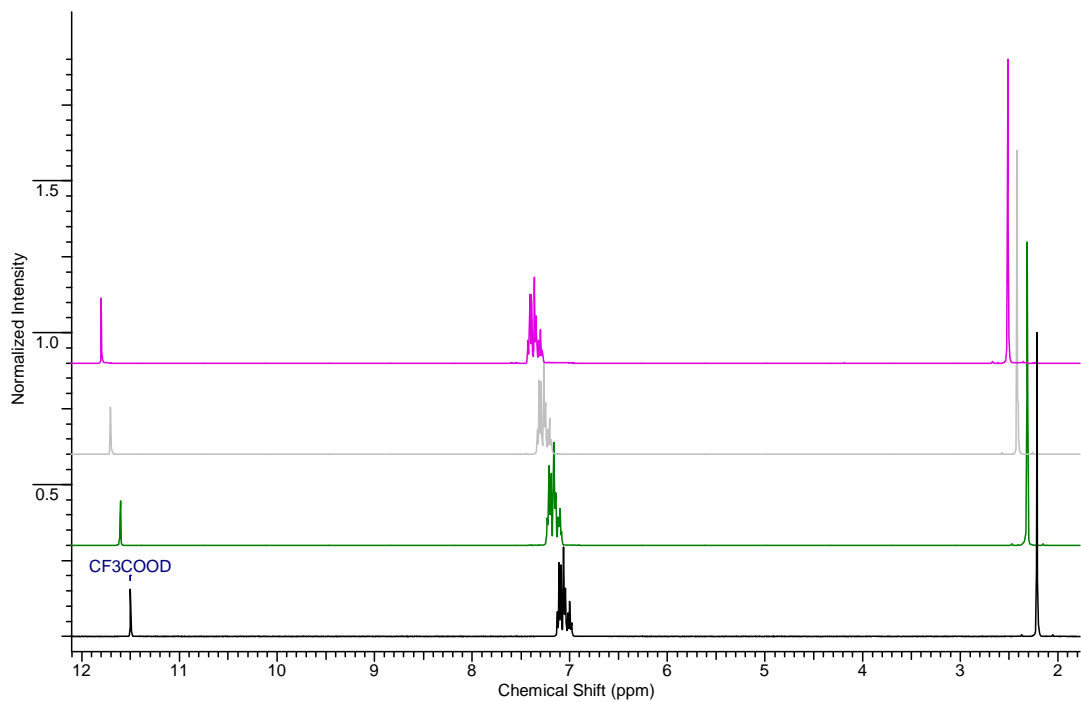


(a)

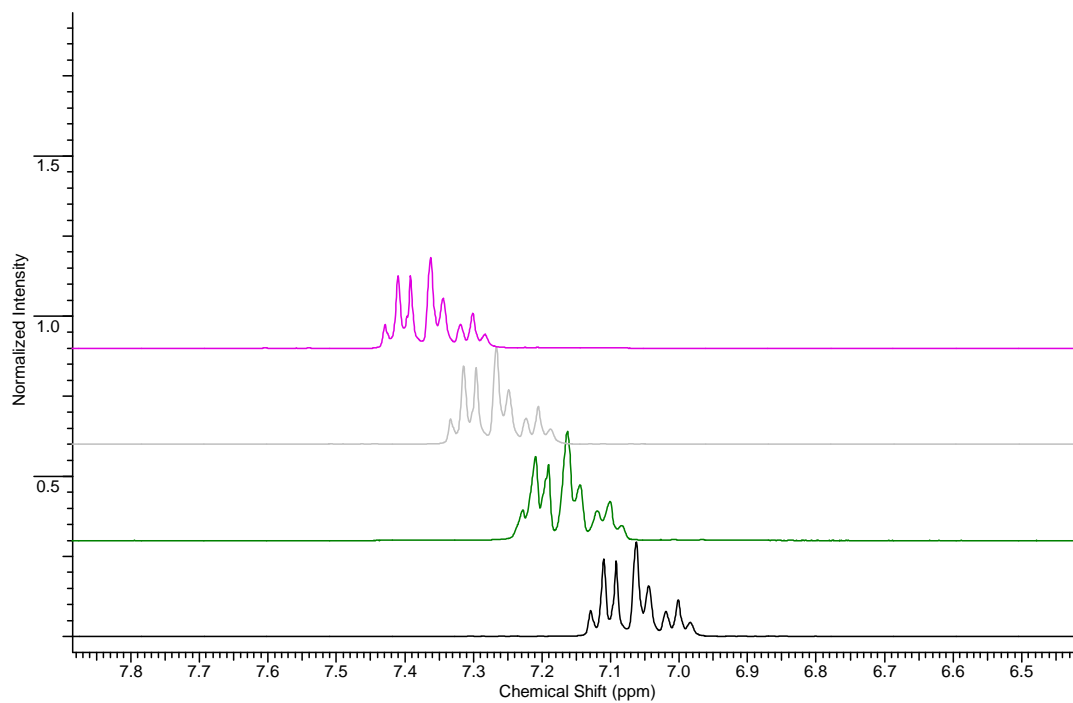


(b)

Figure A.5 (a) Stacked $^1\text{H-NMR}$ of **2.2** mediated toluene H-D exchange in CF_3COOD ; (b) Expanded aromatic area ($^1\text{H-NMR}$ spectrum was recorded every 5 hours).



(a)



(b)

Figure A.6 (a) Stacked ^1H -NMR of control toluene H-D exchange in CF_3COOD ; (b) Expanded aromatic area (^1H -NMR spectrum was recorded every 5 hours).

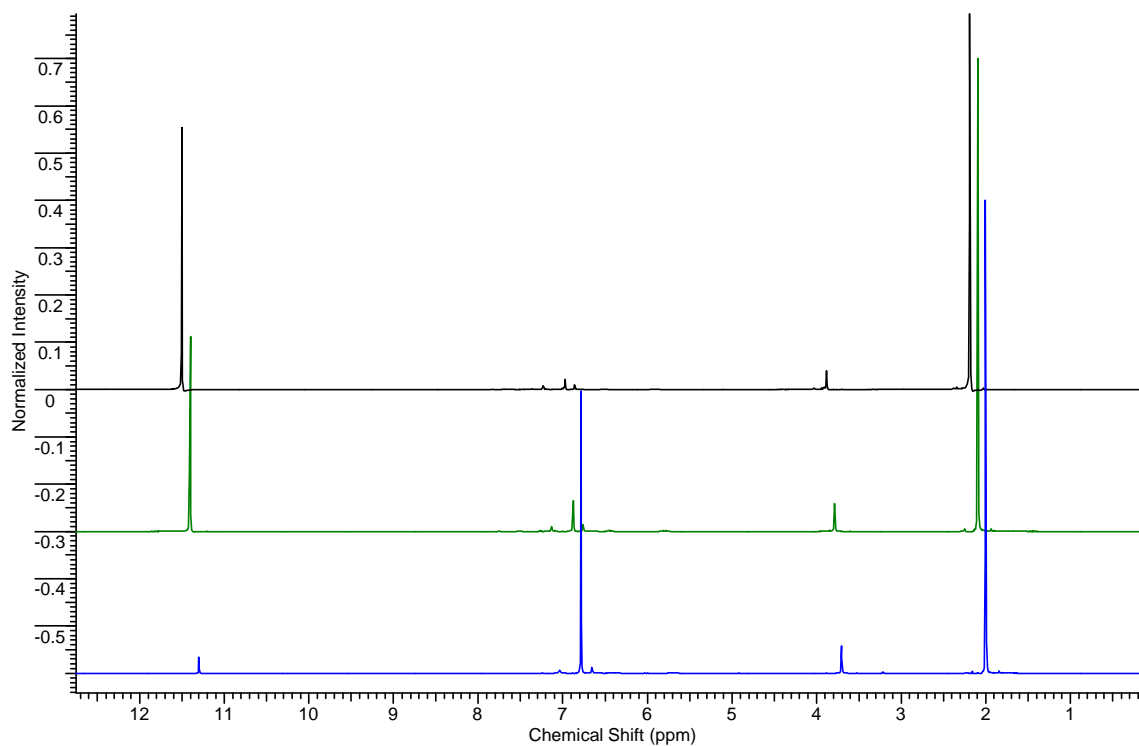


Figure A.7 Stacked ^1H -NMR of **2.3a** mediated *para*-xylene H-D exchange in CF_3COOD (^1H -NMR spectrum was recorded every 5 hours).

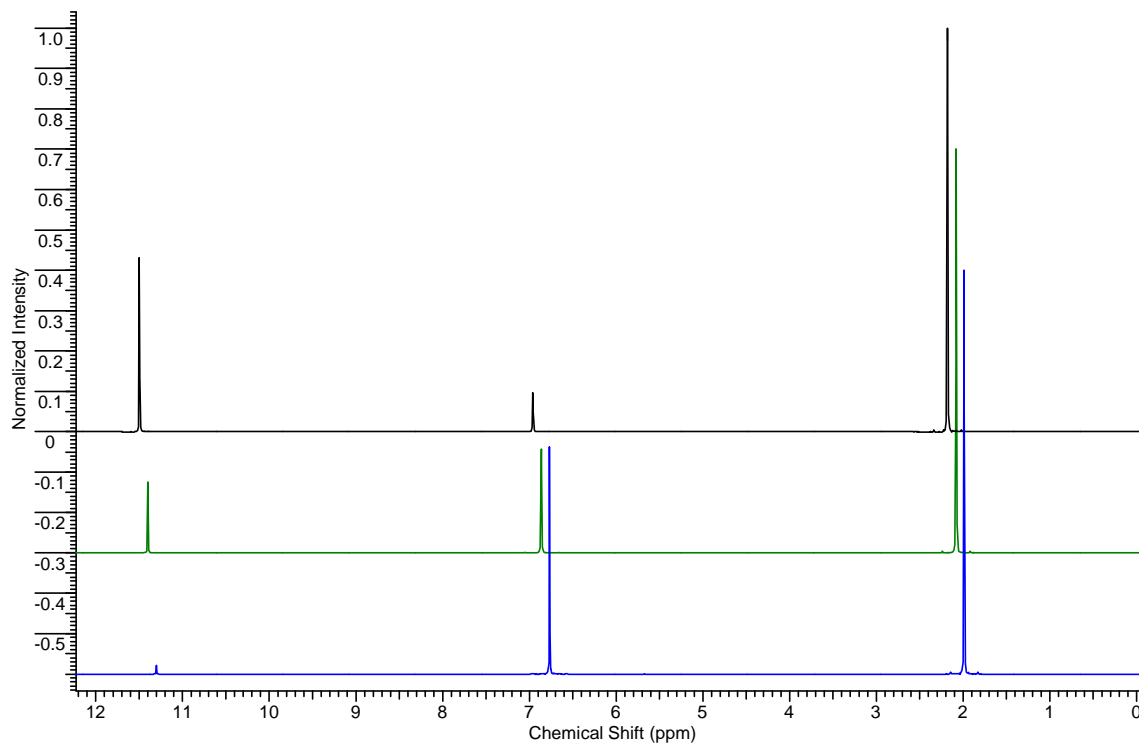


Figure A.8 Stacked ¹H-NMR of control *para*-xylene H-D exchange in CF₃COOD (¹H-NMR spectrum was recorded every 5 hours).

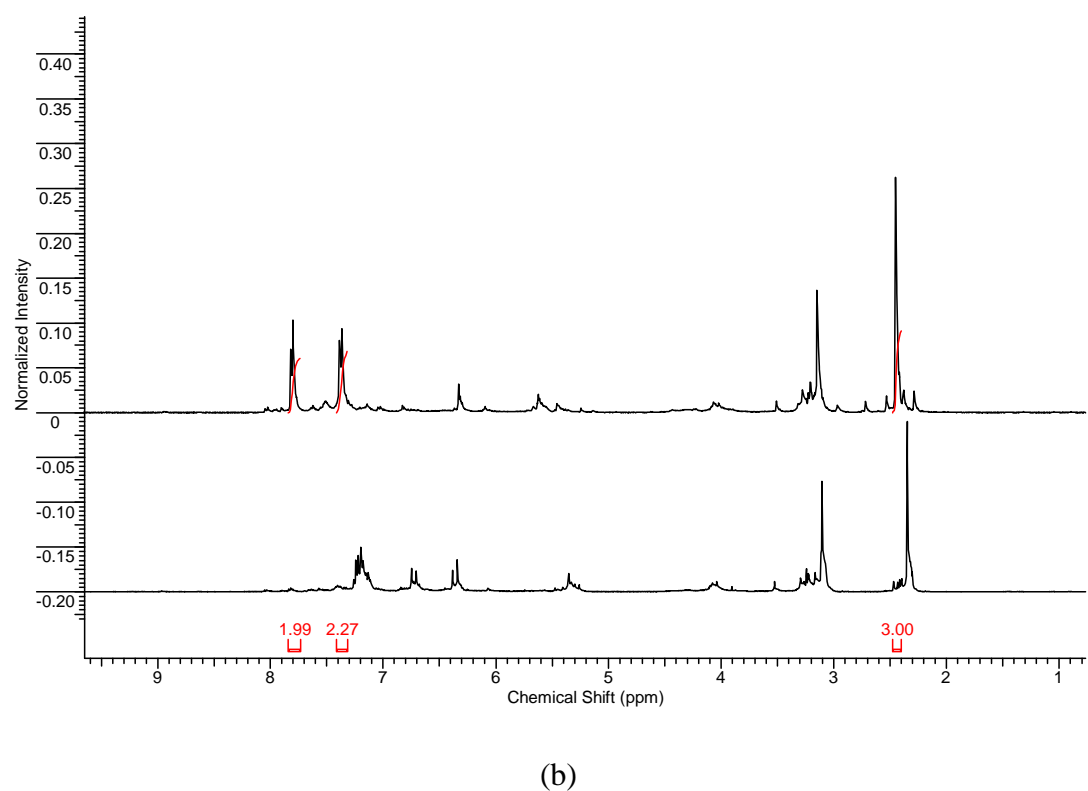
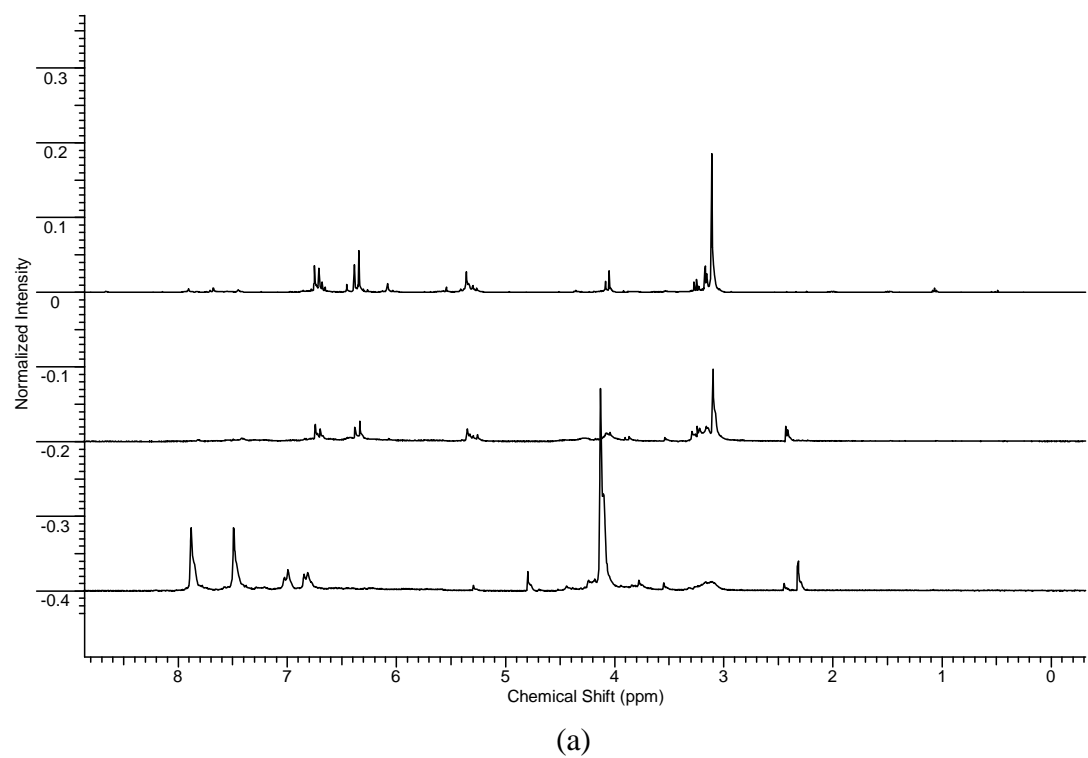
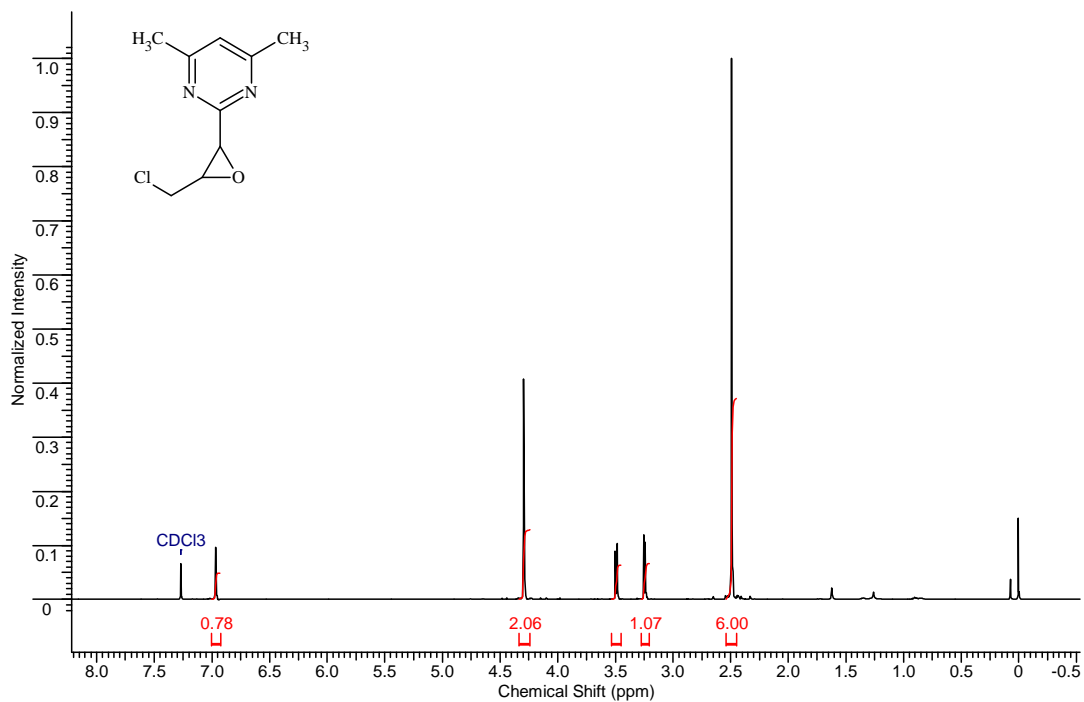
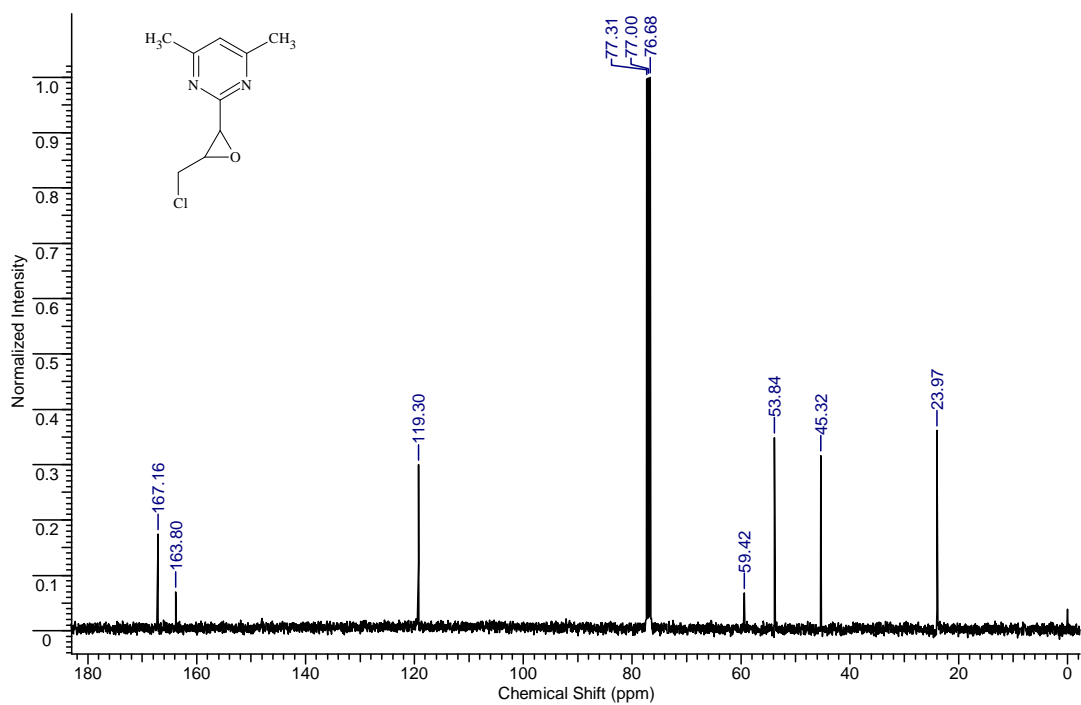


Figure A.9 Stacked $^1\text{H-NMR}$ of **2.2** mediated toluene C-H activation in CF_3COOD in the presence of oxane. (a) **2.2** and oxane in a mixture of CF_3COOD and trifluoroacetic anhydride; (b) Toluene was converted to p-toluenesulfonic acid.

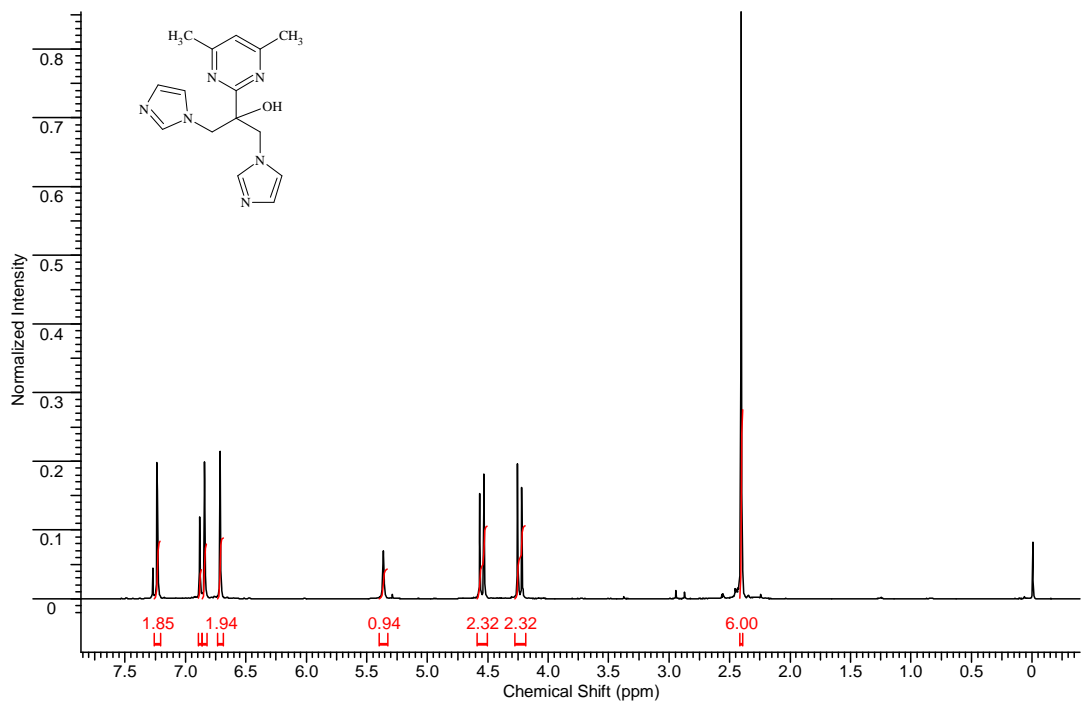


(a)

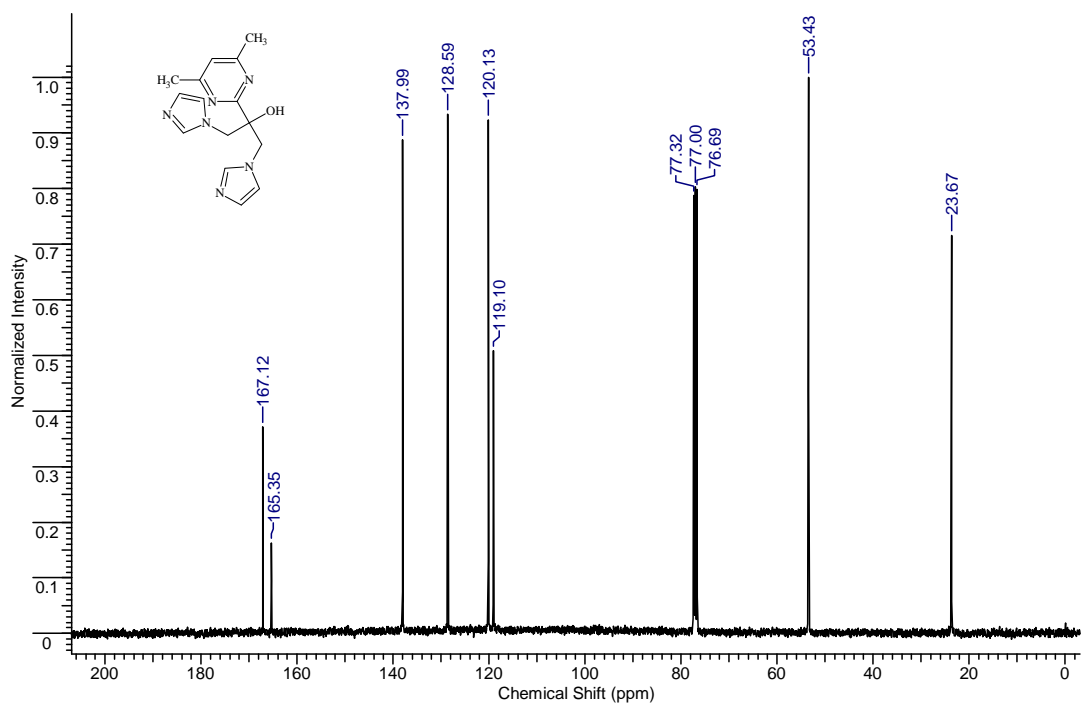


(b)

Figure A.10 (a) ¹H-NMR and (b) ¹³C-NMR of **3.17** (in CDCl₃)



(a)



(b)

Figure A.11 (a) $^1\text{H-NMR}$ and (b) $^{13}\text{C-NMR}$ of **3.18** (in CDCl₃)

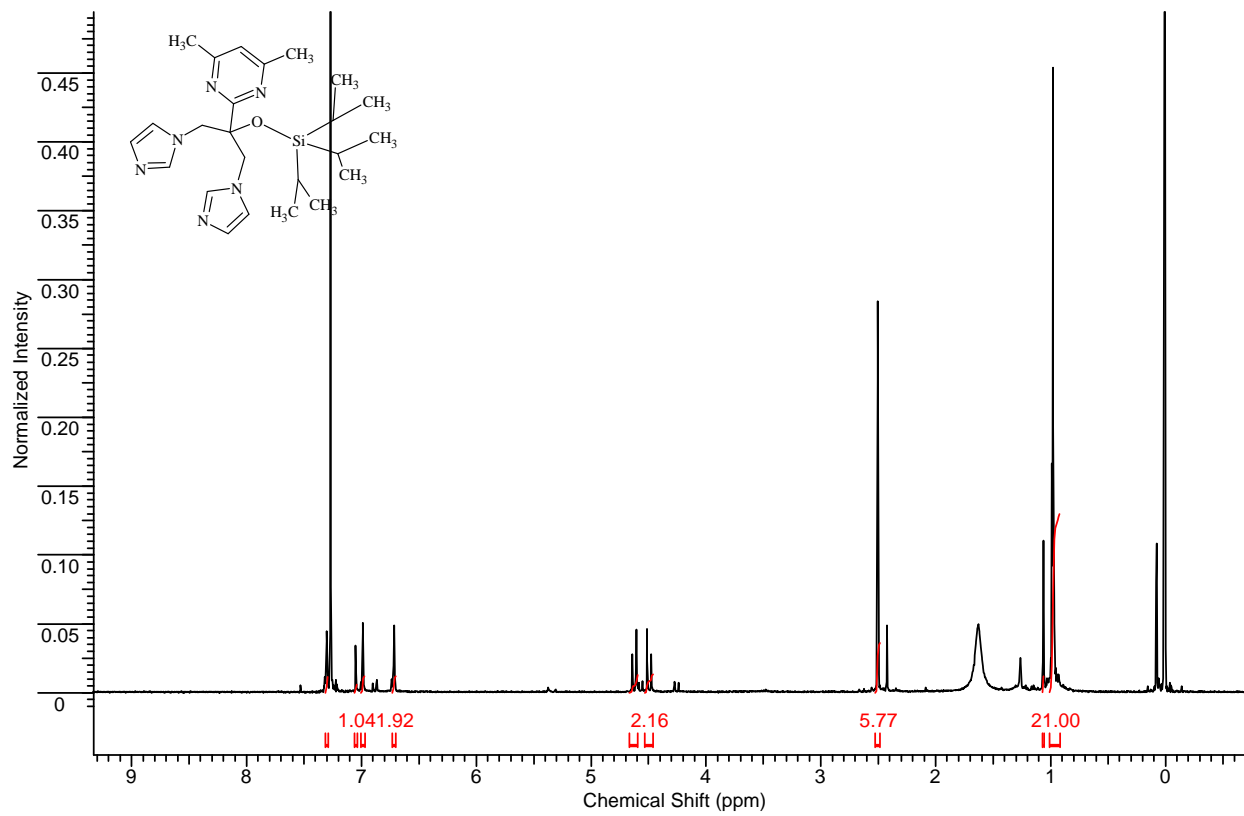


Figure A.12 $^1\text{H-NMR}$ **3.19** (in CDCl_3)

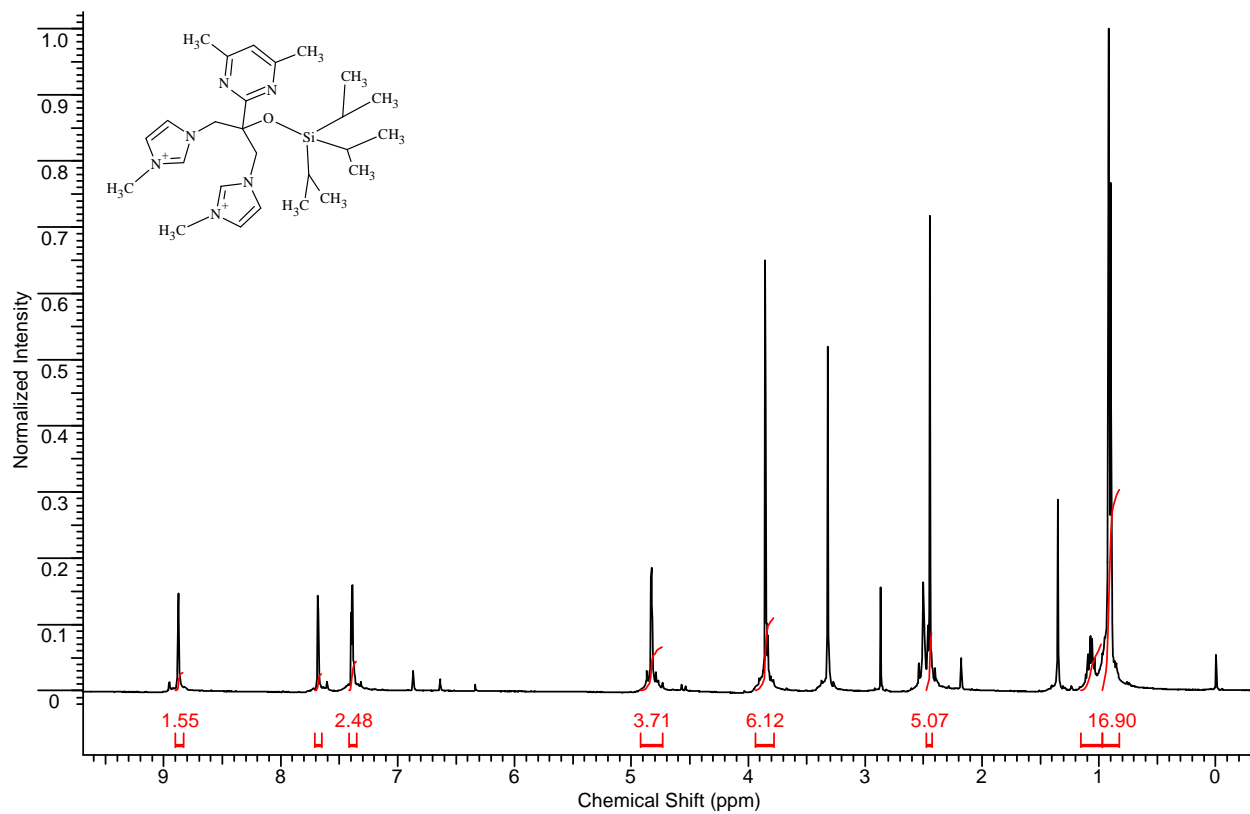


Figure A.13 $^1\text{H-NMR}$ 3.20 (in $\text{DMSO-}d_6$)

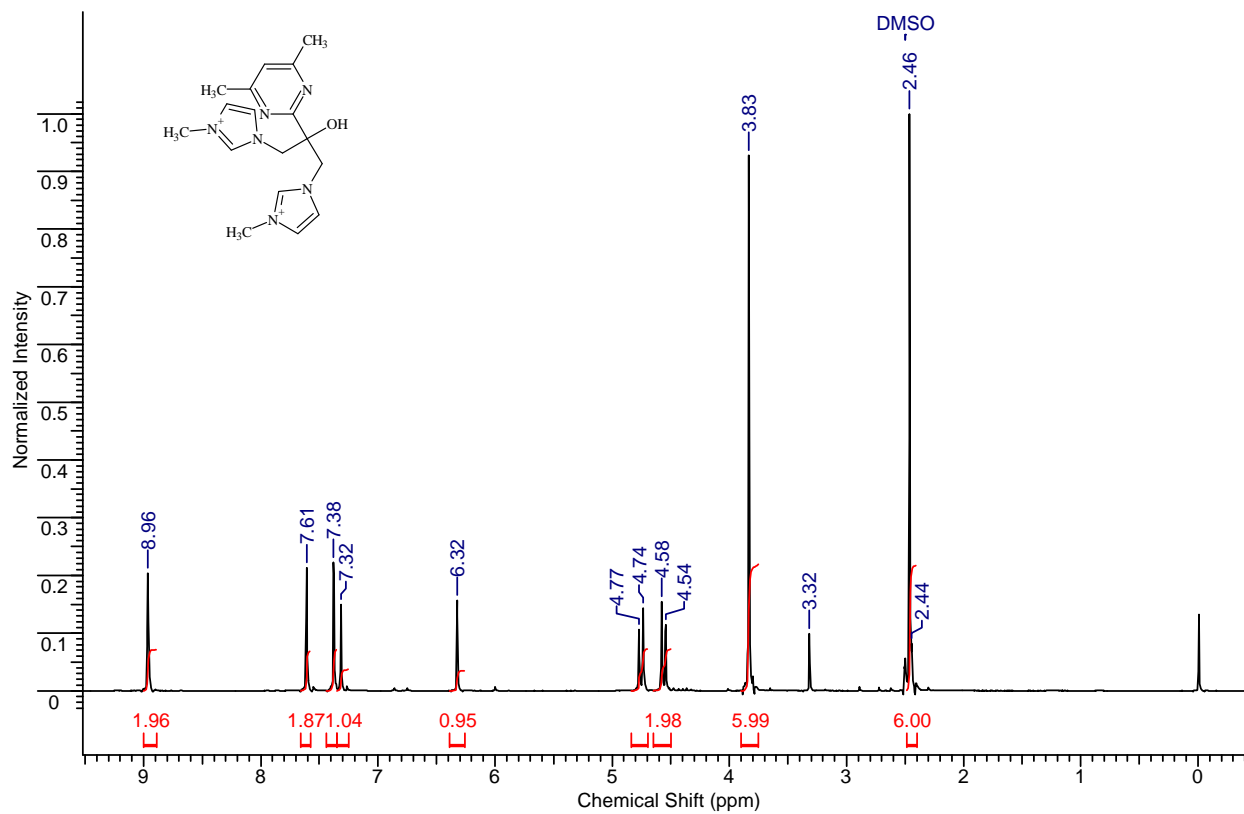


Figure A.14 ¹H-NMR 3.24 (in DMSO-*d*₆)

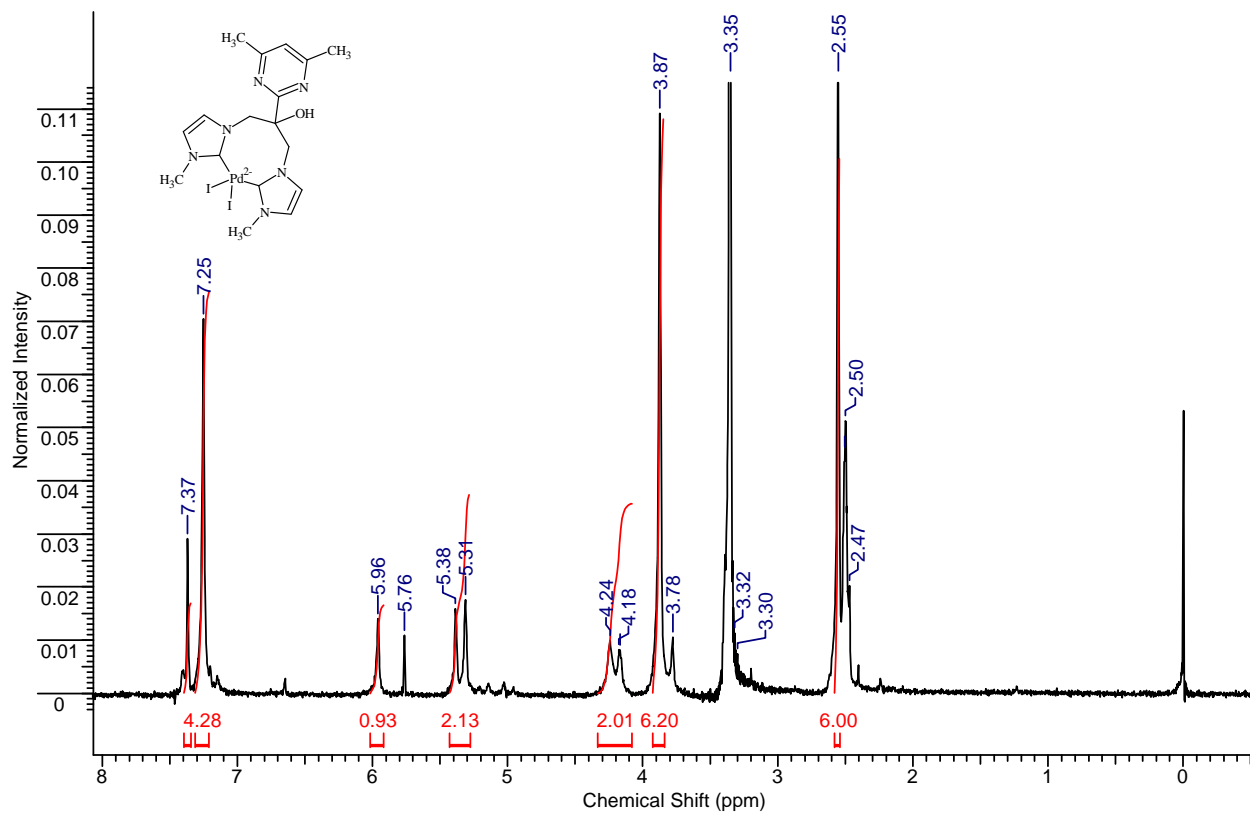


Figure A.15 $^1\text{H-NMR}$ 3.25 (in $\text{DMSO-}d_6$)

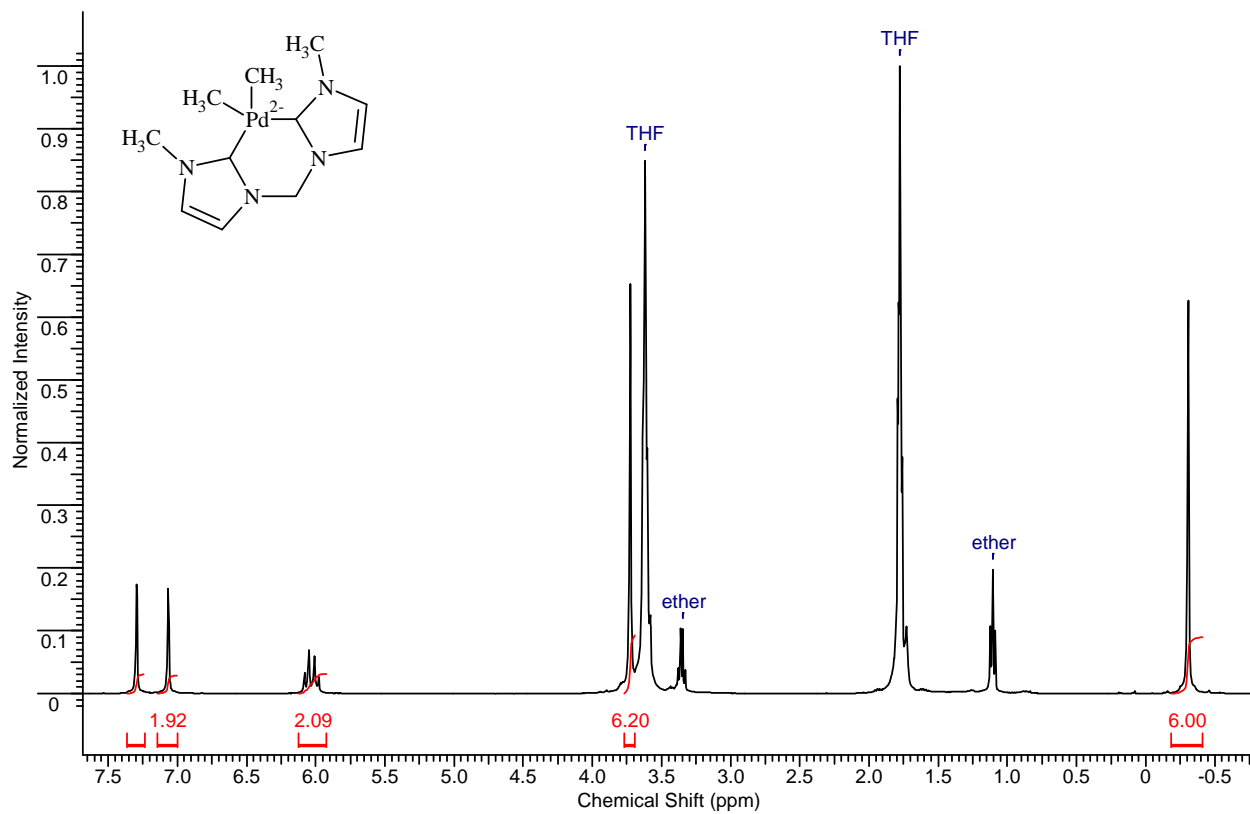


Figure A.16 $^1\text{H-NMR}$ 4.1 (in $\text{THF-}d_8$)

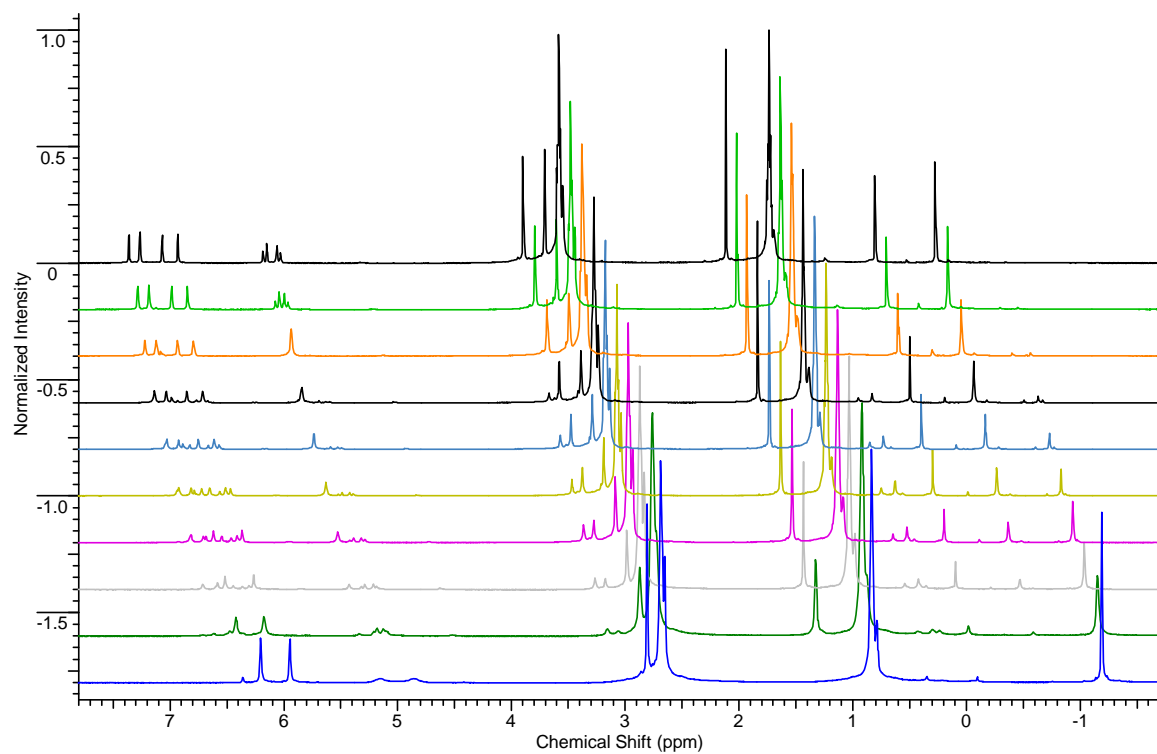


Figure A.17a Stacked $^1\text{H-NMR}$ spectrum of the reaction between palladium complex **4.1** and MeI at $-50\text{ }^\circ\text{C}$. (NMR spectrum was recorded every 10 minutes in $\text{THF-}d_8$)

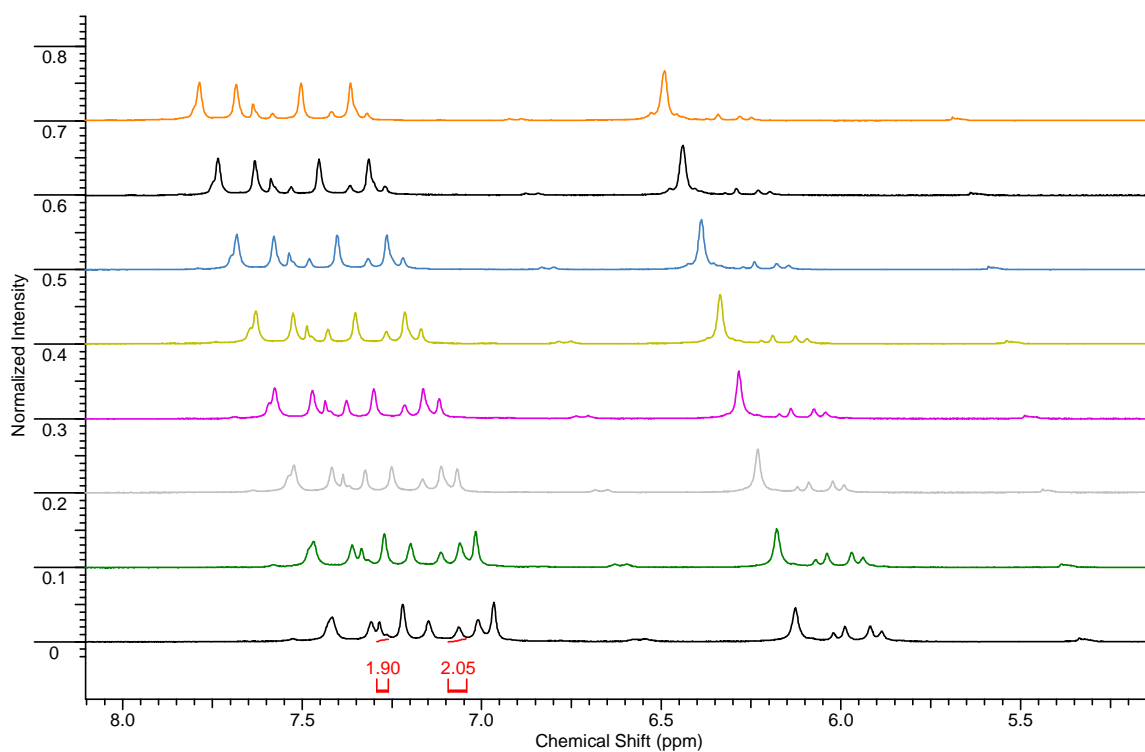


Figure A.17b Stacked ¹H-NMR spectrum of the reaction between palladium complex **4.1** and MeI at -50 °C; (NMR spectrum was recorded every 10 minutes in THF-*d*₈, expanded imidazole and methylene bridge area)

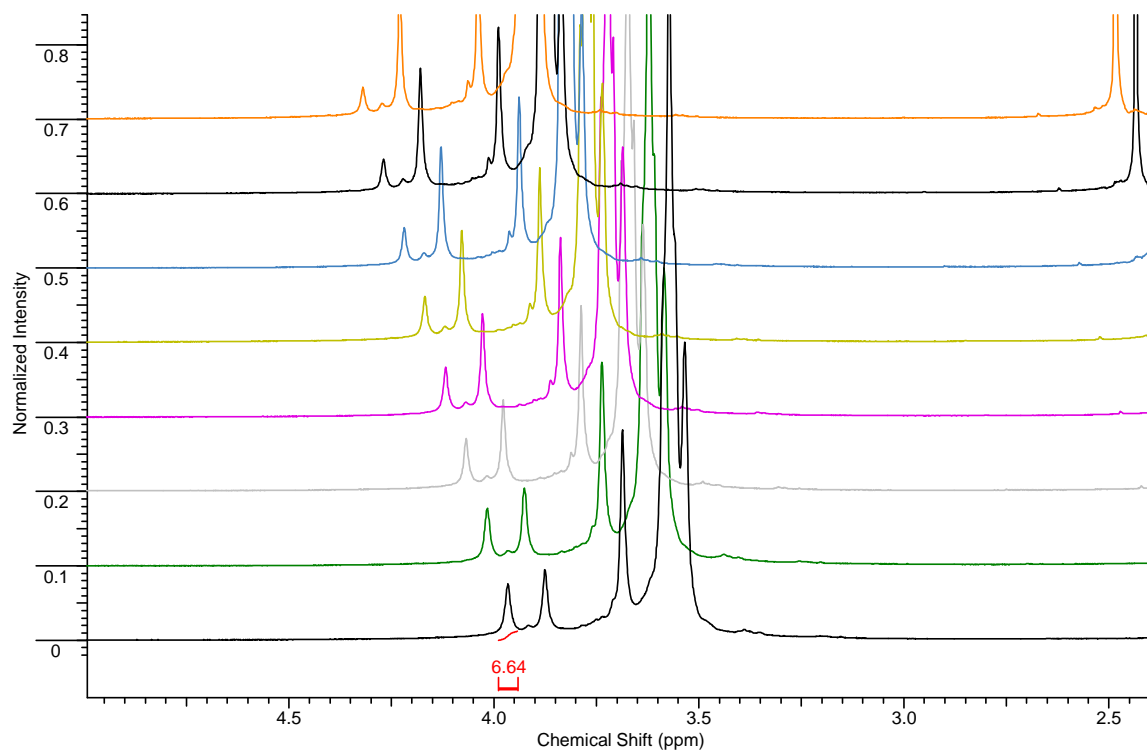


Figure A.17c Stacked ¹H-NMR spectrum of the reaction between palladium complex **4.1** and MeI at -50 °C; (NMR spectrum was recorded every 10 minutes in THF-*d*₈, expanded N-methyl area)

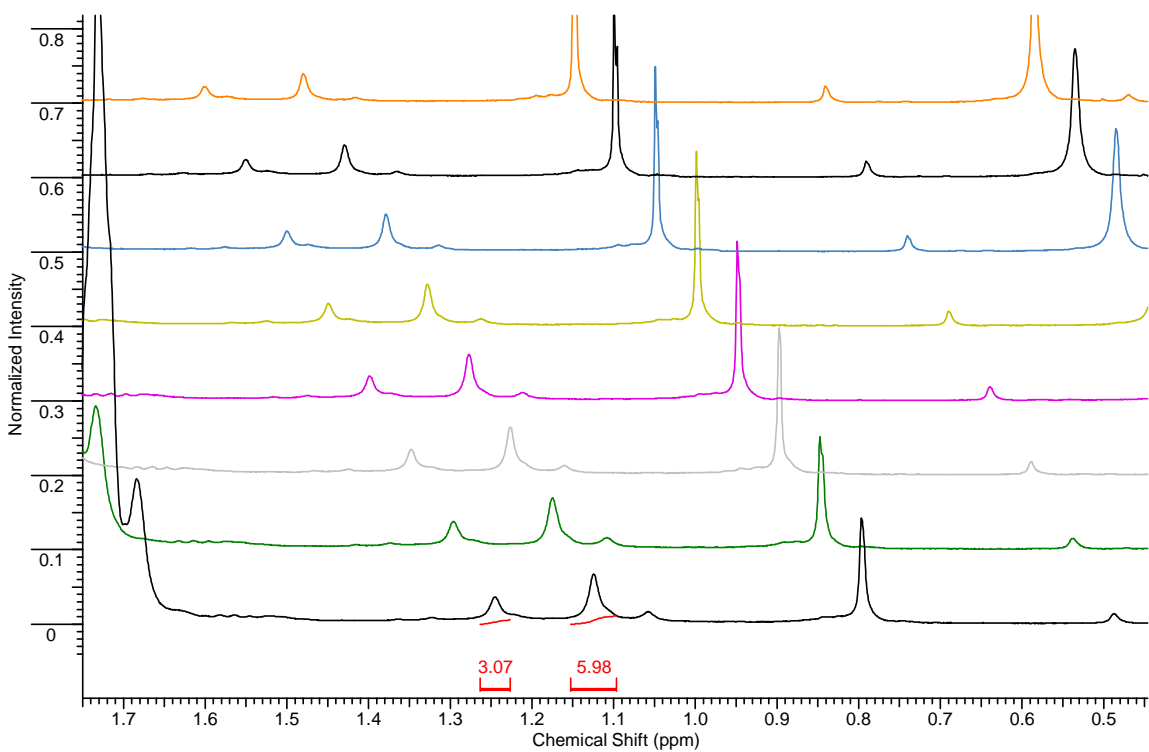


Figure A.17d Stacked $^1\text{H-NMR}$ spectrum of the reaction between palladium complex **4.1** and MeI at $-50\text{ }^\circ\text{C}$; (NMR spectrum was recorded every 10 minutes in $\text{THF-}d_8$, expanded palladium coordinated methyl groups area)

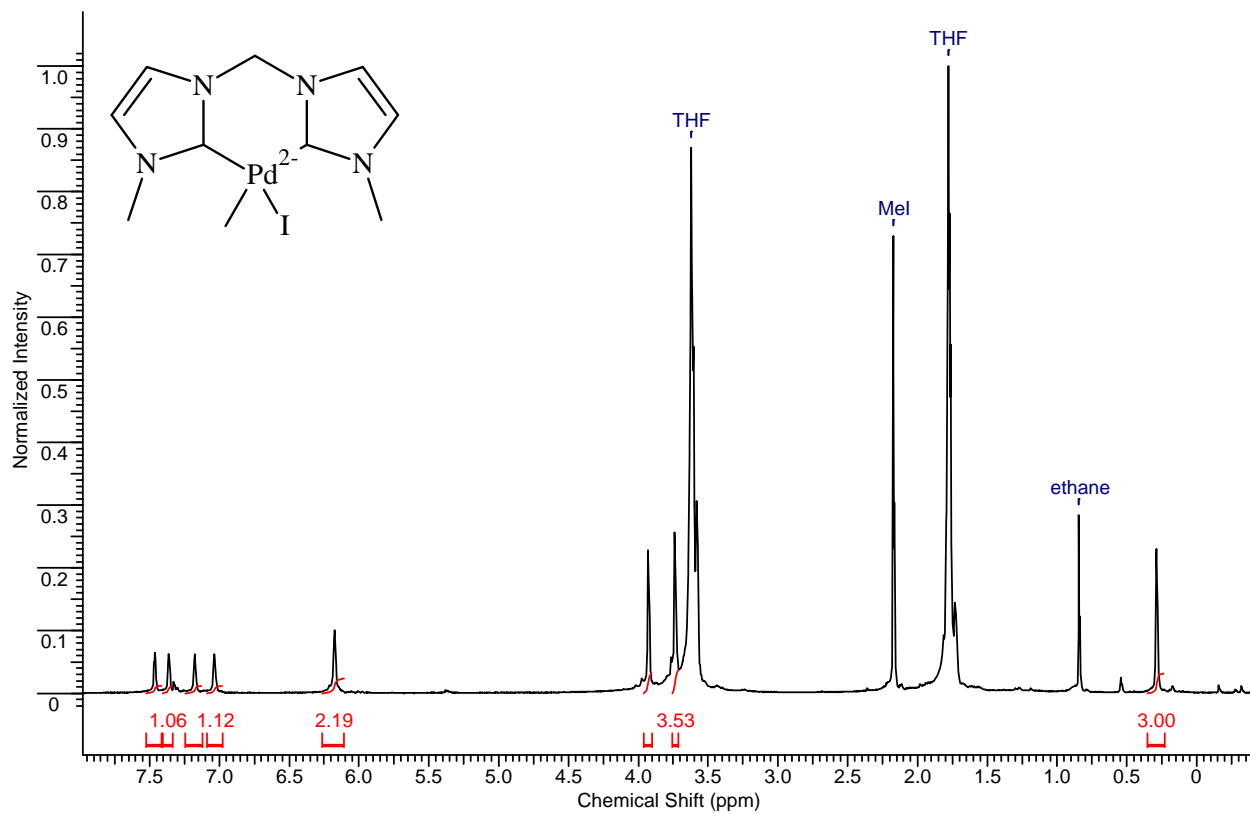


Figure A.18 $^1\text{H-NMR}$ of **4.4** (Spectrum recorded after the completion of the reaction between palladium complex **4.1** and MeI)

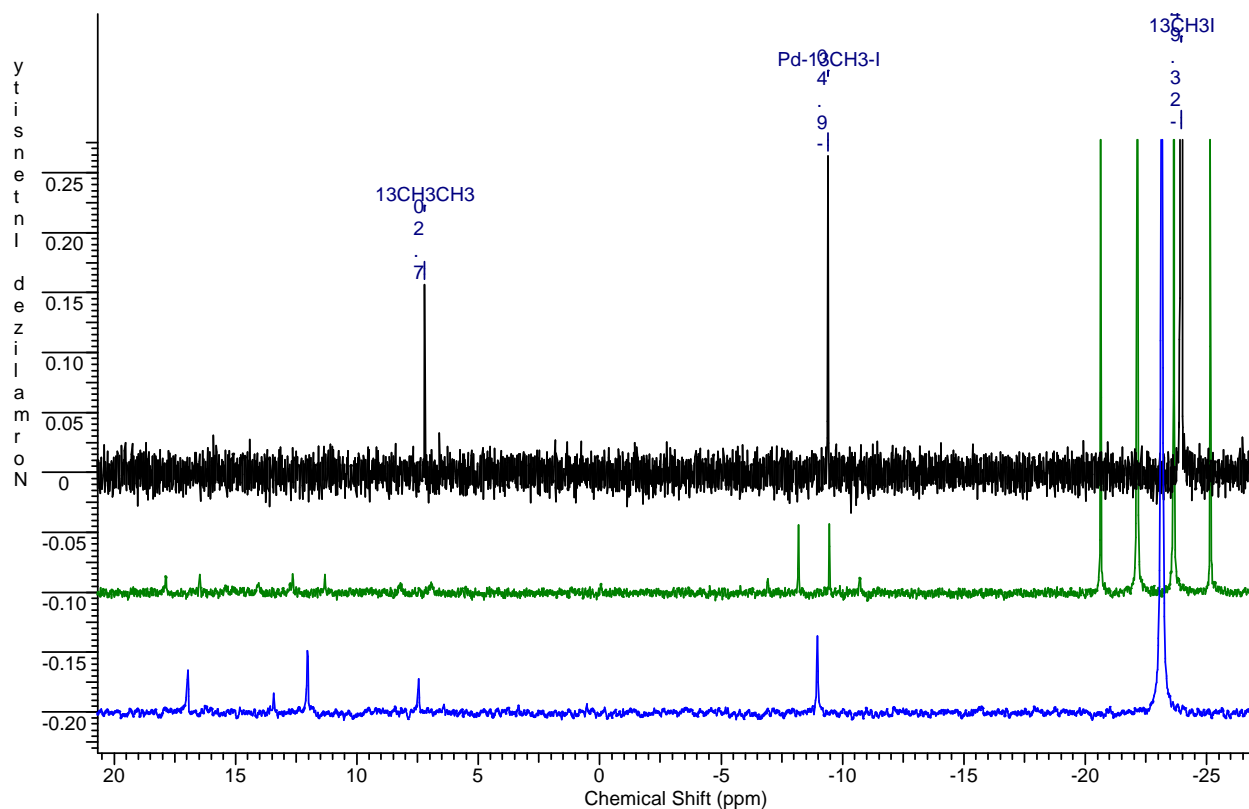


Figure A.19 Stacked ^{13}C -NMR spectrum of the reaction between palladium complex **4.1** and $^{13}\text{CH}_3\text{I}$ (blue: After 20 minutes reaction at $-50\text{ }^\circ\text{C}$, ^{13}C -NMR recorded at $-70\text{ }^\circ\text{C}$; green: After 20 minutes reaction at $-50\text{ }^\circ\text{C}$, ^{13}C -NMR recorded at $-70\text{ }^\circ\text{C}$ with carbon-hydrogen coupling; black: After 60 minutes reaction at $-50\text{ }^\circ\text{C}$, ^{13}C -NMR recorded at $-50\text{ }^\circ\text{C}$)

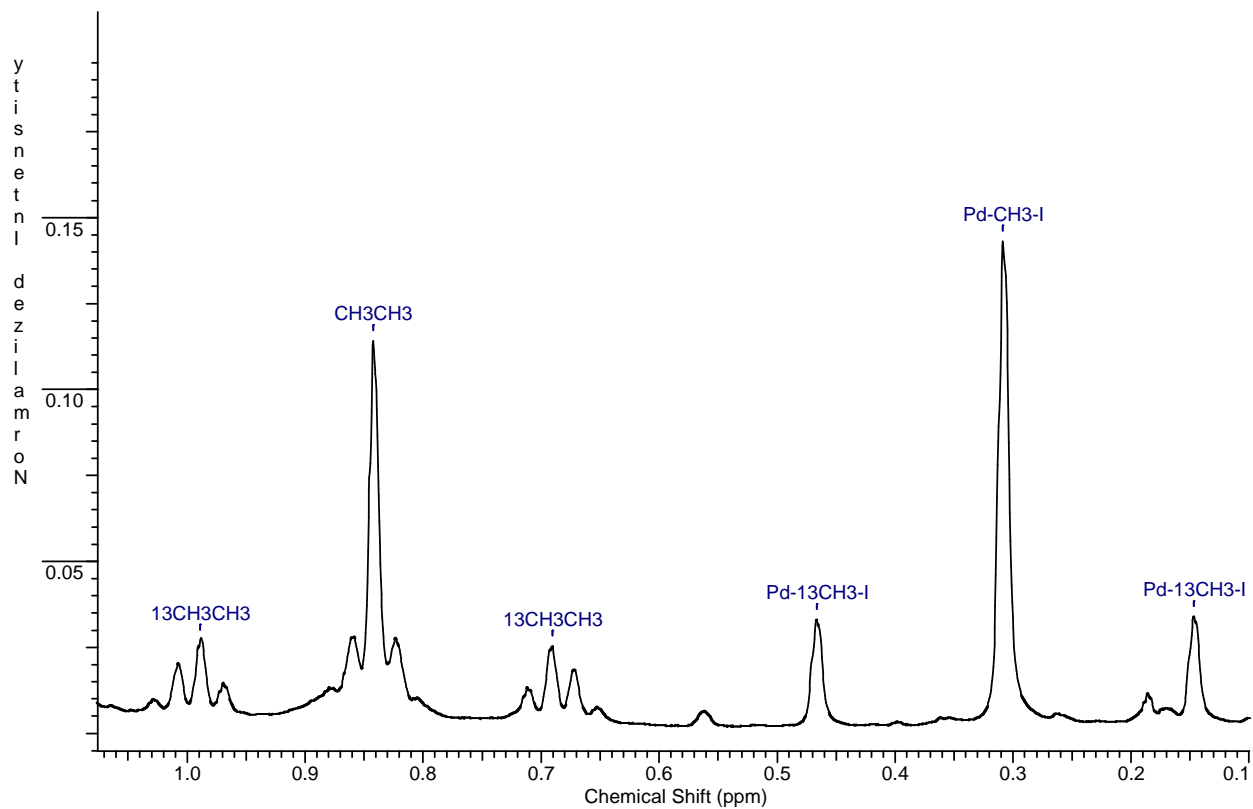


Figure A.20 $^1\text{H-NMR}$ for the products after the completion of the reaction between palladium complex **4.1** and $^{13}\text{CH}_3\text{I}$

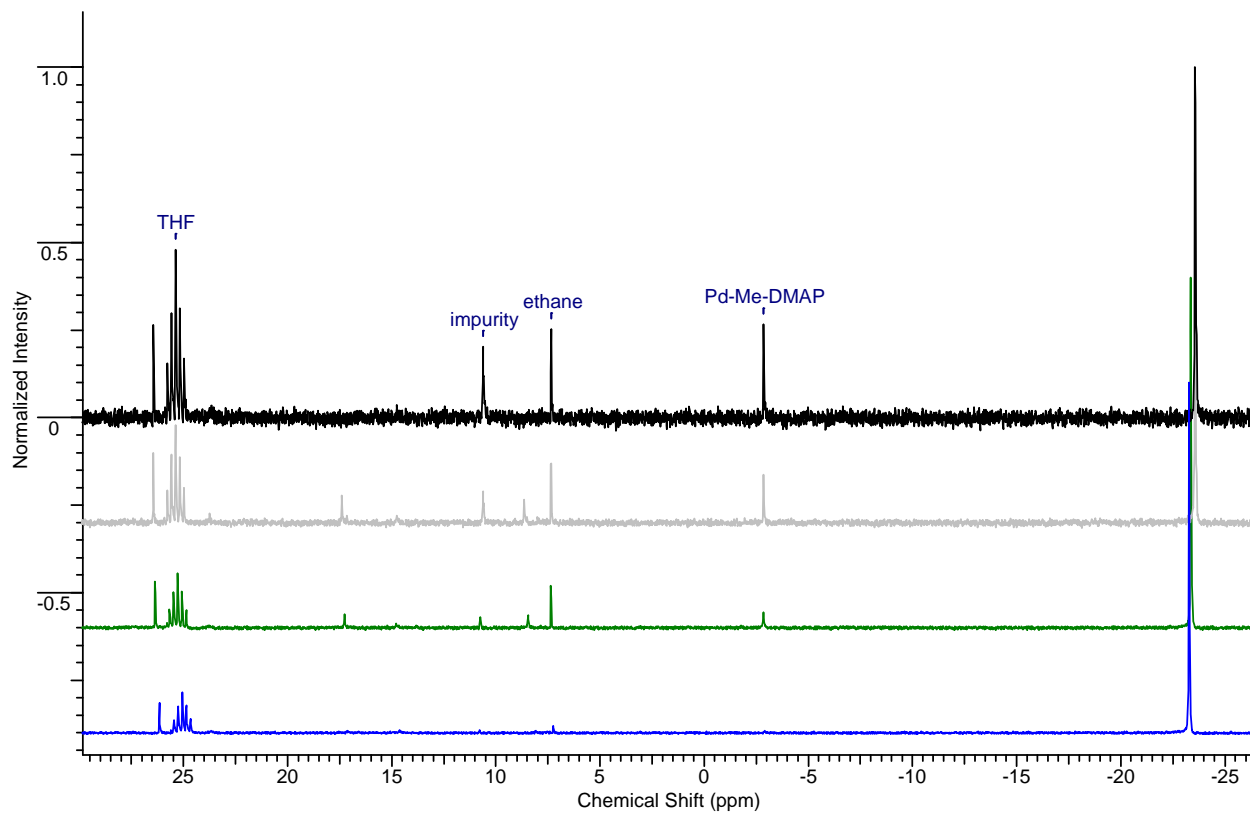


Figure A.21 Stacked ^{13}C -NMR of the reaction between *bis*-NHC-Pd(II)-Me₂ and $^{13}\text{CH}_3\text{I}$ in the presence of DMAP (blue: reaction at -50 °C for 20 min; green: reaction at -30 °C for 20 minutes; gray: reaction at -30 °C for 40 minutes; black: reaction at -30 °C for 60 minutes)

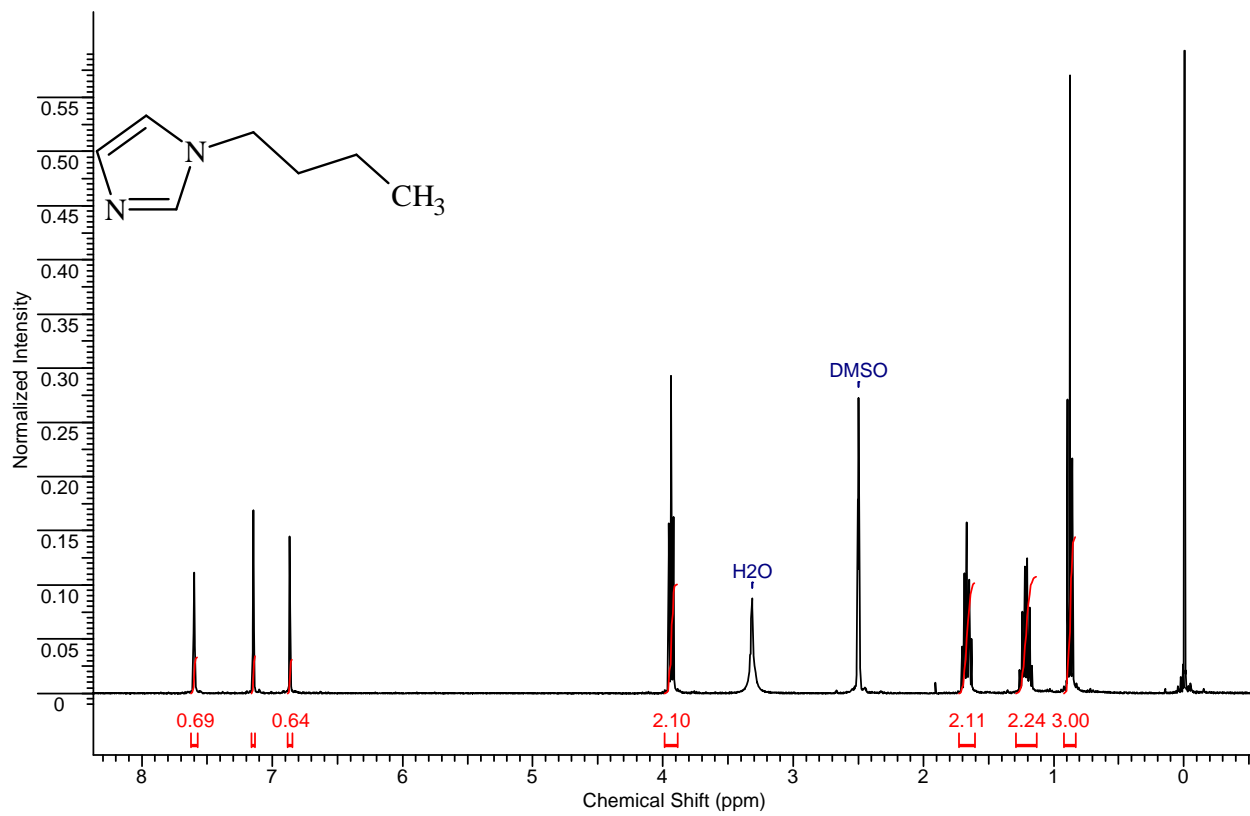


Figure A.22 ¹H-NMR of 5.11

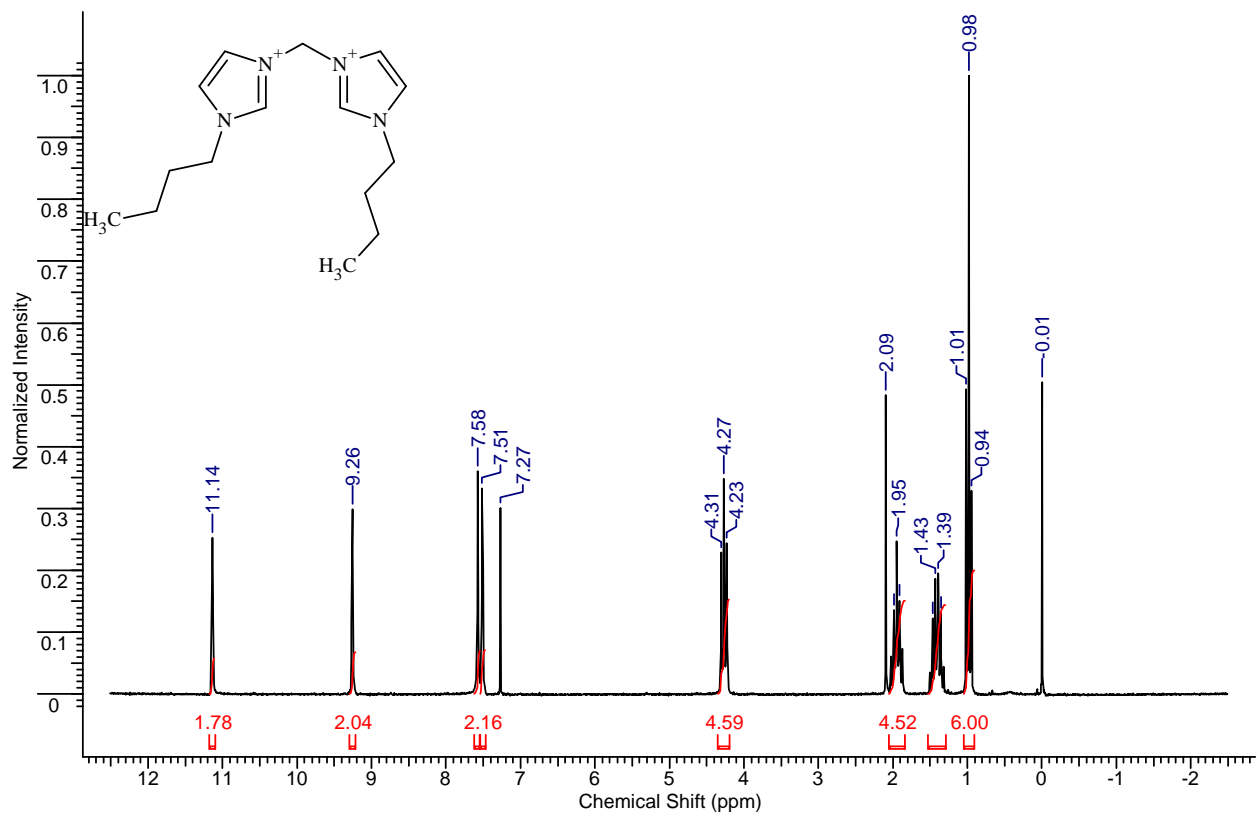
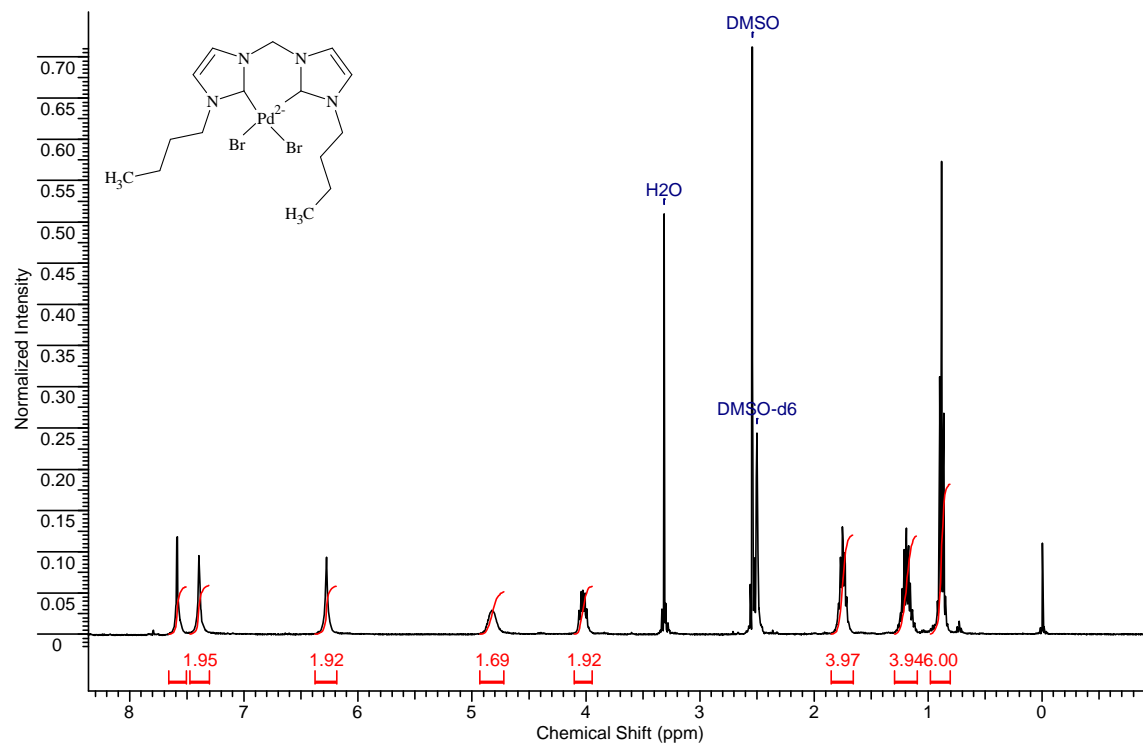
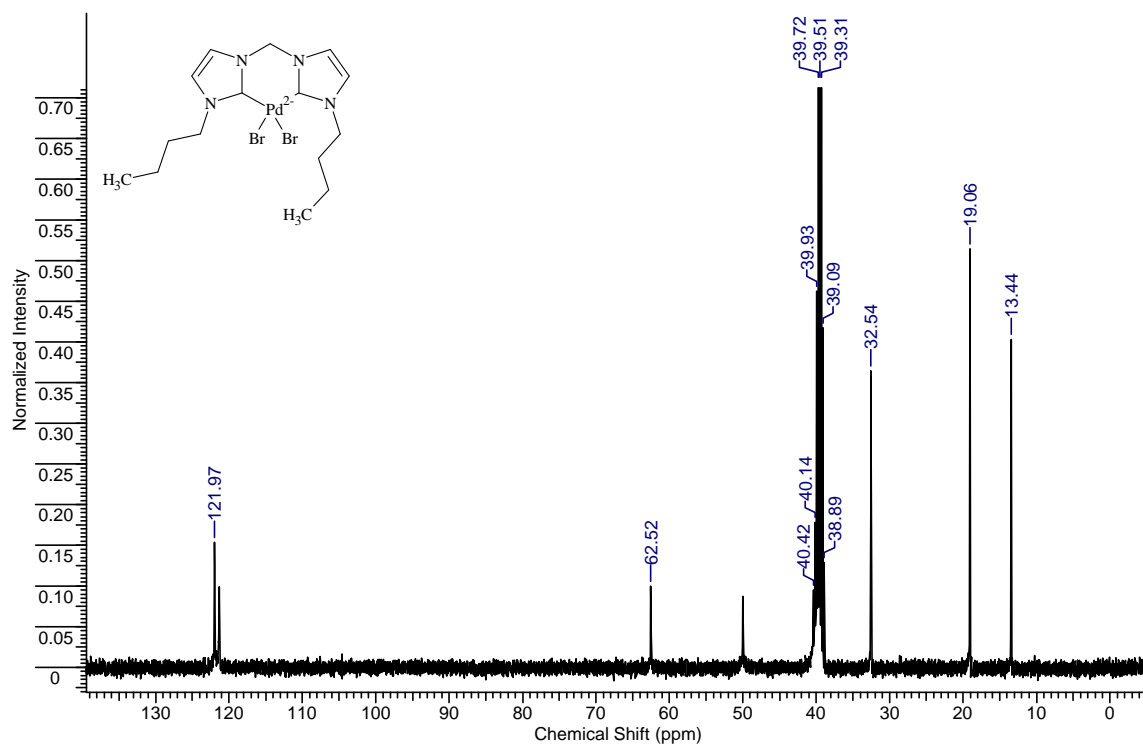


Figure A.23 $^1\text{H-NMR}$ of 5.12



(a)



(b)

Figure A.24 (a) $^1\text{H-NMR}$ and (b) $^{13}\text{C-NMR}$ of 5.13

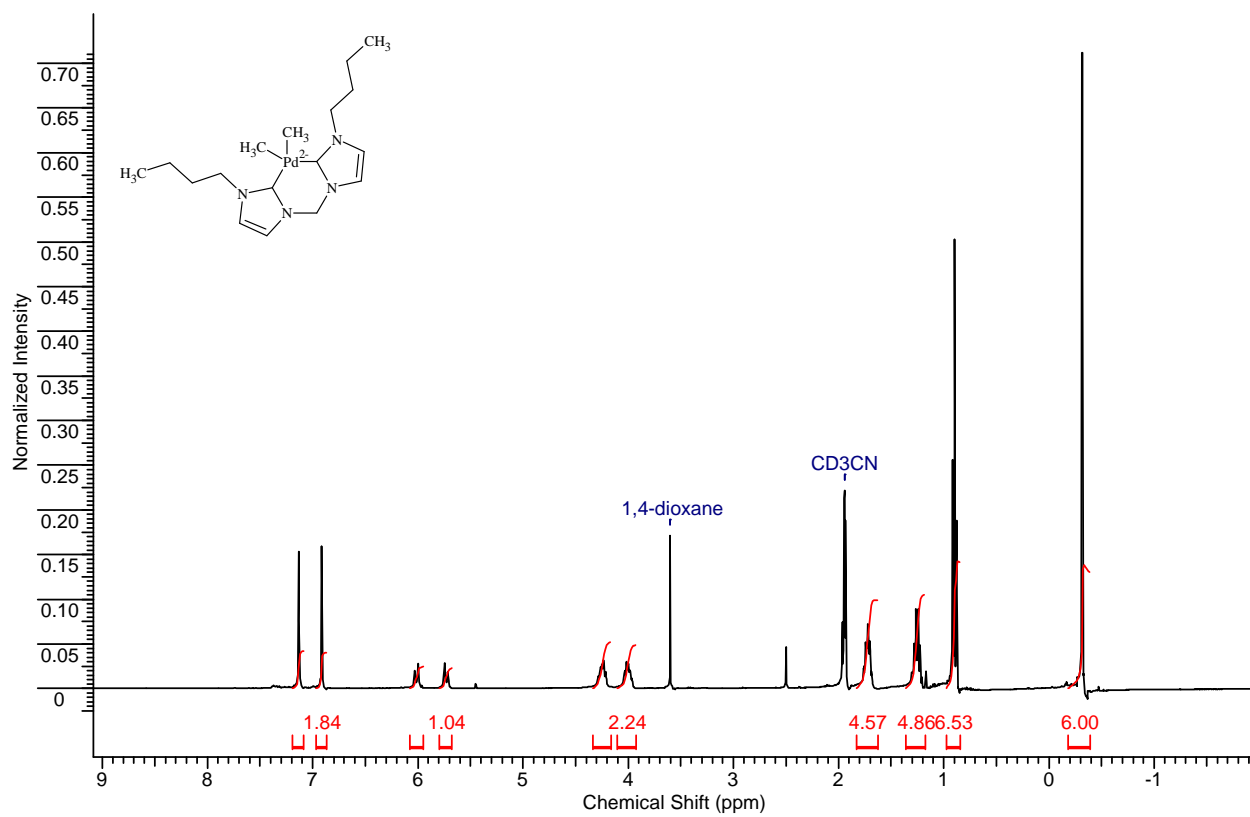


Figure A.25 $^1\text{H-NMR}$ 5.14

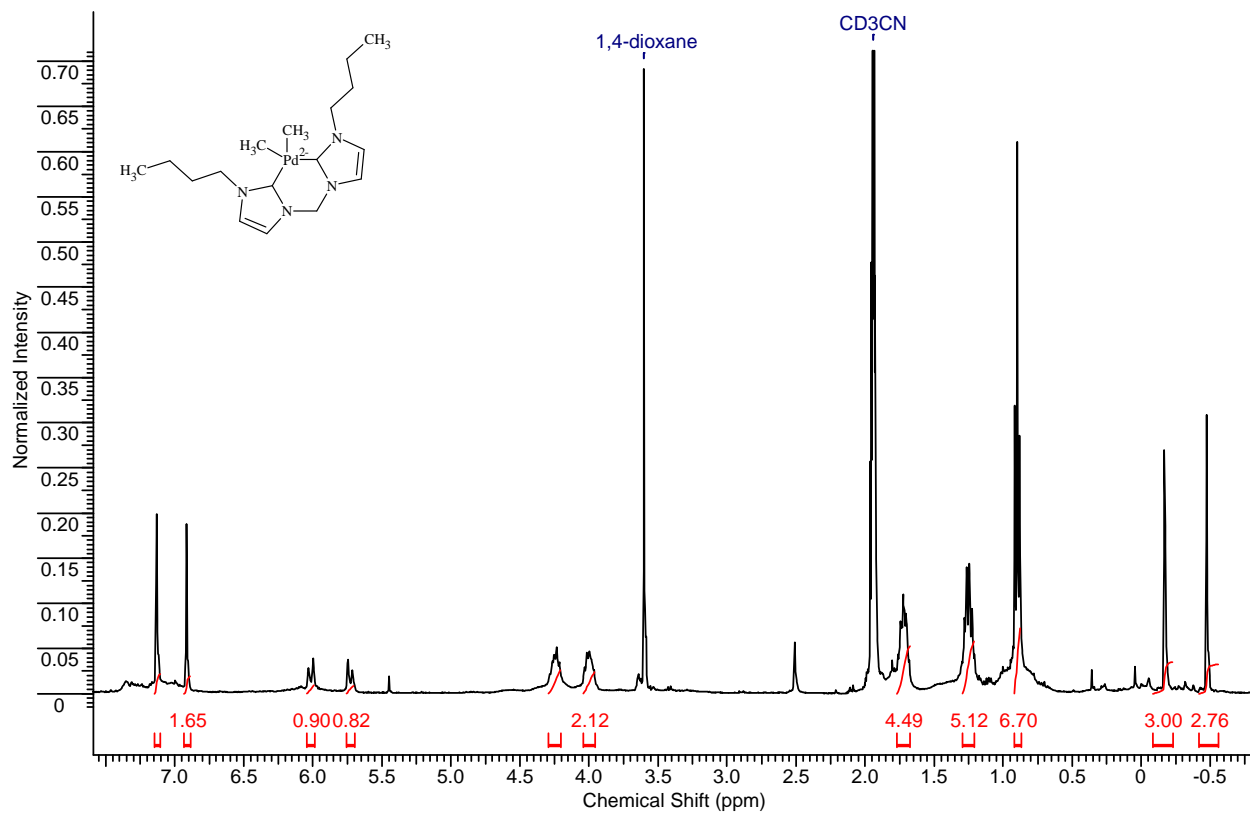


Figure A.26 $^1\text{H-NMR}$ of ^{13}C -labeled *bis*-NHC-Pd(II)- $(^{13}\text{CH}_3)_2$ **5.14'**

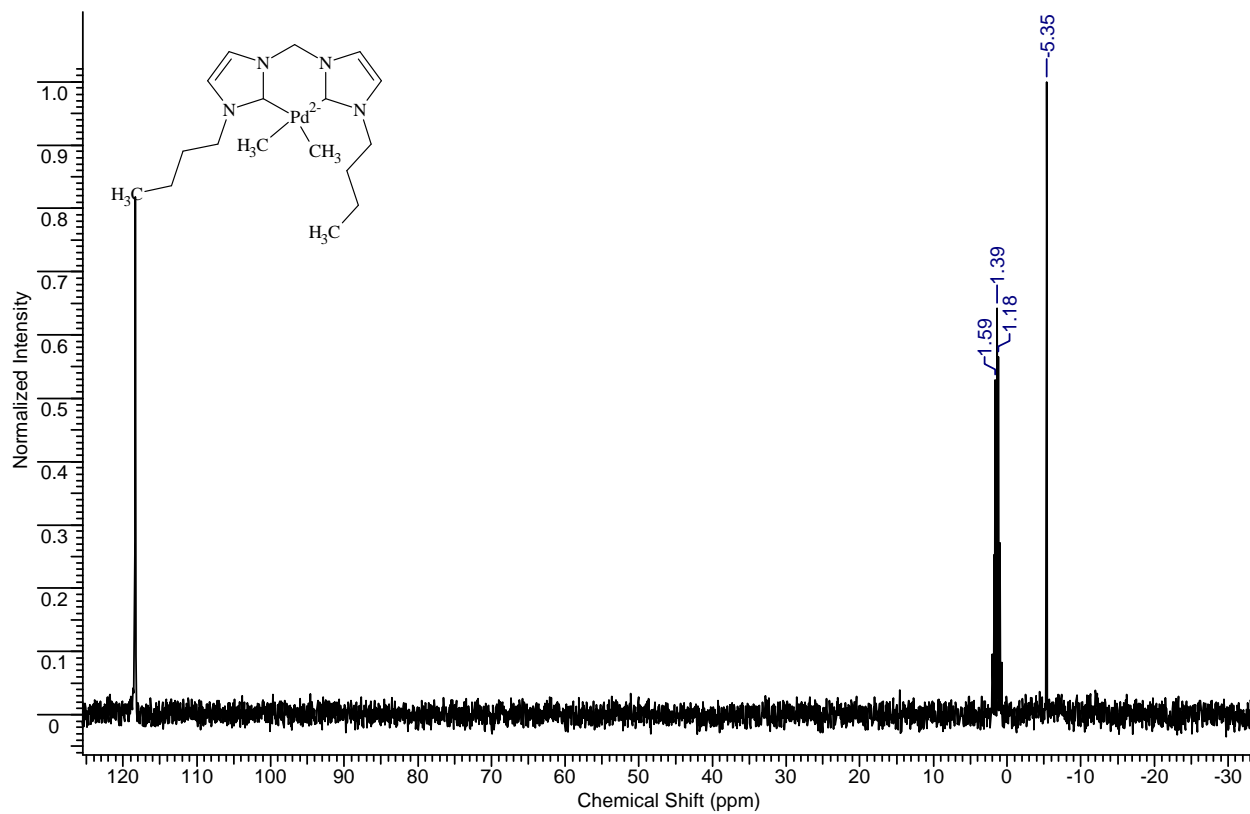


Figure A.27 ^{13}C -NMR of ^{13}C -labeled *bis*-NHC-Pd(II)- $(^{13}\text{CH}_3)_2$ **5.14'** (32 scans)

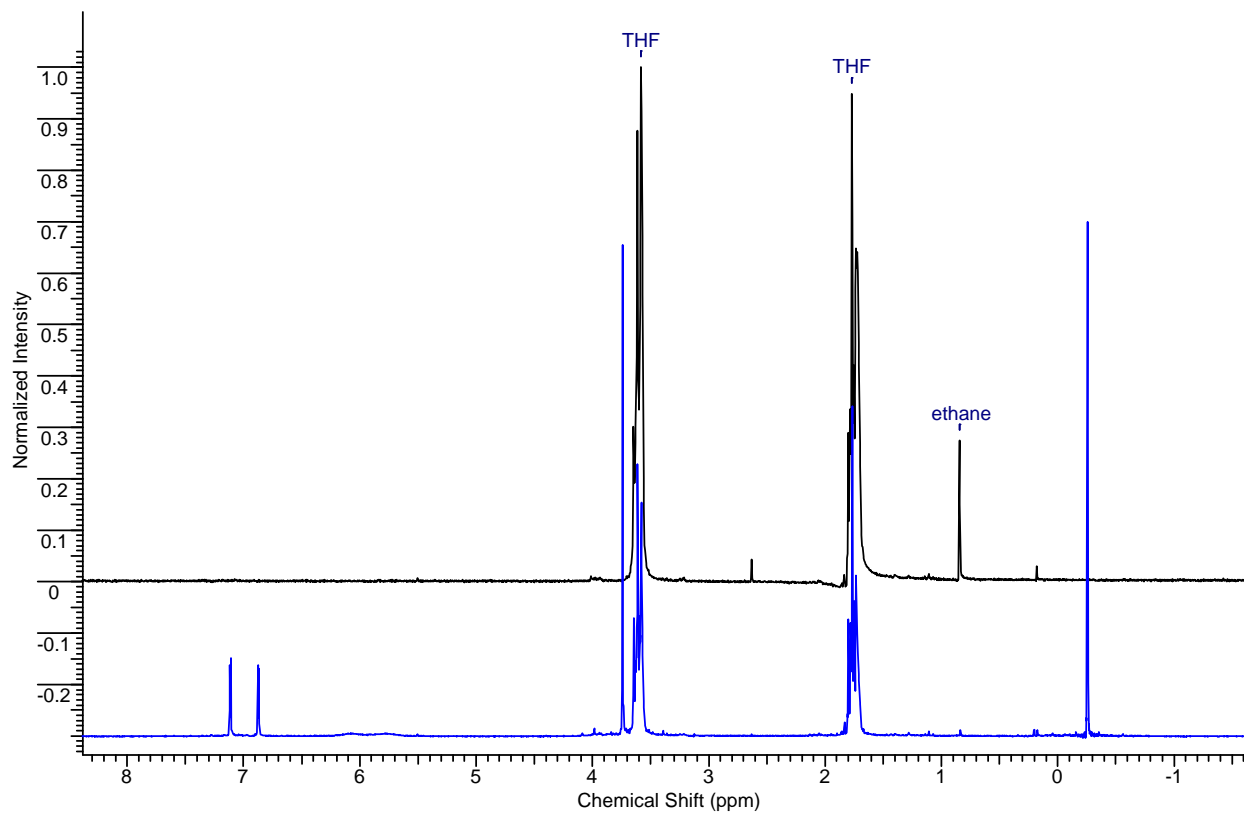


Figure A.28 Stacked $^1\text{H-NMR}$ spectrum of the reaction between *bis*-NHC-Pd-Me₂ (complex **4.1**) and dioxygen. (blue: complex **4.1** in $\text{THF-}d_8$; black: after addition of oxygen for 2 hours)

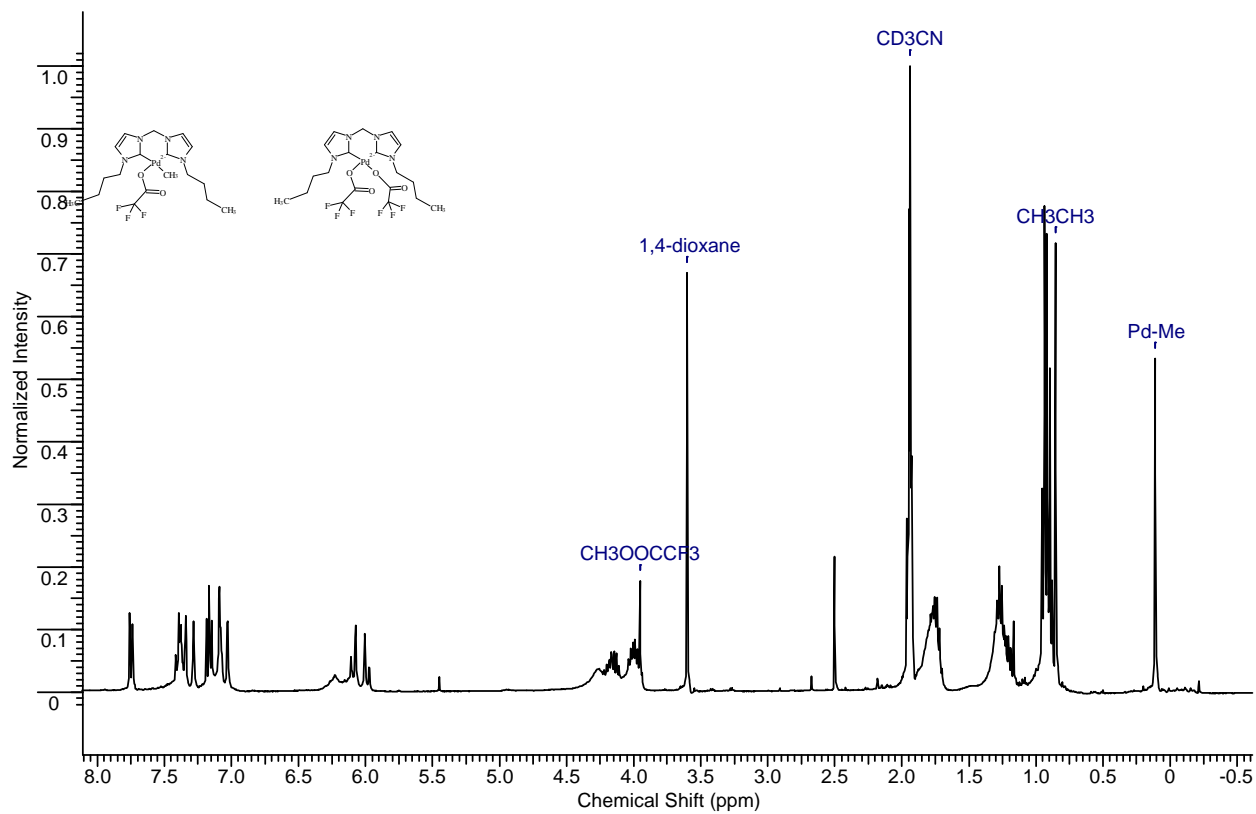
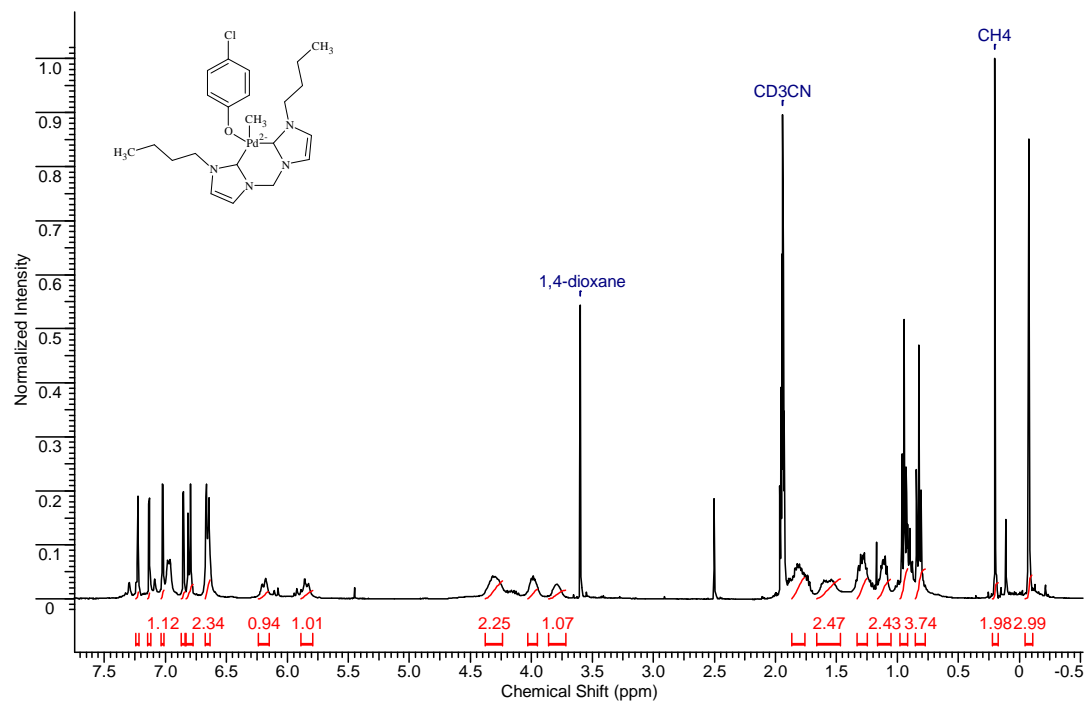
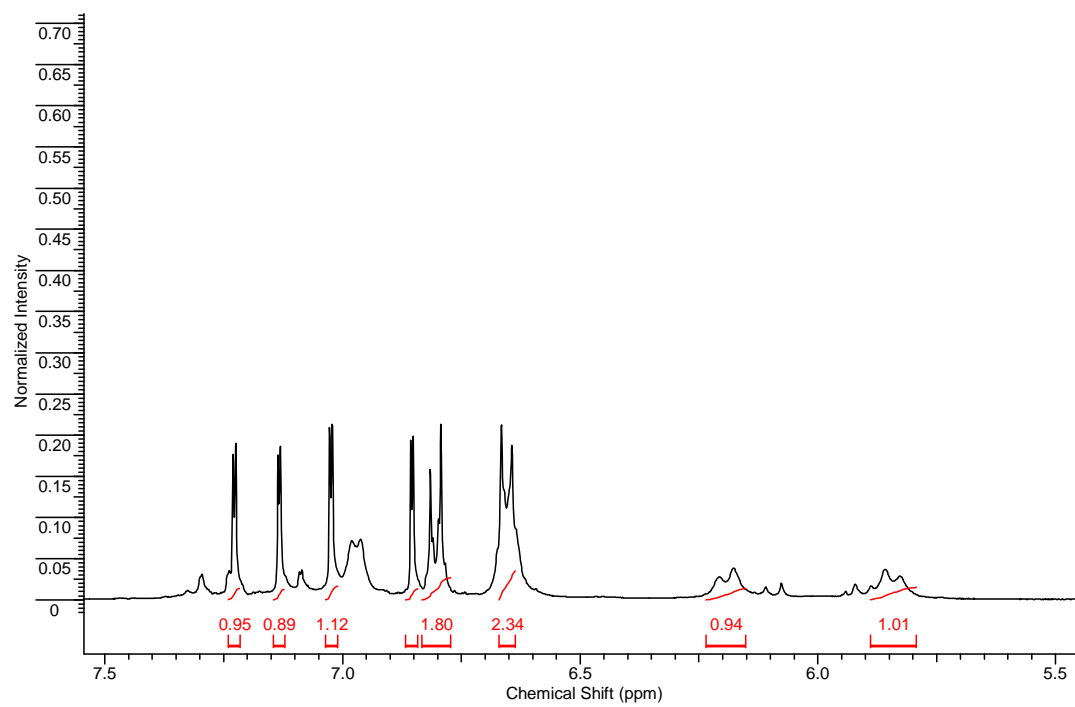


Figure A.29 The reaction between $\text{PhI}(\text{OTFA})_2$ and *bis*-NHC-Pd(II)- $(\text{CH}_3)_2$ **5.14** to generate *bis*-NHC-Pd(II)- (CH_3) - (OTFA) and CH_3OCCF_3 as well as *bis*-NHC-Pd(II)- $(\text{OTFA})_2$ and ethane.



(a)



(b)

Figure A.30 (a) ¹H-NMR of **6.17** (b) Expanded aromatic area

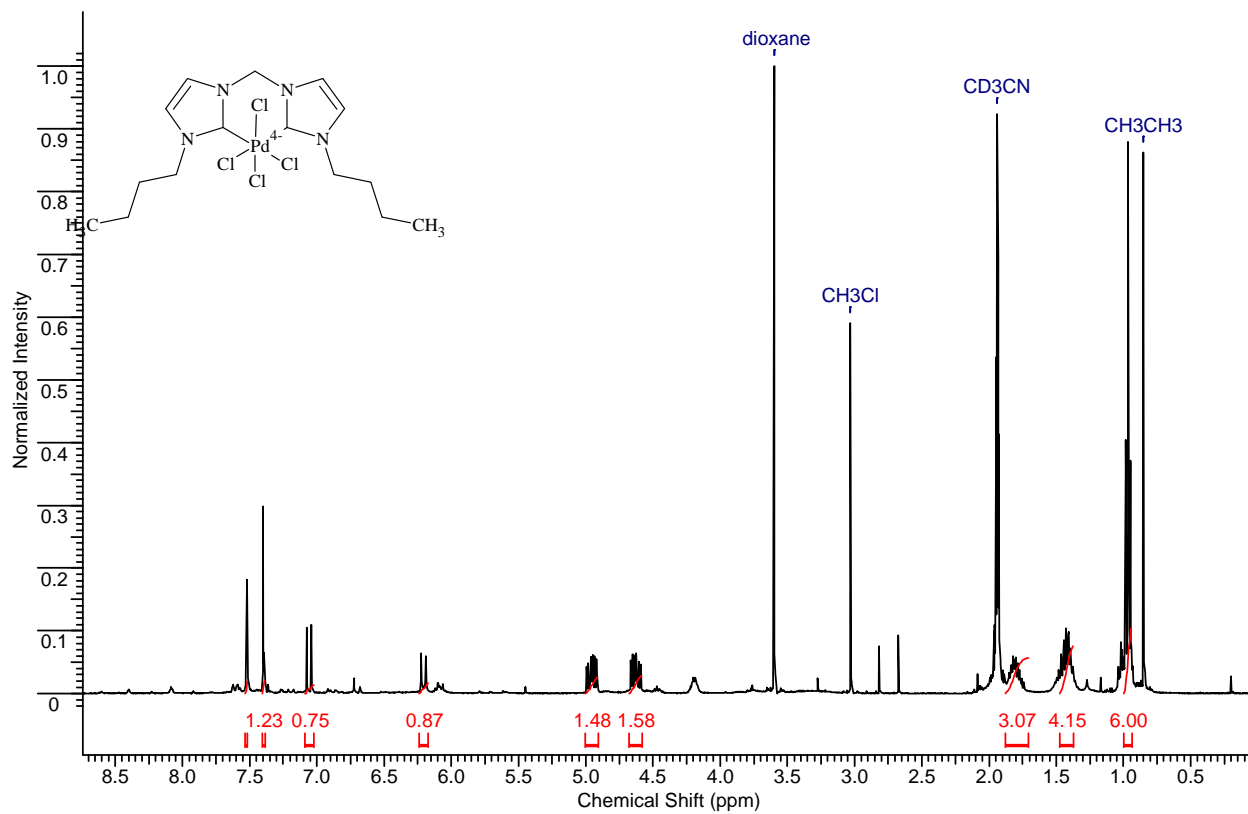


Figure A.31 ¹H-NMR of **7.9** (generated by the reaction between *bis*-NHC-Pd(II)-Me₂ **5.14** and chlorine)

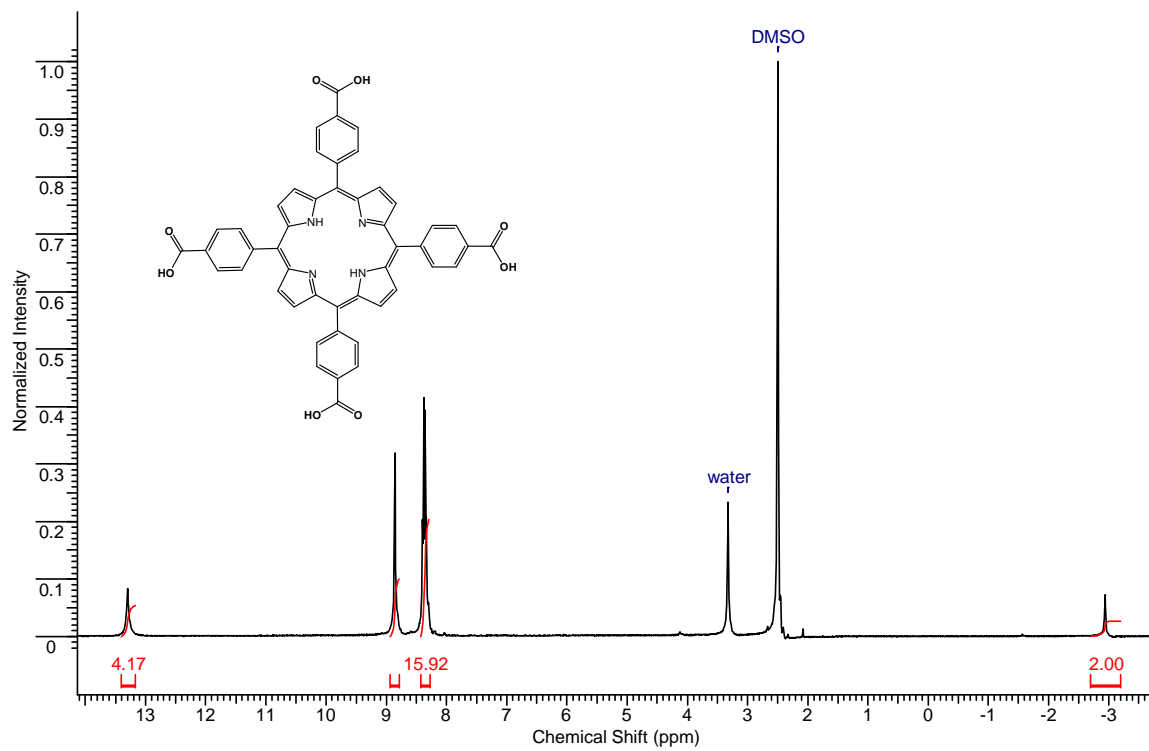


Figure A.32 $^1\text{H-NMR}$ of porphyrin TCPP

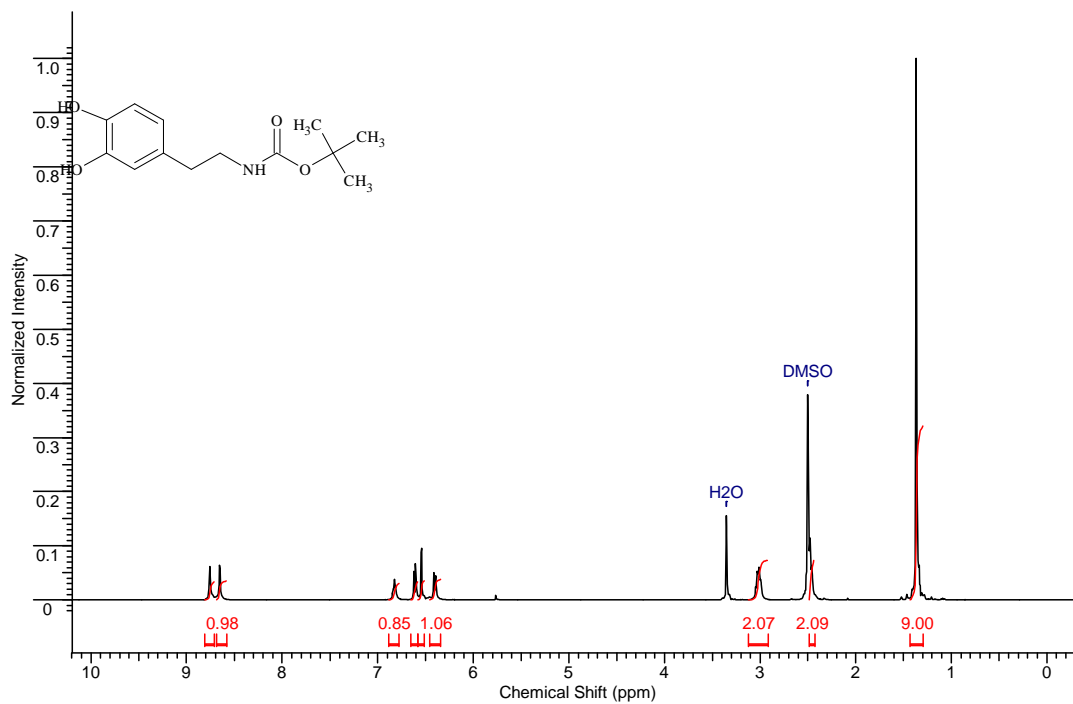


Figure A.33 $^1\text{H-NMR}$ of **9.1**

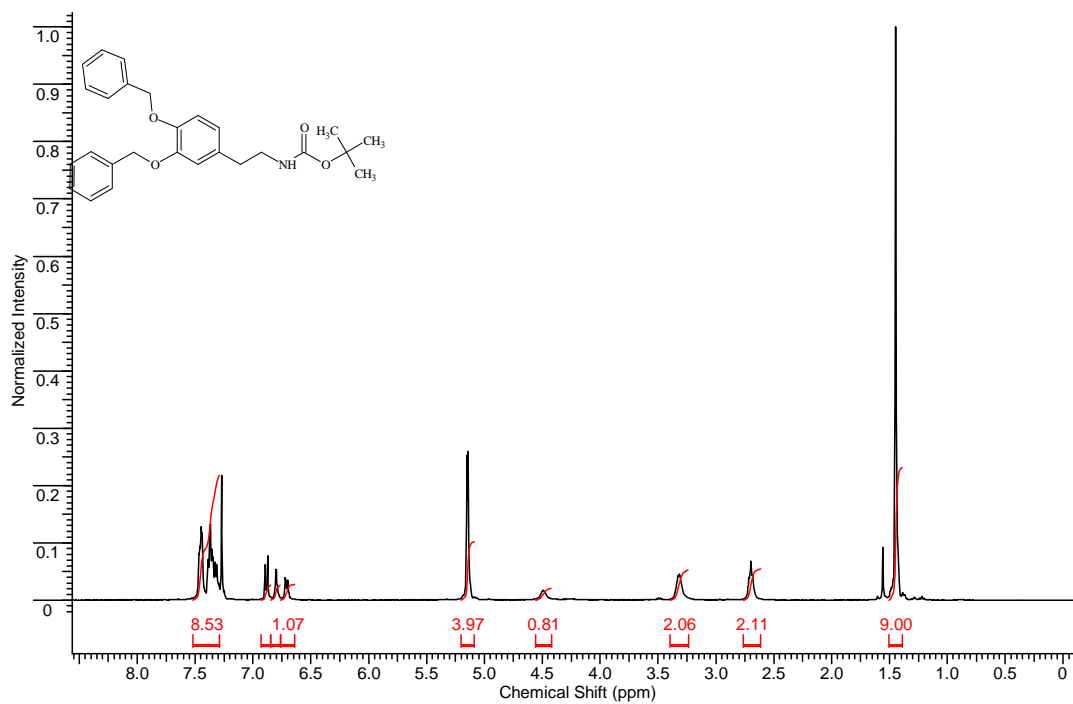


Figure A.34 $^1\text{H-NMR}$ of **9.2**

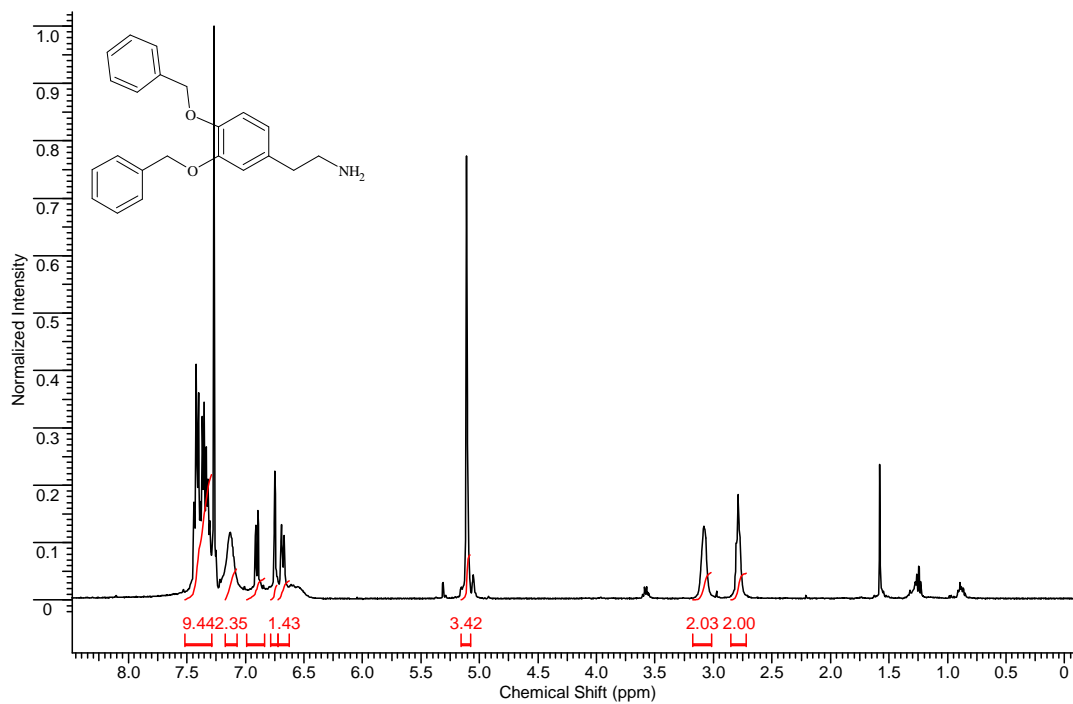


Figure A.35 $^1\text{H-NMR}$ of 9.3

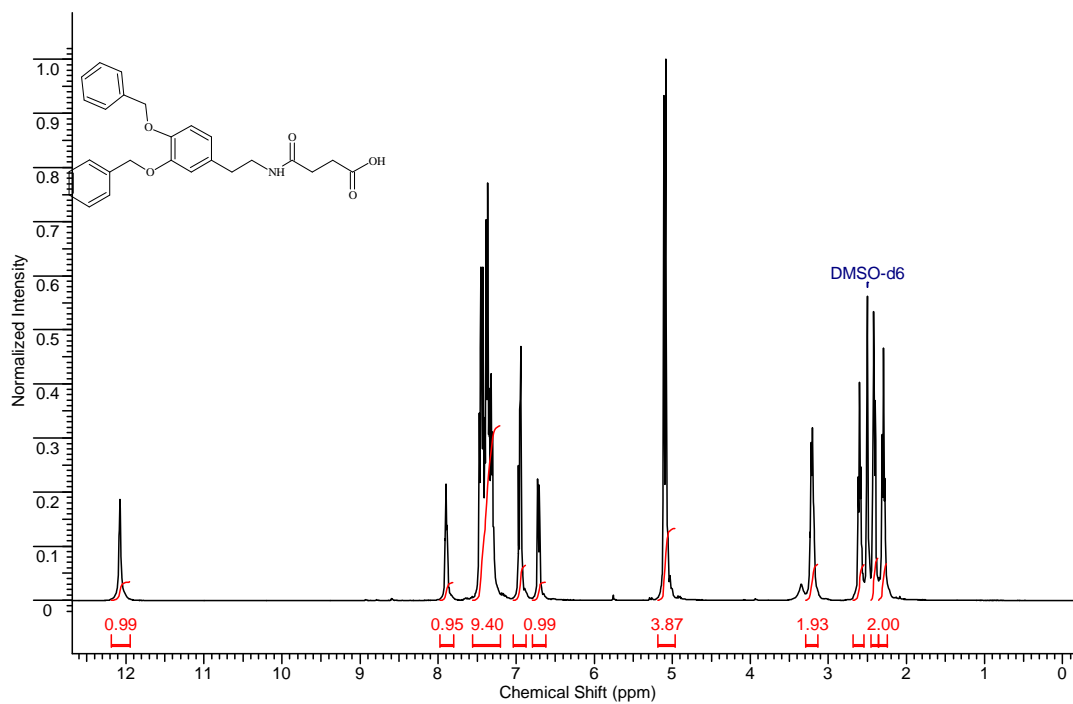


Figure A.35 $^1\text{H-NMR}$ of 9.4

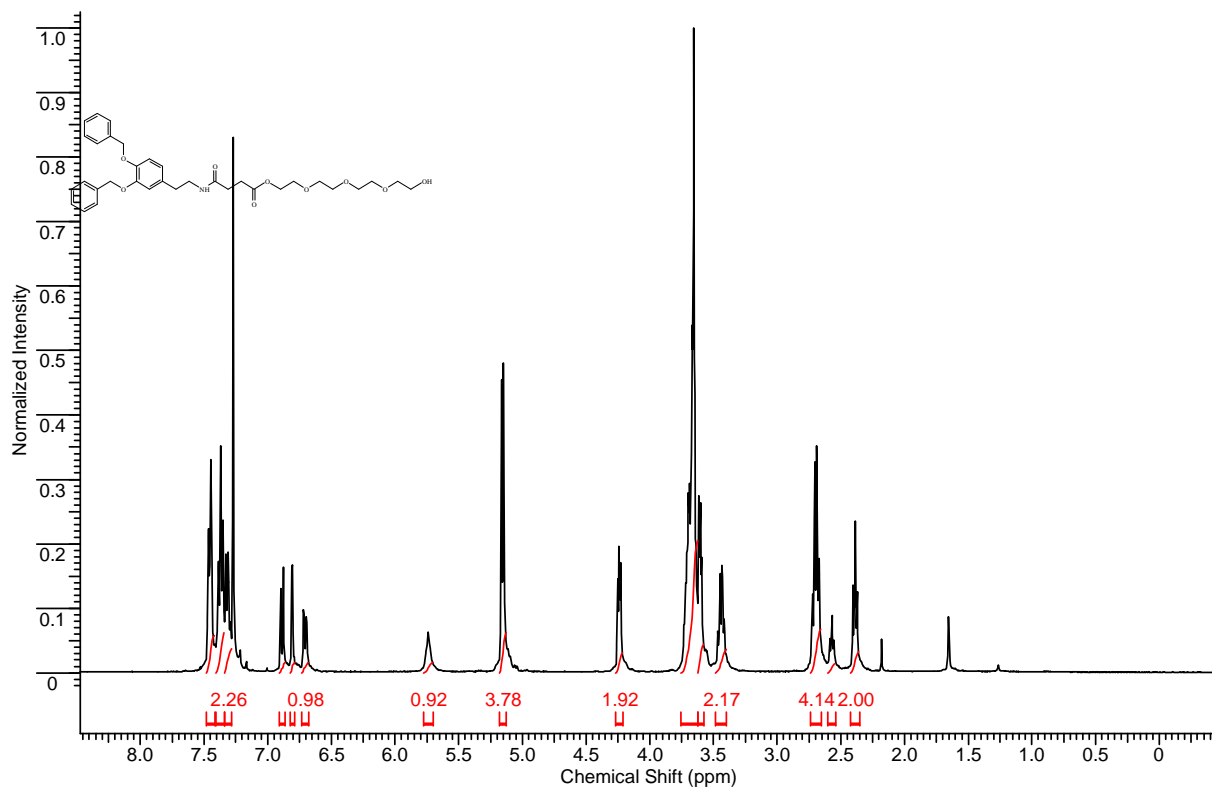


Figure A.36 $^1\text{H-NMR}$ of 9.5

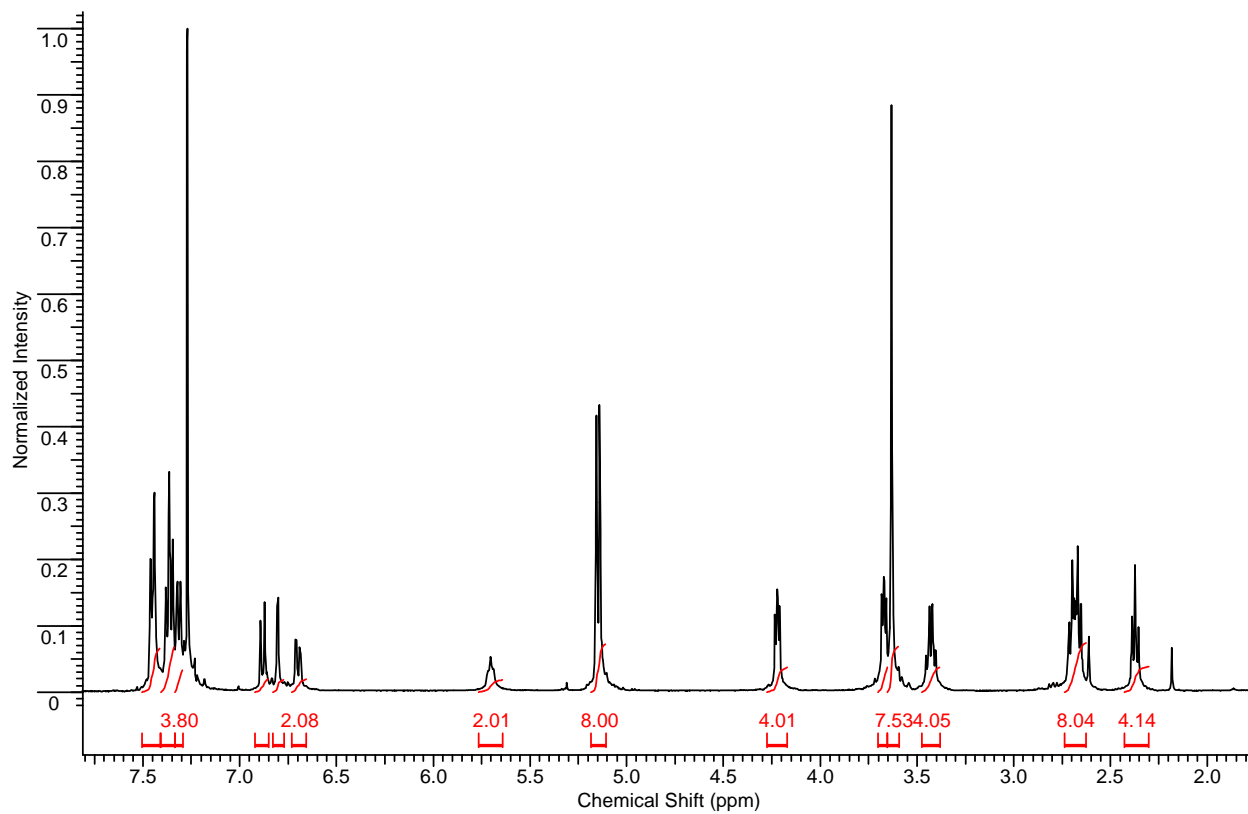


Figure A.37 $^1\text{H-NMR}$ of 9.6

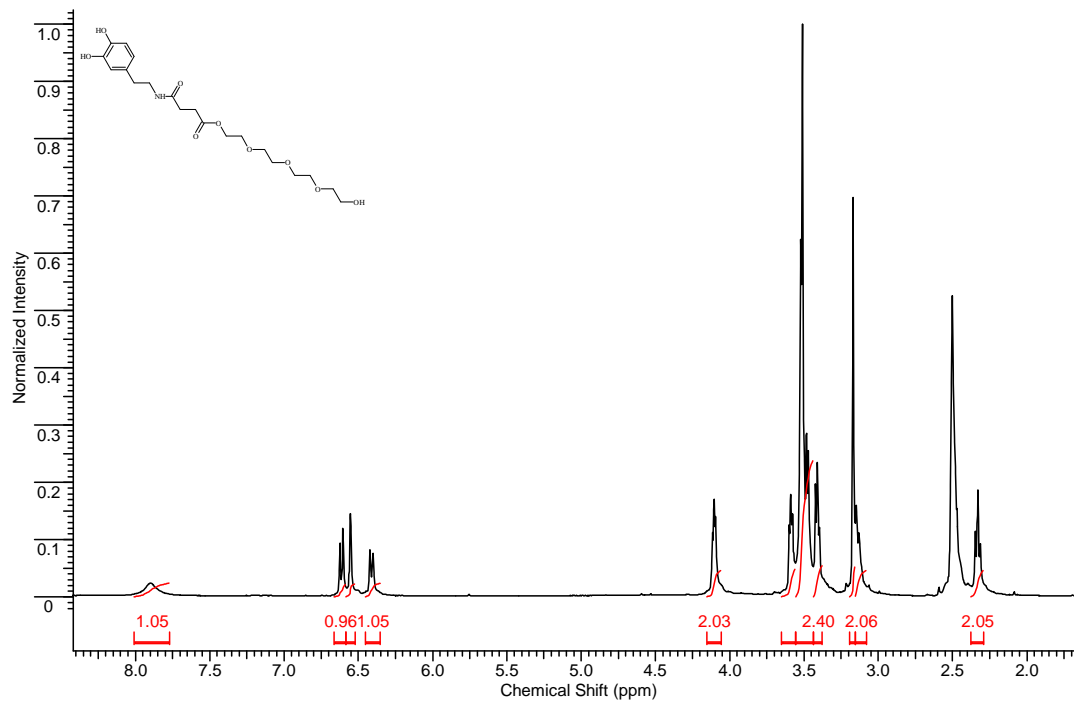
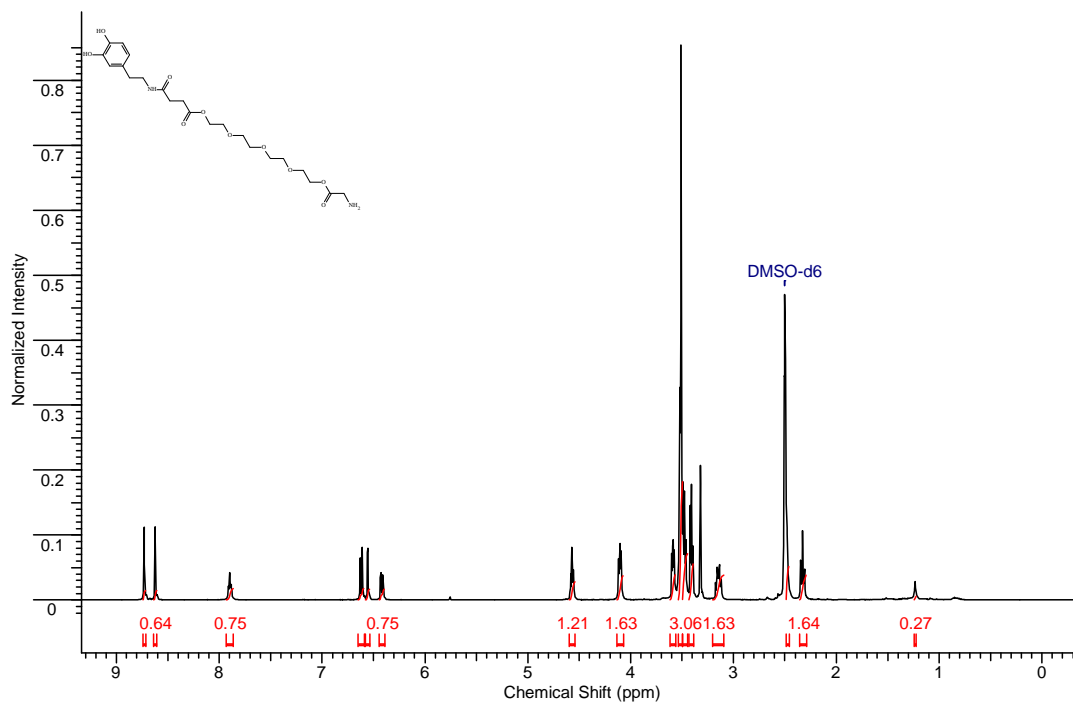
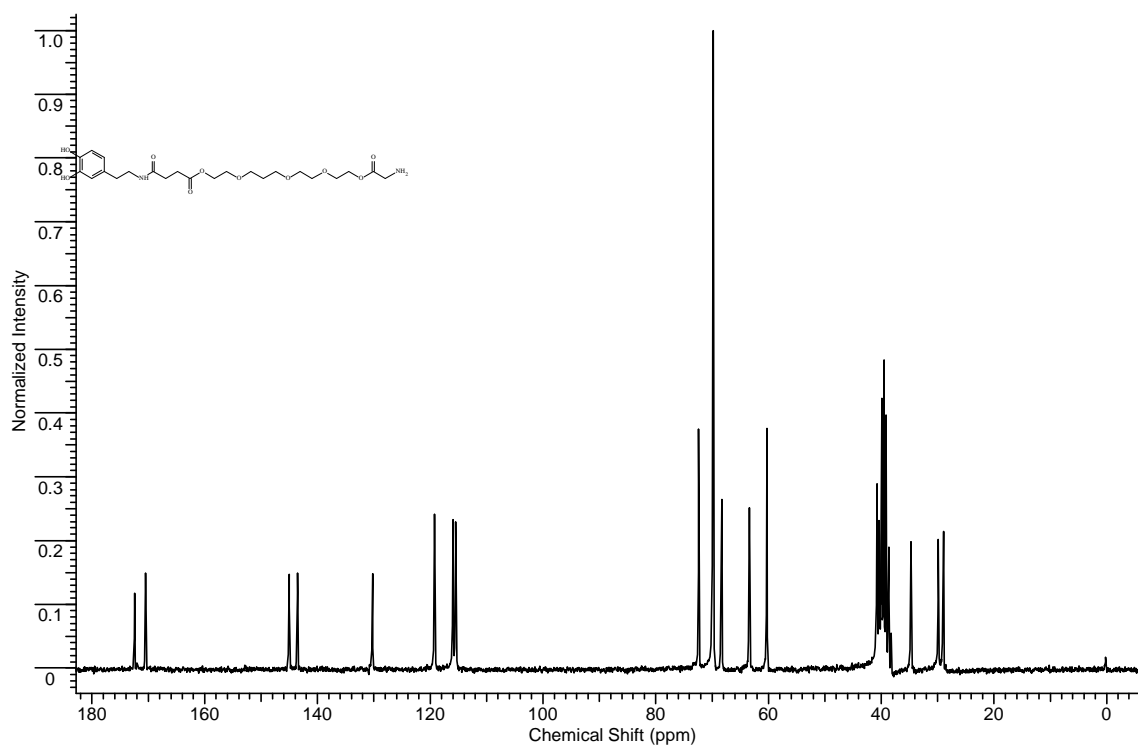


Figure A.38 ¹H-NMR of ligand I



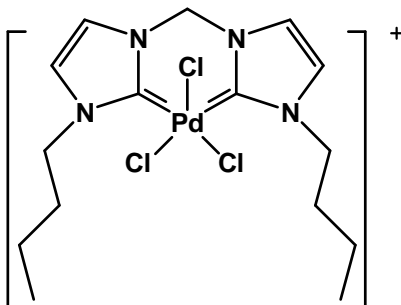
(a)



(b)

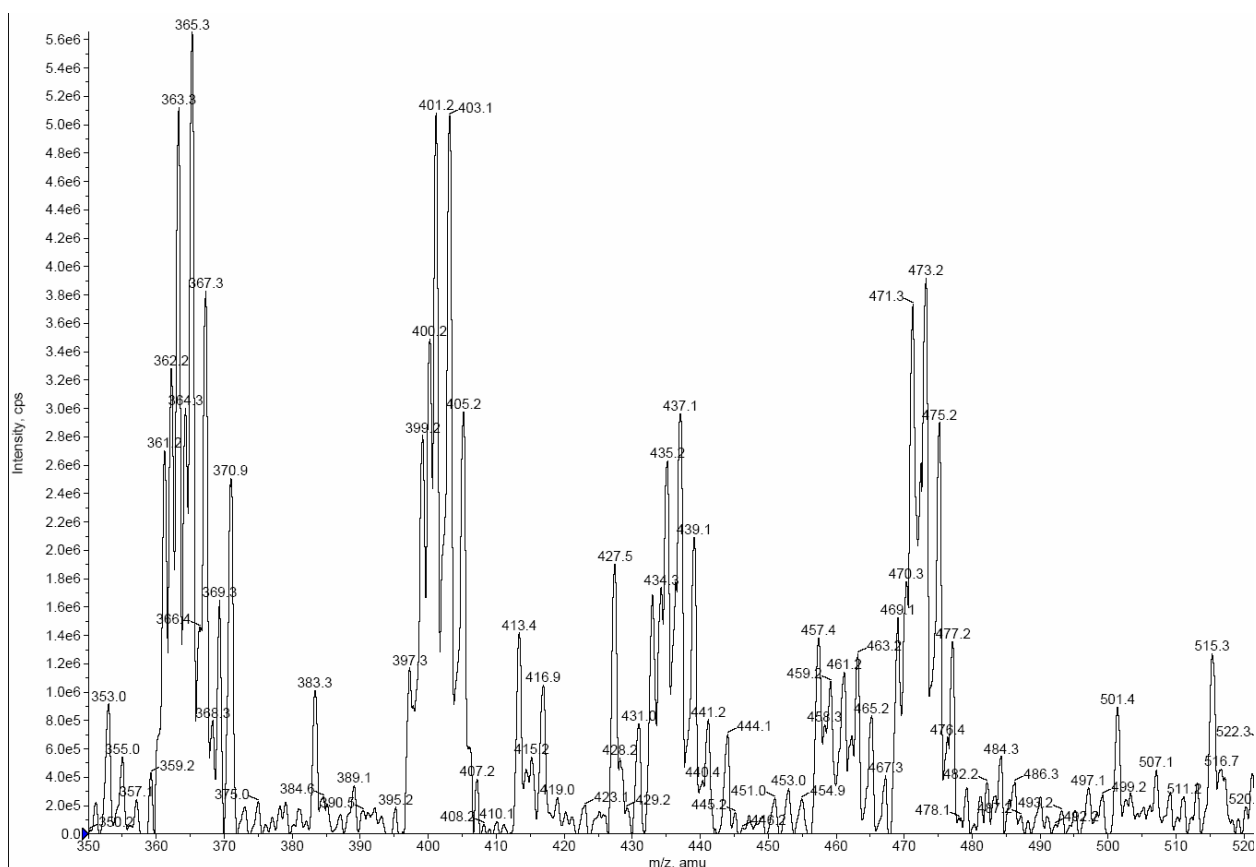
Figure A.39 (a) $^1\text{H-NMR}$ and (b) $^{13}\text{C-NMR}$ of **ligand II**

Appendix B- Mass Spectroscopy Data

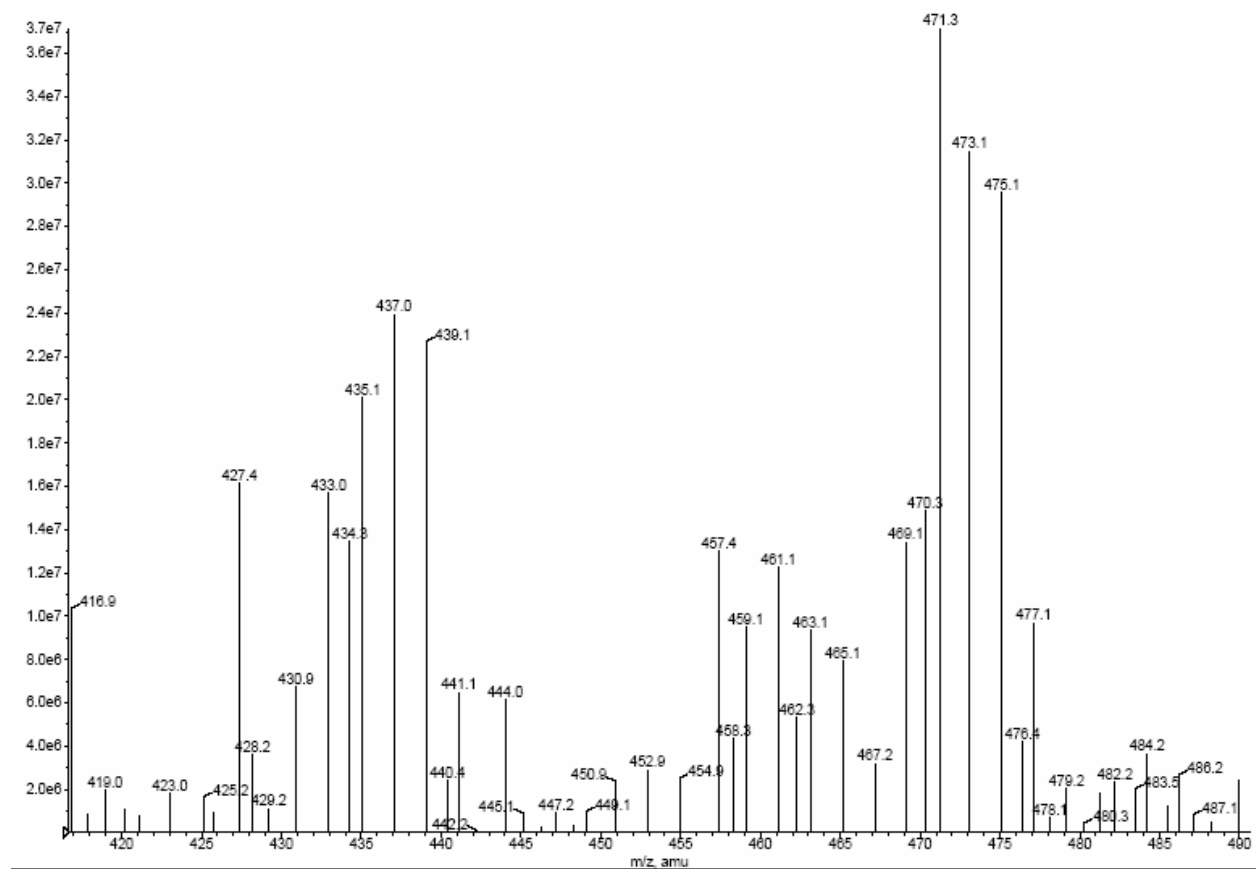


$C_{15}H_{24}Cl_3N_4Pd$
Exact Mass: 471.01

m/z : 473.01 (100.0%), 475.01 (68.3%), 471.01 (68.2%), 470.01 (43.2%), 469.01 (21.4%), 477.01 (20.9%)

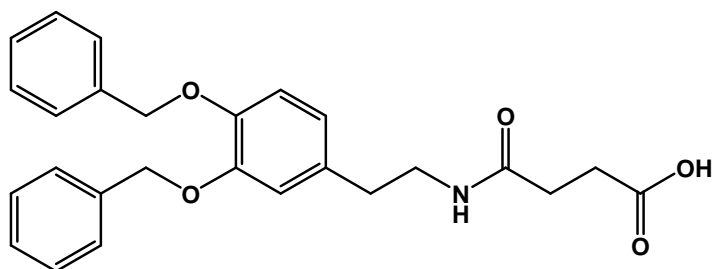


(a)



(b)

Figure B.1 (a) ESI⁺ Mass spectroscopy of the *bis*-NHC-Pd(IV)-Cl₄ **7.9** with stepwise fragmentation. (b) Centroided Mass spectrum for [M-Cl] ion.



$C_{26}H_{27}NO_5$
Exact Mass: 433.19
 $(M+H)^+$ 434.19, $(M+Na)^+$ 456.40

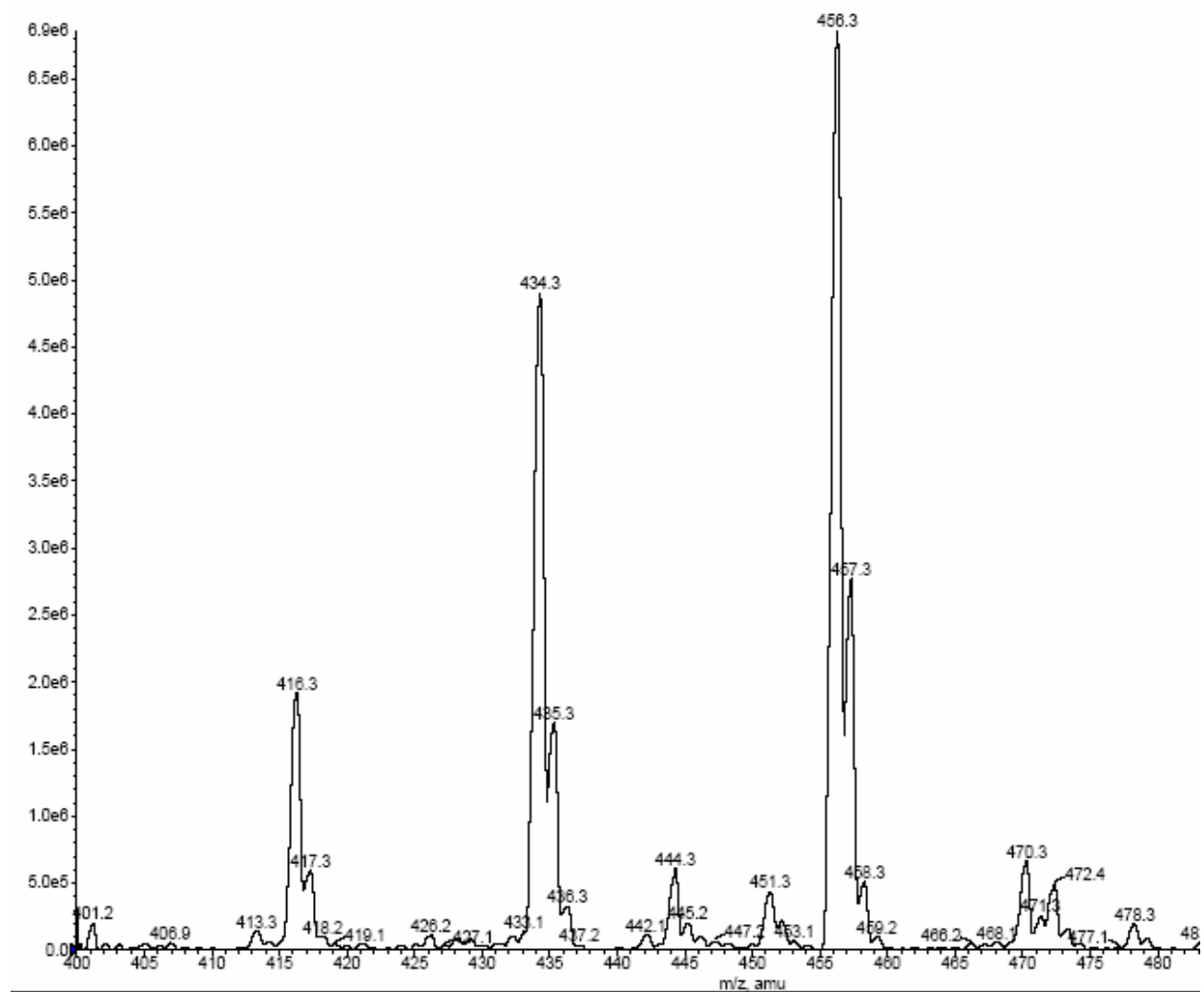
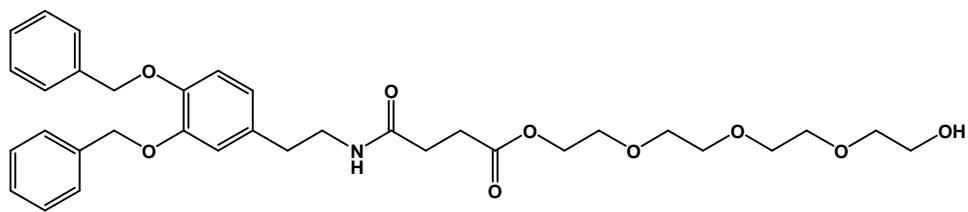


Figure B.2 ESI⁺ Mass spectroscopy of 9.4



$C_{34}H_{43}NO_9$
Exact Mass: 609.29
 m/z : (M+H)⁺ 610.40, (M+Na)⁺ 632.30, (M+K)⁺ 648.3

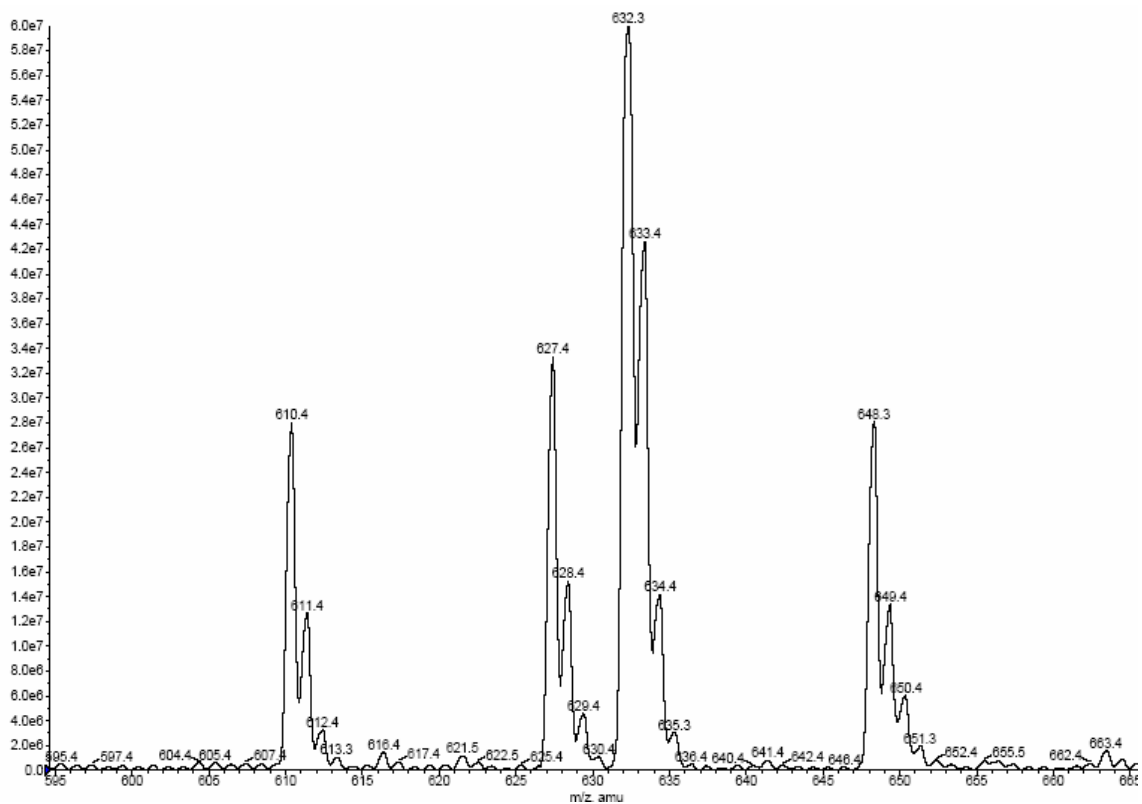
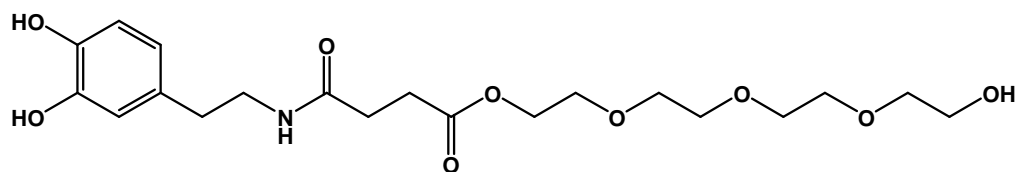


Figure B.3 ESI⁺ Mass spectroscopy of 9.5



$C_{20}H_{31}NO_9$
Exact Mass: 429.2
 $m/e: (M+H)^+ 430.20, (M+Na)^+ 452.20$

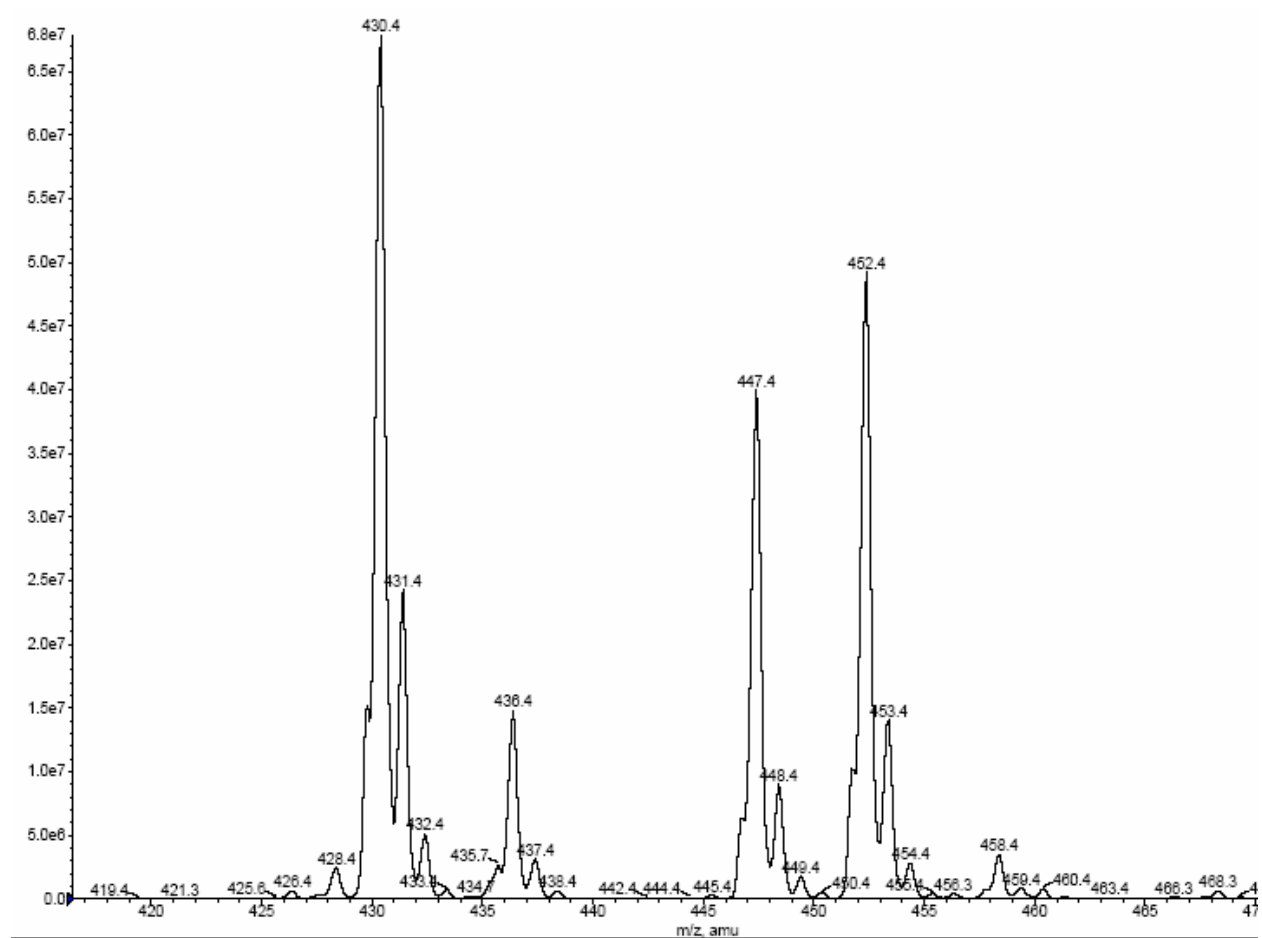
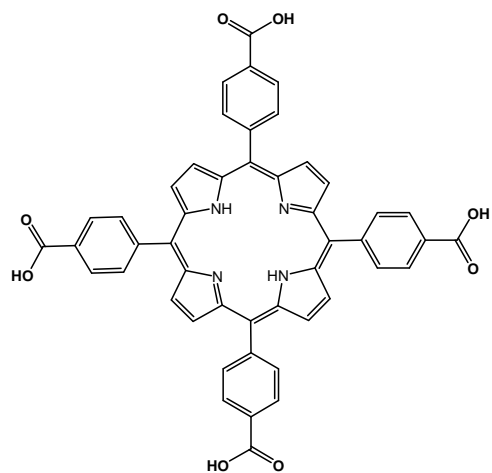


Figure B.4 ESI⁺ Mass spectroscopy of **ligand I**



$C_{48}H_{30}N_4O_8$
Exact Mass: 790.21
 $m/e: (M+H)^+ 791.21$

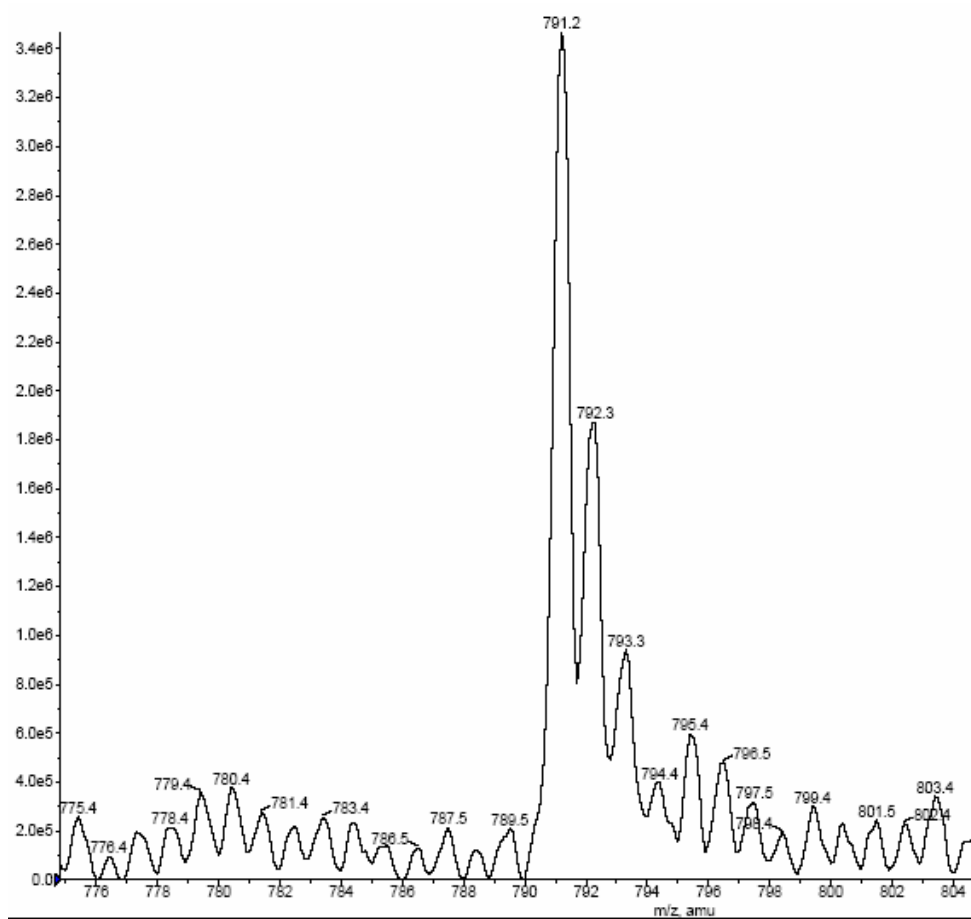


Figure B.5 ESI⁺ Mass spectroscopy of porphyrin TCPP

Appendix C- Crystal Data and Structure Refinements

Table C.1 Crystal data and structure refinement for **3.25**

Empirical formula	C ₁₉ H ₂₈ I ₂ N ₆ O ₂ Pd S	
Formula weight	764.73	
Temperature	120(2) K	
Wavelength	0.71073 Å	
Crystal system	Triclinic	
Space group	P-1	
Unit cell dimensions	a = 11.4450(6) Å	α = 71.772(2)°.
	b = 11.8474(6) Å	β = 64.040(2)°.
	c = 12.0978(6) Å	γ = 62.941(2)°.
Volume	1300.13(11) Å ³	
Z	2	
Density (calculated)	1.953 g/cm ³	
Absorption coefficient	3.195 mm ⁻¹	
F(000)	736	
Crystal size	0.26 x 0.24 x 0.06 mm ³	
Theta range for data collection	2.23 to 32.58°.	
Index ranges	-17 ≤ h ≤ 17, -16 ≤ k ≤ 17, -18 ≤ l ≤ 18	
Reflections collected	27872	
Independent reflections	9131 [R(int) = 0.0320]	
Completeness to theta = 32.58°	96.4 %	
Absorption correction	None	
Max. and min. transmission	0.8314 and 0.4905	
Refinement method	Full-matrix least-squares on F ²	
Data / restraints / parameters	9131 / 0 / 289	
Goodness-of-fit on F ²	1.042	
Final R indices [I > 2σ(I)]	R1 = 0.0279, wR2 = 0.0639	
R indices (all data)	R1 = 0.0358, wR2 = 0.0675	
Largest diff. peak and hole	1.051 and -0.741 e.Å ⁻³	

Table C.2 Crystal data and structure refinement for **7.9'**

Empirical formula	C ₂₁ H ₃₀ Cl ₁₄ N ₈ Pd ₂	
Formula weight	1103.63	
Temperature	120(2) K	
Wavelength	0.71073 Å	
Crystal system	Monoclinic	
Space group	P2(1)/n	
Unit cell dimensions	a = 7.6703(6) Å	α = 90°.
	b = 18.5451(11) Å	β = 91.644(4)°.
	c = 13.1767(8) Å	γ = 90°.
Volume	1873.6(2) Å ³	
Z	2	
Density (calculated)	1.956 g/cm ³	
Absorption coefficient	1.989 mm ⁻¹	
F(000)	1084	
Crystal size	0.25 x 0.05 x 0.05 mm ³	
Theta range for data collection	2.20 to 32.03°.	
Index ranges	-11 ≤ h ≤ 3, -27 ≤ k ≤ 24, -19 ≤ l ≤ 19	
Reflections collected	19678	
Independent reflections	5968 [R(int) = 0.0462]	
Completeness to theta = 30.00°	97.2 %	
Absorption correction	None	
Max. and min. transmission	0.9071 and 0.6362	
Refinement method	Full-matrix least-squares on F ²	
Data / restraints / parameters	5968 / 9 / 223	
Goodness-of-fit on F ²	1.056	
Final R indices [I > 2σ(I)]	R ₁ = 0.0465, wR ₂ = 0.1070	
R indices (all data)	R ₁ = 0.0710, wR ₂ = 0.1172	
Largest diff. peak and hole	1.758 and -1.083 e.Å ⁻³	